



Arabian Sea Mixed Layer Dynamics Experiment

Data Report

by

Mark F. Baumgartner

Nancy J. Brink

William M. Ostrom

Richard P. Trask

Robert A. Weller

Upper Ocean Processes Group

Woods Hole Oceanographic Institution

Tommy D. Dickey

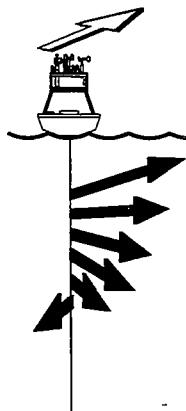
Ocean Physics Laboratory

University of California, Santa Barbara

John Marra

Lamont-Doherty Earth Observatory

Columbia University



WHOI-97-08
UOP Report 97-03

**Arabian Sea Mixed Layer Dynamics Experiment
Data Report**

by

Mark F. Baumgartner
Nancy J. Brink
William M. Ostrom
Richard P. Trask
Robert A. Weller
*Upper Ocean Processes Group
Woods Hole Oceanographic Institution*

Tommy D. Dickey
*Ocean Physics Laboratory
University of California, Santa Barbara*

John Marra
*Lamont-Doherty Earth Observatory
Columbia University*

Upper Ocean Processes Group
Woods Hole Oceanographic Institution
Woods Hole, Massachusetts 02543-1541

July 1997


Technical Report

Funding provided by the Office of Naval Research under
Contract No. N00014-94-1-0161.

Reproduction in whole or in part is permitted for any purpose of the United States
Government. This report should be cited as:
Woods Hole Oceanog. Inst. Tech. Rept., WHOI-97-08

Approved for publication; distribution unlimited.

Approved for Distribution:



Philip L. Richardson, Chair
Department of Physical Oceanography

Abstract

The Arabian Sea is characterized by strong, large-scale atmospheric forcing during the summer (southwest) and winter (northeast) monsoons. To investigate air-sea interactions related to this unique surface forcing, a moored array was deployed from 15 October 1994 to 19 October 1995 just south of a region that experiences the climatological maximum winds during the summer monsoon. The array consisted of two Scripps Institution of Oceanography surface toroid buoys, two University of Washington subsurface moorings and a surface 3 m discus buoy deployed by the Woods Hole Oceanographic Institution (WHOI). The WHOI buoy carried redundant meteorological packages to measure wind speed and direction, air temperature, relative humidity, barometric pressure, incoming short- and long-wave radiation and precipitation. Oceanographic instrumentation was deployed on the WHOI buoy's bridle and mooring line to collect time series of temperature, salinity and velocity at various depths. Four multi-variable moored systems (MVMS) were also deployed along the mooring line by the Lamont-Doherty Earth Observatory and the University of California at Santa Barbara to record both bio-optical and physical parameters. This report describes the instrumentation deployed on the WHOI buoy and the processing and editing of the returned data. The data are then summarized in graphical and tabular formats.

Table of Contents

Abstract	i
List of Figures	iii
List of Tables	vii
Section 1: Introduction	1
Section 2. Instrumentation	4
Section 3: Data Processing	14
Section 4: Data Summary	23
Acknowledgments	106
Literature Cited	107
Appendix A: Ancillary Data	109
Appendix B: Instrument Serial Numbers	155
Appendix C: VMCM Record Format	157

List of Figures

Figure 1.	Arabian Sea moored array	2
Figure 2.	3 m discus buoy	7
Figure 3.	Buoy tower top configuration	8
Figure 4.	Mooring schematic	11
Figure 5.	Discus buoy bridle configuration	12
Figure 6.	Booby signal in long-wave radiation measurements	21
Figure 7.	Hourly time series of meteorological observations	38
Figure 8.	Time series of meteorological observations for October 1994	39
Figure 9.	Time series of meteorological observations for November 1994	40
Figure 10.	Time series of meteorological observations for December 1994	41
Figure 11.	Time series of meteorological observations for January 1995	42
Figure 12.	Time series of meteorological observations for February 1995	43
Figure 13.	Time series of meteorological observations for March 1995	44
Figure 14.	Time series of meteorological observations for April 1995	45
Figure 15.	Time series of meteorological observations for May 1995	46
Figure 16.	Time series of meteorological observations for June 1995	47
Figure 17.	Time series of meteorological observations for July 1995	48
Figure 18.	Time series of meteorological observations for August 1995	49
Figure 19.	Time series of meteorological observations for September 1995	50
Figure 20.	Time series of meteorological observations for October 1995	51
Figure 21.	Hourly time series of precipitation and evaporation	52
Figure 22.	Hourly time series of estimated heat and momentum fluxes	53
Figure 23.	Time series of heat and momentum fluxes for October 1994	54
Figure 24.	Time series of heat and momentum fluxes for November 1994	55
Figure 25.	Time series of heat and momentum fluxes for December 1994	56
Figure 26.	Time series of heat and momentum fluxes for January 1995	57
Figure 27.	Time series of heat and momentum fluxes for February 1995	58
Figure 28.	Time series of heat and momentum fluxes for March 1995	59
Figure 29.	Time series of heat and momentum fluxes for April 1995	60
Figure 30.	Time series of heat and momentum fluxes for May 1995	61
Figure 31.	Time series of heat and momentum fluxes for June 1995	62
Figure 32.	Time series of heat and momentum fluxes for July 1995	63
Figure 33.	Time series of heat and momentum fluxes for August 1995	64

Figure 34. Time series of heat and momentum fluxes for September 1995	65
Figure 35. Time series of heat and momentum fluxes for October 1995	66
Figure 36. Contour plot of temperature and mixed layer depth	67
Figure 37. Contour plot of temperature and mixed layer depth for October 1994	68
Figure 38. Contour plot of temperature and mixed layer depth for November 1994	69
Figure 39. Contour plot of temperature and mixed layer depth for December 1994	70
Figure 40. Contour plot of temperature and mixed layer depth for January 1995	71
Figure 41. Contour plot of temperature and mixed layer depth for February 1995	72
Figure 42. Contour plot of temperature and mixed layer depth for March 1995	73
Figure 43. Contour plot of temperature and mixed layer depth for April 1995	74
Figure 44. Contour plot of temperature and mixed layer depth for May 1995	75
Figure 45. Contour plot of temperature and mixed layer depth for June 1995	76
Figure 46. Contour plot of temperature and mixed layer depth for July 1995	77
Figure 47. Contour plot of temperature and mixed layer depth for August 1995	78
Figure 48. Contour plot of temperature and mixed layer depth for September 1995	79
Figure 49. Contour plot of temperature and mixed layer depth for October 1995	80
Figure 50. VMCM and MVMS velocity stick plots from WHOI mooring	81
Figure 51. VMCM and MVMS velocity stick plots from UW South mooring	82
Figure 52. Time series of velocity at selected depths for October 1994	83
Figure 53. Time series of velocity at selected depths for November 1994	84
Figure 54. Time series of velocity at selected depths for December 1994	85
Figure 55. Time series of velocity at selected depths for January 1995	86
Figure 56. Time series of velocity at selected depths for February 1995	87
Figure 57. Time series of velocity at selected depths for March 1995	88
Figure 58. Time series of velocity at selected depths for April 1995	89
Figure 59. Time series of velocity at selected depths for May 1995	90
Figure 60. Time series of velocity at selected depths for June 1995	91
Figure 61. Time series of velocity at selected depths for July 1995	92
Figure 62. Time series of velocity at selected depths for August 1995	93
Figure 63. Time series of velocity at selected depths for September 1995	94
Figure 64. Time series of velocity at selected depths for October 1995	95
Figure 65. Progressive vectors from VMCM and MVMS current meters	96
Figure 66. Monthly progressive vectors	97
Figure 67. Autospectra of meteorological parameters	100
Figure 68. Autospectra of heat and momentum fluxes	101
Figure 69. Autospectra of temperature at various depths	102

Figure 70. Rotary autospectra of velocity at various depths	104
Figure A1. Shipboard meteorological observations during cruise TN040	112
Figure A2. Shipboard meteorological observations during cruise TN042	113
Figure A3. Shipboard meteorological observations during cruise TN044	114
Figure A4. Shipboard meteorological observations during cruise TN046	115
Figure A5. Shipboard meteorological observations during cruise TN048	116
Figure A6. Shipboard meteorological observations during cruise TN051	117
Figure A7. Shipboard meteorological observations during cruise TN052	118
Figure A8. Estimated heat and momentum fluxes during cruise TN040	119
Figure A9. Estimated heat and momentum fluxes during cruise TN042	120
Figure A10. Estimated heat and momentum fluxes during cruise TN044	121
Figure A11. Estimated heat and momentum fluxes during cruise TN046	122
Figure A12. Estimated heat and momentum fluxes during cruise TN048	123
Figure A13. Estimated heat and momentum fluxes during cruise TN051	124
Figure A14. Estimated heat and momentum fluxes during cruise TN052	125
Figure A15. Near-surface temperatures during DriftAR experiment 1	126
Figure A16. Near-surface temperatures during DriftAR experiment 2	127
Figure A17. Near-surface temperatures during DriftAR experiment 3	128
Figure A18. ECMWF vs. VAWR wind speed comparison	129
Figure A19. ECMWF vs. VAWR wind direction comparison	130
Figure A20. ECMWF vs. VAWR barometric pressure comparison	131
Figure A21. ECMWF vs. VAWR air temperature comparison	132
Figure A22. ECMWF vs. VAWR relative humidity comparison	133
Figure A23. ECMWF vs. VAWR specific humidity comparison	134
Figure A24. ECMWF vs. VAWR sea surface temperature comparison	135
Figure A25. ECMWF vs. VAWR sensible heat flux comparison	136
Figure A26. ECMWF vs. VAWR latent heat flux comparison	137
Figure A27. ECMWF vs. VAWR net short-wave radiation comparison	138
Figure A28. ECMWF vs. VAWR net long-wave radiation comparison	139
Figure A29. ECMWF vs. VAWR net heat flux comparison	140
Figure A30. ECMWF vs. VAWR wind stress magnitude comparison	141
Figure A31. NCEP vs VAWR wind speed comparison	142
Figure A32. NCEP vs VAWR wind direction comparison	143
Figure A33. NCEP vs VAWR barometric pressure comparison	144
Figure A34. NCEP vs VAWR air temperature comparison	145

Figure A35.NCEP vs VAWR relative humidity comparison	146
Figure A36.NCEP vs VAWR specific humidity comparison	147
Figure A37.NCEP vs VAWR sea surface temperature comparison	148
Figure A38.NCEP vs VAWR sensible heat flux comparison	149
Figure A39.NCEP vs VAWR latent heat flux comparison	150
Figure A40.NCEP vs VAWR net short-wave radiation comparison	151
Figure A41.NCEP vs VAWR net long-wave radiation comparison	152
Figure A42.NCEP vs VAWR net heat flux comparison	153
Figure A43.NCEP vs VAWR wind stress magnitude comparison	154

List of Tables

Table 1. Mooring deployment and recovery dates (UTC) and anchor positions	1
Table 2. Sensors heights (in meters) above the mean water line	4
Table 3. VAWR sensor specifications	5
Table 4. IMET sensor specifications	6
Table 5. Subsurface instrumentation	10
Table 6. WHOI subsurface instrumentation deployed on the UW moorings	13
Table 7. Data return of meteorological instruments	14
Table 8. Data return of temperature measurements	14
Table 9. Data return of temperature measurements on UW moorings	15
Table 10. Data return of salinity measurements	15
Table 11. Data return of currents	15
Table 12. Processing and edits of meteorological data	16
Table 13. Processing and edits of temperature data	17
Table 14. Processing and edits of salinity data	18
Table 15. Offsets applied to Arab 1 10 and 35 m MVMS salinity	18
Table 16. Constants for 10 m MVMS time dependent salinity drift correction	18
Table 17. Processing and edits of current data	19
Table 18. Parameters used in bulk flux algorithm	22
Table 19. Statistics of observables and fluxes for the entire deployment	24
Table 20. Statistics of observables and fluxes for October 1994	25
Table 21. Statistics of observables and fluxes for November 1994	26
Table 22. Statistics of observables and fluxes for December 1994	27
Table 23. Statistics of observables and fluxes for January 1995	28
Table 24. Statistics of observables and fluxes for February 1995	29
Table 25. Statistics of observables and fluxes for March 1995	30
Table 26. Statistics of observables and fluxes for April 1995	31
Table 27. Statistics of observables and fluxes for May 1995	32
Table 28. Statistics of observables and fluxes for June 1995	33
Table 29. Statistics of observables and fluxes for July 1995	34
Table 30. Statistics of observables and fluxes for August 1995	35
Table 31. Statistics of observables and fluxes for September 1995	36
Table 32. Statistics of observables and fluxes for October 1995	37

Table A1. Statistics of differences between ECMWF model and buoy observations 111

Table A2. Statistics of differences between NCEP model and buoy observations 111

Table B1. Serial numbers of meteorological instrumentation 155

Table B2. Serial numbers of WHOI instrumentation deployed on UW moorings 155

Table B3. Serial numbers of subsurface instrumentation 156

Section 1: Introduction

Meteorological forcing in the Arabian Sea is characterized by an intense atmospheric circulation during the summer or southwest monsoon known as the Findlater Jet and persistent, moderate winds during the winter or northeast monsoon. These conditions are rather unique when compared to other basins at similar latitudes since the wind forcing is much larger during the summer than in the winter. The annual cycle of sea surface temperatures (SST) in the Arabian Sea is also unique; the summer SST is nearly as low as the winter SST. Unfortunately, few in situ meteorological and oceanographic measurements have been collected in this region. To better understand the air-sea interactions in this region, a moored array was deployed for one year just south of the climatological axis of the Findlater Jet.

The array consisted of five moorings: a Woods Hole Oceanographic Institution (WHOI) surface mooring, two Scripps Institution of Oceanography (SIO) surface moorings and two University of Washington (UW) subsurface moorings (Figure 1). At all of the mooring sites except for the UW northeast site, the one year time series of meteorological and/or oceanographic measurements were recorded in two consecutive six month deployments. All mooring work was conducted from the R/V *Thomas Thompson*, beginning with the initial deployment in mid-October 1994 during cruise 40. The first set of moorings were recovered and the second set deployed in mid-April 1995 during cruise 46. The final recovery occurred in mid-October 1995 during cruise 52. Deployment and recovery times and mooring sites are presented in Table 1.

Table 1. Mooring deployment and recovery dates (UTC) and anchor positions.

Mooring	Deployment Date/Time	Recovery Date/Time	Anchor Position
<i>Arab 1</i>			
WHOI Central	15 Oct 1994 1048	20 Apr 1995 0105	15° 30.04'N, 61° 29.99'E
SIO Northwest	17 Oct 1994 0723	16 Apr 1995 1055	15° 43.53'N, 61° 15.94'E
SIO Southwest	18 Oct 1994 0649	23 Apr 1995 0652	15° 16.53'N, 61° 16.11'E
UW Northeast	23 Oct 1994 1000		15° 43.90'N, 61° 44.53'E
UW Southeast	19 Oct 1994 morning	18 Apr 1995 0150	15° 16.37'N, 61° 44.07'E
<i>Arab 2</i>			
WHOI Central	22 Apr 1995 0939	10 Oct 1995 1000	15° 30.07'N, 61° 30.05'E
SIO Northwest	17 Apr 1995 0715	19 Oct 1995 0601	15° 43.39'N, 61° 15.86'E
SIO Southwest	24 Apr 1995 0716	18 Oct 1995 0712	15° 16.52'N, 61° 16.12'E
UW Northeast		16 Oct 1995 0210	15° 43.90'N, 61° 44.53'E
UW Southeast	25 Apr 1995 0650	17 Oct 1995 1000	15° 16.11'N, 61° 43.82'E

The two SIO toroid buoys in the northwest and southwest corners of the array each supported redundant meteorological packages that measured wind speed and direction, air temperature, barometric pressure and incoming short-wave radiation, an acoustic doppler current profiler (ADCP) and ten subsurface temperature recorders. The UW subsurface moorings each carried a profiling current meter (PCM) and two temperature recorders. The southeastern UW mooring also carried five deep, vector measuring current meters (VMCM). The WHOI 3 m discus buoy supported two complete suites of meteorological instrumentation and a single stand-alone module capable of measuring all of the bulk parameters required for estimating heat, freshwater and momentum fluxes at the sea surface. The buoy and the mooring line also carried subsurface instrumentation to measure both physical and bio-optical properties.

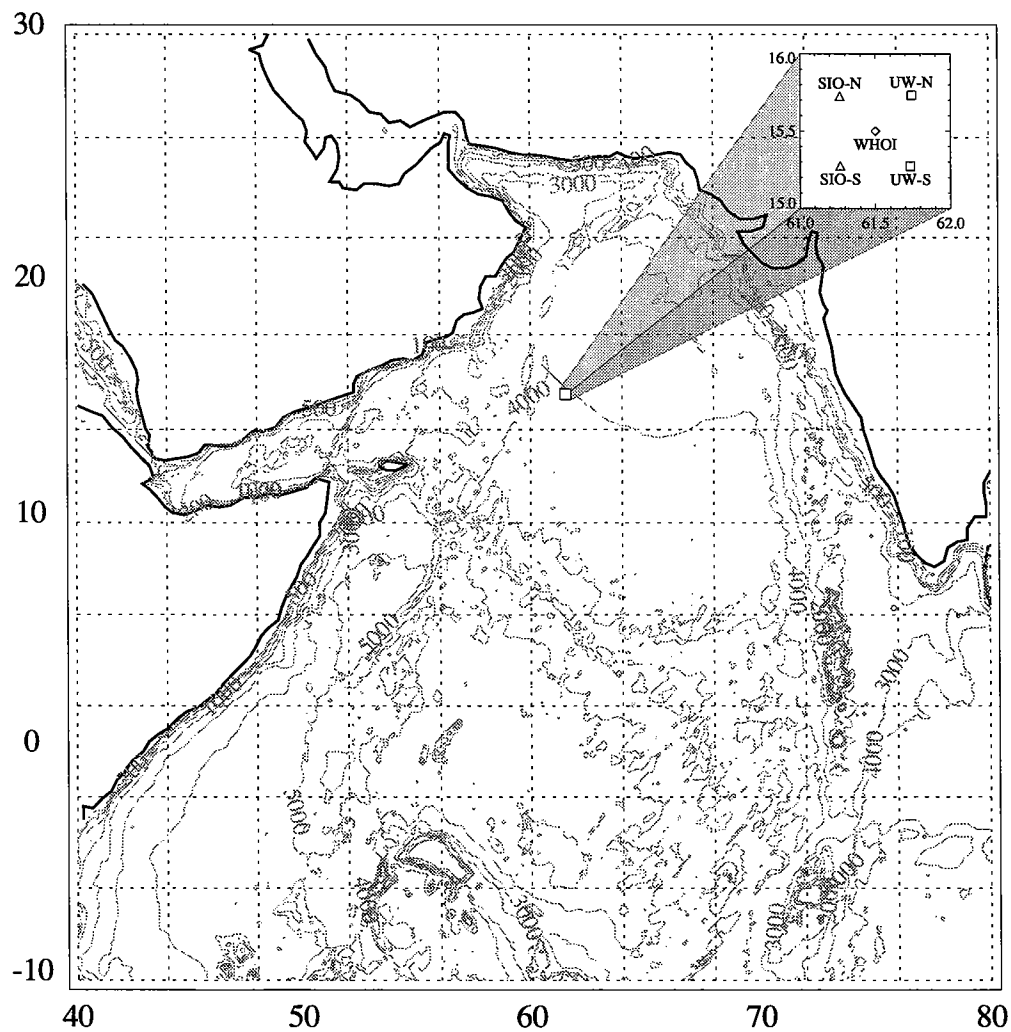


Figure 1. Arabian Sea moored array. Depth contours are in meters.

This report documents the meteorological and oceanographic data returned from the central WHOI mooring. Section 2 describes the instrumentation deployed at the central mooring site, Section 3 briefly describes the post-recovery data processing and Section 4 provides a tabular and graphical summary of the data.

Section 2: Instrumentation

Meteorological

Two meteorological packages, the Vector Averaging Wind Recorder (VAWR) and the Improved Meteorological (IMET) system, were deployed on the 3 m diameter discus buoy. Instrument heights above the mean water line for each meteorological system are provided in Table 2. The VAWR (Weller *et al.*, 1990) logged measurements of air temperature, relative humidity, barometric pressure, wind speed and direction, short-wave and long-wave radiation and sea temperature every 7.5 minutes (Table 3). The IMET system (Hosom *et al.*, 1995) logged the same parameters as the VAWR as well as precipitation and aspirated temperature every minute (Table 4). The IMET relative humidity module also contained a collocated air temperature sensor. In addition to the meteorological packages, a stand-alone, internally logging, humidity/temperature instrument was also deployed (Way, 1996). This module contained collocated relative humidity and temperature sensors which were sampled every 3.75 minutes. Further details about the meteorological instrumentation can be found in Trask *et al.* (1995a), Trask *et al.* (1995b) and Ostrom *et al.* (1996).

Table 2. Sensors heights (in meters) above the mean water line.

Parameter	VAWR		IMET		Stand-alone	
	Arab 1	Arab 2	Arab 1	Arab 2	Arab 1	Arab 2
Air temperature	2.68	2.70	2.74	2.76	2.98	2.98
Relative humidity	2.69	2.72	2.74	2.79	2.98	2.98
Barometric pressure	2.76	2.76	2.77	2.86		
Wind speed	3.36	3.34	3.16	3.25		
Wind direction	3.07	3.07	3.16	3.25		
Short-wave radiation	3.42	3.41	3.42	3.41		
Long-wave radiation	3.42	3.41	3.42	3.42		
Sea temperature	-0.92	-0.92	-0.89	-0.89		
Aspirated air temperature			2.20	2.19		
Precipitation			3.14	3.12		

The instrumented buoy is shown in Figure 2 and the tower top layout is provided in Figure 3. The tower was designed to eliminate shading for some instruments while maximizing air flow for others. The short- and long-wave sensors were placed above all other sensors so that they were afforded an unobstructed view of the sky.

Table 3. VAWR sensor specifications.

Parameter	Sensor Type	Nominal Accuracy	Sampling
Air temperature	Thermistor Yellow Springs #44034 5K @ 25°C	±0.2°C when wind > 5ms ⁻¹	1.875 min average ^a
Relative humidity	Variable Dielectric Conductor Vaisala Humicap 0062HM	±2% RH	3.515 sec burst sample ^b
Barometric pressure	Quartz crystal Digiquartz Paroscientific Model 215, 216	±0.2mbar when wind < 20ms ⁻¹	2.636 sec burst sample ^b
Wind speed	3 cup anemometer R.M. Young	±2% above 0.7ms ⁻¹	7.5 min vector averaged ^c
Wind direction	Integral vane w/ vane follower WHOI / EG&G	±5.6°	7.5 min vector averaged
Short-wave radiation	Pyranometer Eppley 8-48	±3% of value	7.5 min average
Long-wave radiation		±10%	
<i>Thermopile</i>	Pyrgeometer Eppley PIR		7.5 min average
<i>Body Temperature</i>	Thermistor 10K @ 25°C		1.875 min average ^d
<i>Dome Temperature</i>	Thermistor 10K @ 25°C		1.875 min average ^e
Sea temperature	Thermistor Thermometrics 4K @ 25°C	±0.005°C	1.875 min average ^f

^a Air temperature is measured during the second quarter of the sampling interval for one quarter of the record time.

^b Relative humidity and barometric pressure are burst samples taken in the middle of the sampling interval.

^c Overestimation of wind speed by about 5% is characteristic of cup anemometers.

^d Long-wave radiation body temperature is measured during the third quarter of the sampling interval for one quarter of the record time.

^e Long-wave radiation dome temperature is measured during the fourth quarter of the sampling interval for one quarter of the record time.

^f Sea temperature is measured during the first quarter of the sampling interval for one quarter of the record time.

Table 4. IMET sensor specifications.

Parameter	Sensor Type	Nominal Accuracy	Sampling
Air temperature	Platinum Resistance Thermometer	$\pm 0.25^{\circ}\text{C}$	Burst sample every 1 min
Relative humidity	Rotronic MP-100F	$\pm 3\%$ RH	Burst sample every 1 min
Barometric pressure	Quartz crystal AIR DB-1A	$\pm 0.5\text{mbar}$	Burst sample every 1 min
Wind speed	Wind monitor R.M. Young Model 5103	$\pm 2\%$	1 min average ^{ab}
Wind direction	Wind monitor R.M. Young Model 5103	$\pm 1.5^{\circ}$	1 min average ^a
Short-wave radiation	Temperature compensated Thermopile Eppley PSP	$\pm 3\%$ of value	1 min average ^c
Long-wave radiation	Pyrgometer Eppley PIR	$\pm 10\%$	Burst sample every 1 min
Sea temperature	Platinum Resistance Thermometer	$\pm 0.005^{\circ}\text{C}$	Burst sample every 1 min
Precipitation	Self-siphoning rain gauge R.M. Young Model 50201	$\pm 10\%$	Burst sample every 1 min
Aspirated air temperature	Platinum Resistance Thermometer with R. M. Young Aspirated Shield Model 43408	$\pm 0.2^{\circ}\text{C}$ when short-wave $< 1080 \text{ W m}^{-2}$	Burst sample every 1 min

^a The vane on the wind module is sampled at one second intervals and averaged over 15 seconds. The compass is sampled every 15 seconds and the wind speed is averaged every 15 seconds. East and north components are computed every 15 seconds. Once a minute the logger stores average east and north components computed from the most recent four 15 second averages.

^b Underestimation of wind speed by about 3% is characteristic of propeller anemometers.

^c Short-wave radiation is sampled every 10 seconds and the average of the six most recent samples is logged.

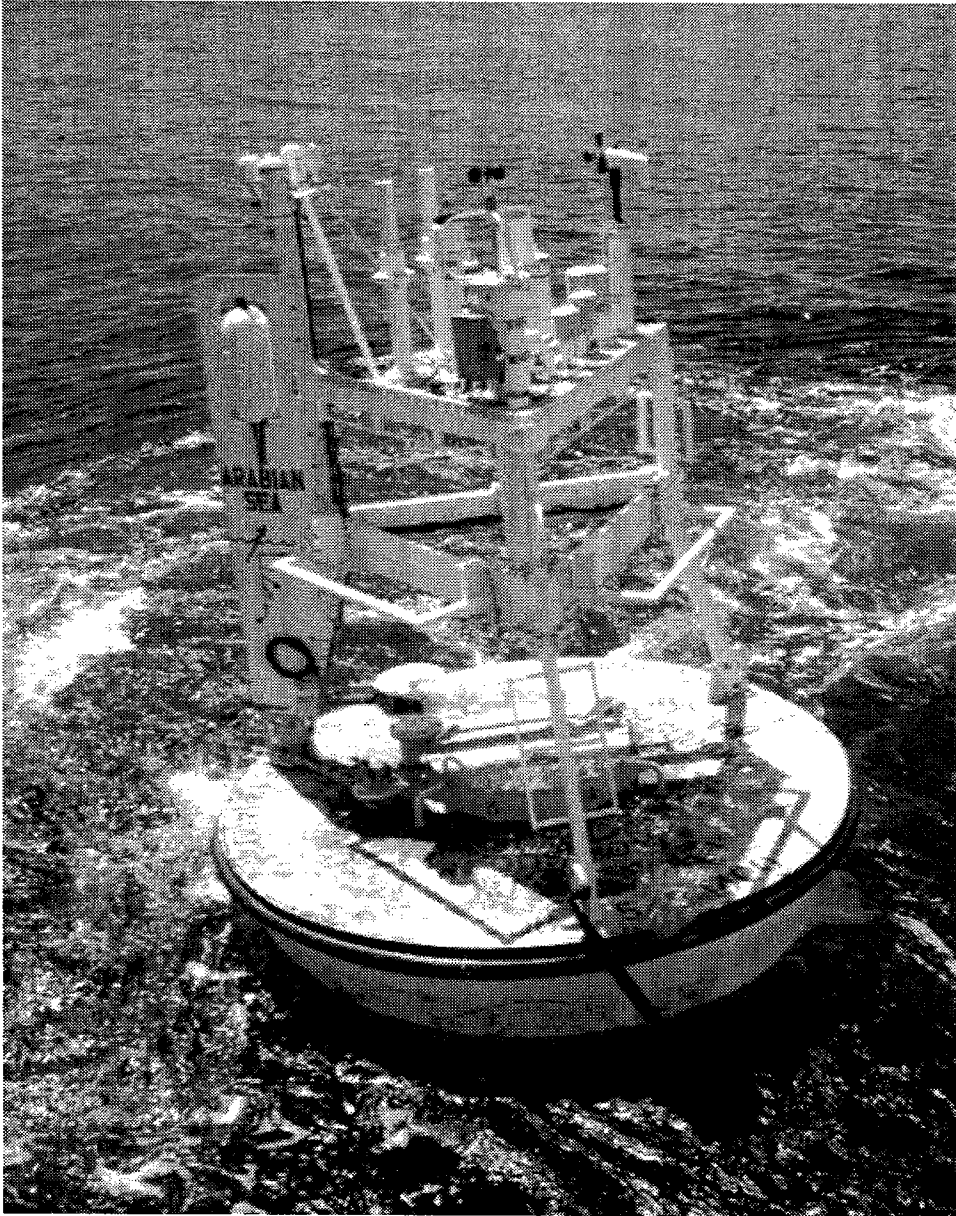


Figure 2. Arabian Sea 3m discus buoy.

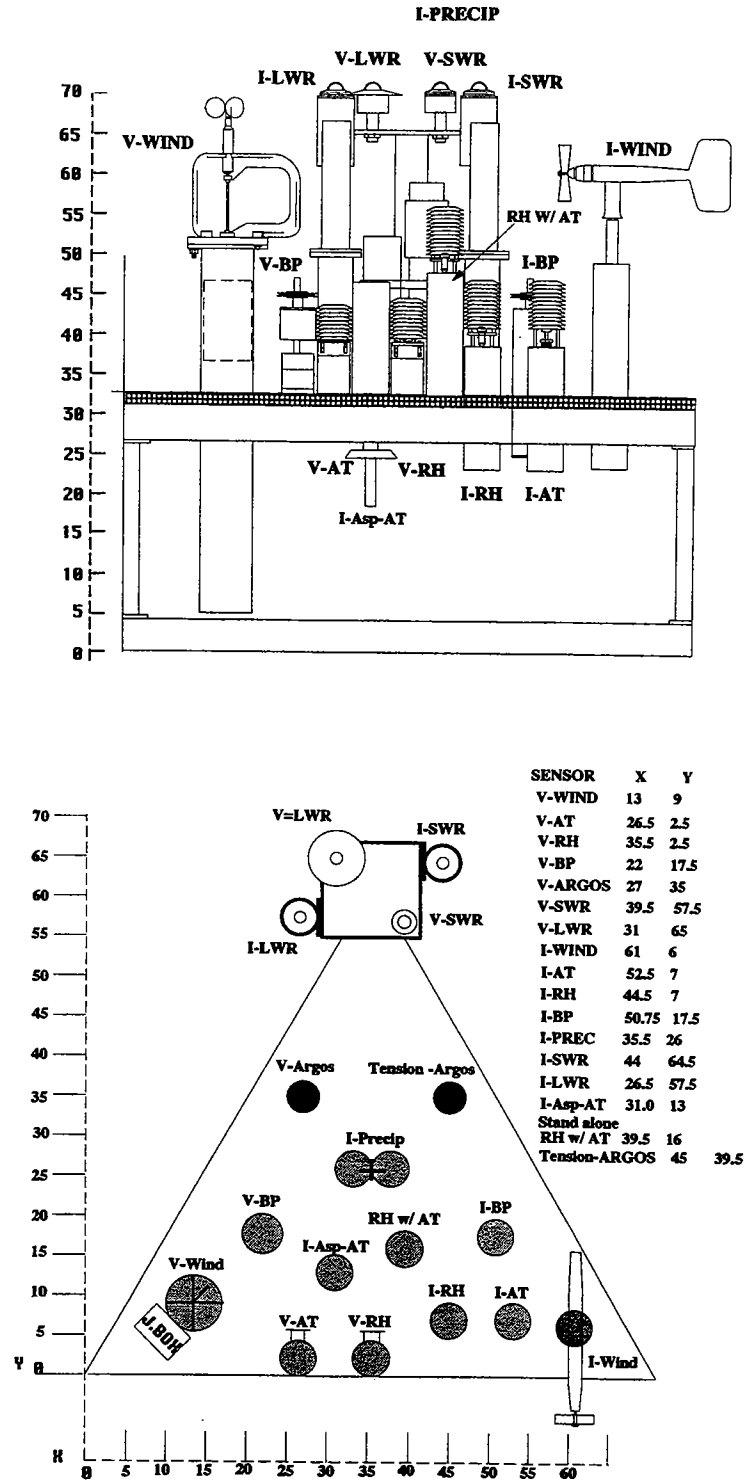


Figure 3. Buoy tower top configuration.

Oceanographic

Subsurface instrumentation measured water temperature, conductivity, currents, dissolved oxygen, photosynthetically available radiation (PAR), light transmission and natural and stimulated fluorescence (Table 5; Figures 4 and 5). Brancker temperature sensors (Richard Brancker Research, Ltd.) were deployed in a near-surface array at depths of 0.17, 0.43, 0.92, 1.37 (first deployment only), 1.41, 1.91 and 2.42 m. Each of these sensors was enclosed in a multi-plate radiation shield to reduce solar heating. Twelve more Brancker temperature sensors were deployed along the mooring line at depths of 4.5, 20, 30, 40, 50, 60, 72.5, 90, 125, 175, 225 and 300 m. All of the Branckers sampled a single point measurement every 15 minutes.

Both conductivity and temperature were measured using five Seacat instruments (SeaBird, Inc.). The shallowest was mounted on the buoy bridle at a depth of 1.42 m while the remaining instruments were deployed along the mooring line at depths of 100, 150, 200 and 250 m. The Seacats sampled a single point measurement every 7.5 minutes.

A total of five Vector Measuring Current Meters (VMCM) (Weller and Davis, 1980) were deployed to measure horizontal water velocity and temperature. The VMCMs were deployed in-line at 5, 15, 25, 45 and 55 m depth. Each VMCM recorded current and temperature measurements every 3.75 minutes. A description of the VMCM sampling scheme is provided in Appendix C. Five additional VMCMs were deployed on the University of Washington southeastern mooring at depths of 300, 500, 750, 1500 and 3025 m (Table 6). The sampling rate for these instruments was 7.5 minutes.

A Pacific Marine Environmental Lab (PMEL) miniature temperature recorder (MTR) was deployed in-line at 3.5 m depth. This instrument sampled a single point measurement every 7.5 minutes. A Lamont-Doherty Earth Observatory (LDEO) dissolved oxygen sensor provided by Dr. Chris Langdon was mounted to the buoy bridle at a depth of 1.42 m.

Four Multi-Variable Moored Systems (MVMS) were deployed to measure a suite of bio-optical and physical parameters. Two University of California at Santa Barbara Ocean Physics Laboratory MVMS instruments were deployed at 35 and 80 m (Sigurdson *et al.*, 1995, 1996). These systems measured temperature, conductivity, dissolved oxygen, current, PAR, light transmission (660 nm), natural fluorescence (683 nm) and stimulated chlorophyll fluorescence. Two LDEO MVMS instruments were deployed at 10 and 65 m (Ho *et al.*, 1996, 1997). These systems measured temperature, conductivity, dissolved oxygen, current, PAR, light transmission, stimulated fluorescence and upward vertical radiance (683 nm).

Table 5. Subsurface instrumentation.

Depth (m)	Sensor	Sample Interval (minutes)	Parameters Measured
0.17	Brancker	15	Temperature
0.43	Brancker	15	Temperature
0.92	Brancker	15	Temperature
1.37	Brancker	15	Temperature
1.41	Brancker	15	Temperature
1.42	LDEO DO		Dissolved oxygen
1.42	Seacat	7.5	Temperature, Salinity
1.91	Brancker	15	Temperature
2.42	Brancker	15	Temperature
3.5	PMEL MTR	7.5	Temperature
4.5	Brancker	15	Temperature
5	VMCM	3.75	Velocity, Temperature
10	LDEO MVMS	4 (7.5 for velocity)	Temperature, Salinity, Velocity, PAR, Dissolved Oxygen, Light Transmission, Natural (683nm) and Stimulated Fluorescence
15	VMCM	3.75	Velocity, Temperature
20	Brancker	15	Temperature
25	VMCM	3.75	Velocity, Temperature
30	Brancker	15	Temperature
35	UCSB MVMS	3.75	Temperature, Salinity, Velocity, PAR, Dissolved Oxygen and DO temperature, Light Transmission, Natural (683nm) and Stimulated Fluorescence
40	Bio-Acoustic	60	Acoustic backscattering
40	Brancker	15	Temperature
45	VMCM	3.75	Velocity, Temperature
50	Brancker	15	Temperature
55	VMCM	3.75	Velocity, Temperature
60	Brancker	15	Temperature
65	LDEO MVMS	4 (7.5 for velocity)	Temperature, Salinity, Velocity, PAR, Dissolved Oxygen, Light Transmission, Natural (683nm) and Stimulated Fluorescence
72.5	Brancker	15	Temperature
80	UCSB MVMS	3.75	Temperature, Salinity, Velocity, PAR, Dissolved Oxygen and DO temperature, Light Transmission, Natural (683nm) and Stimulated Fluorescence
90	Brancker	15	Temperature
100	Seacat	7.5	Temperature, Salinity
125	Brancker	15	Temperature
150	Seacat	7.5	Temperature, Salinity
175	Brancker	15	Temperature
200	Seacat	7.5	Temperature, Salinity
225	Brancker	15	Temperature
250	Seacat	7.5	Temperature, Salinity
300	Brancker	15	Temperature

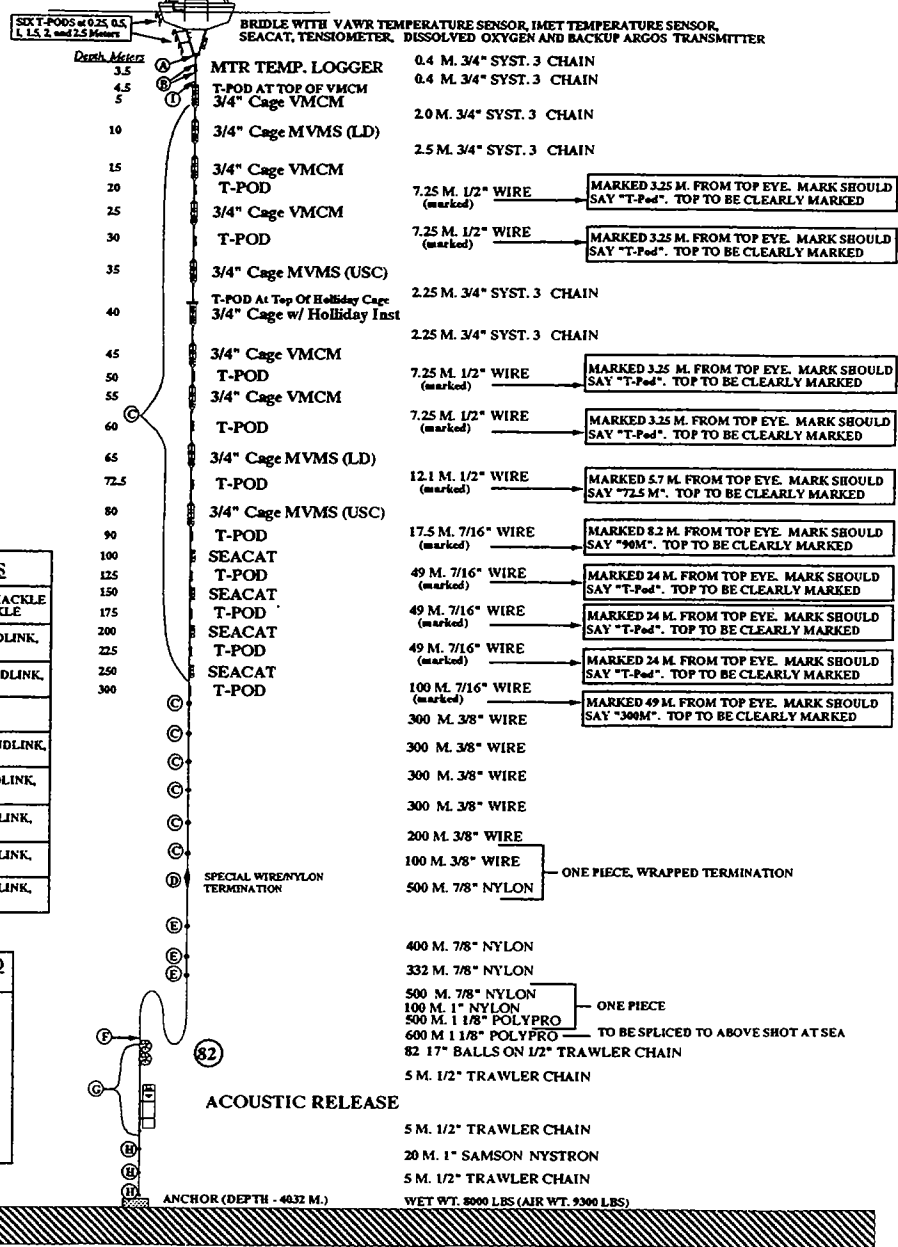
MAXIMUM DIAMETER OF BUOY
WATCH CIRCLE = 3.5 N. MILES

3 meter Discus Buoy with VAWR (With Argos Telemetry), IMET, and Tension Argos Transmitter

TEMPERATURE PODS	
NO.	DEPTH (M)
1	0.25M Buoy Pipe
2	0.5M Buoy Pipe
3	1 M-Bridle Pipe
4	1.5 M-Bridle Pipe
5	2 M-Bridle Pipe
6	2.5 M-Bridle Pipe
7	3.5 M (MTR)
8	4.5 M-VMCM Cage
9	20
10	30
11	40 M Cage
12	50
13	60
14	72.5
15	90
16	125
17	175
18	225
19	300

TERMINATION CODES	
(A)	BRIDLE: U-JOINT, 1" CHAIN SHACKLE, 1" ENDLINK, 7/8" CHAIN SHACKLE
(B)	7/8" CHAIN SHACKLE, 7/8" ENDLINK, 7/8" CHAIN SHACKLE
(C)	3/4" CHAIN SHACKLE, 7/8" ENDLINK, 3/4" CHAIN SHACKLE
(D)	7/8" ANCHOR SHACKLE
(E)	3/4" ANCHOR SHACKLE, 7/8" ENDLINK, 3/4" ANCHOR SHACKLE
(F)	1" ANCHOR SHACKLE, 7/8" ENDLINK, 5/8" CHAIN SHACKLE
(G)	5/8" CHAIN SHACKLE, 7/8" ENDLINK, 5/8" CHAIN SHACKLE
(H)	5/8" CHAIN SHACKLE, 7/8" ENDLINK, 7/8" ANCHOR SHACKLE
(I)	7/8" CHAIN SHACKLE, 7/8" ENDLINK, 3/4" CHAIN SHACKLE

HARDWARE REQUIRED (INCLUDES APPROX. 20% SPARES)	
1" CHAIN SHACKLES	5
1" ANCHOR SHACKLES	5
1" WELDLESS ENDLINKS	5
7/8" ANCHOR SHACKLES	5
7/8" CHAIN SHACKLES	10
7/8" WELDLESS ENDLINKS	85
3/4" CHAIN SHACKLES	85
3/4" ANCHOR SHACKLES	10
5/8" CHAIN SHACKLES	65



ARABIAN SEA MOORING
NOMINAL POSITION - 15.5° N 61.5° E

C. TUPPER /R. TRASK
APRIL 4, 1994
REV 18 MAY 94
REV 15 JUN 94
REV 20 OCT 94

Figure 4. Mooring schematic showing subsurface instrumentation.

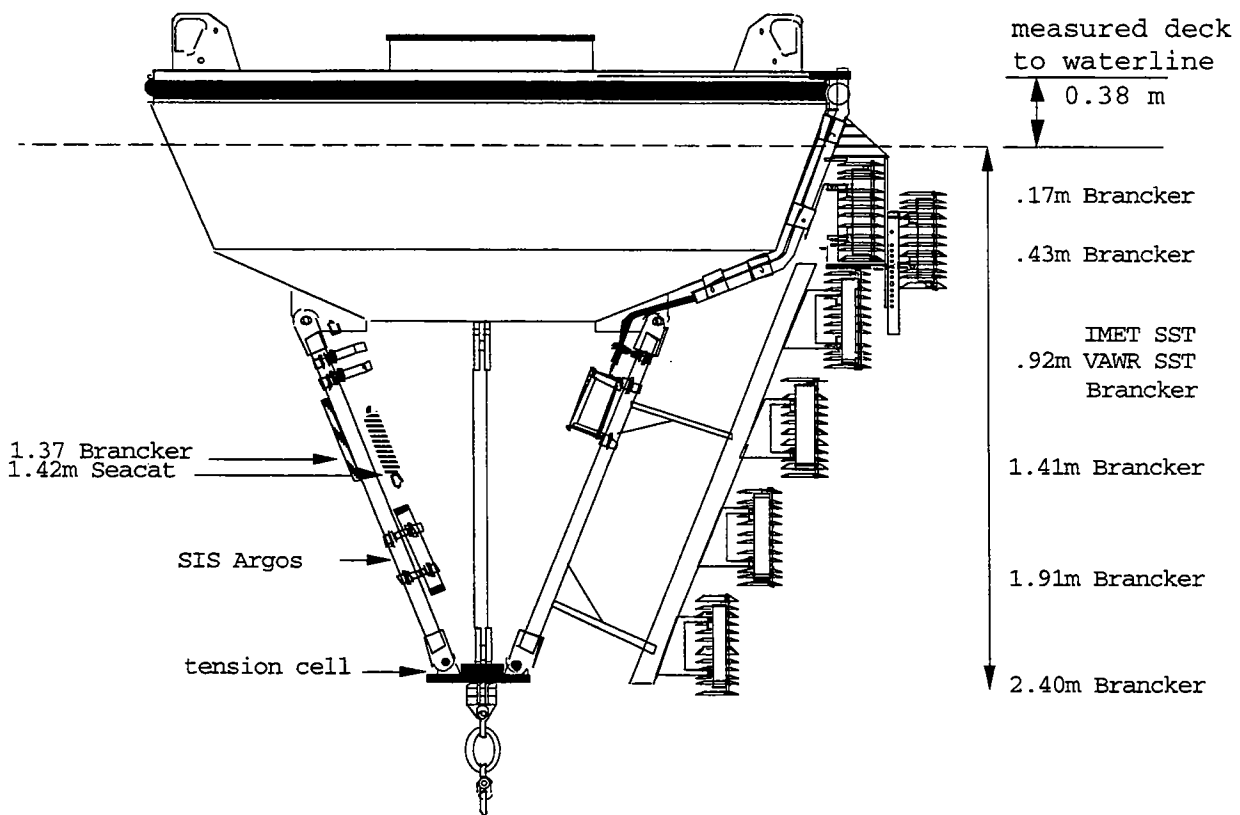


Figure 5. Disc buoy bridle instrumentation.

Table 6. WHOI subsurface instrumentation deployed on the UW moorings.

Depth	Sensor	Sample Interval (minute)	Parameters Measured
<i>UW North</i>			
20.0	Brancker	15.0	Temperature
250.0	Brancker	15.0	Temperature
<i>UW South</i>			
20.0	Brancker	15.0	Temperature
250.0	Brancker	15.0	Temperature
300.0	VMCM	7.5	Velocity, Temperature
500.0	VMCM	7.5	Velocity, Temperature
750.0	VMCM	7.5	Velocity, Temperature
1500.0	VMCM	7.5	Velocity, Temperature
3025.0	VMCM	7.5	Velocity, Temperature

Section 3: Data Processing

Data Return

The following tables show the percentage of time that a particular instrument was returning good data for both deployments. Data return for the meteorological instruments is provided in Table 7 while data return for the oceanographic instrumentation is provided in tables 8 through 11.

Table 7. Data return (percent) of meteorological instruments.

	Arab 1	Arab 2
<u>V A W R</u>		
Wind speed/direction	100	100
Sea surface temperature	100	100
Air temperature	100	100
Barometric pressure	100	0
Relative humidity	100	100
Incoming short-wave radiation	100	100
Incoming long-wave radiation	100	100
<u>I M E T</u>		
Wind speed/direction	100	100
Sea surface temperature	100	100
Air temperature	100	100
Barometric pressure	100	100
Relative humidity	100	100
Incoming short-wave radiation	100	100
Incoming long-wave radiation	100	100
Precipitation	100	100
<u>Stand-alone</u>		
Air temperature	100	100
Relative humidity	100	100

Table 8. Data return (percent) of temperature measurements.

Depth (m)	Instrument	Arab 1	Arab 2	Total
0.17	Brancker	100	100	100
0.43	Brancker	100	100	100
0.92	Brancker	69	100	84
1.37	Brancker	100	-	100
1.41	Brancker	100	100	100
1.42	Seacat	100	100	100
1.91	Brancker	100	100	100
2.42	Brancker	100	100	100
3.5	MTR	100	100	100
4.5	Brancker	100	100	100
5	VMCM	100	100	100
10	MVMS	99	100	99
15	VMCM	100	100	100
20	Brancker	100	100	100
25	VMCM	100	100	100
30	Brancker	100	100	100
35	MVMS	100	100	100
40	Brancker	100	100	100
45	VMCM	100	96	98
50	Brancker	100	100	100
55	VMCM	100	100	100
60	Brancker	100	100	100
65	MVMS	99	100	99
72.5	Brancker	23	0	12
80	MVMS	100	100	100
90	Brancker	100	100	100
100	Seacat	100	100	100
125	Brancker	100	100	100
150	Seacat	78	100	89
175	Brancker	100	100	100
200	Seacat	100	100	100
225	Brancker	100	100	100
250	Seacat	100	100	100
300	Brancker	100	0	51

Note: No temperature sensor was deployed at 1.37 m during Arab 2.

Table 9. Data return (percent) of temperature measurements on UW moorings.

Depth (m)	Instrument	Arab 1	Arab 2	Total
<i>UW North</i>				
20	Brancker	72	-	36
250	Brancker	72	-	36
<i>UW South</i>				
20	Brancker	52	100	75
250	Brancker	100	100	100
300	VMCM	0	100	48
500	VMCM	0	100	48
750	VMCM	100	100	100
1500	VMCM	100	100	100
3000	VMCM	100	100	100

Note: The UW Northeast mooring broke free on 15 July 1995.

Table 10. Data return (percent) of salinity (conductivity) measurements.

Depth (m)	Instrument	Arab 1	Arab 2	Total
1.8	Seacat	100	100	100
10	MVMS	69	78	74
35	MVMS	98	53	76
65	MVMS	99	47	73
80	MVMS	0	100	49
100	Seacat	100	100	100
150	Seacat	73	100	86
200	Seacat	100	100	100
250	Seacat	100	100	100

Processing

The raw VAWR and subsurface data were processed using the WHOI UOP software package (Prada, 1992). Pre-deployment calibrations were applied to each instrument initially and post-deployment calibrations were only used when the post-deployment calibrations yielded better agreement during intercomparisons with other sensors. All calibrated data were converted to EPIC-compliant NetCDF files (Denbo and Zhu, 1993; Rew *et al.*, 1993).

After initial processing, qualitative checks were performed on the data to identify sensor problems such as spikes, drop-outs or gross errors. Subsequent intercomparisons with other buoy and shipboard instruments revealed time dependent problems, linear biases and offsets in some

Table 11. Data return (percent) of currents.

Depth (m)	Instrument	Arab 1	Arab 2	Total
5	VMCM	100	100	100
10	MVMS	82	100	91
15	VMCM	100	100	100
25	VMCM	100	100	100
35	MVMS	100	100	100
45	VMCM	100	100	100
55	VMCM	100	100	100
65	MVMS	95	100	97
80	MVMS	100	100	100
300	VMCM	98	98	98
500	VMCM	0	98	48
750	VMCM	86	98	92
1500	VMCM	5	0	2
3000	VMCM	0	0	0

Note: VMCMs at and below 300 m are from the UW southeast mooring.

sensors. Empirical adjustments were applied to the data to improve agreement among these collocated sensors. These adjustments are summarized in Tables 12–17.

Solar radiative heating errors occur in air temperature measurements when the sensor itself or its housing is heated by the sun. All of the temperature sensors deployed in the Arabian Sea except the IMET aspirated module were housed in Gill multi-plate radiation shields (Gill, 1983) which reduce radiative heating errors, but do not eliminate them. The aspirated air temperature was fan-aspirated at 3 m s^{-1} and was specified to have an error of no more than $\pm 0.2^\circ\text{C}$ under 1080 W m^{-2} heating. Differences between the shielded and aspirated daytime air temperatures were attributed to solar radiative heating and these errors were detected in all of the shielded air temperature measurements. A detailed analysis of radiative heating was possible (Anderson and

Table 12. Processing and edits of meteorological data.

	Arab 1	Arab 2
<u>VAWR</u>		
Air temperature		
Relative humidity		
Barometric pressure		Failed ^a
Wind speed		
Wind direction		
Short-wave radiation		
Long-wave radiation	Removed booby signal ^b and daytime values	Removed booby signal ^b
Sea temperature		
<u>IMET</u>		
Air temperature	Adjusted for radiative heating	Adjusted for radiative heating
Relative humidity	Applied linear correction ^c , $c_1 = 0.952794$, $c_0 = 5.7102\%$	Applied linear correction ^c , $c_1 = 0.775654$, $c_0 = 24.2117\%$
RH air temperature	Add 0.2160°C offset	Add -0.0831°C offset
Barometric pressure		
Wind speed		
Wind direction		
Short-wave radiation		
Long-wave radiation	Removed booby signal ^b , daytime values and spikes in thermopile	Removed booby signal ^b , daytime values and spikes in thermopile
Sea temperature		
Aspirated air temperature		
Precipitation		
<u>Stand-alone</u>		
Air temperature	Add -0.0626°C offset	Add -0.0661°C offset
Relative humidity	5 – 7%RH too high (moist)	

^a Filled with IMET barometric pressure.

^b See text.

^c Corrected RH = $(\text{RH} - c_0) / c_1$

Table 13. Processing and edits of temperature data.

Depth (m)	Sensor	Arab 1	Arab 2
0.17	Brancker		Add 0.0314°C offset
0.43	Brancker		
0.92	Brancker	Failed on 22 Feb 95	
1.37	Brancker		No sensor deployed at this depth
1.41	Brancker		
1.42	Seacat		
1.91	Brancker		
2.42	Brancker		
3.5	PMEL MTR		
4.5	Brancker		
5	VMCM		
10	LDEO MVMS		
15	VMCM		
20	Brancker		
25	VMCM		
30	Brancker		
35	UCSB MVMS	Add 0.049°C offset	Add 0.193°C offset
40	Brancker		
45	VMCM		Several hot spikes edited
50	Brancker		Several cold spikes edited
55	VMCM		
60	Brancker		
65	LDEO MVMS		
72.5	Brancker	Failed 28 Nov 94	Failed
80	UCSB MVMS	Add 0.055°C offset	
90	Brancker		
100	Seacat		
125	Brancker		
150	Seacat	Failed on 10 Mar 1995	
175	Brancker		
200	Seacat		
225	Brancker		
250	Seacat		
300	Brancker		Failed ^b
300 ^a	VMCM	Failed	
500 ^a	VMCM	Failed	
750 ^a	VMCM		
1500 ^a	VMCM		
3025 ^a	VMCM		

^a From the UW southeast mooring.

^b Filled with UW southeast 300 m VMCM temperature data

Table 14. Processing and edits of salinity data.

Depth (m)	Sensor	Arab 1	Arab 2
1.42	Seacat		
10	MVMS	16 Jan 95 1340 – 12 Mar 95 0340 discarded	Failed on 10 Sep 95 0945
35	MVMS	17 Jan 95 0430 – 20 Jan 95 1300 discarded	Failed on 28 Jul 95 0000
65	MVMS		23 Apr 95 2007 – 28 Jul 95 0100 discarded
80	MVMS		
100	Seacat		
150	Seacat	Failed on 28 Feb 95	
200	Seacat		
250	Seacat		

Table 15. Offsets applied to Arab 1 LDEO 10 m MVMS and UCSB 35 m MVMS salinity during various periods*.

Depth (m)	Start of Period	End of Period	Offset (PSU)
10	14 Dec 94 0223	17 Jan 95 0416	0.1165
10	11 Mar 95 1609	17 Apr 95 2207	0.4500
35	12 Dec 94 2151	17 Jan 95 0416	0.1893
35	20 Jan 95 1306	20 Apr 95 1642	0.4141

* Corrected salinity = salinity + offset

Table 16. Constants for 10m LDEO MVMS time dependent salinity drift correction*.

Deployment	Start of Period	End of Period	c_1 (PSU day ⁻¹)	c_0 (PSU)
Arab 1	16 Nov 94 0845	14 Dec 94 0215	0.0090456	0.0153
Arab 2	5 Jul 95 0500	11 Sep 95 1900	0.0067624	0.0380

* Corrected salinity = salinity + [c_1 (number of days since start of period) + c_0]

Table 17. Processing and edits of current data.

Depth (m)	Sensor	Arab 1	Arab 2
5	VMCM		
10	LDEO MVMS	Rotated 18.71° east of north	Rotated 18.71° east of north
15	VMCM		
25	VMCM		
35	UCSB MVMS		
45	VMCM		
55	VMCM		
65	LDEO MVMS	Rotated 18.71° east of north	Rotated 18.71° east of north
80	UCSB MVMS		
300	VMCM		
500	VMCM	Failed	
750	VMCM	Compass failed on 25 Mar 95 2307	
1500	VMCM	Failed	Failed
3025	VMCM	Failed	Failed

Baumgartner, 1997) due to the availability of so many collocated air temperature measurements (i.e., VAWR, IMET, IMET aspirated, IMET relative humidity/air temperature module and the stand-alone relative humidity/air temperature module). This analysis yielded a model of heat exchange that could be used with empirically derived constants to adjust air temperatures for radiative heating errors. Since the IMET aspirated air temperature module was designed to operate for only the first two months of each six month deployment due to power constraints, the IMET air temperature measurements were adjusted for radiative heating errors to provide a complete time series of air temperature for the buoy. This time series of adjusted air temperature was used in the bulk aerodynamic formulae to derive heat fluxes (described below).

The IMET incoming long-wave radiation was contaminated by daytime errors roughly proportional to incoming short-wave during both deployments. The VAWR pyrgeometer showed similar errors during the first deployment. These errors are, as yet, unexplained and no simple empirical correction was determined. All of the deployed pyrgeometers were designed to account for daytime heating by measuring both body and dome temperatures, so these errors are unrelated to daytime heating of the sensor. An anomalous diurnal signal in the thermopile output voltage seems to be responsible for the daytime errors. The Arab 1 VAWR daytime long-wave measurements were replaced by values linearly interpolated in time between the median long-wave radiation one hour before sunrise and one hour after sunset. The adjusted Arab 1 VAWR and the uncontaminated Arab 2 VAWR long-wave measurements were used in the bulk aerodynamic formulae.

Based on observations during recovery and a qualitative analysis of both long-wave time series, it was determined that a bird (tentatively identified as a booby during recovery) alternately sat on the VAWR and IMET pyrgeometers during the inter-monsoon periods (Figure 6). Apparently the IMET pyrgeometer provides a more comfortable seat for a booby, since the bird spent almost three times more time on the IMET sensor (93 hours) than on the VAWR (33 hours). This signal was replaced by values linearly interpolated in time between the average long-wave radiation one-half hour before the booby sat down and one-half hour after it got up.

The 10 and 35 m MVMS salinity (conductivity) measurements were suspect at many times during the one year experiment. A significant effort was invested in recovering these salinity measurements, since the shallowest salinity observations after the 1.42 m Seacat were from the 65 m LDEO MVMS. The variability in the salinity measurements at 10 and 35 m often matched that of the 1.42 or 65 m, but offsets were detected. The 10 m MVMS seemed to have time dependent drifts in some instances. To determine offsets and drifts, the 10 and 35 m MVMS salinity measurements were compared to an 'expected' salinity that was interpolated in temperature/salinity space from the 1.42 m Seacat and the 65 m MVMS. This approach assumed that the 1.42 and 65 m temperature and salinity observations are from the same water mass and are conservative. The latter assumption is not a very good one for the surface Seacat, so this analysis is quite crude. However, the aim of the adjustment was to preserve the observed variability in the 10 and 35 m measurements and to shift the mean values so that they agree with surrounding sensors and make sense in context with their corresponding temperature measurements. The resulting time series of vertical density distribution yields few inversions over the entire year which suggests that the adjustments were reasonable.

All current meters had a magnetic variation correction of -0.79° (west of north) applied. A magnetic variation of -19.5° had been applied to the LDEO MVMS current measurements during calibration on the advice of the University of Washington, however this was incorrect. A rotation of 18.71° (east of north) was applied to the 10 and 65 m MVMS currents to account for the incorrect magnetic variation and to apply the true -0.79° value.

Freshwater, Heat and Momentum Fluxes

Air-sea fluxes were estimated from the meteorological and near-surface oceanographic measurements using a bulk flux algorithm developed for TOGA COARE (Fairall *et al.*, 1996a). This algorithm is based on methods developed by Liu *et al.* (1979) with modifications for, but not limited to, low wind regimes. Consequently, these bulk formulae are appropriate for the low wind

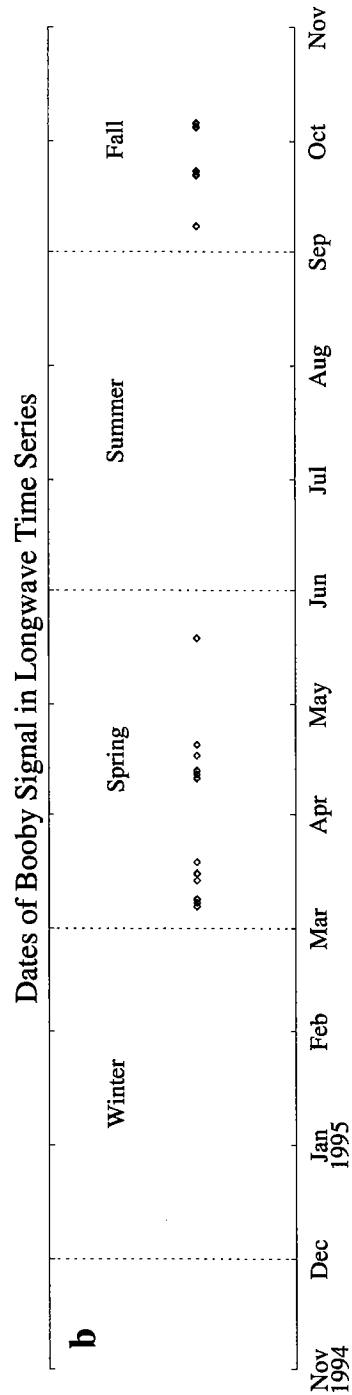
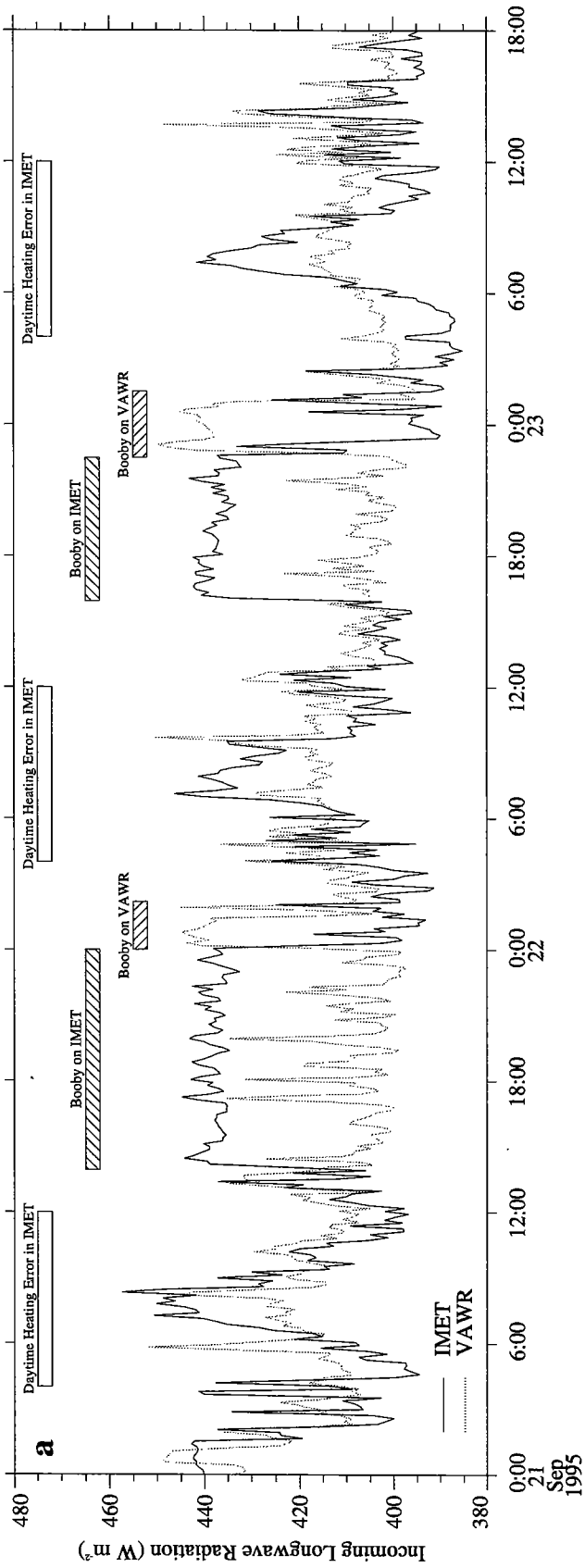


Figure 6. (a) Booby signal in IMET and VAWR incoming long-wave radiation time series. (b) Dates of booby signal.

inter-monsoonal period observed during the one year deployment. The algorithm also includes cool skin and warm layer adjustments based on Fairall *et al.* (1996b) to account for the cooling of the upper few millimeters of the ocean due to sensible, latent and outgoing long-wave radiation heat loss and warming of the upper few meters of the ocean due to absorption of short-wave radiation. The parameters used in the bulk algorithm (version 2.5) were derived from both the VAWR and IMET meteorological packages, the 0.17 m Brancker temperature sensor and the 5 m VMCM (Table 18).

Table 18. Parameters used in bulk flux algorithm.

Parameter	Arab 1	Arab 2
Air temperature	IMET adjusted for radiative heating	IMET adjusted for radiative heating
Specific humidity	Computed from IMET RH	Computed from IMET RH
Barometric pressure	VAWR	IMET
Incoming short-wave radiation	VAWR	VAWR
Incoming long-wave radiation	VAWR	VAWR
Sea surface temperature	0.17 m Brancker	0.17 m Brancker
Wind speed/direction relative to surface current	VAWR wind speed relative to 5 m VMCM current	VAWR wind speed relative to 5 m VMCM current

Since only incoming short- and long-wave radiation were measured, the outgoing components of radiation were estimated. Surface albedo was derived from the atmospheric transmittance and solar elevation angle using Payne's algorithm (1972). The atmospheric transmittance was estimated from the difference between the theoretical clear sky radiation (List, 1984) and the observed incoming short-wave radiation on a cloud-free day. The atmospheric transmittance determined from the VAWR pyranometer was 0.72. Outgoing long-wave radiation was estimated as $\epsilon\sigma T^4$ where ϵ is the emissivity of the sea surface ($\epsilon = 0.97$), σ is the Stefan-Boltzmann constant and T is the sea surface temperature in °K. The skin temperature from the cool skin adjustment was used as the sea surface temperature, since the outgoing long-wave radiation is dependent on the interfacial temperature which may be quite different from the shallowest temperature measurement at 0.17 m.

Section 4: Data Summary

Yearly statistics of the meteorological measurements and estimated heat, momentum and freshwater fluxes are presented in Table 19 and monthly statistics are provided in Tables 20–32. Each table contains the mean, standard deviation, minimum and maximum of the meteorological measurements and fluxes. Yearly time series of the meteorological observations are presented in Figure 7 and monthly time series are provided in Figures 8–20. A yearly time series of precipitation and evaporation are shown in Figure 21. Yearly time series of the heat and momentum fluxes are presented in Figure 22 and monthly time series are provided in Figures 23–35.

Yearly and monthly contour plots of subsurface temperature are presented in Figure 36 and Figures 37–49, respectively. The mixed layer depth in these plots was computed as the depth at which the temperature differs from the sea surface temperature (measured at 0.17 m) by 0.1°C . Stick plots depicting the VMCM and MVMS currents are presented in Figures 50 and 51. Monthly stick plots of velocity with current speed overlaid are presented in Figures 52–64. Integrated velocity for the current meters between 5 and 80 m are presented as progressive vector diagrams in Figure 65 (integrated over the entire year) and Figure 66 (integrated over each month).

Autospectra of the meteorological measurements and heat and momentum fluxes are presented in Figures 67 and 68, respectively. Rotary autospectra are presented for vector quantities (i.e., wind and wind stress). Autospectra of temperature and rotary autospectra of velocity at various depths are presented in Figures 69 and 70, respectively. Band averaging was used in each of the autospectra plots and the 95% confidence limits are shown. The first 5 frequencies were averaged over 3 bands and the number of bands averaged was doubled every 10 frequencies thereafter (i.e., frequencies 6-15 were averaged over 6 bands, frequencies 16-25 were averaged over 12 bands, frequencies 26-35 were averaged over 24 bands, etc.).

Table 19. Statistics of observables and fluxes for the entire deployment.

Variable	Unit	Mean	Std. Dev.	Minimum	Maximum
Air temperature	°C	26.65	1.63	22.60	31.47
Relative humidity	%	77.4	9.2	47.3	97.7
Barometric pressure	mbar	1010.4	4.5	997.0	1020.3
East wind	m s ⁻¹	1.35	5.73	-14.78	14.82
North wind	m s ⁻¹	0.13	4.27	-10.66	16.32
Wind speed ^a	m s ⁻¹	6.50	3.27	0.04	18.34
Wind direction ^b	°	157	0	0	0
Wind speed ^c	m s ⁻¹	1.35	0.00	0.00	0.00
Wind direction ^d	°	84	0	0	0
Incoming short-wave radiation	W m ⁻²	258.0	341.4	-0.7	1214.7
Incoming long-wave radiation	W m ⁻²	400.0	29.7	335.2	506.5
Sea surface temperature ^e	°C	27.24	1.57	24.58	32.23
Specific humidity	g kg ⁻¹	16.83	2.94	8.59	22.64
Precipitation rate	mm hr ⁻¹	0.0053	0.2690	0.0000	38.5243
Evaporation rate	mm hr ⁻¹	0.1800	0.0831	0.0117	0.5516
Evaporation rate - precipitation rate	mm hr ⁻¹	0.1747	0.2817	-38.4665	0.5516
Wind stress	N m ⁻²	0.1007	0.1085	0.0001	0.8772
Sensible heat flux	W m ⁻²	-1.7	6.6	-55.4	25.9
Latent heat flux	W m ⁻²	-122.6	56.6	-375.8	-7.9
Net short-wave radiation	W m ⁻²	243.3	328.6	-0.2	1170.0
Net long-wave radiation	W m ⁻²	-58.7	26.2	-109.6	26.8
Net heat flux	W m ⁻²	60.3	335.7	-498.0	1011.4
Skin temperature ^f	°C	27.03	1.58	24.52	32.17
10m wind speed ^g	m s ⁻¹	7.12	3.64	0.09	20.30
2m air temperature ^g	°C	26.67	1.63	22.65	31.47
2m relative humidity ^g	%	78.0	8.7	48.1	99.2
2m specific humidity ^g	g kg ⁻¹	16.95	2.91	8.78	22.74

^a Scalar averaged

^b Vector averaged from components of a unit vector oriented in the direction of the wind

^c Vector averaged

^d Computed as the arctangent of the average east and north components

^e Measured at 0.17 m depth

^f The temperature of the upper few millimeters of the ocean. Computed from Fairall *et al.* (1996b)

^g Estimated from boundary layer profiles in flux algorithm

Table 20. Statistics of observables and fluxes for October 1994.

Variable	Unit	Mean	Std. Dev.	Minimum	Maximum
Air temperature	°C	27.24	0.43	24.88	28.53
Relative humidity	%	77.0	7.9	49.9	97.7
Barometric pressure	mbar	1011.6	1.5	1004.9	1015.1
East wind	m s ⁻¹	-3.49	1.98	-14.78	4.56
North wind	m s ⁻¹	-2.54	2.86	-10.66	16.32
Wind speed ^a	m s ⁻¹	5.29	1.67	1.63	17.39
Wind direction ^b	°	234			
Wind speed ^c	m s ⁻¹	4.32			
Wind direction ^d	°	234			
Incoming short-wave radiation	W m ⁻²	250.5	344.7	-0.2	1078.1
Incoming long-wave radiation	W m ⁻²	393.9	15.2	356.3	444.7
Sea surface temperature ^e	°C	27.91	0.21	27.31	28.41
Specific humidity	g kg ⁻¹	17.55	1.87	11.19	20.58
Precipitation rate	mm hr ⁻¹	0.0557	0.7195	0.0000	13.4636
Evaporation rate	mm hr ⁻¹	0.1769	0.0555	0.0625	0.3697
Evaporation rate - precipitation rate	mm hr ⁻¹	0.1212	0.7182	-13.1743	0.3697
Wind stress	N m ⁻²	0.0597	0.0592	0.0068	0.8772
Sensible heat flux	W m ⁻²	-3.9	4.4	-55.4	4.2
Latent heat flux	W m ⁻²	-120.5	37.8	-251.9	-42.6
Net short-wave radiation	W m ⁻²	235.9	331.0	-0.1	1038.7
Net long-wave radiation	W m ⁻²	-68.4	14.7	-101.9	-17.7
Net heat flux	W m ⁻²	43.0	333.8	-348.6	896.6
Skin temperature ^f	°C	27.67	0.24	27.16	28.26
10m wind speed ^g	m s ⁻¹	6.17	1.81	1.99	20.30
2m air temperature ^g	°C	27.26	0.42	24.94	28.53
2m relative humidity ^g	%	79.2	7.8	52.5	99.2
2m specific humidity ^g	g kg ⁻¹	17.67	1.84	11.38	20.63

^a Scalar averaged

^b Vector averaged from components of a unit vector oriented in the direction of the wind

^c Vector averaged

^d Computed as the arctangent of the average east and north components

^e Measured at 0.17 m depth

^f The temperature of the upper few millimeters of the ocean. Computed from Fairall *et al.* (1996b)

^g Estimated from boundary layer profiles in flux algorithm

Table 21. Statistics of observables and fluxes for November 1994.

Variable	Unit	Mean	Std. Dev.	Minimum	Maximum
Air temperature	°C	27.23	0.55	24.63	28.32
Relative humidity	%	75.6	8.0	51.8	90.7
Barometric pressure	mbar	1012.7	1.4	1009.2	1017.0
East wind	m s ⁻¹	-5.08	1.51	-8.46	0.15
North wind	m s ⁻¹	-3.25	1.42	-7.31	3.09
Wind speed ^a	m s ⁻¹	6.26	1.20	1.40	10.19
Wind direction ^b	°	237			
Wind speed ^c	m s ⁻¹	6.02			
Wind direction ^d	°	237			
Incoming short-wave radiation	W m ⁻²	237.2	321.0	-0.1	987.2
Incoming long-wave radiation	W m ⁻²	390.8	14.3	359.9	441.8
Sea surface temperature ^e	°C	27.52	0.51	26.55	28.34
Specific humidity	g kg ⁻¹	17.01	2.13	11.83	20.57
Precipitation rate	mm hr ⁻¹	0.0099	0.3177	0.0000	15.8448
Evaporation rate	mm hr ⁻¹	0.1998	0.0662	0.0658	0.4656
Evaporation rate - precipitation rate	mm hr ⁻¹	0.1900	0.3252	-15.6822	0.4656
Wind stress	N m ⁻²	0.0724	0.0287	0.0045	0.2089
Sensible heat flux	W m ⁻²	0.0	4.0	-34.8	15.8
Latent heat flux	W m ⁻²	-136.2	45.1	-317.2	-44.9
Net short-wave radiation	W m ⁻²	222.1	307.4	0.0	949.4
Net long-wave radiation	W m ⁻²	-69.1	12.5	-97.5	-20.1
Net heat flux	W m ⁻²	16.8	311.4	-392.2	789.3
Skin temperature ^f	°C	27.29	0.54	26.22	28.18
10m wind speed ^g	m s ⁻¹	7.01	1.41	1.58	11.35
2m air temperature ^g	°C	27.23	0.55	24.69	28.32
2m relative humidity ^g	%	76.9	8.1	53.2	95.2
2m specific humidity ^g	g kg ⁻¹	17.14	2.10	12.08	20.62

^a Scalar averaged

^b Vector averaged from components of a unit vector oriented in the direction of the wind

^c Vector averaged

^d Computed as the arctangent of the average east and north components

^e Measured at 0.17 m depth

^f The temperature of the upper few millimeters of the ocean. Computed from Fairall *et al.* (1996b)

^g Estimated from boundary layer profiles in flux algorithm

Table 22. Statistics of observables and fluxes for December 1994.

Variable	Unit	Mean	Std. Dev.	Minimum	Maximum
Air temperature	°C	25.53	0.57	23.71	27.20
Relative humidity	%	67.1	5.0	52.6	82.8
Barometric pressure	mbar	1015.8	1.4	1012.0	1019.4
East wind	m s ⁻¹	-4.48	2.01	-8.34	4.09
North wind	m s ⁻¹	-4.31	2.01	-9.55	2.23
Wind speed ^a	m s ⁻¹	6.64	1.63	1.81	10.78
Wind direction ^b	°	227			
Wind speed ^c	m s ⁻¹	6.22			
Wind direction ^d	°	226			
Incoming short-wave radiation	W m ⁻²	221.9	305.7	0.0	1003.3
Incoming long-wave radiation	W m ⁻²	377.0	13.5	345.6	431.4
Sea surface temperature ^e	°C	26.34	0.25	25.66	26.94
Specific humidity	g kg ⁻¹	13.59	1.19	9.77	16.39
Precipitation rate	mm hr ⁻¹	0.0005	0.0360	0.0000	2.7786
Evaporation rate	mm hr ⁻¹	0.2890	0.0772	0.0744	0.5516
Evaporation rate - precipitation rate	mm hr ⁻¹	0.2886	0.0855	-2.5433	0.5516
Wind stress	N m ⁻²	0.0860	0.0442	0.0048	0.2464
Sensible heat flux	W m ⁻²	-5.7	5.0	-23.7	6.1
Latent heat flux	W m ⁻²	-196.9	52.6	-375.8	-50.7
Net short-wave radiation	W m ⁻²	206.7	291.7	0.0	961.8
Net long-wave radiation	W m ⁻²	-75.1	12.6	-102.8	-22.4
Net heat flux	W m ⁻²	-71.0	301.3	-498.0	760.6
Skin temperature ^f	°C	26.04	0.27	25.34	26.74
10m wind speed ^g	m s ⁻¹	7.32	1.83	1.71	11.96
2m air temperature ^g	°C	25.55	0.57	23.75	27.19
2m relative humidity ^g	%	68.4	4.8	53.3	84.3
2m specific humidity ^g	g kg ⁻¹	13.76	1.17	9.98	16.51

^a Scalar averaged

^b Vector averaged from components of a unit vector oriented in the direction of the wind

^c Vector averaged

^d Computed as the arctangent of the average east and north components

^e Measured at 0.17 m depth

^f The temperature of the upper few millimeters of the ocean. Computed from Fairall *et al.* (1996b)

^g Estimated from boundary layer profiles in flux algorithm

Table 23. Statistics of observables and fluxes for January 1995.

Variable	Unit	Mean	Std. Dev.	Minimum	Maximum
Air temperature	°C	24.21	0.36	22.90	25.51
Relative humidity	%	67.6	8.3	47.3	85.3
Barometric pressure	mbar	1015.8	1.5	1011.8	1020.3
East wind	m s ⁻¹	-3.99	1.64	-10.23	2.51
North wind	m s ⁻¹	-4.23	1.55	-9.42	1.13
Wind speed ^a	m s ⁻¹	6.03	1.58	0.55	10.89
Wind direction ^b	°	223			
Wind speed ^c	m s ⁻¹	5.81			
Wind direction ^d	°	223			
Incoming short-wave radiation	W m ⁻²	237.0	323.4	-0.1	1067.7
Incoming long-wave radiation	W m ⁻²	367.1	16.5	335.2	420.6
Sea surface temperature ^e	°C	25.30	0.34	24.91	26.28
Specific humidity	g kg ⁻¹	12.61	1.49	8.59	15.41
Precipitation rate	mm hr ⁻¹	0.0004	0.0314	0.0000	2.4203
Evaporation rate	mm hr ⁻¹	0.2510	0.0834	0.0642	0.5408
Evaporation rate - precipitation rate	mm hr ⁻¹	0.2506	0.0894	-2.2208	0.5408
Wind stress	N m ⁻²	0.0662	0.0393	0.0008	0.2450
Sensible heat flux	W m ⁻²	-7.6	3.8	-34.1	4.0
Latent heat flux	W m ⁻²	-171.0	56.9	-368.5	-43.7
Net short-wave radiation	W m ⁻²	221.3	309.2	0.0	1024.2
Net long-wave radiation	W m ⁻²	-78.6	15.8	-107.9	-25.4
Net heat flux	W m ⁻²	-36.0	319.3	-484.8	745.3
Skin temperature ^f	°C	25.00	0.31	24.52	25.98
10m wind speed ^g	m s ⁻¹	6.43	1.76	0.50	11.86
2m air temperature ^g	°C	24.24	0.36	22.96	25.52
2m relative humidity ^g	%	68.8	8.2	48.1	88.0
2m specific humidity ^g	g kg ⁻¹	12.76	1.46	8.78	15.51

^a Scalar averaged

^b Vector averaged from components of a unit vector oriented in the direction of the wind

^c Vector averaged

^d Computed as the arctangent of the average east and north components

^e Measured at 0.17 m depth

^f The temperature of the upper few millimeters of the ocean. Computed from Fairall *et al.* (1996b)

^g Estimated from boundary layer profiles in flux algorithm

Table 24. Statistics of observables and fluxes for February 1995.

Variable	Unit	Mean	Std. Dev.	Minimum	Maximum
Air temperature	°C	24.19	0.51	22.60	27.47
Relative humidity	%	69.9	6.2	49.5	86.8
Barometric pressure	mbar	1014.1	1.5	1009.9	1018.2
East wind	m s ⁻¹	-2.28	2.04	-6.59	3.18
North wind	m s ⁻¹	-2.23	1.90	-7.61	3.77
Wind speed ^a	m s ⁻¹	3.95	1.53	0.06	7.74
Wind direction ^b	°	227			
Wind speed ^c	m s ⁻¹	3.19			
Wind direction ^d	°	226			
Incoming short-wave radiation	W m ⁻²	270.5	358.3	0.0	1214.7
Incoming long-wave radiation	W m ⁻²	367.2	12.9	336.3	423.7
Sea surface temperature ^e	°C	25.35	0.35	24.89	27.18
Specific humidity	g kg ⁻¹	13.00	1.32	8.66	15.87
Precipitation rate	mm hr ⁻¹	0.0000	0.0000	0.0000	0.0000
Evaporation rate	mm hr ⁻¹	0.1625	0.0632	0.0333	0.3512
Evaporation rate - precipitation rate	mm hr ⁻¹	0.1625	0.0632	0.0333	0.3512
Wind stress	N m ⁻²	0.0291	0.0198	0.0001	0.1082
Sensible heat flux	W m ⁻²	-5.4	3.1	-18.4	3.9
Latent heat flux	W m ⁻²	-110.7	43.1	-239.3	-22.7
Net short-wave radiation	W m ⁻²	254.0	344.2	0.0	1170.0
Net long-wave radiation	W m ⁻²	-78.8	12.3	-106.4	-25.2
Net heat flux	W m ⁻²	59.1	348.6	-357.1	1011.4
Skin temperature ^f	°C	25.06	0.39	24.52	26.97
10m wind speed ^g	m s ⁻¹	4.21	1.67	0.11	8.46
2m air temperature ^g	°C	24.22	0.50	22.65	27.43
2m relative humidity ^g	%	70.7	6.2	51.5	87.5
2m specific humidity ^g	g kg ⁻¹	13.13	1.30	8.84	15.96

^a Scalar averaged

^b Vector averaged from components of a unit vector oriented in the direction of the wind

^c Vector averaged

^d Computed as the arctangent of the average east and north components

^e Measured at 0.17 m depth

^f The temperature of the upper few millimeters of the ocean. Computed from Fairall *et al.* (1996b)

^g Estimated from boundary layer profiles in flux algorithm

Table 25. Statistics of observables and fluxes for March 1995.

Variable	Unit	Mean	Std. Dev.	Minimum	Maximum
Air temperature	°C	25.30	0.68	23.82	28.69
Relative humidity	%	73.2	6.6	52.0	89.1
Barometric pressure	mbar	1013.2	2.1	1008.1	1017.7
East wind	m s ⁻¹	-2.27	2.84	-9.33	5.03
North wind	m s ⁻¹	-1.92	2.12	-8.04	5.86
Wind speed ^a	m s ⁻¹	4.26	1.80	0.04	9.53
Wind direction ^b	°	226			
Wind speed ^c	m s ⁻¹	2.97			
Wind direction ^d	°	230			
Incoming short-wave radiation	W m ⁻²	300.6	386.6	0.0	1169.2
Incoming long-wave radiation	W m ⁻²	372.9	14.6	338.9	427.3
Sea surface temperature ^e	°C	26.25	0.76	25.24	28.78
Specific humidity	g kg ⁻¹	14.47	1.46	10.20	17.72
Precipitation rate	mm hr ⁻¹	0.0000	0.0000	0.0000	0.0000
Evaporation rate	mm hr ⁻¹	0.1646	0.0756	0.0221	0.4214
Evaporation rate - precipitation rate	mm hr ⁻¹	0.1646	0.0756	0.0221	0.4214
Wind stress	N m ⁻²	0.0354	0.0278	0.0001	0.1742
Sensible heat flux	W m ⁻²	-4.2	3.0	-15.4	3.5
Latent heat flux	W m ⁻²	-112.1	51.5	-287.2	-15.0
Net short-wave radiation	W m ⁻²	283.9	372.8	0.0	1129.0
Net long-wave radiation	W m ⁻²	-78.7	15.0	-109.6	-23.5
Net heat flux	W m ⁻²	88.8	375.7	-386.1	952.2
Skin temperature ^f	°C	25.98	0.79	24.88	29.13
10m wind speed ^g	m s ⁻¹	4.57	1.99	0.11	10.45
2m air temperature ^e	°C	25.32	0.68	23.85	28.69
2m relative humidity ^e	%	73.5	6.5	52.7	88.4
2m specific humidity ^e	g kg ⁻¹	14.60	1.43	10.44	17.80

^a Scalar averaged

^b Vector averaged from components of a unit vector oriented in the direction of the wind

^c Vector averaged

^d Computed as the arctangent of the average east and north components

^e Measured at 0.17 m depth

^f The temperature of the upper few millimeters of the ocean. Computed from Fairall *et al.* (1996b)

^g Estimated from boundary layer profiles in flux algorithm

Table 26. Statistics of observables and fluxes for April 1995.

Variable	Unit	Mean	Std. Dev.	Minimum	Maximum
Air temperature	°C	27.19	1.00	25.05	31.47
Relative humidity	%	74.0	5.8	52.7	83.8
Barometric pressure	mbar	1011.2	1.5	1007.4	1015.6
East wind	m s ⁻¹	-1.17	2.26	-7.33	4.55
North wind	m s ⁻¹	-1.17	2.06	-6.77	5.40
Wind speed ^a	m s ⁻¹	3.17	1.42	0.09	7.89
Wind direction ^b	°	226			
Wind speed ^c	m s ⁻¹	1.65			
Wind direction ^d	°	225			
Incoming short-wave radiation	W m ⁻²	318.9	400.0	-0.3	1148.6
Incoming long-wave radiation	W m ⁻²	383.2	13.3	359.4	442.7
Sea surface temperature ^e	°C	28.47	0.90	27.11	31.85
Specific humidity	g kg ⁻¹	16.46	1.83	10.48	20.55
Precipitation rate	mm hr ⁻¹	0.0000	0.0000	0.0000	0.0000
Evaporation rate	mm hr ⁻¹	0.1435	0.0626	0.0264	0.4922
Evaporation rate - precipitation rate	mm hr ⁻¹	0.1435	0.0626	0.0264	0.4922
Wind stress	N m ⁻²	0.0191	0.0150	0.0001	0.1153
Sensible heat flux	W m ⁻²	-5.0	2.9	-14.2	2.9
Latent heat flux	W m ⁻²	-97.8	42.6	-335.4	-18.0
Net short-wave radiation	W m ⁻²	301.9	386.4	-0.1	1111.0
Net long-wave radiation	W m ⁻²	-81.8	9.9	-108.5	-27.8
Net heat flux	W m ⁻²	117.3	386.5	-414.0	939.9
Skin temperature ^f	°C	28.18	0.97	26.69	31.86
10m wind speed ^g	m s ⁻¹	3.35	1.54	0.13	8.61
2m air temperature ^g	°C	27.22	0.99	25.08	31.47
2m relative humidity ^g	%	74.3	6.1	52.5	84.1
2m specific humidity ^g	g kg ⁻¹	16.60	1.82	10.70	20.68

^a Scalar averaged

^b Vector averaged from components of a unit vector oriented in the direction of the wind

^c Vector averaged

^d Computed as the arctangent of the average east and north components

^e Measured at 0.17 m depth

^f The temperature of the upper few millimeters of the ocean. Computed from Fairall *et al.* (1996b)

^g Estimated from boundary layer profiles in flux algorithm

Table 27. Statistics of observables and fluxes for May 1995.

Variable	Unit	Mean	Std. Dev.	Minimum	Maximum
Air temperature	°C	28.86	0.48	27.41	31.39
Relative humidity	%	75.9	5.8	60.8	88.1
Barometric pressure	mbar	1008.7	1.7	1003.9	1012.7
East wind	m s ⁻¹	3.06	3.23	-3.25	9.60
North wind	m s ⁻¹	0.05	2.46	-5.88	6.94
Wind speed ^a	m s ⁻¹	4.46	2.43	0.04	10.50
Wind direction ^b	°	103			
Wind speed ^c	m s ⁻¹	3.06			
Wind direction ^d	°	89			
Incoming short-wave radiation	W m ⁻²	313.5	381.1	-0.3	1067.0
Incoming long-wave radiation	W m ⁻²	406.7	14.3	373.3	458.2
Sea surface temperature ^e	°C	29.84	0.51	29.21	32.23
Specific humidity	g kg ⁻¹	18.73	1.64	14.46	22.35
Precipitation rate	mm hr ⁻¹	0.0000	0.0000	0.0000	0.0000
Evaporation rate	mm hr ⁻¹	0.1686	0.0547	0.0268	0.3466
Evaporation rate - precipitation rate	mm hr ⁻¹	0.1686	0.0547	0.0268	0.3466
Wind stress	N m ⁻²	0.0436	0.0428	0.0001	0.2182
Sensible heat flux	W m ⁻²	-3.7	3.2	-16.4	5.5
Latent heat flux	W m ⁻²	-114.9	37.3	-236.2	-18.3
Net short-wave radiation	W m ⁻²	297.0	368.4	-0.1	1032.4
Net long-wave radiation	W m ⁻²	-67.4	13.6	-99.6	-15.4
Net heat flux	W m ⁻²	111.0	365.9	-309.3	872.2
Skin temperature ^f	°C	29.58	0.51	28.87	32.17
10m wind speed ^g	m s ⁻¹	4.80	2.70	0.09	11.60
2m air temperature ^g	°C	28.88	0.48	27.46	31.34
2m relative humidity ^g	%	76.6	5.8	61.2	88.4
2m specific humidity ^g	g kg ⁻¹	18.88	1.62	14.70	22.44

^a Scalar averaged

^b Vector averaged from components of a unit vector oriented in the direction of the wind

^c Vector averaged

^d Computed as the arctangent of the average east and north components

^e Measured at 0.17 m depth

^f The temperature of the upper few millimeters of the ocean. Computed from Fairall *et al.* (1996b)

^g Estimated from boundary layer profiles in flux algorithm

Table 28. Statistics of observables and fluxes for June 1995.

Variable	Unit	Mean	Std. Dev.	Minimum	Maximum
Air temperature	°C	29.25	0.69	28.07	30.56
Relative humidity	%	82.3	2.1	70.8	88.4
Barometric pressure	mbar	1005.2	2.1	999.3	1010.8
East wind	m s ⁻¹	8.74	2.44	0.92	13.77
North wind	m s ⁻¹	4.35	2.25	-3.22	8.69
Wind speed ^a	m s ⁻¹	9.91	2.85	1.38	15.23
Wind direction ^b	°	66			
Wind speed ^c	m s ⁻¹	9.76			
Wind direction ^d	°	64			
Incoming short-wave radiation	W m ⁻²	264.8	330.2	-0.3	1030.4
Incoming long-wave radiation	W m ⁻²	436.4	10.1	412.6	506.5
Sea surface temperature ^e	°C	29.45	0.73	28.57	31.22
Specific humidity	g kg ⁻¹	20.69	0.73	18.74	22.64
Precipitation rate	mm hr ⁻¹	0.0008	0.0600	0.0000	4.5548
Evaporation rate	mm hr ⁻¹	0.2429	0.0540	0.0712	0.4073
Evaporation rate - precipitation rate	mm hr ⁻¹	0.2421	0.0807	-4.3108	0.4073
Wind stress	N m ⁻²	0.2123	0.1163	0.0037	0.5427
Sensible heat flux	W m ⁻²	0.1	3.0	-16.8	10.0
Latent heat flux	W m ⁻²	-165.5	36.8	-277.6	-48.5
Net short-wave radiation	W m ⁻²	251.0	319.2	-0.1	997.0
Net long-wave radiation	W m ⁻²	-37.0	11.7	-64.6	26.8
Net heat flux	W m ⁻²	48.7	322.8	-318.1	833.3
Skin temperature ^f	°C	29.31	0.70	28.43	31.11
10m wind speed ^g	m s ⁻¹	10.86	3.21	1.46	16.89
2m air temperature ^g	°C	29.26	0.68	28.08	30.56
2m relative humidity ^g	%	82.4	1.9	72.1	87.4
2m specific humidity ^g	g kg ⁻¹	20.81	0.74	18.89	22.74

^a Scalar averaged

^b Vector averaged from components of a unit vector oriented in the direction of the wind

^c Vector averaged

^d Computed as the arctangent of the average east and north components

^e Measured at 0.17 m depth

^f The temperature of the upper few millimeters of the ocean. Computed from Fairall *et al.* (1996b)

^g Estimated from boundary layer profiles in flux algorithm

Table 29. Statistics of observables and fluxes for July 1995.

Variable	Unit	Mean	Std. Dev.	Minimum	Maximum
Air temperature	°C	27.42	0.80	25.83	28.78
Relative humidity	%	86.3	2.3	80.7	93.9
Barometric pressure	mbar	1002.5	2.3	997.0	1007.9
East wind	m s ⁻¹	10.01	1.63	5.47	14.82
North wind	m s ⁻¹	7.18	1.47	1.87	13.65
Wind speed ^a	m s ⁻¹	12.37	1.89	6.50	18.34
Wind direction ^b	°	54			
Wind speed ^c	m s ⁻¹	12.32			
Wind direction ^d	°	54			
Incoming short-wave radiation	W m ⁻²	198.1	267.9	-0.5	988.9
Incoming long-wave radiation	W m ⁻²	440.6	11.1	411.3	479.5
Sea surface temperature ^e	°C	27.00	1.10	24.95	28.59
Specific humidity	g kg ⁻¹	19.37	0.58	18.08	20.76
Precipitation rate	mm hr ⁻¹	0.0004	0.0278	0.0000	2.1422
Evaporation rate	mm hr ⁻¹	0.1796	0.0703	0.0281	0.3430
Evaporation rate - precipitation rate	mm hr ⁻¹	0.1792	0.0753	-1.8992	0.3430
Wind stress	N m ⁻²	0.3248	0.1215	0.0567	0.8332
Sensible heat flux	W m ⁻²	9.0	5.1	-7.3	22.1
Latent heat flux	W m ⁻²	-122.4	47.9	-233.7	-19.2
Net short-wave radiation	W m ⁻²	188.0	258.7	-0.1	956.5
Net long-wave radiation	W m ⁻²	-18.6	9.6	-50.5	15.6
Net heat flux	W m ⁻²	56.0	268.7	-280.4	850.6
Skin temperature ^f	°C	26.93	1.07	24.91	28.52
10m wind speed ^g	m s ⁻¹	13.50	2.16	6.76	20.07
2m air temperature ^e	°C	27.42	0.81	25.82	28.78
2m relative humidity ^e	%	85.7	2.2	79.5	91.8
2m specific humidity ^e	g kg ⁻¹	19.43	0.59	18.12	20.84

^a Scalar averaged

^b Vector averaged from components of a unit vector oriented in the direction of the wind

^c Vector averaged

^d Computed as the arctangent of the average east and north components

^e Measured at 0.17 m depth

^f The temperature of the upper few millimeters of the ocean. Computed from Fairall *et al.* (1996b)

^g Estimated from boundary layer profiles in flux algorithm

Table 30. Statistics of observables and fluxes for August 1995.

Variable	Unit	Mean	Std. Dev.	Minimum	Maximum
Air temperature	°C	26.46	0.26	25.07	27.03
Relative humidity	%	89.6	1.5	84.6	94.6
Barometric pressure	mbar	1006.2	2.0	1001.7	1011.5
East wind	m s ⁻¹	7.16	1.62	2.96	11.93
North wind	m s ⁻¹	5.88	0.81	3.12	9.06
Wind speed ^a	m s ⁻¹	9.33	1.47	4.53	13.32
Wind direction ^b	°	50			
Wind speed ^c	m s ⁻¹	9.27			
Wind direction ^d	°	51			
Incoming short-wave radiation	W m ⁻²	230.2	306.3	-0.7	994.3
Incoming long-wave radiation	W m ⁻²	432.0	12.1	402.6	465.9
Sea surface temperature ^e	°C	25.93	0.49	24.58	26.71
Specific humidity	g kg ⁻¹	18.94	0.34	17.99	19.78
Precipitation rate	mm hr ⁻¹	0.0000	0.0000	0.0000	0.0000
Evaporation rate	mm hr ⁻¹	0.0877	0.0286	0.0117	0.1951
Evaporation rate - precipitation rate	mm hr ⁻¹	0.0877	0.0286	0.0117	0.1951
Wind stress	N m ⁻²	0.1706	0.0608	0.0353	0.3962
Sensible heat flux	W m ⁻²	8.9	5.2	-21.1	25.9
Latent heat flux	W m ⁻²	-59.8	19.5	-132.9	-7.9
Net short-wave radiation	W m ⁻²	218.8	295.8	-0.2	962.1
Net long-wave radiation	W m ⁻²	-20.8	11.5	-52.2	10.0
Net heat flux	W m ⁻²	147.0	295.7	-167.9	880.2
Skin temperature ^f	°C	25.89	0.48	24.58	26.67
10m wind speed ^g	m s ⁻¹	10.40	1.59	5.41	14.91
2m air temperature ^g	°C	26.45	0.27	25.11	27.02
2m relative humidity ^g	%	89.0	1.3	84.1	92.8
2m specific humidity ^g	g kg ⁻¹	18.98	0.34	18.03	19.82

^a Scalar averaged

^b Vector averaged from components of a unit vector oriented in the direction of the wind

^c Vector averaged

^d Computed as the arctangent of the average east and north components

^e Measured at 0.17 m depth

^f The temperature of the upper few millimeters of the ocean. Computed from Fairall *et al.* (1996b)

^g Estimated from boundary layer profiles in flux algorithm

Table 31. Statistics of observables and fluxes for September 1995.

Variable	Unit	Mean	Std. Dev.	Minimum	Maximum
Air temperature	°C	26.77	0.38	23.53	27.59
Relative humidity	%	87.5	2.3	77.3	94.3
Barometric pressure	mbar	1009.4	2.3	1002.4	1014.6
East wind	m s ⁻¹	6.03	2.24	-1.08	11.94
North wind	m s ⁻¹	2.83	1.95	-4.43	8.96
Wind speed ^a	m s ⁻¹	6.82	2.58	0.28	13.95
Wind direction ^b	°	66			
Wind speed ^c	m s ⁻¹	6.66			
Wind direction ^d	°	65			
Incoming short-wave radiation	W m ⁻²	255.6	335.8	-0.4	1068.3
Incoming long-wave radiation	W m ⁻²	421.6	18.4	386.9	481.6
Sea surface temperature ^e	°C	27.21	0.57	26.19	28.55
Specific humidity	g kg ⁻¹	18.90	0.55	15.32	20.05
Precipitation rate	mm hr ⁻¹	0.0230	0.7059	0.0000	38.5243
Evaporation rate	mm hr ⁻¹	0.1184	0.0275	0.0269	0.2334
Evaporation rate - precipitation rate	mm hr ⁻¹	0.0954	0.7075	-38.4665	0.2334
Wind stress	N m ⁻²	0.1008	0.0820	0.0003	0.4598
Sensible heat flux	W m ⁻²	-1.8	4.7	-34.4	15.7
Latent heat flux	W m ⁻²	-80.7	18.8	-159.1	-18.3
Net short-wave radiation	W m ⁻²	242.1	323.9	-0.1	1032.6
Net long-wave radiation	W m ⁻²	-38.0	19.1	-74.7	20.9
Net heat flux	W m ⁻²	121.6	319.2	-219.4	957.7
Skin temperature ^f	°C	27.09	0.54	26.11	28.40
10m wind speed ^g	m s ⁻¹	7.59	2.94	0.23	15.81
2m air temperature ^g	°C	26.79	0.38	23.60	27.59
2m relative humidity ^g	%	87.5	2.2	71.0	94.8
2m specific humidity ^g	g kg ⁻¹	18.98	0.55	15.45	20.12

^a Scalar averaged

^b Vector averaged from components of a unit vector oriented in the direction of the wind

^c Vector averaged

^d Computed as the arctangent of the average east and north components

^e Measured at 0.17 m depth

^f The temperature of the upper few millimeters of the ocean. Computed from Fairall *et al.* (1996b)

^g Estimated from boundary layer profiles in flux algorithm

Table 32. Statistics of observables and fluxes for October 1995.

Variable	Unit	Mean	Std. Dev.	Minimum	Maximum
Air temperature	°C	27.26	0.35	26.36	29.77
Relative humidity	%	80.6	2.3	72.4	86.6
Barometric pressure	mbar	1010.4	1.6	1005.7	1013.7
East wind	m s ⁻¹	3.13	1.68	-1.64	7.68
North wind	m s ⁻¹	-0.82	1.94	-4.40	6.25
Wind speed ^a	m s ⁻¹	3.88	1.40	0.17	7.78
Wind direction ^b	°	108			
Wind speed ^c	m s ⁻¹	3.23			
Wind direction ^d	°	105			
Incoming short-wave radiation	W m ⁻²	259.0	340.7	-0.1	1068.4
Incoming long-wave radiation	W m ⁻²	406.7	11.0	381.2	454.1
Sea surface temperature ^e	°C	28.41	0.28	28.00	30.26
Specific humidity	g kg ⁻¹	18.16	0.65	16.89	19.96
Precipitation rate	mm hr ⁻¹	0.0000	0.0000	0.0000	0.0000
Evaporation rate	mm hr ⁻¹	0.1280	0.0415	0.0291	0.2756
Evaporation rate - precipitation rate	mm hr ⁻¹	0.1280	0.0415	0.0291	0.2756
Wind stress	N m ⁻²	0.0266	0.0176	0.0001	0.1024
Sensible heat flux	W m ⁻²	-5.6	2.1	-13.2	0.0
Latent heat flux	W m ⁻²	-87.2	28.2	-187.8	-19.8
Net short-wave radiation	W m ⁻²	244.3	327.9	0.0	1031.7
Net long-wave radiation	W m ⁻²	-59.0	10.4	-80.9	-13.1
Net heat flux	W m ⁻²	92.4	326.5	-248.2	895.7
Skin temperature ^f	°C	28.18	0.33	27.68	30.44
10m wind speed ^g	m s ⁻¹	4.12	1.51	0.11	8.27
2m air temperature ^g	°C	27.29	0.35	26.39	29.78
2m relative humidity ^g	%	81.7	2.1	74.0	88.0
2m specific humidity ^g	g kg ⁻¹	18.27	0.64	17.01	20.06

^a Scalar averaged

^b Vector averaged from components of a unit vector oriented in the direction of the wind

^c Vector averaged

^d Computed as the arctangent of the average east and north components

^e Measured at 0.17 m depth

^f The temperature of the upper few millimeters of the ocean. Computed from Fairall *et al.* (1996b)

^g Estimated from boundary layer profiles in flux algorithm

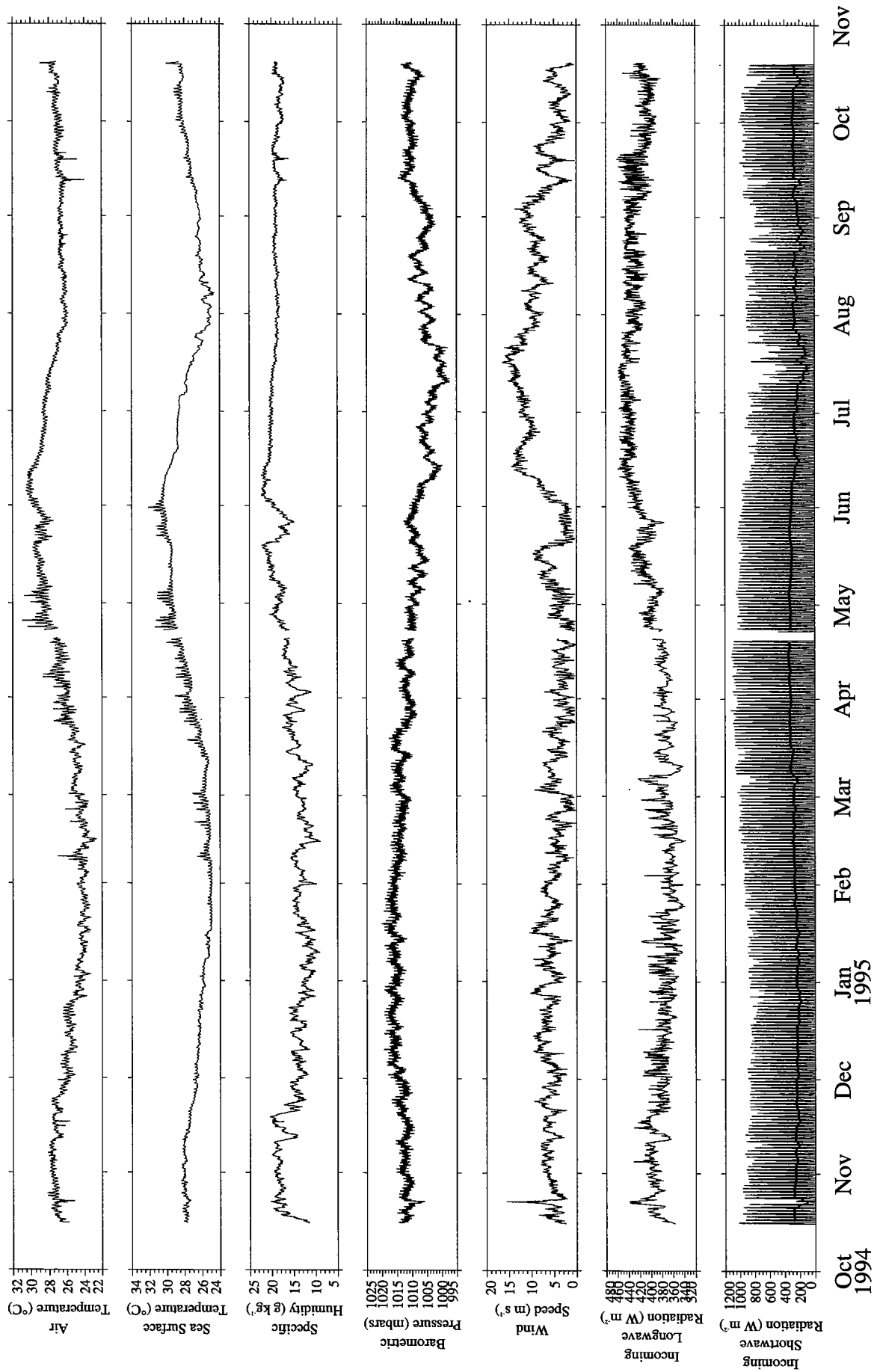


Figure 7. Hourly time series of meteorological observations. Incoming short-wave radiation has a 48 hour running mean superimposed on the hourly time series.

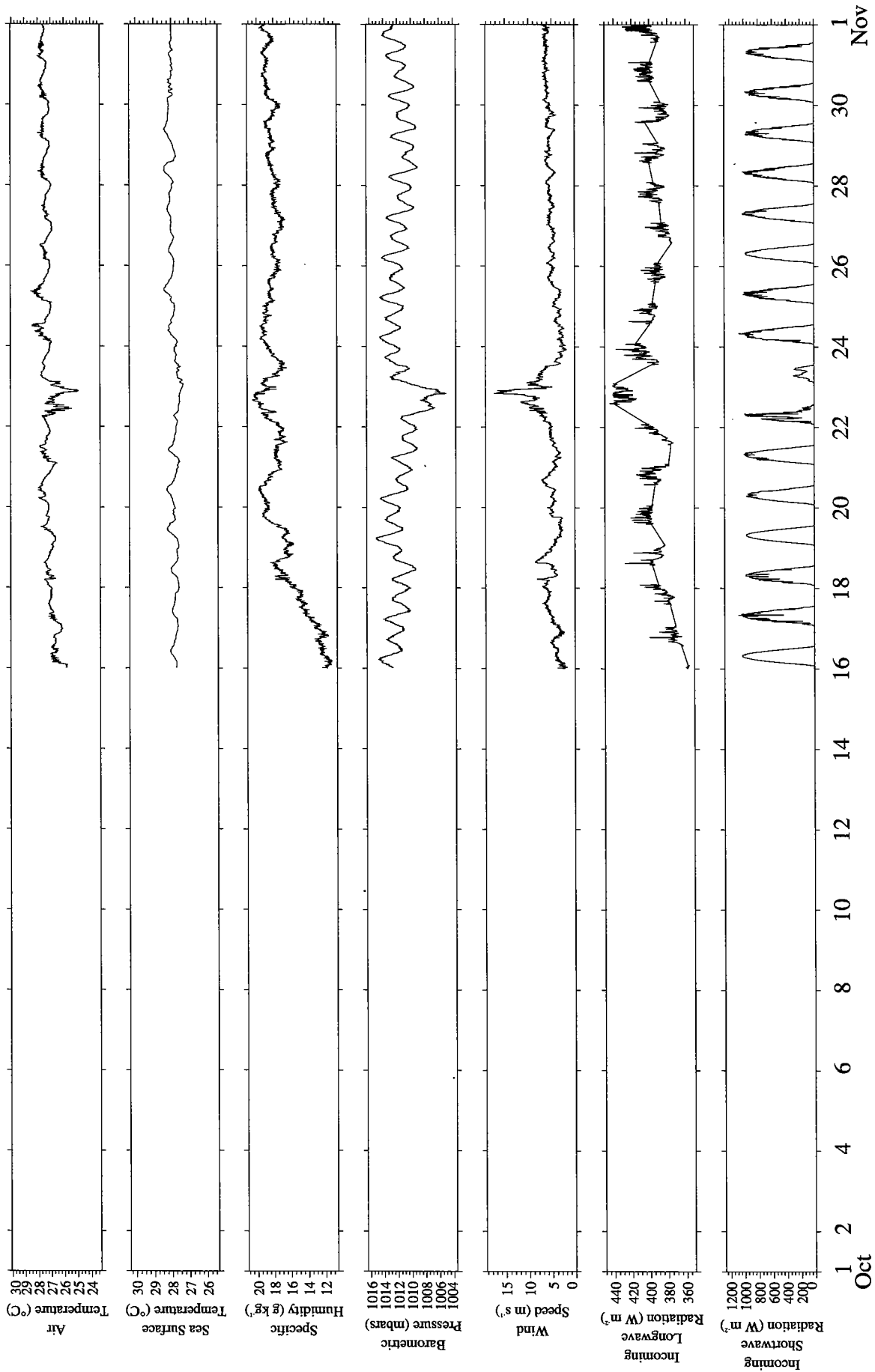


Figure 8. Four hundred fifty second time series of meteorological observations for October 1994.

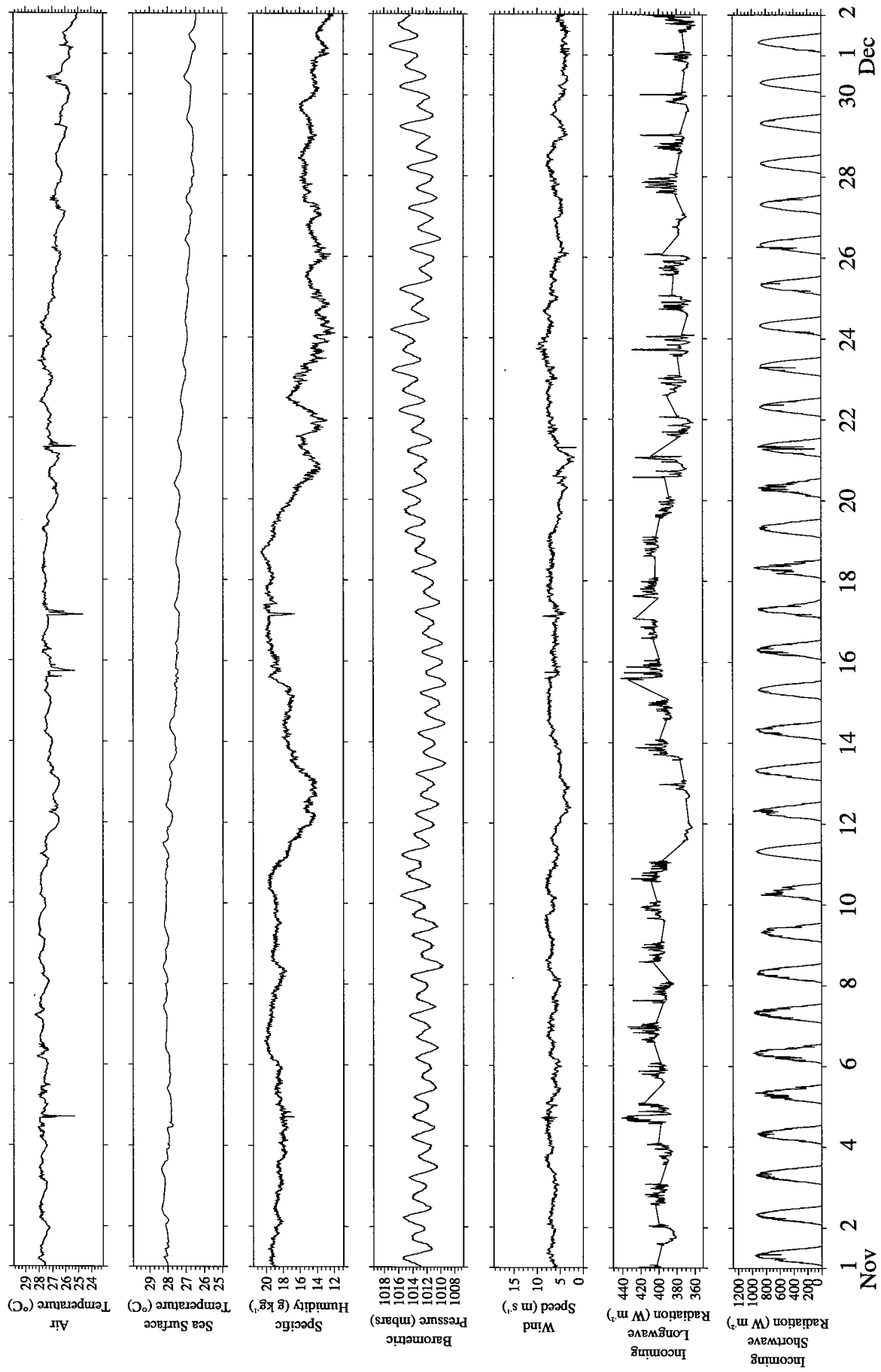


Figure 9. Four hundred fifty second time series of meteorological observations for November 1994.

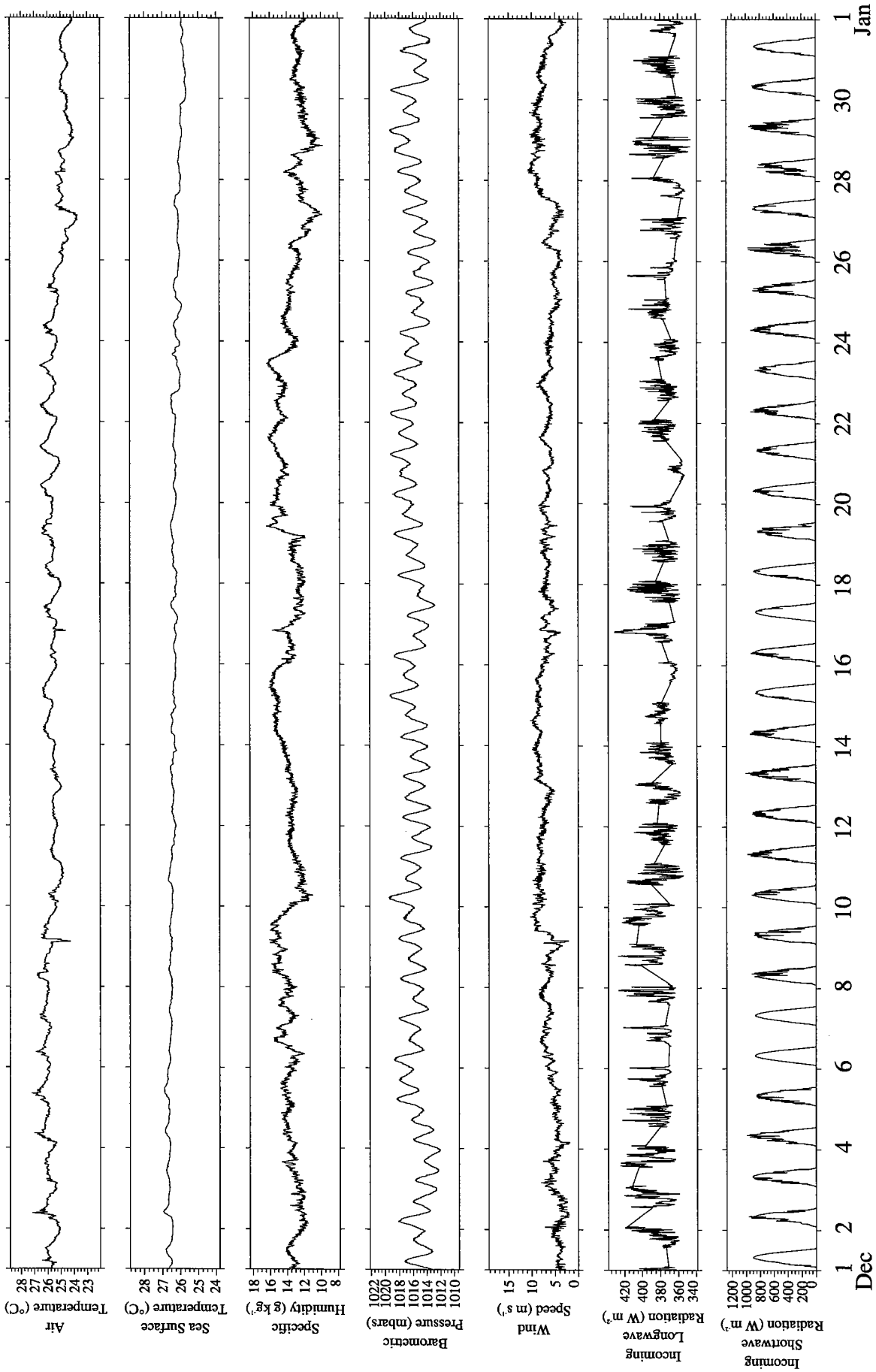


Figure 10. Four hundred fifty second time series of meteorological observations for December 1994.

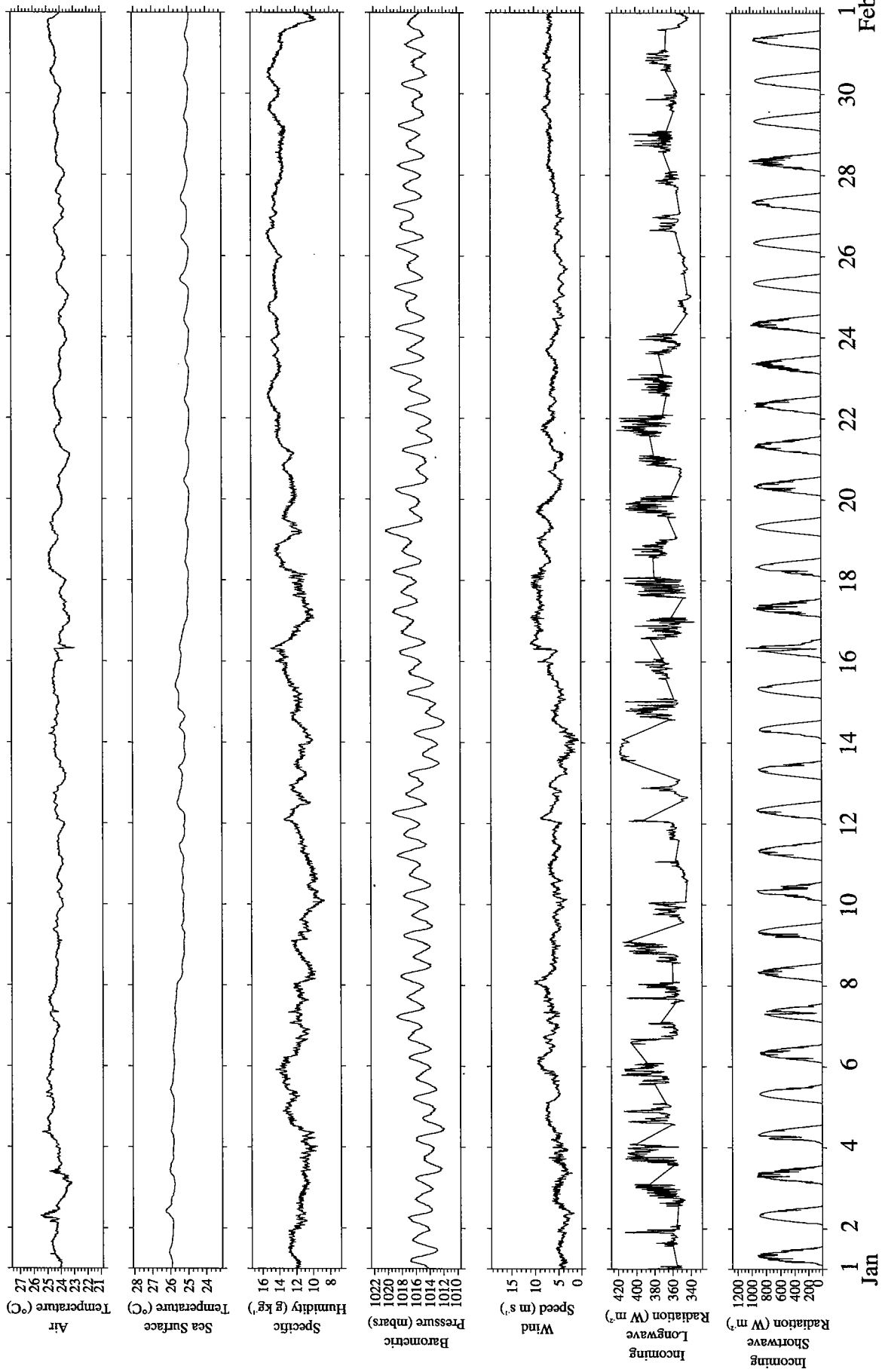


Figure 11. Four hundred fifty second time series of meteorological observations for January 1995.

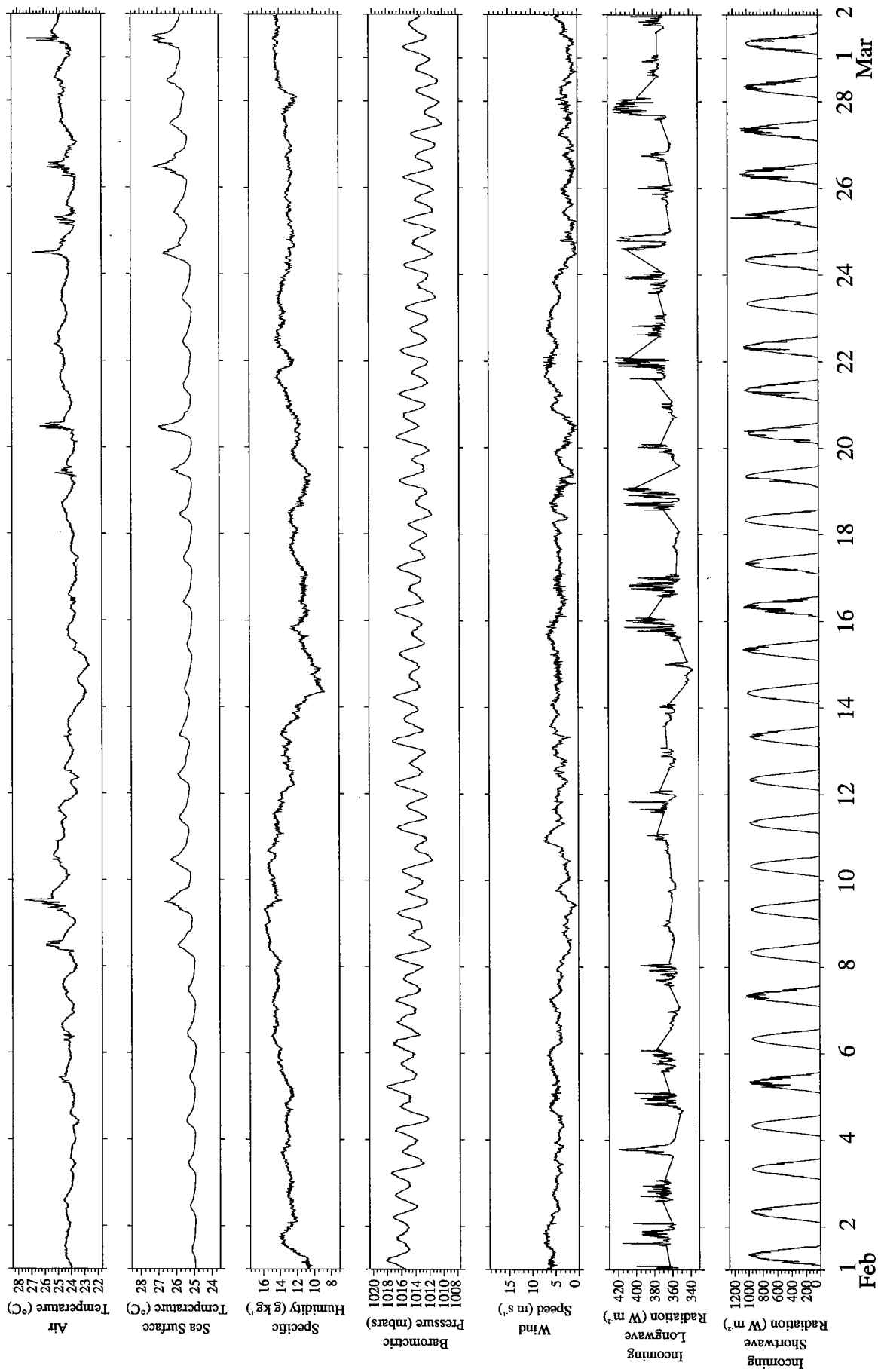


Figure 12. Four hundred fifty second time series of meteorological observations for February 1995.

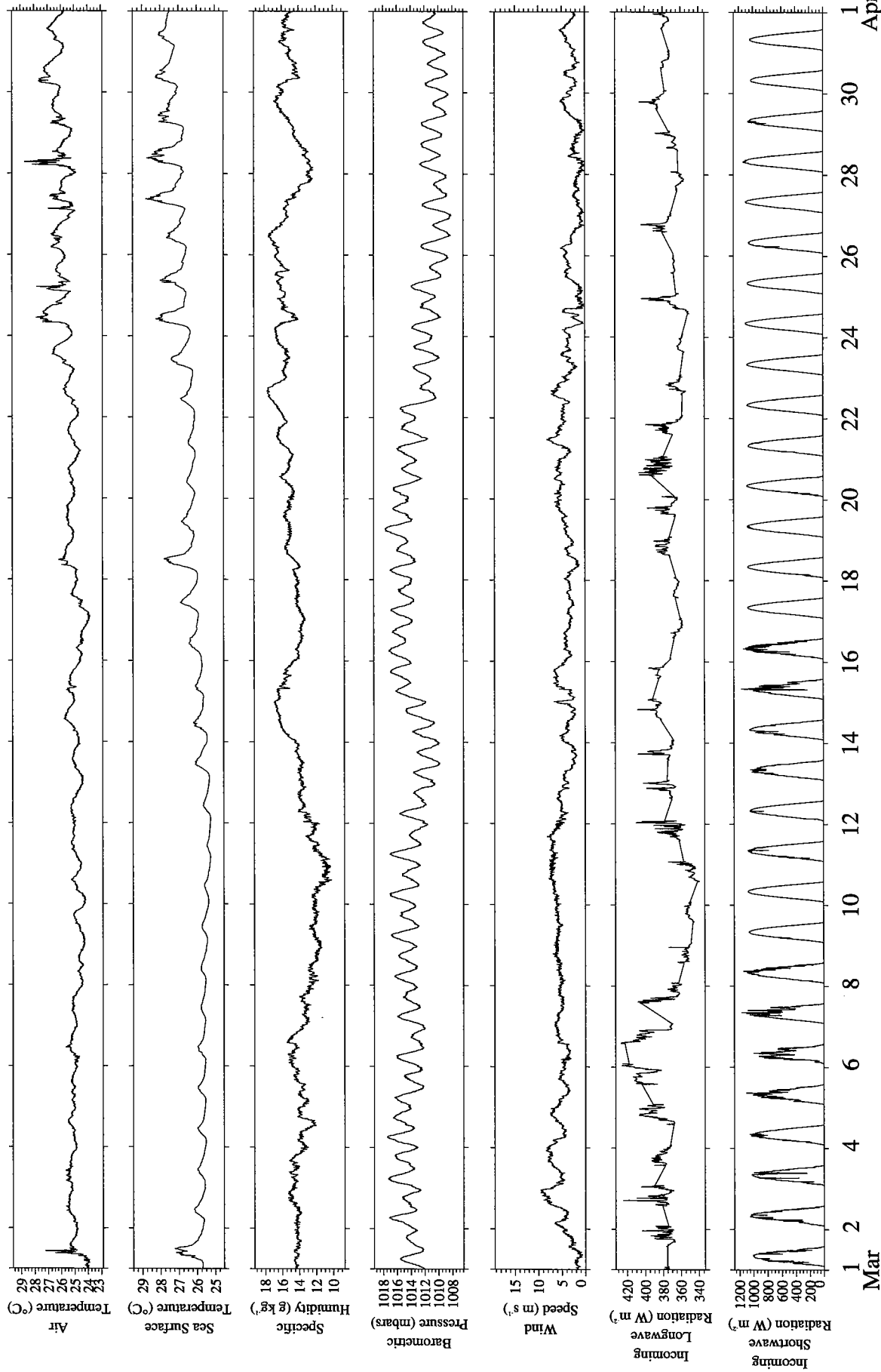


Figure 13. Four hundred fifty second time series of meteorological observations for March 1995.

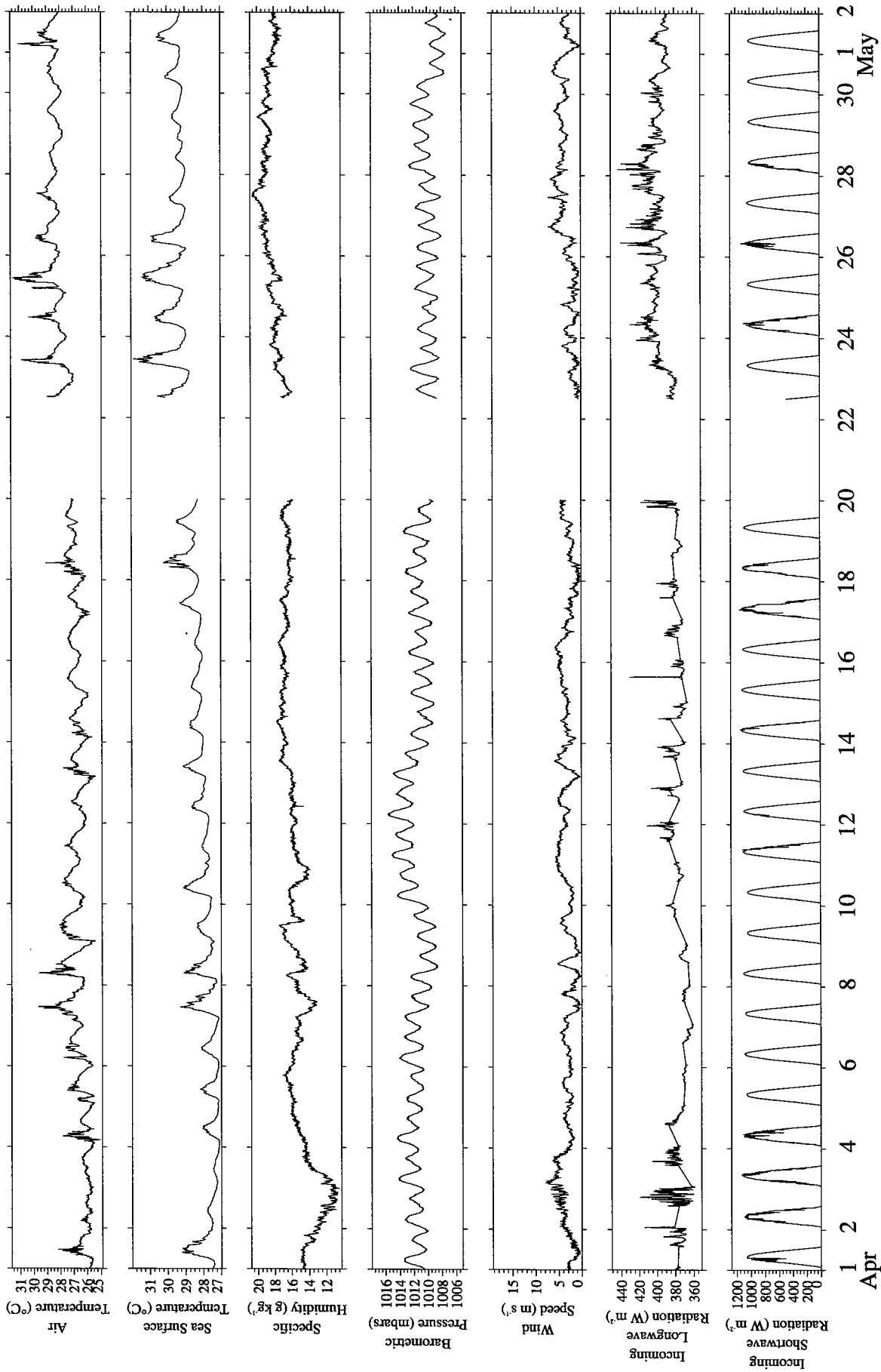


Figure 14. Four hundred fifty second time series of meteorological observations for April 1995.

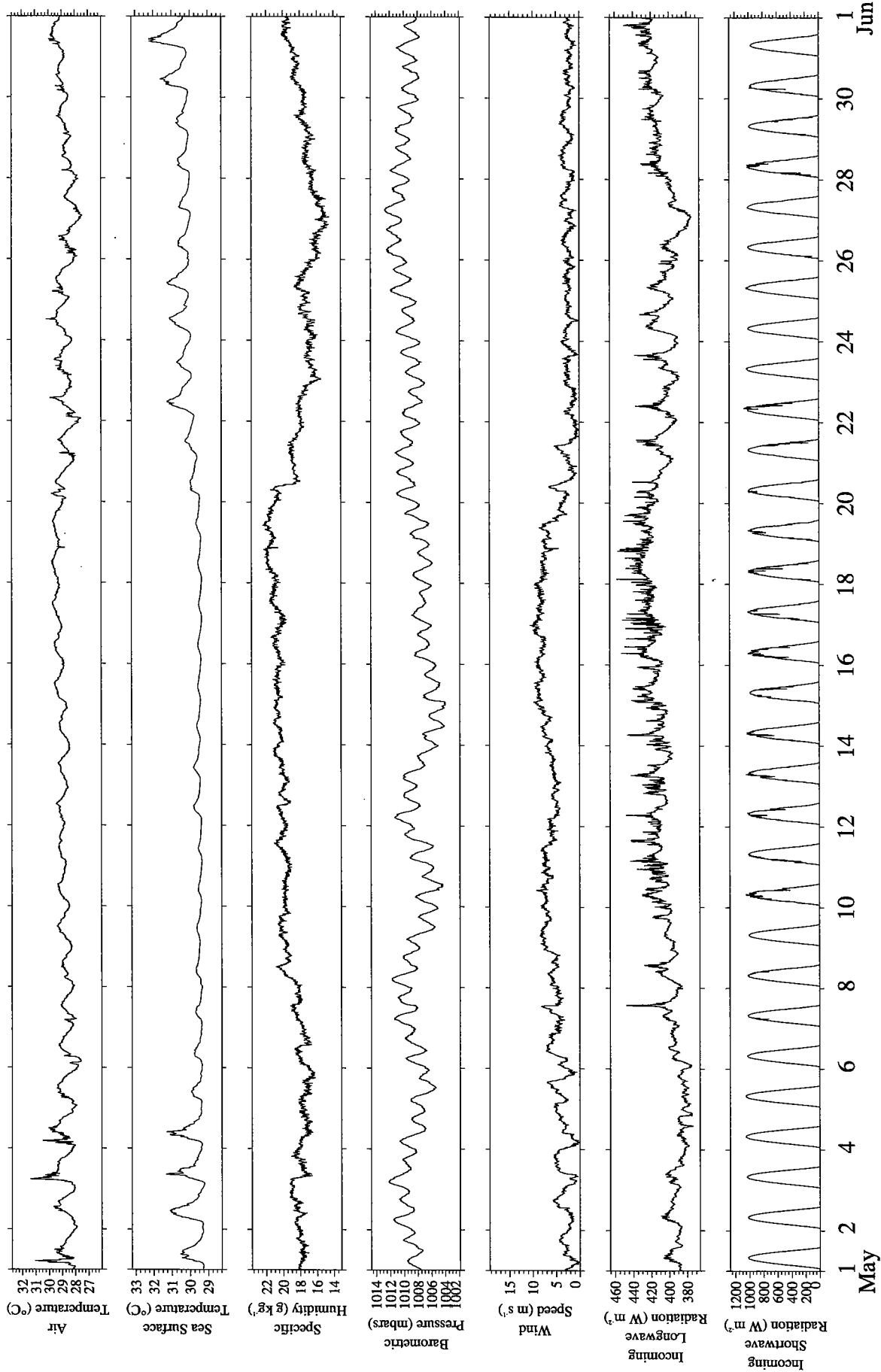


Figure 15. Four hundred fifty second time series of meteorological observations for May 1995.

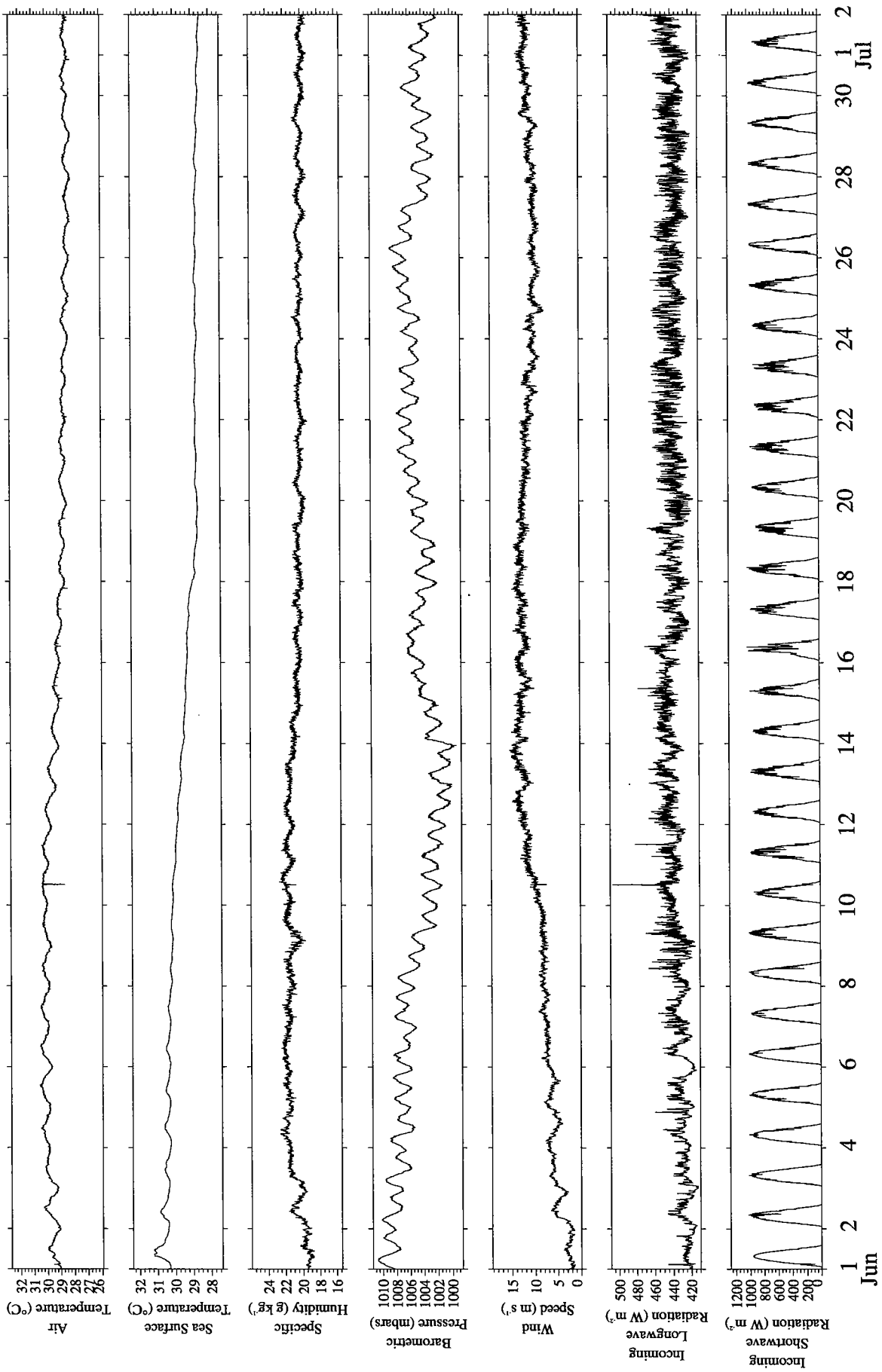


Figure 16. Four hundred fifty second time series of meteorological observations for June 1995.

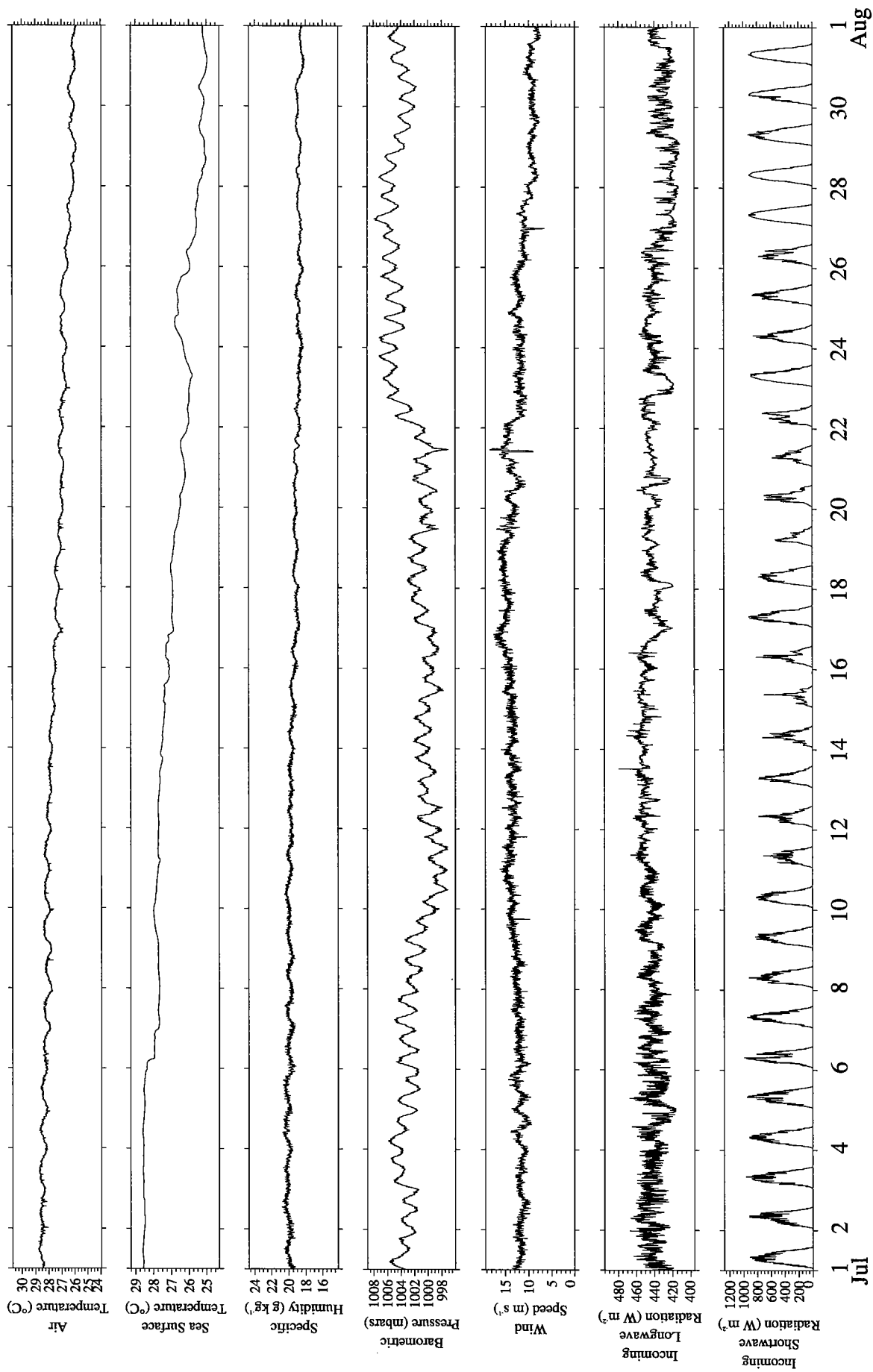


Figure 17. Four hundred fifty second time series of meteorological observations for July 1995.

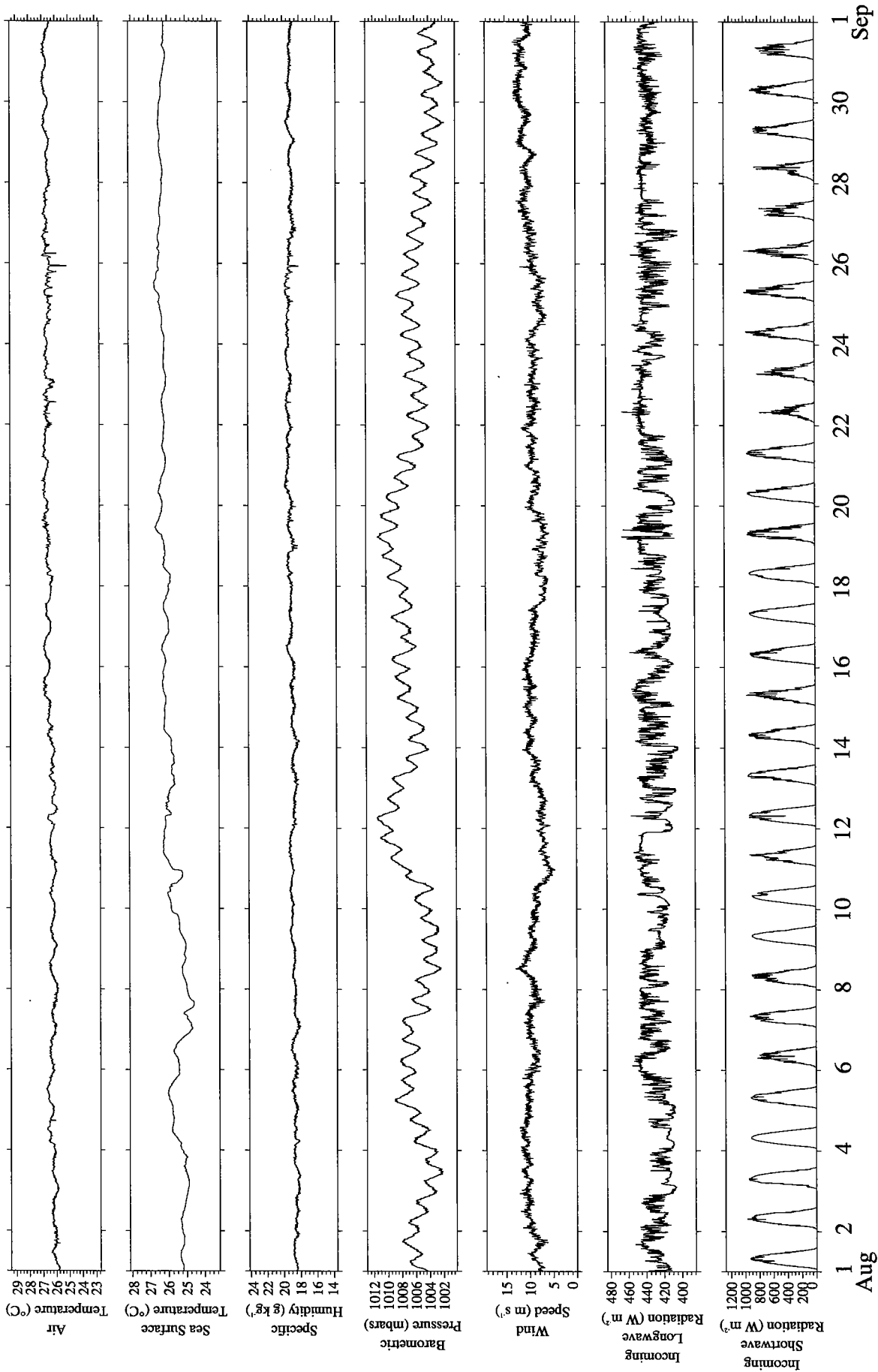


Figure 18. Four hundred fifty second time series of meteorological observations for August 1995.

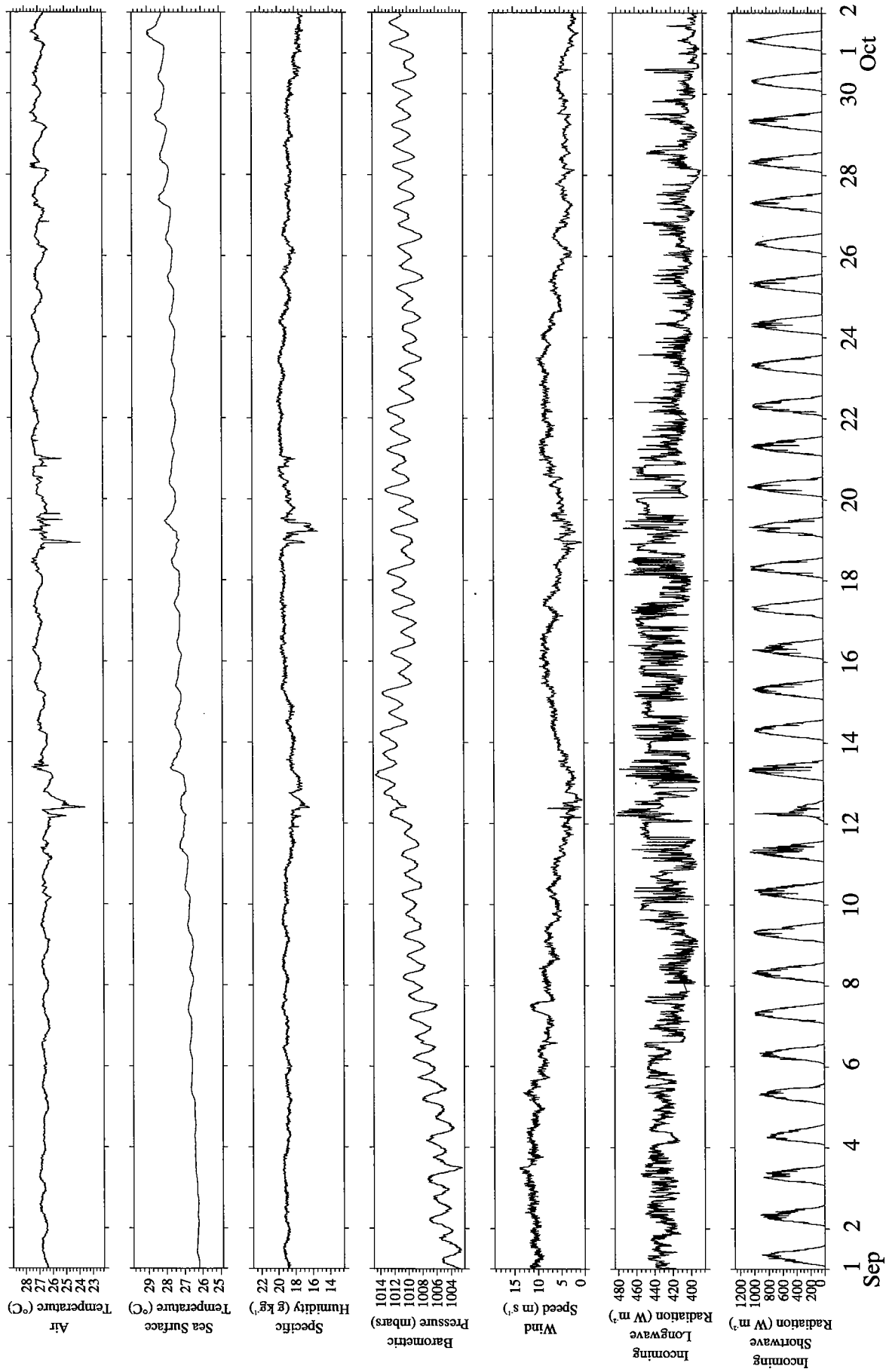


Figure 19. Four hundred fifty second time series of meteorological observations for September 1995.

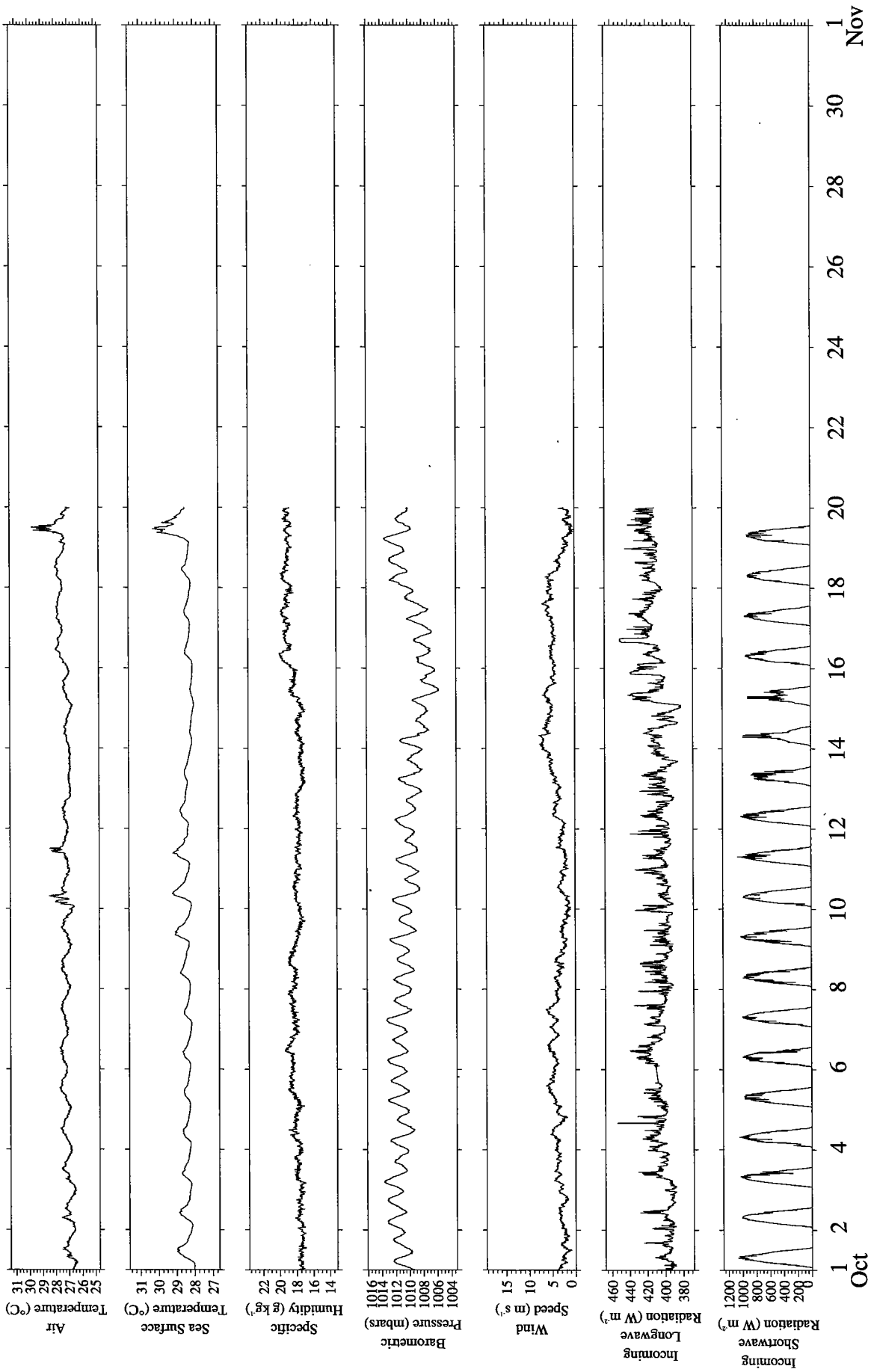


Figure 20. Four hundred fifty second time series of meteorological observations for October 1995.

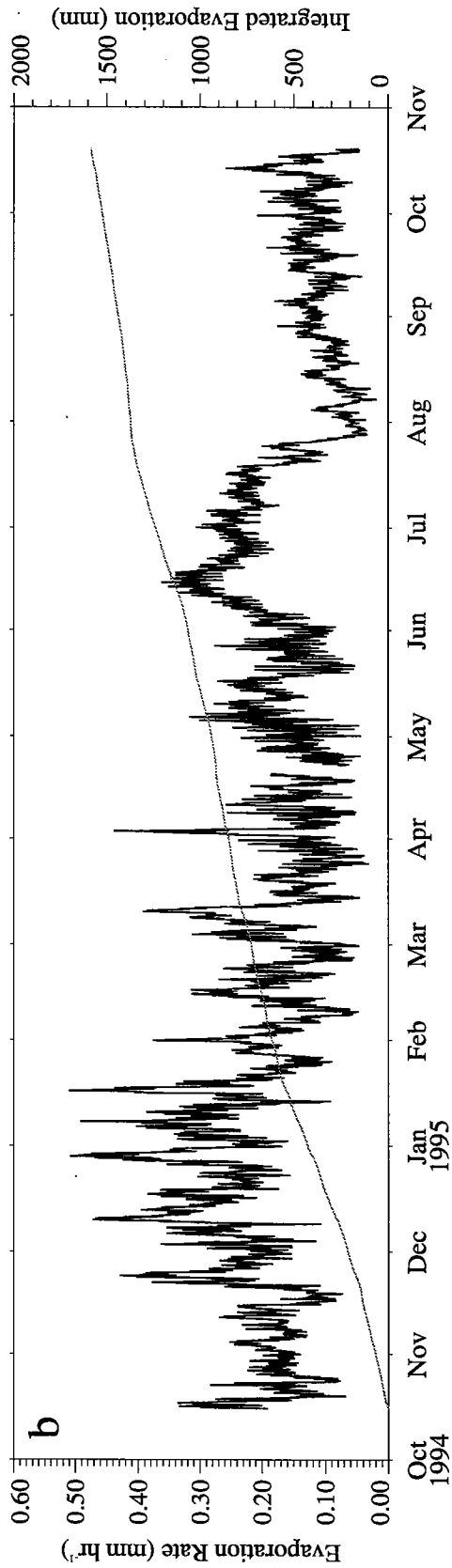
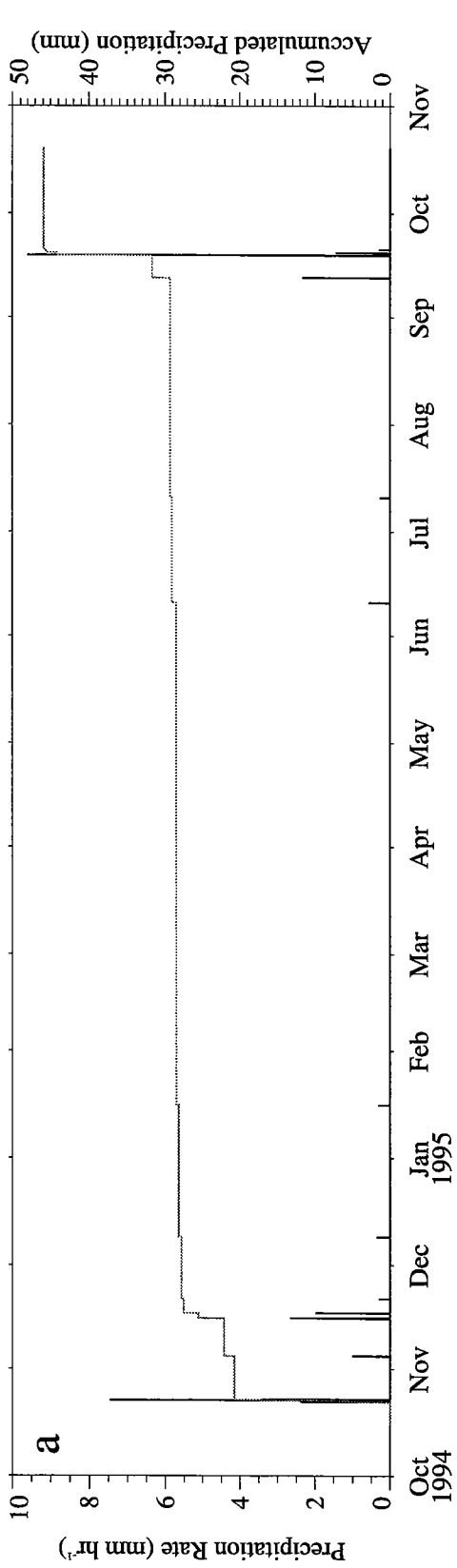


Figure 21. (a) Hourly averaged precipitation rate (black) and accumulated precipitation (gray) from IMET self-siphoning rain gauge. (b) Hourly averaged evaporation rate (black) and integrated evaporation (gray) from bulk formulae.

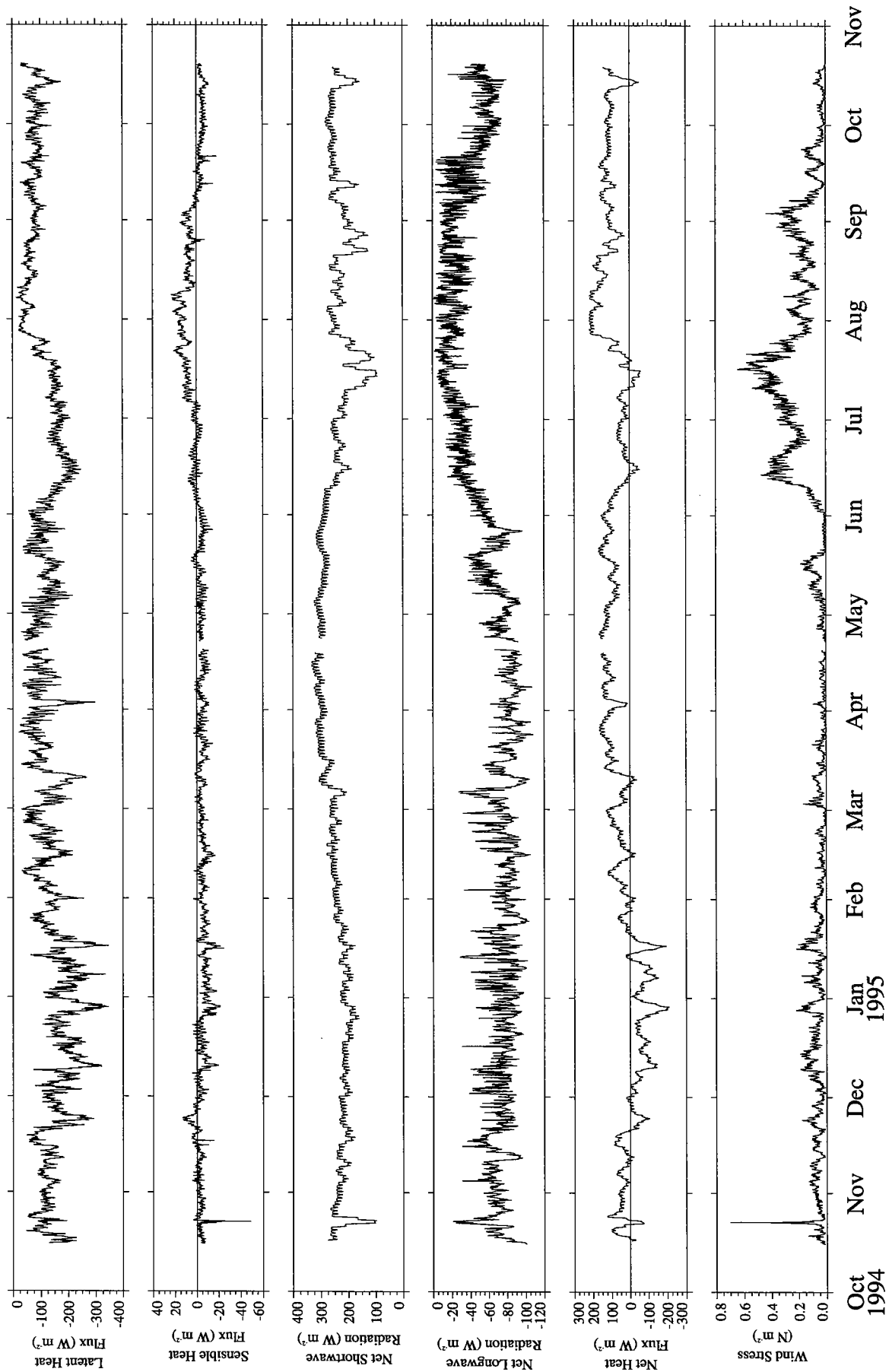


Figure 22. Hourly time series of estimated heat and momentum fluxes. Net short-wave and net heat flux each have a 48 hour running mean applied.

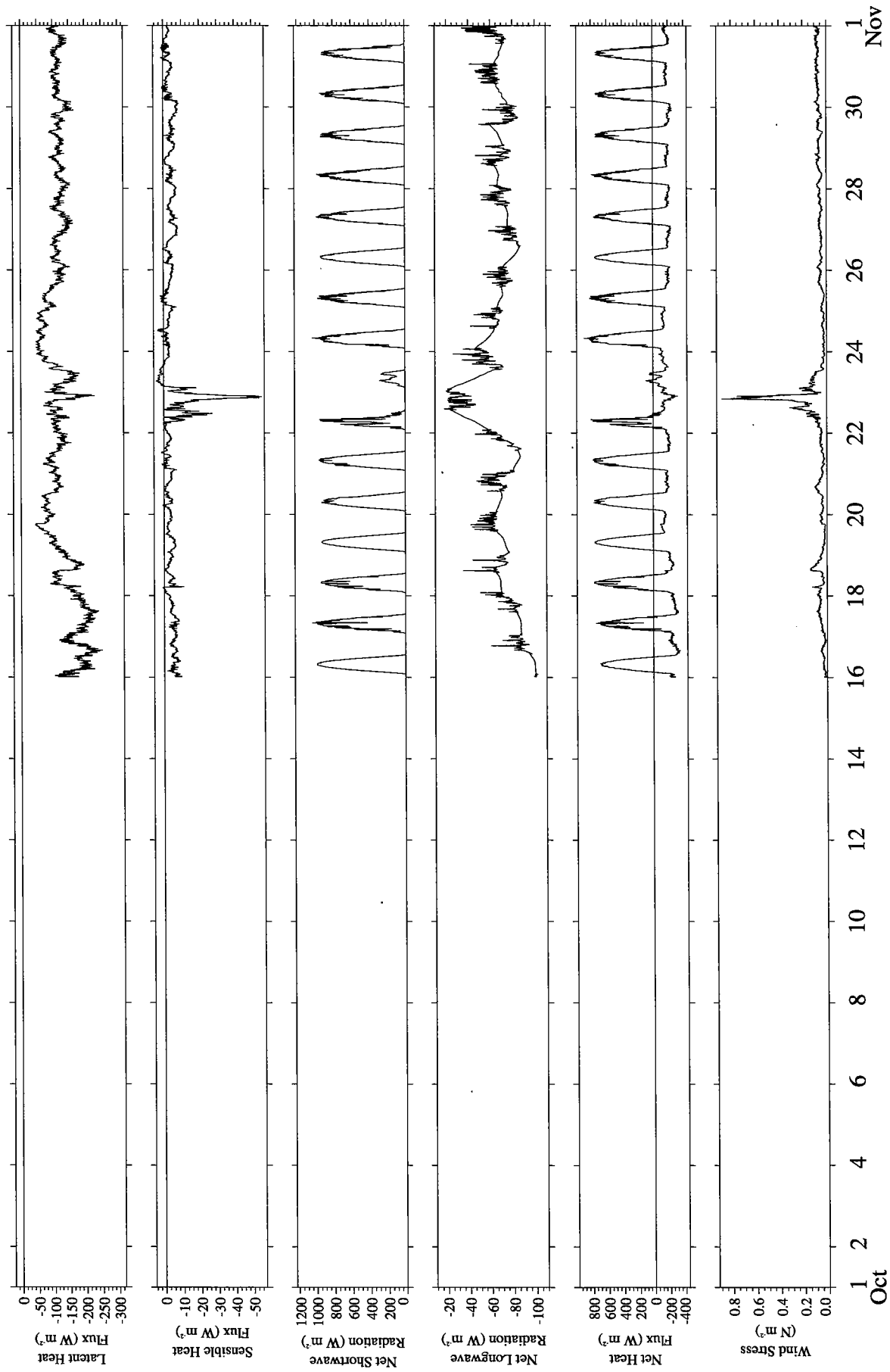


Figure 23. Four hundred fifty second time series of estimated heat and momentum fluxes for October 1994.

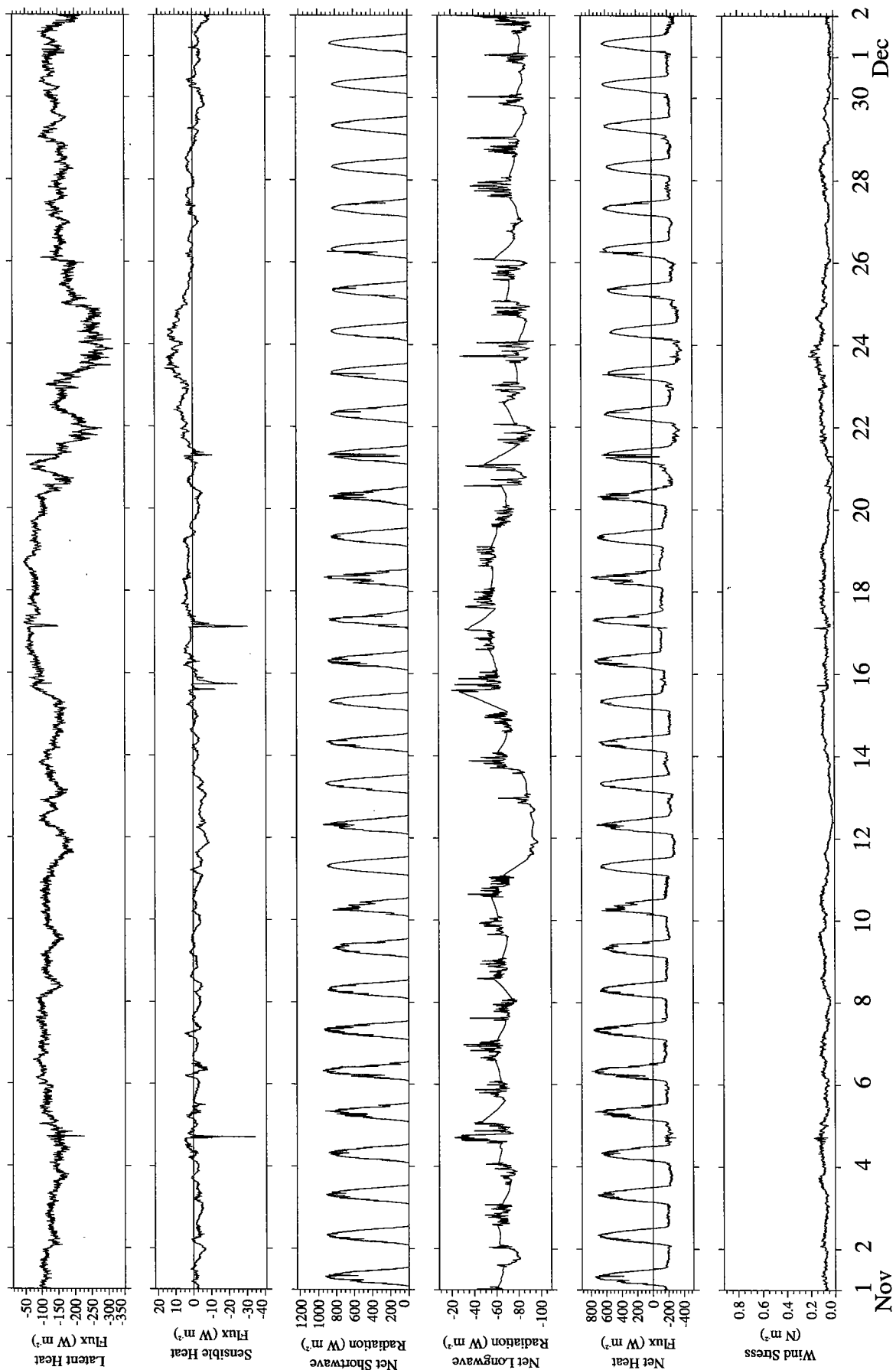


Figure 24. Four hundred fifty second time series of estimated heat and momentum fluxes for November 1994.

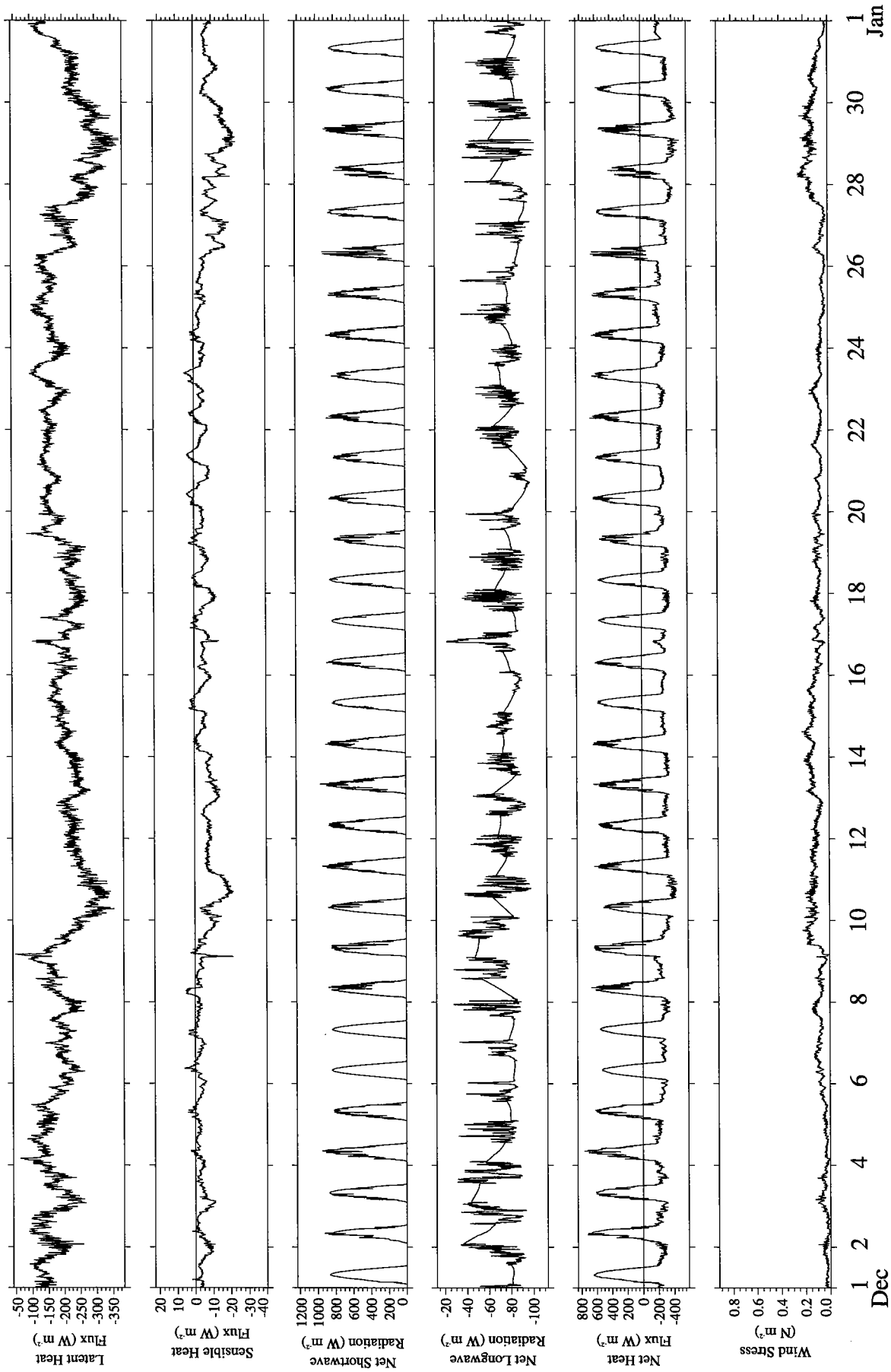


Figure 25. Four hundred fifty second time series of estimated heat and momentum fluxes for December 1994.

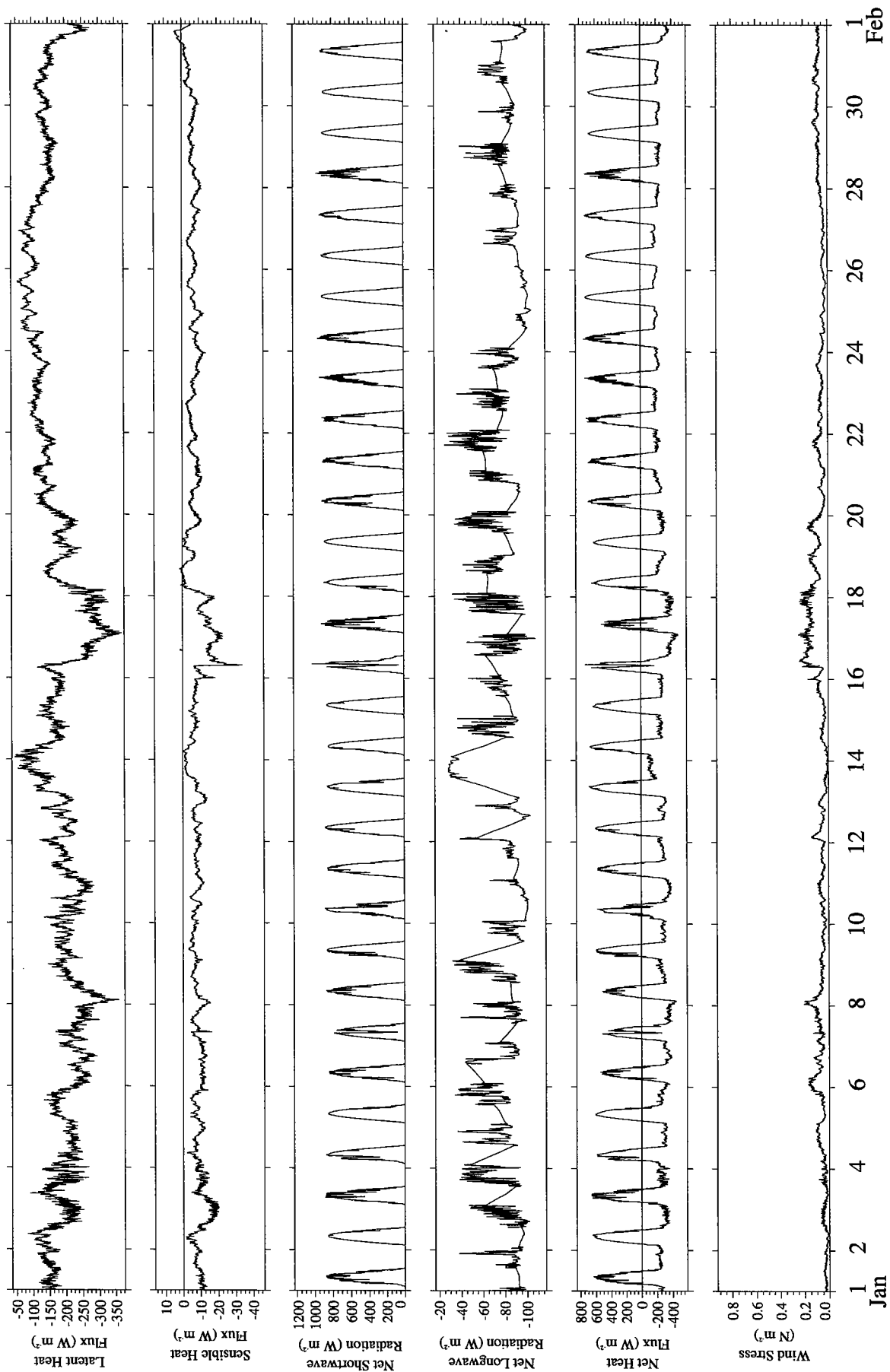


Figure 26. Four hundred fifty second time series of estimated heat and momentum fluxes for January 1995.

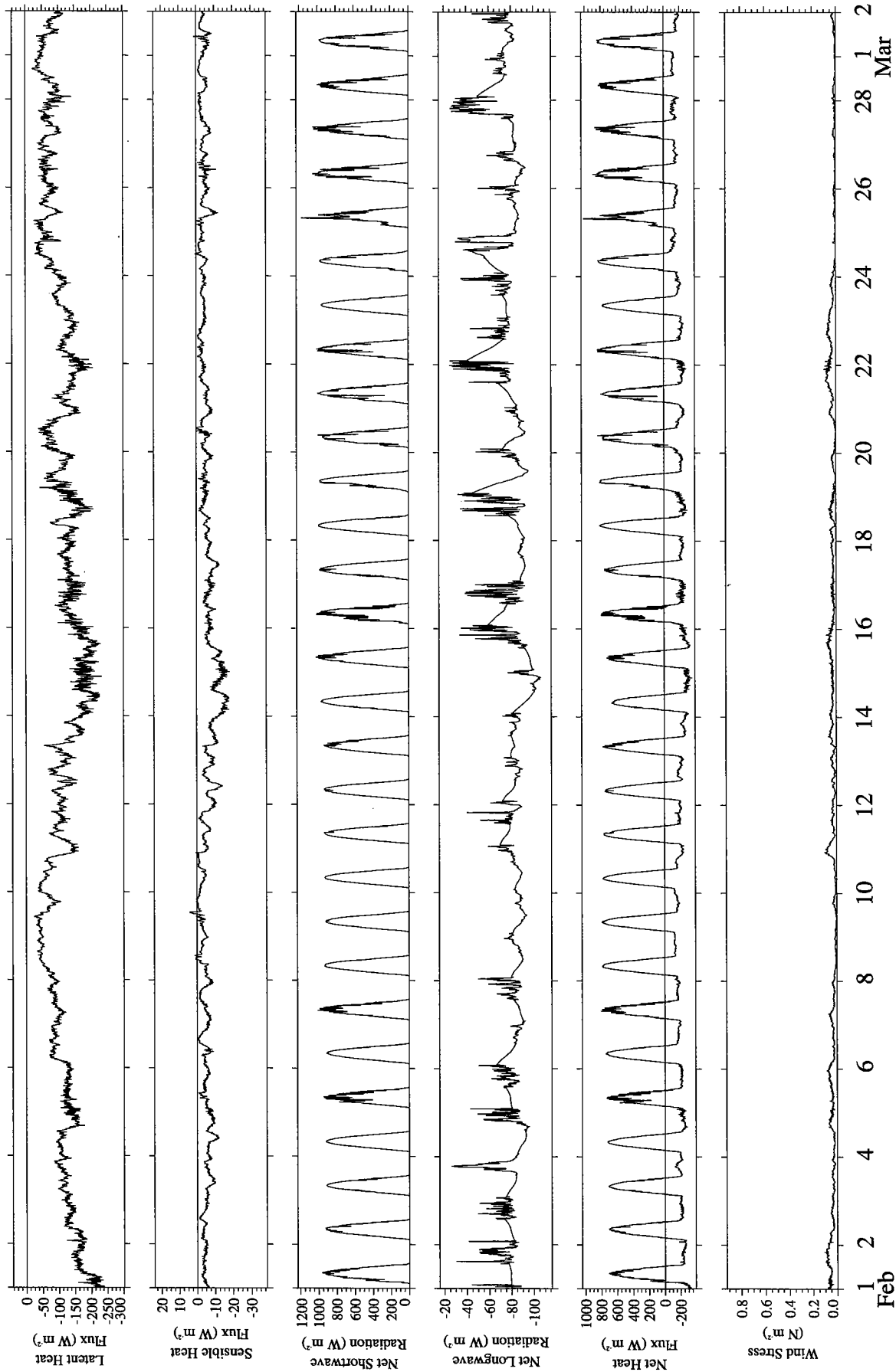


Figure 27. Four hundred fifty second time series of estimated heat and momentum fluxes for February 1995.

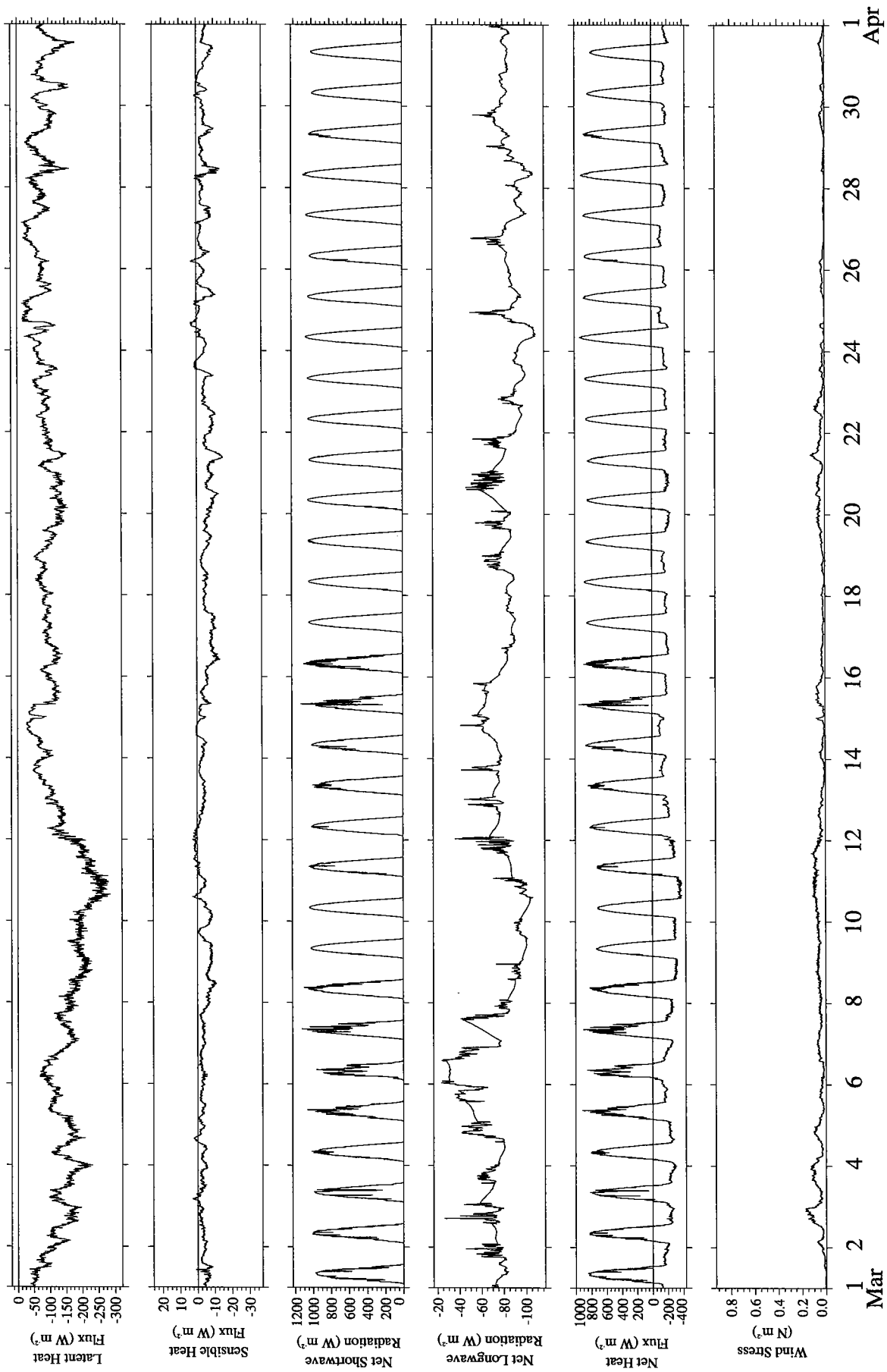


Figure 28. Four hundred fifty second time series of estimated heat and momentum fluxes for March 1995.

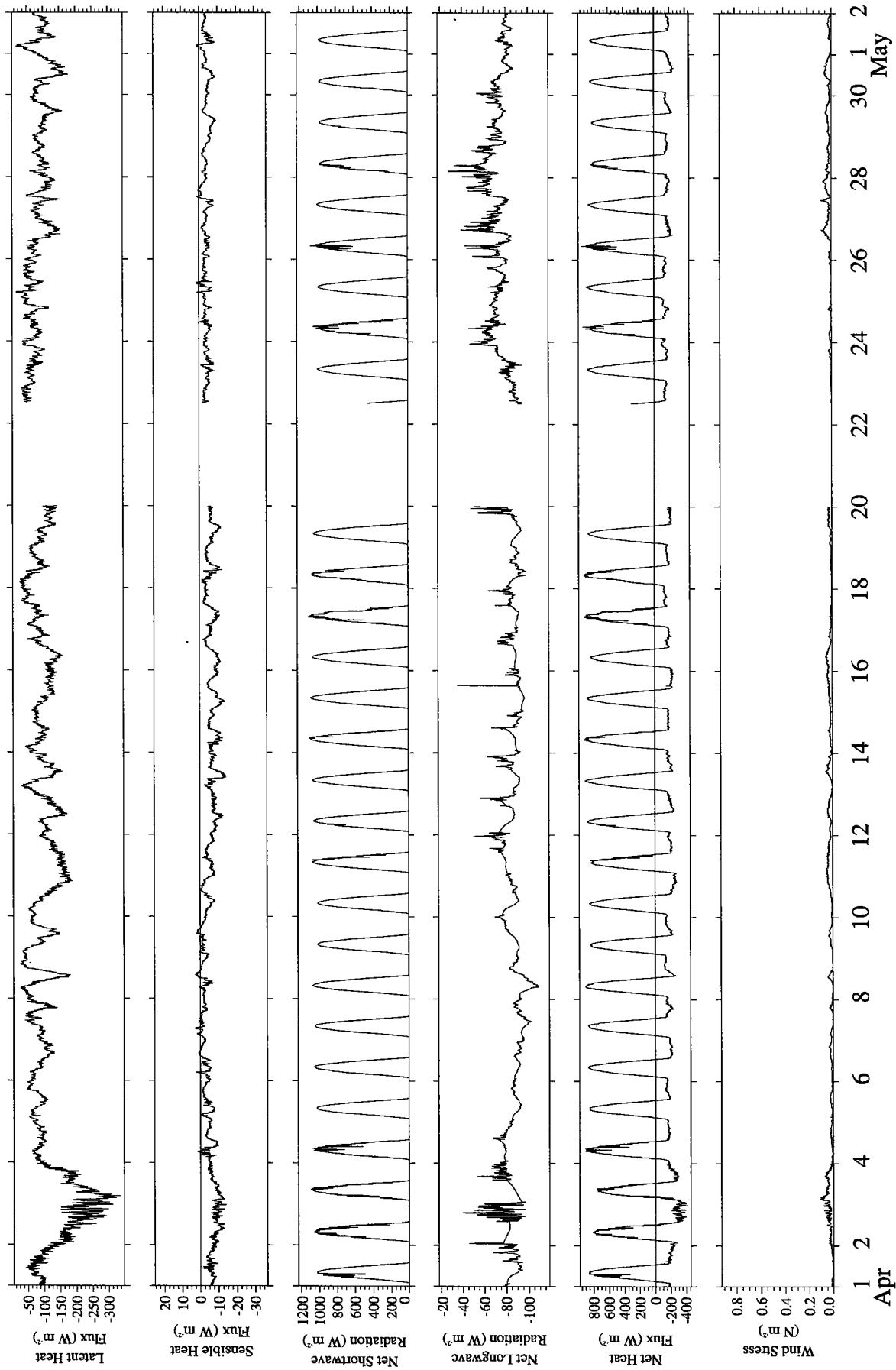


Figure 29. Four hundred fifty second time series of estimated heat and momentum fluxes for April 1995.

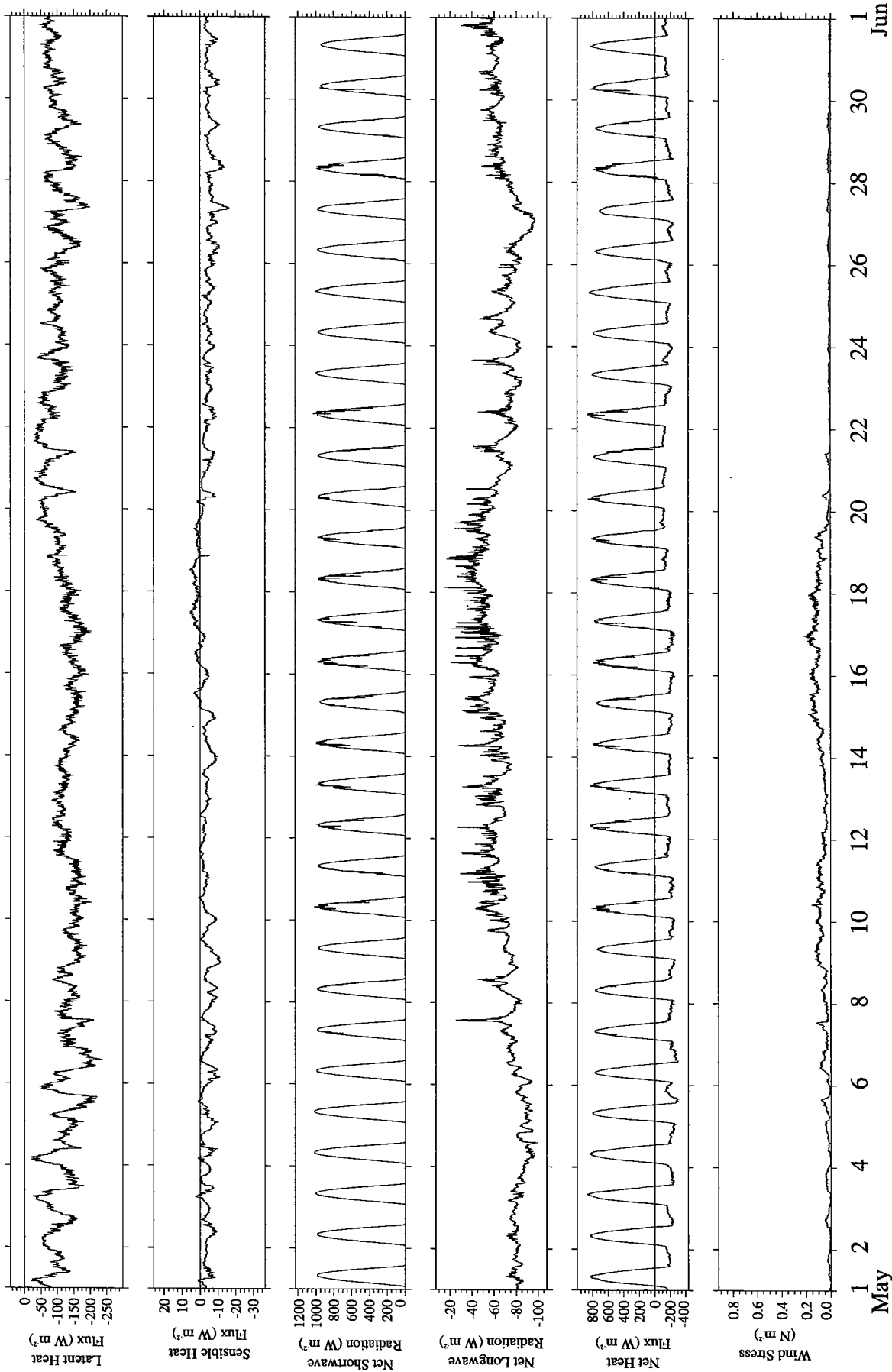


Figure 30. Four hundred fifty second time series of estimated heat and momentum fluxes for May 1995.

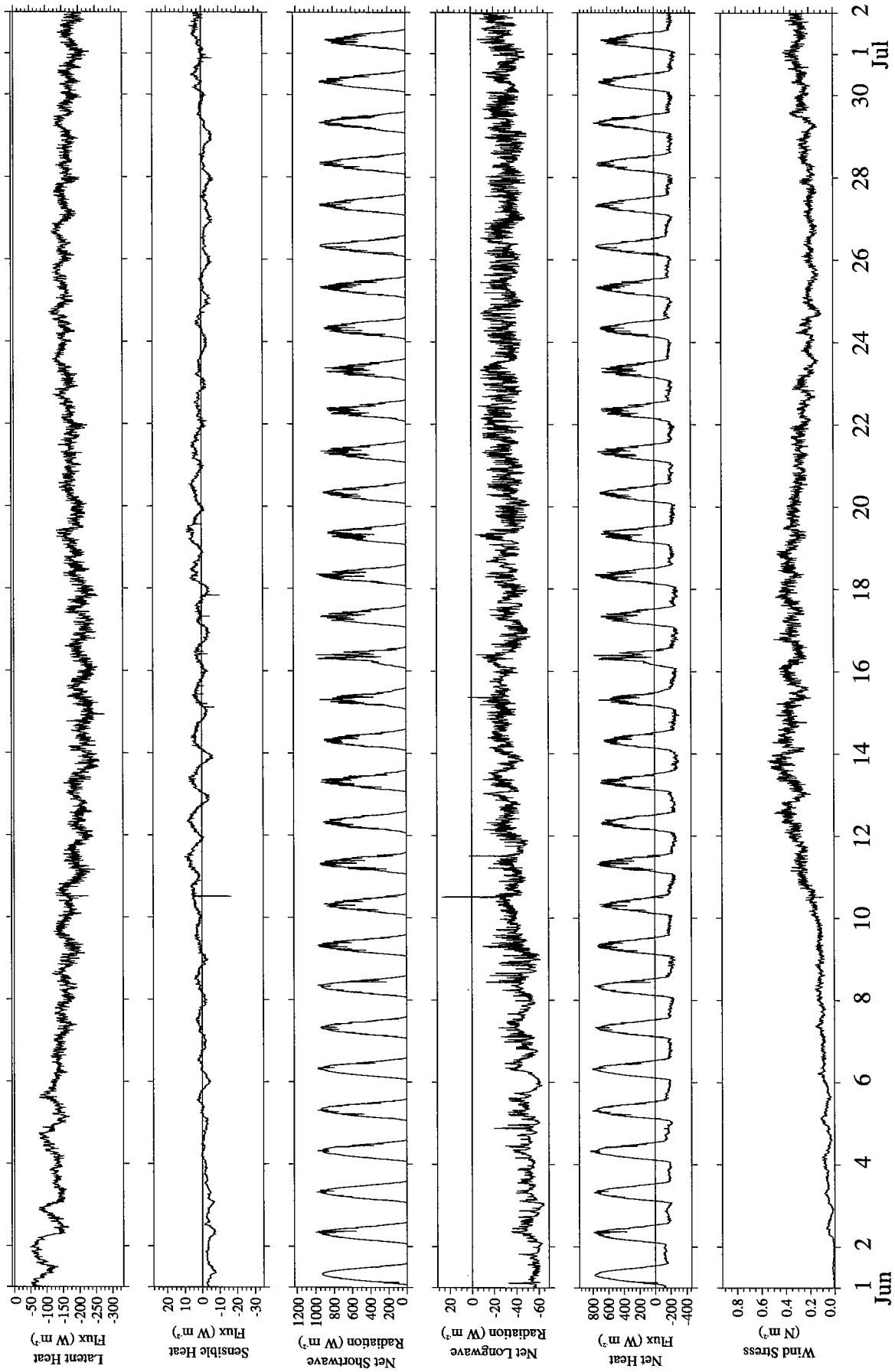


Figure 31. Four hundred fifty second time series of estimated heat and momentum fluxes for June 1995.

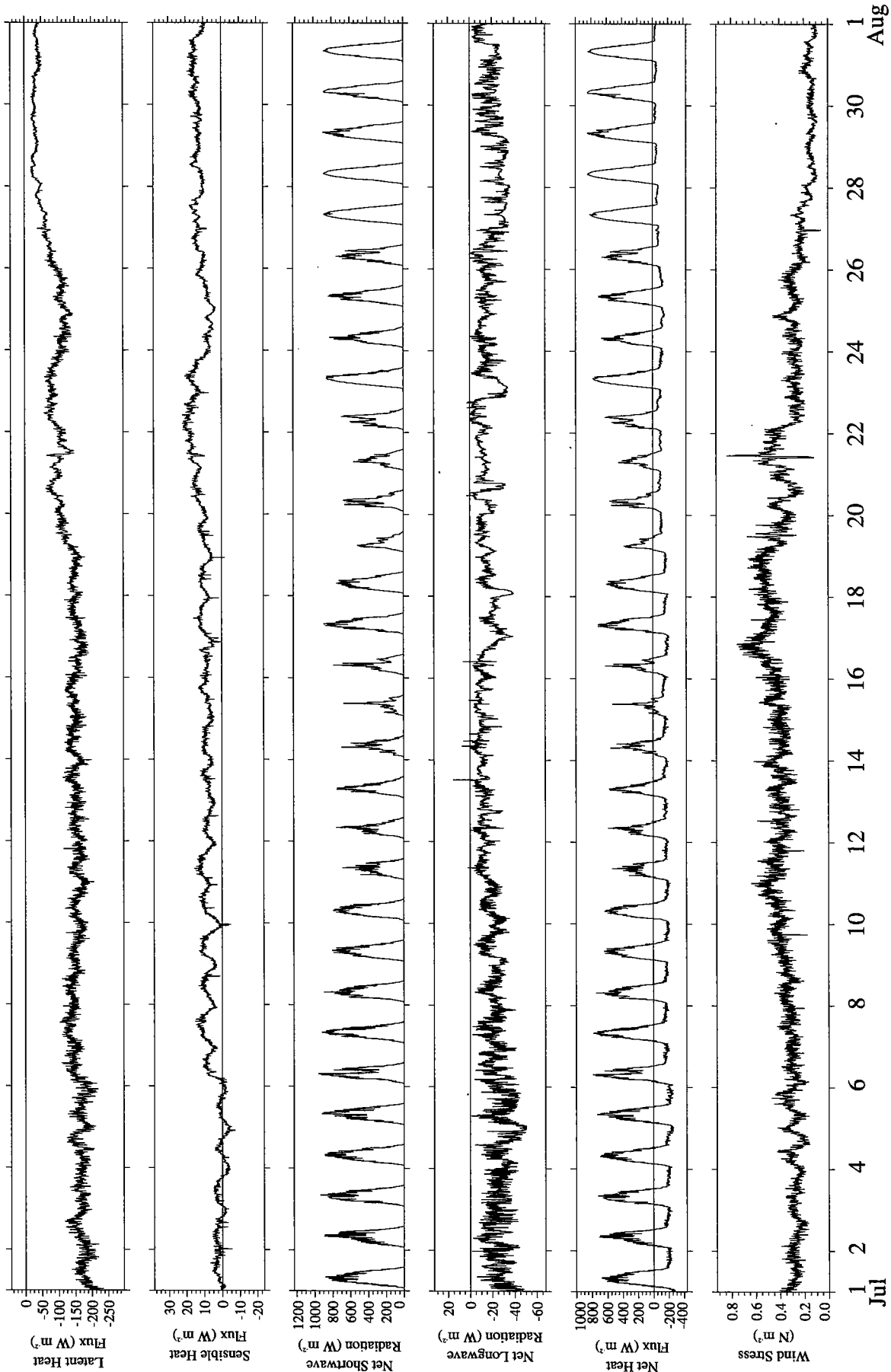


Figure 32. Four hundred fifty second time series of estimated heat and momentum fluxes for July 1995.

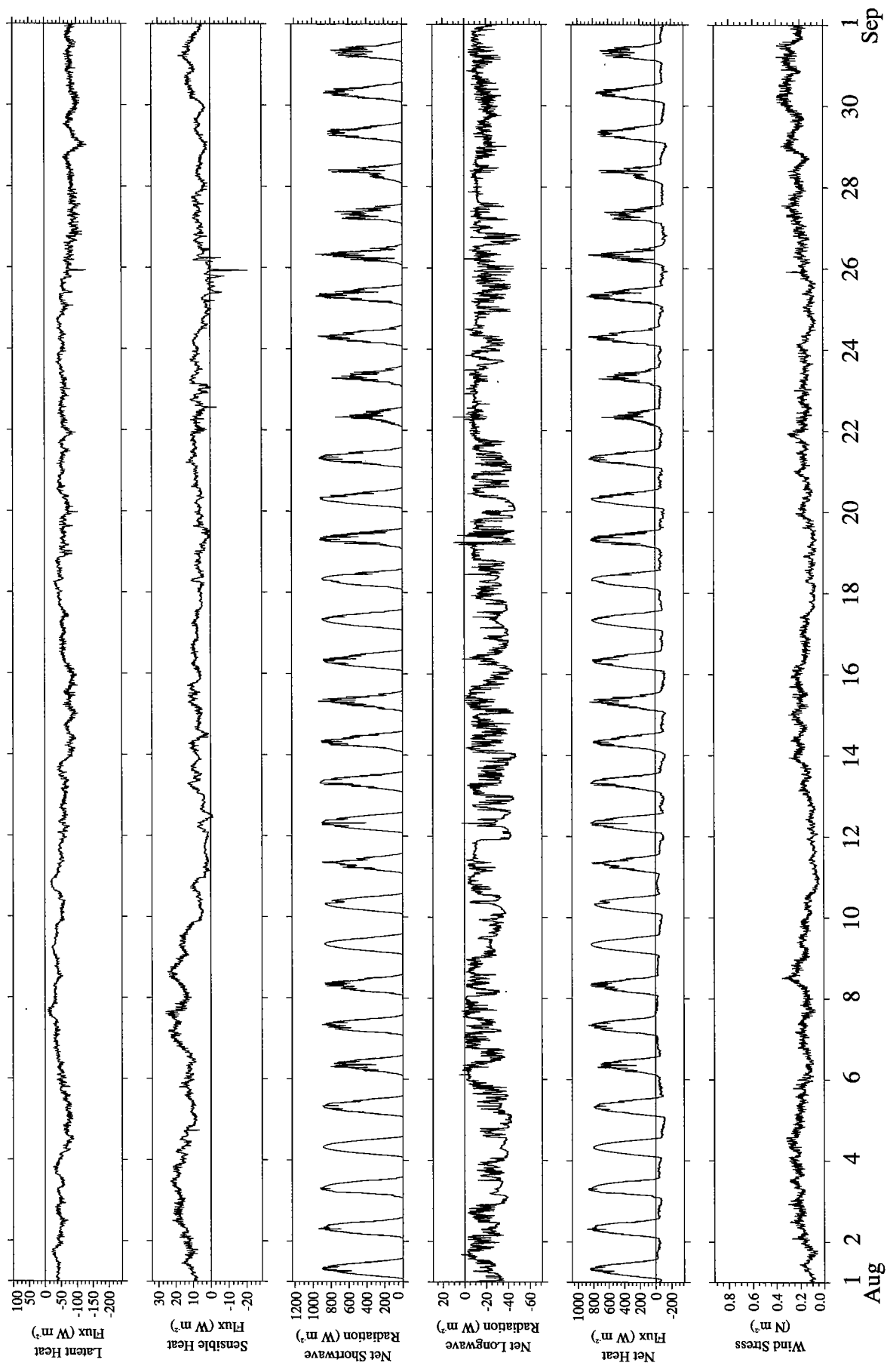


Figure 33. Four hundred fifty second time series of estimated heat and momentum fluxes for August 1995.

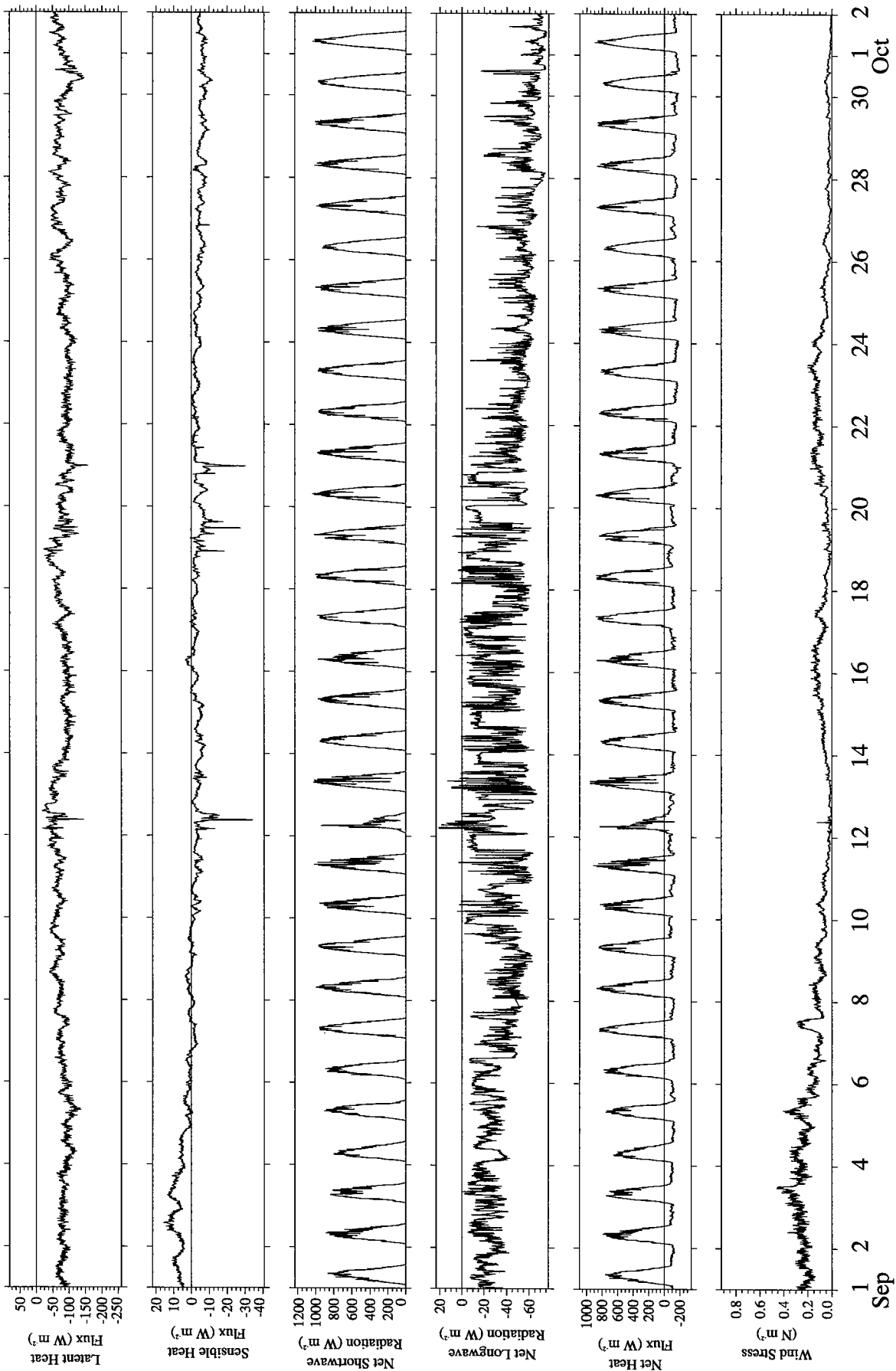


Figure 34. Four hundred fifty second time series of estimated heat and momentum fluxes for September 1995.

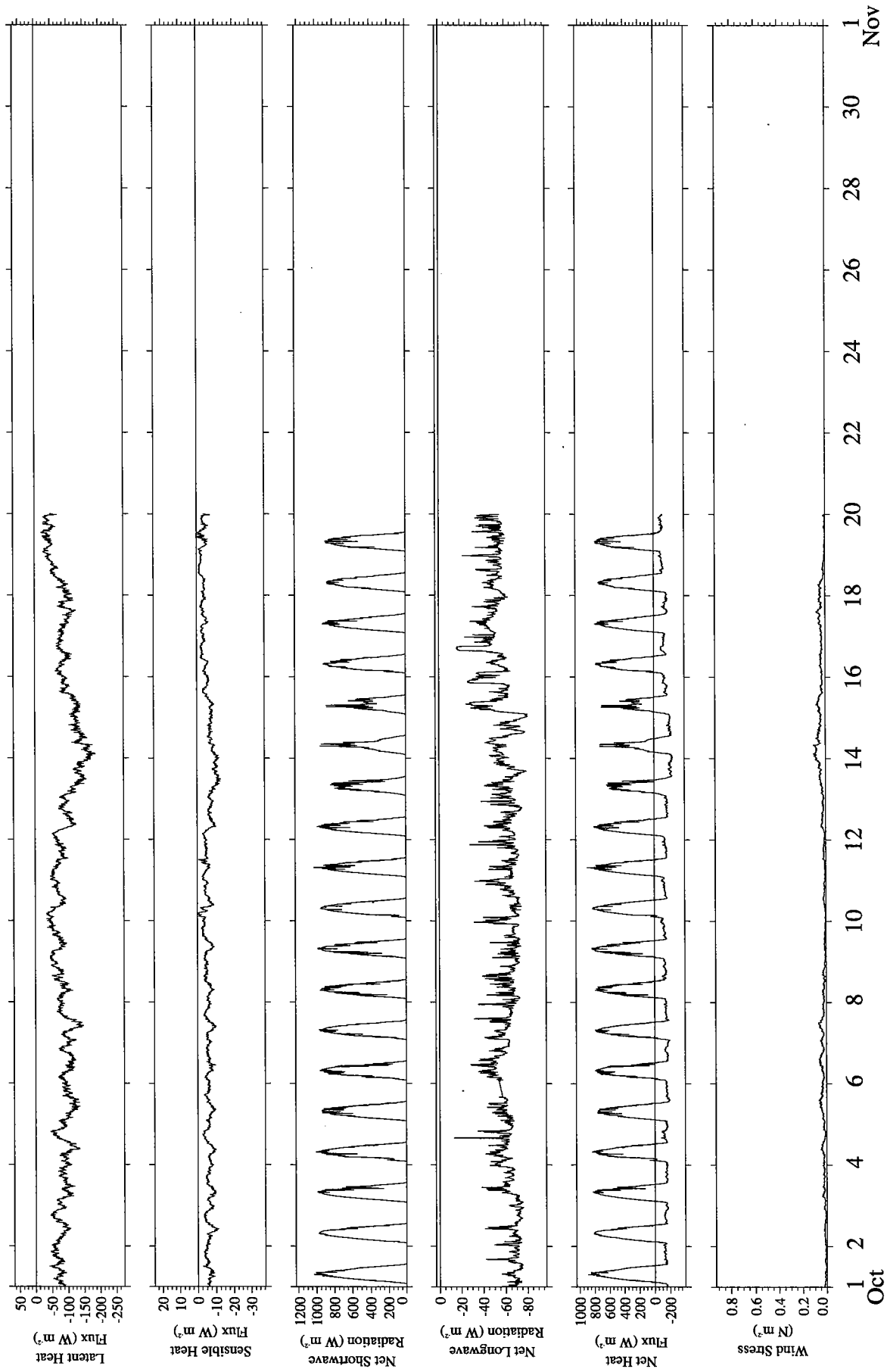


Figure 35. Four hundred fifty second time series of estimated heat and momentum fluxes for October 1995.

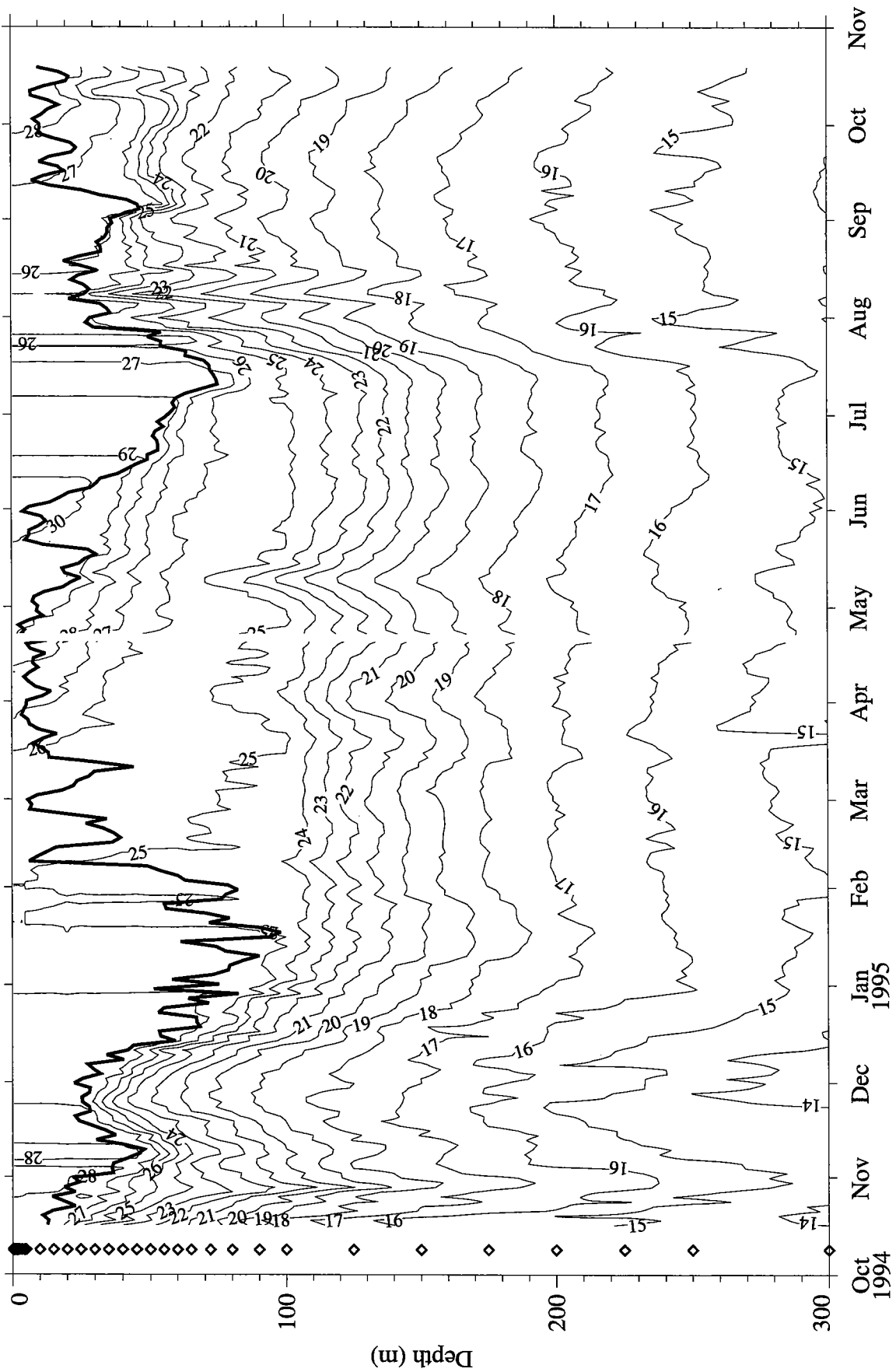


Figure 36. Contour plot of 36 hour averaged temperature and mixed layer depth (thick). Diamonds indicate measurement depths. Isotherms are in units of °C.

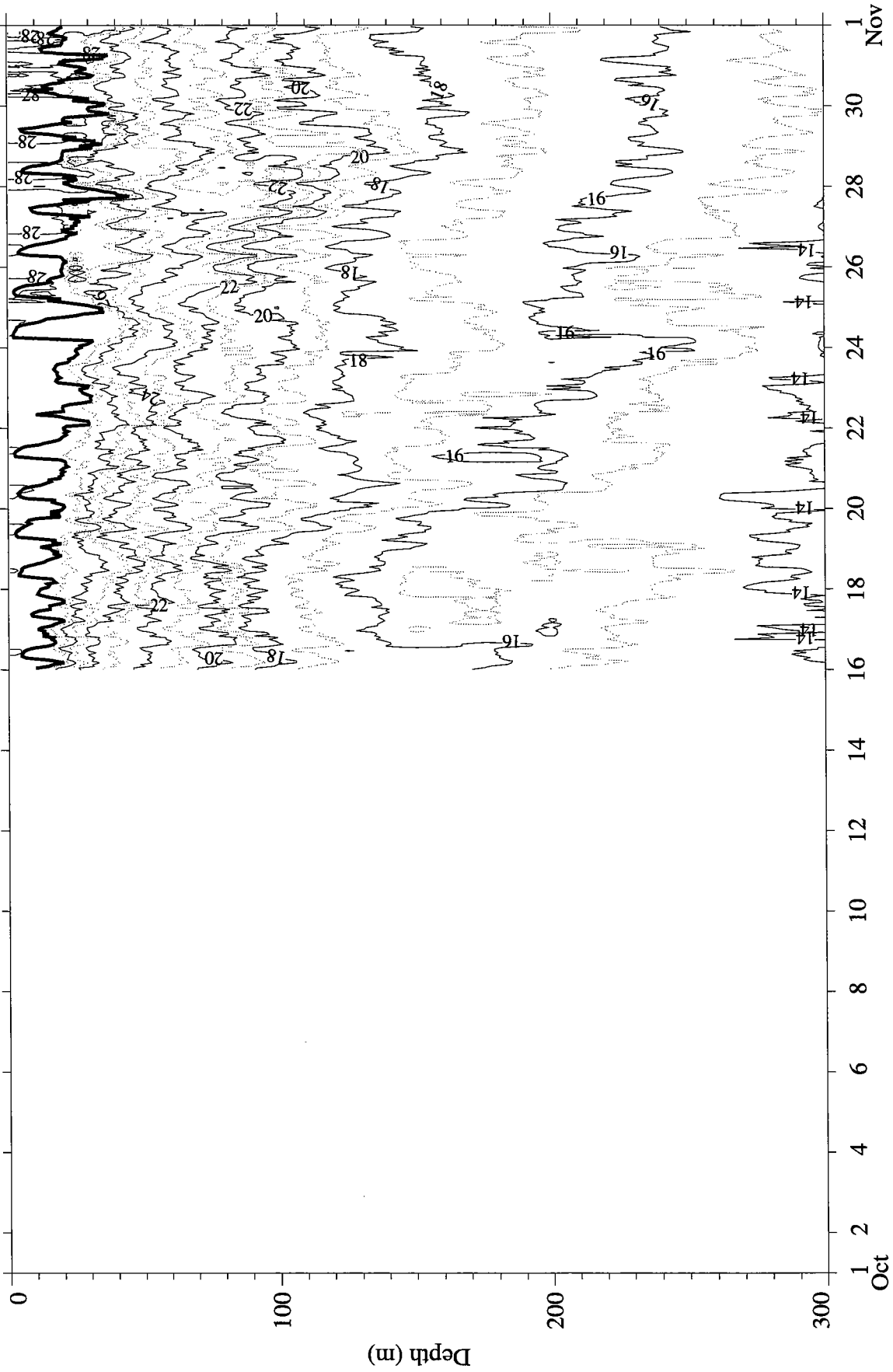


Figure 37. Contour plot of hourly averaged temperature and mixed layer depth (thick) for October, 1994. Isotherms are in units of °C.

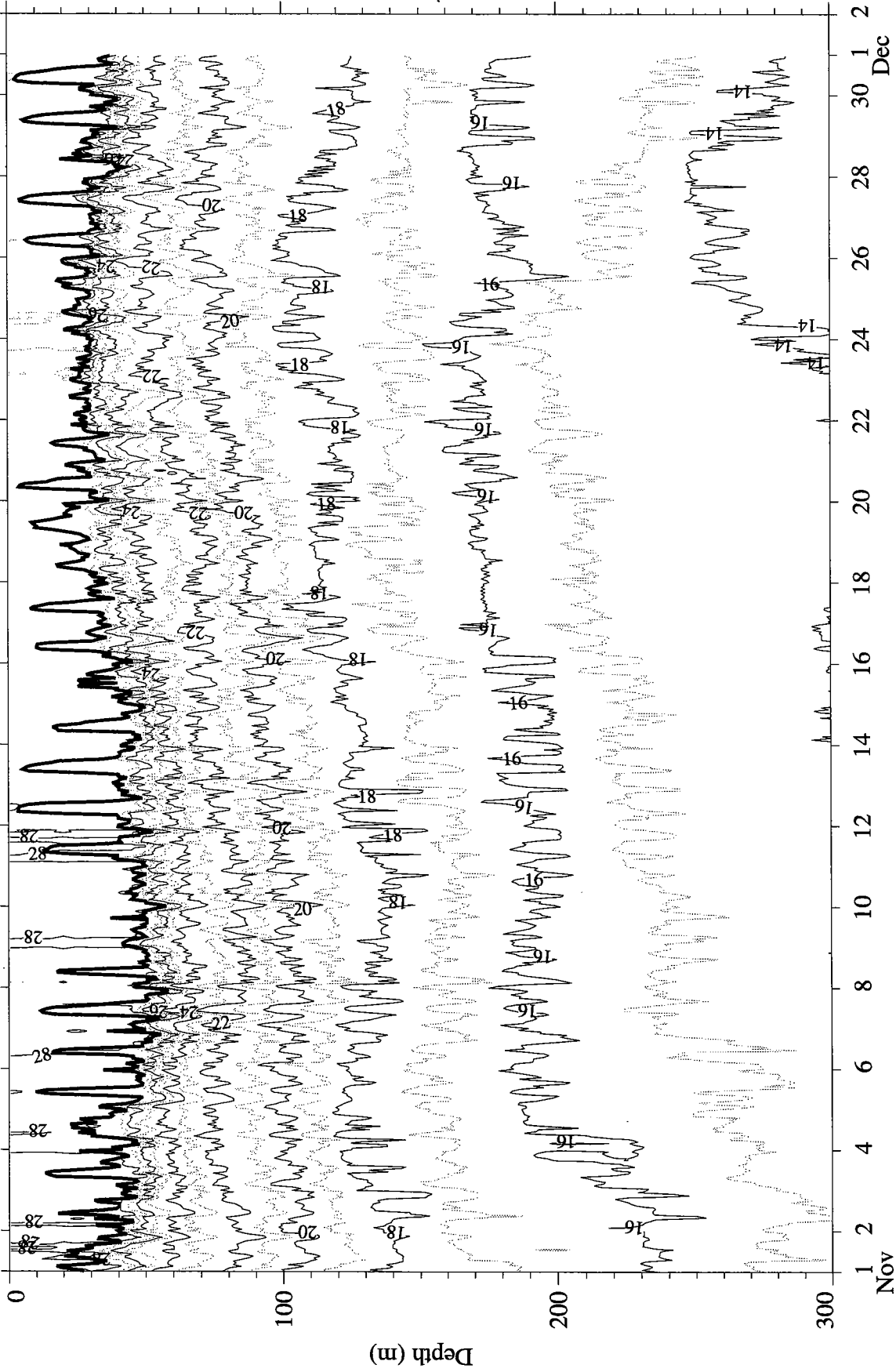


Figure 38. Contour plot of hourly averaged temperature and mixed layer depth (thick) for November, 1994. Isotherms are in units of °C.

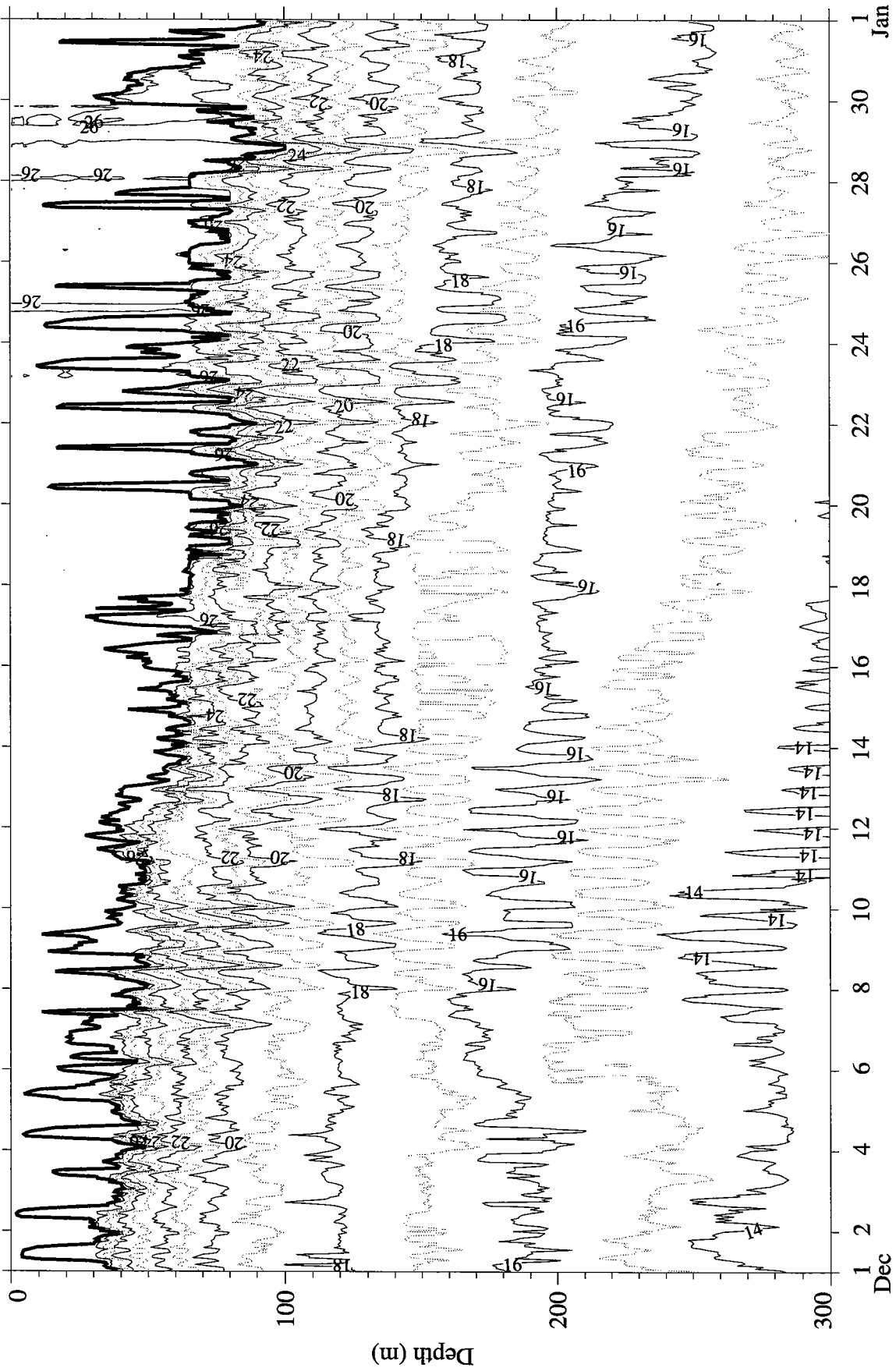


Figure 39. Contour plot of hourly averaged temperature and mixed layer depth (thick) for December, 1994. Isotherms are in units of °C.

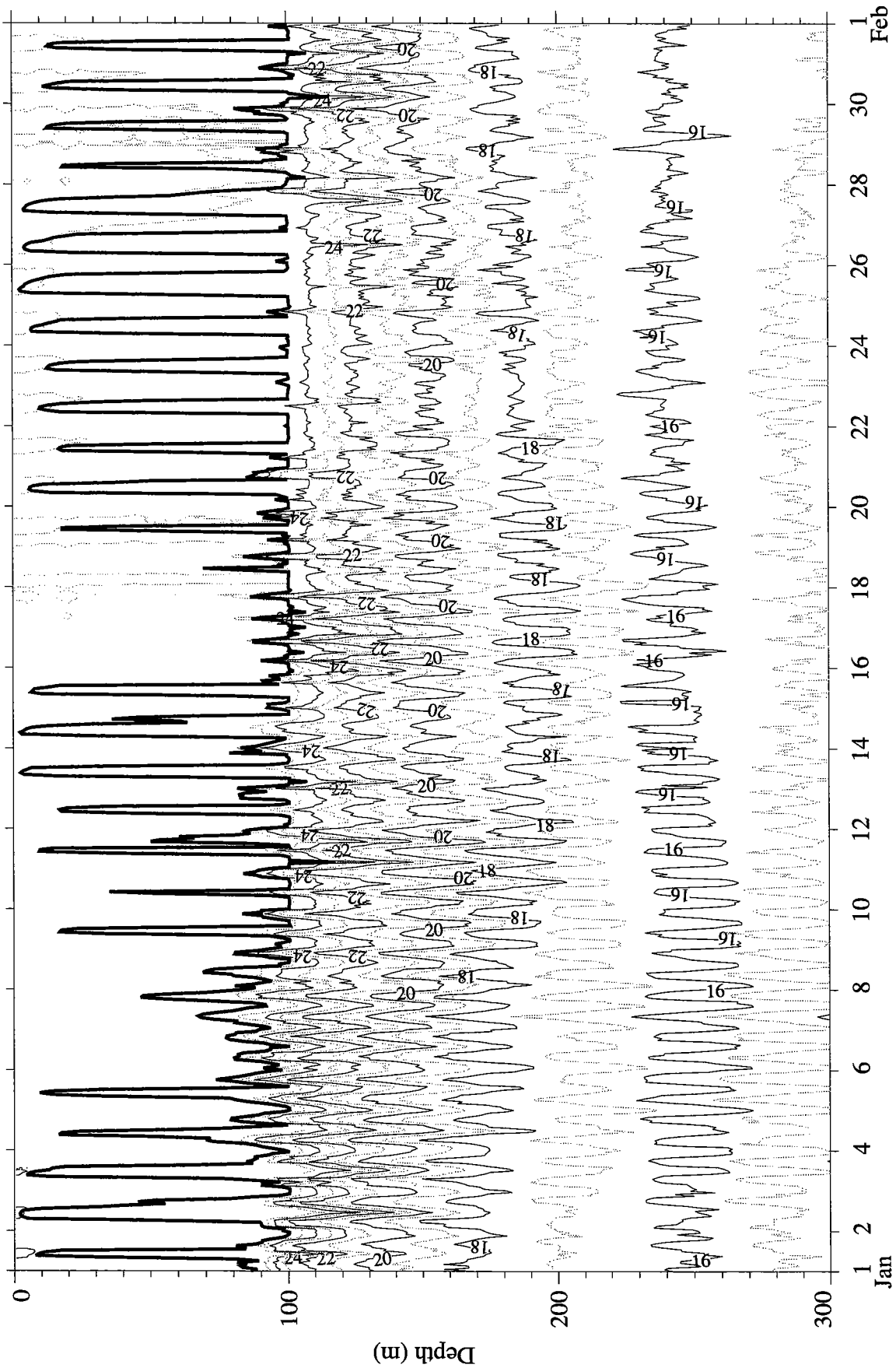


Figure 40. Contour plot of hourly averaged temperature and mixed layer depth (thick) for January, 1995. Isotherms are in units of °C.

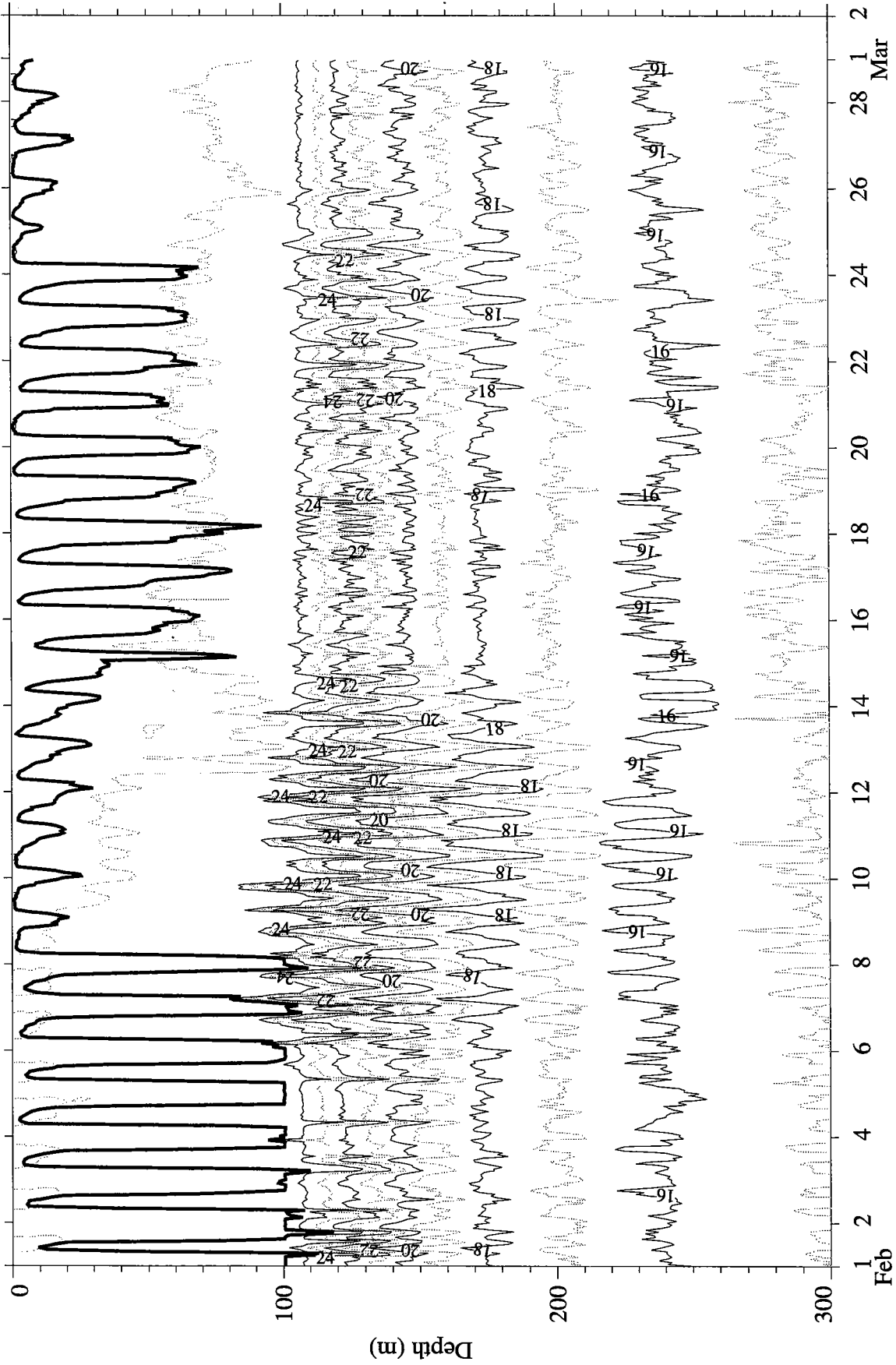


Figure 41. Contour plot of hourly averaged temperature and mixed layer depth (thick) for February, 1995. Isotherms are in units of °C.

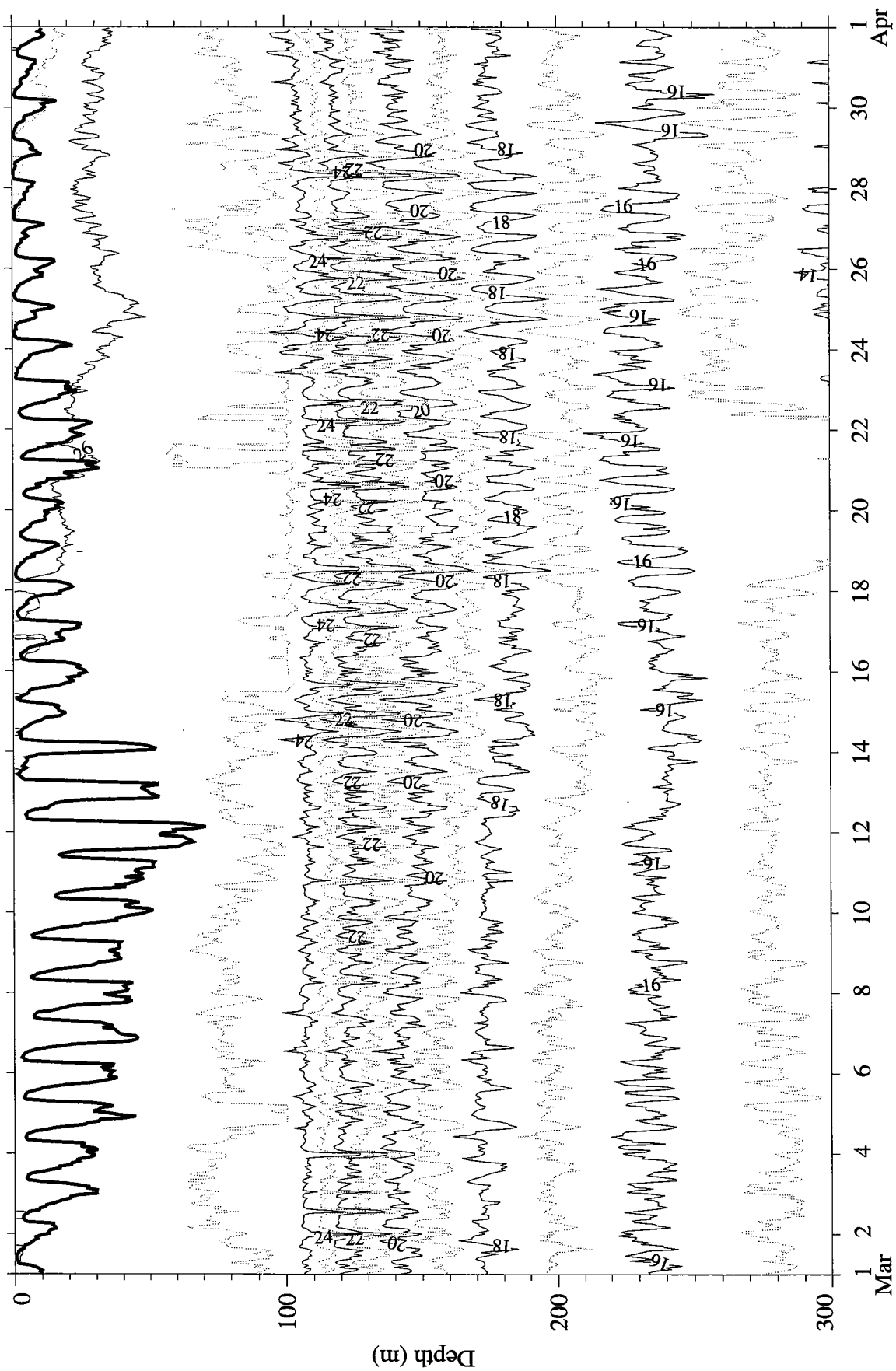


Figure 42. Contour plot of hourly averaged temperature and mixed layer depth (thick) for March, 1995. Isotherms are in units of °C.

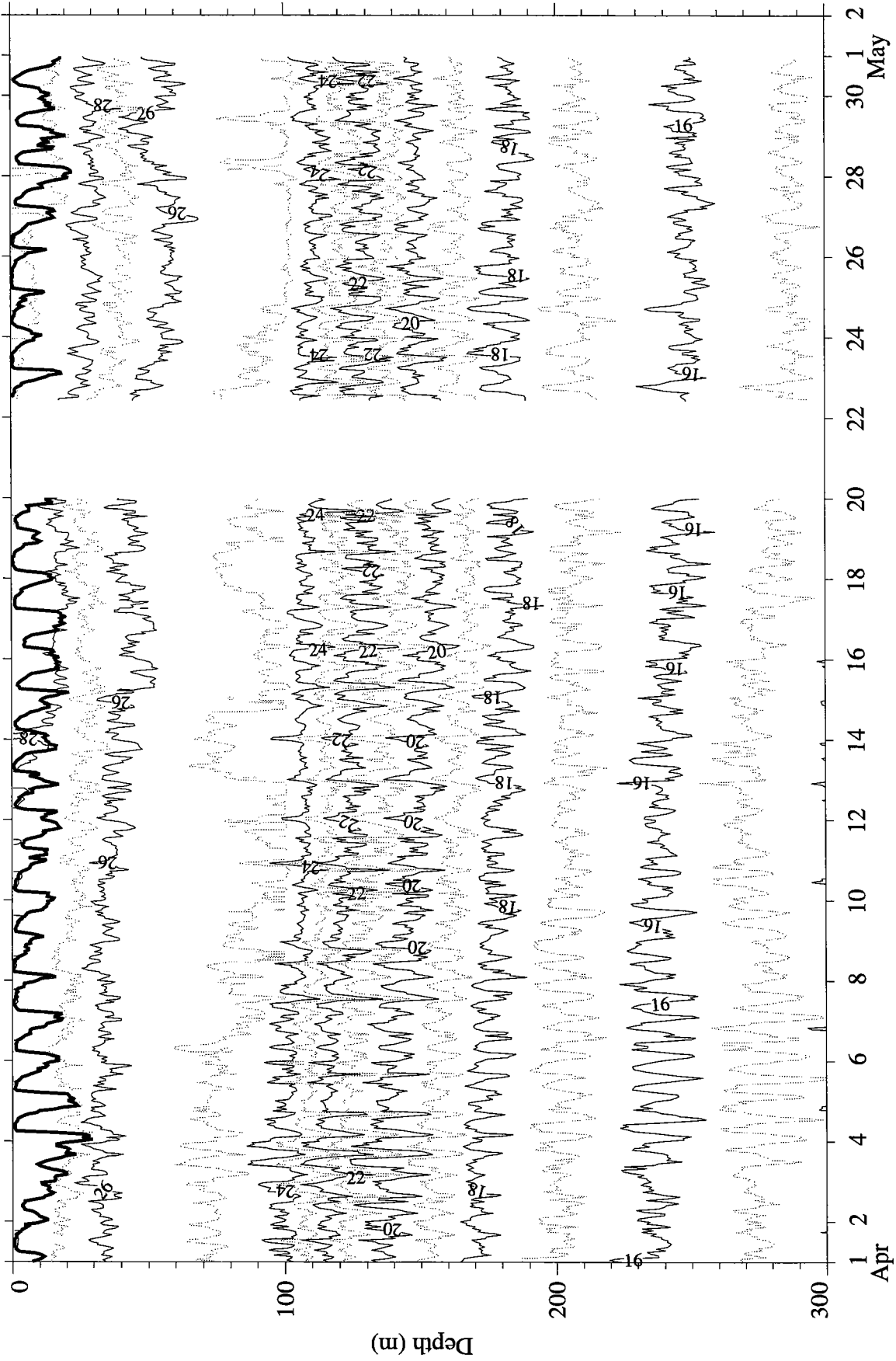


Figure 43. Contour plot of hourly averaged temperature and mixed layer depth (thick) for April, 1995. Isotherms are in units of °C.

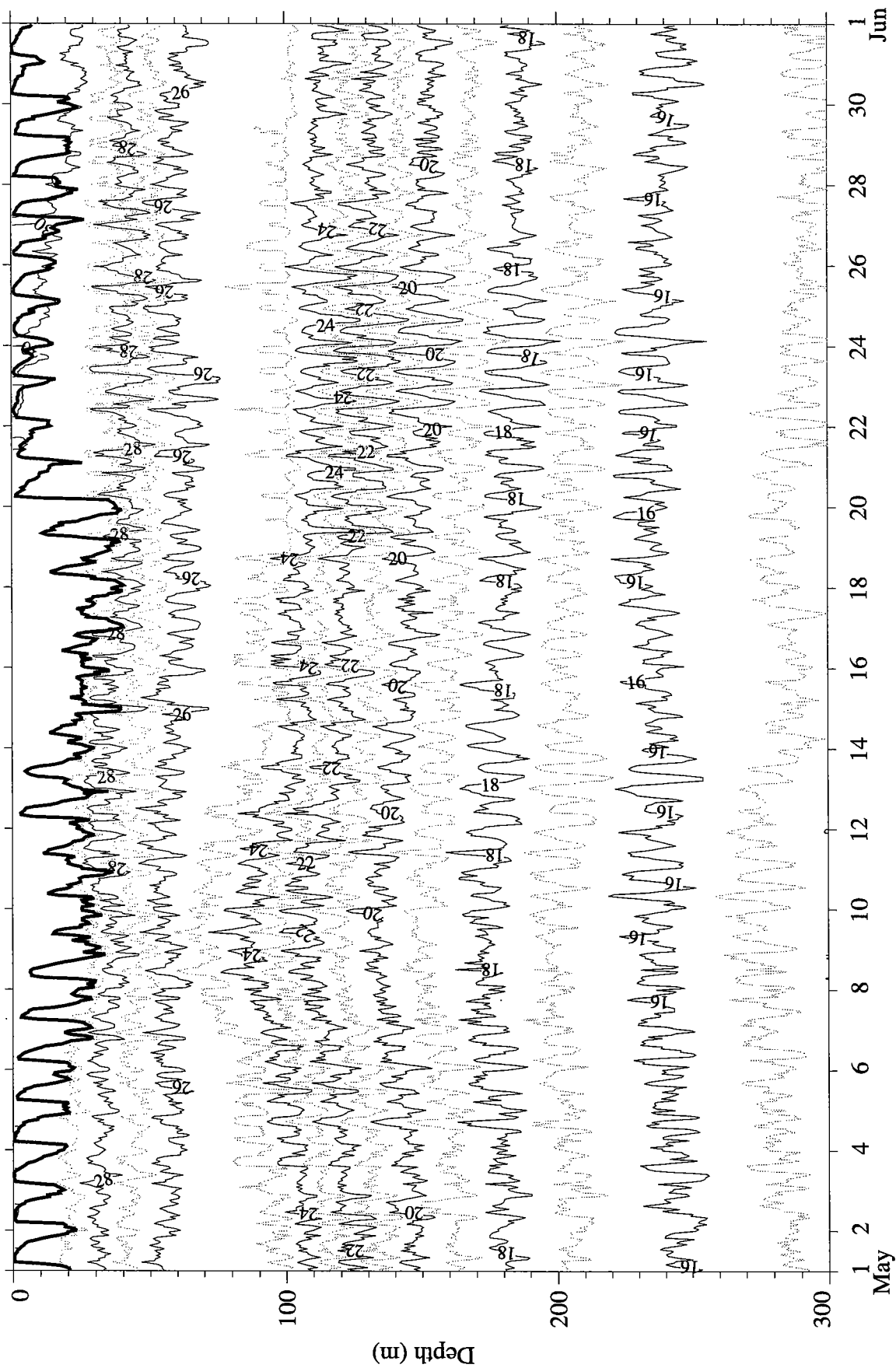


Figure 44. Contour plot of hourly averaged temperature and mixed layer depth (thick) for May, 1995. Isotherms are in units of °C.

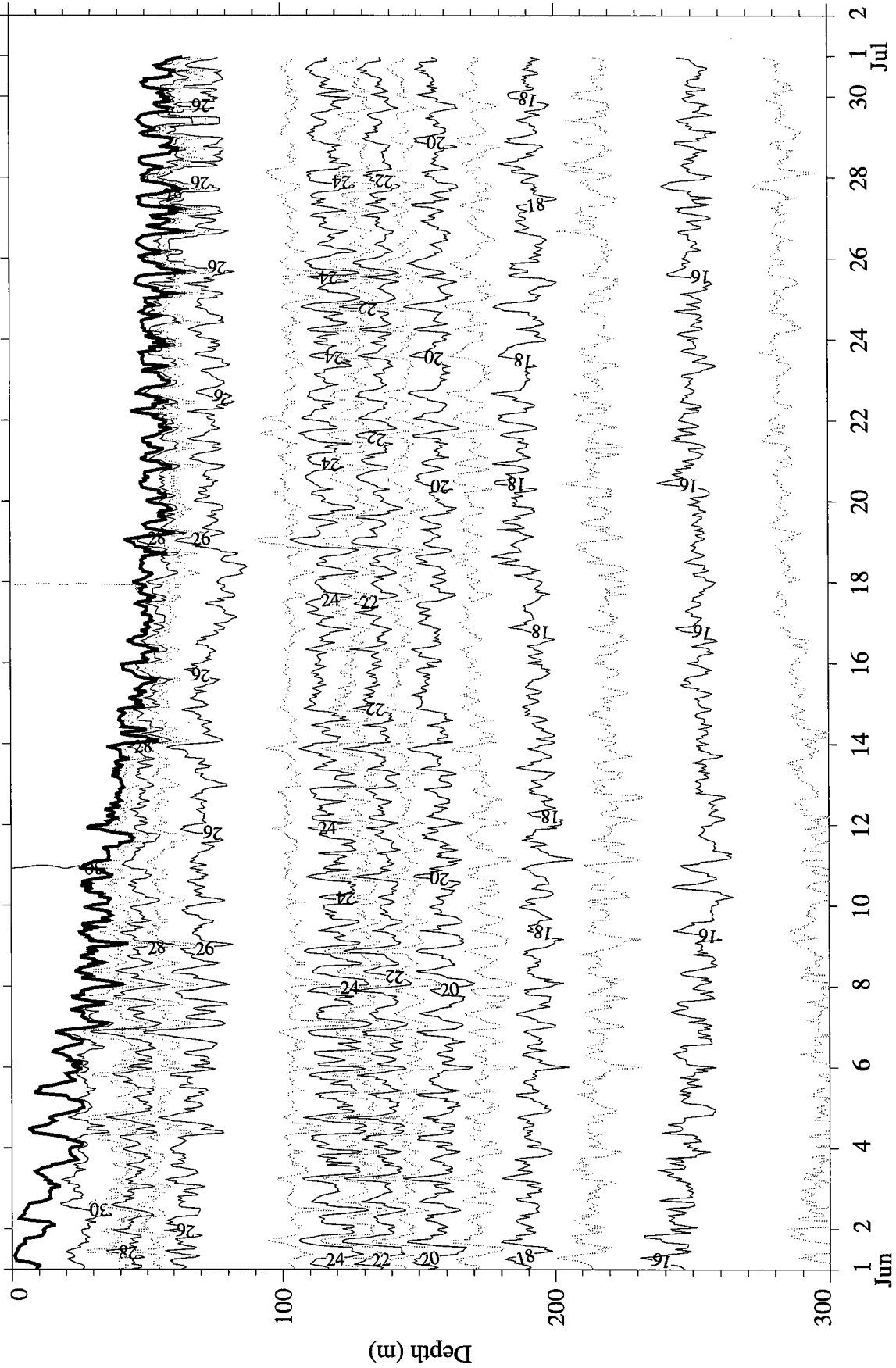


Figure 45. Contour plot of hourly averaged temperature and mixed layer depth (thick) for June, 1995. Isotherms are in units of °C.

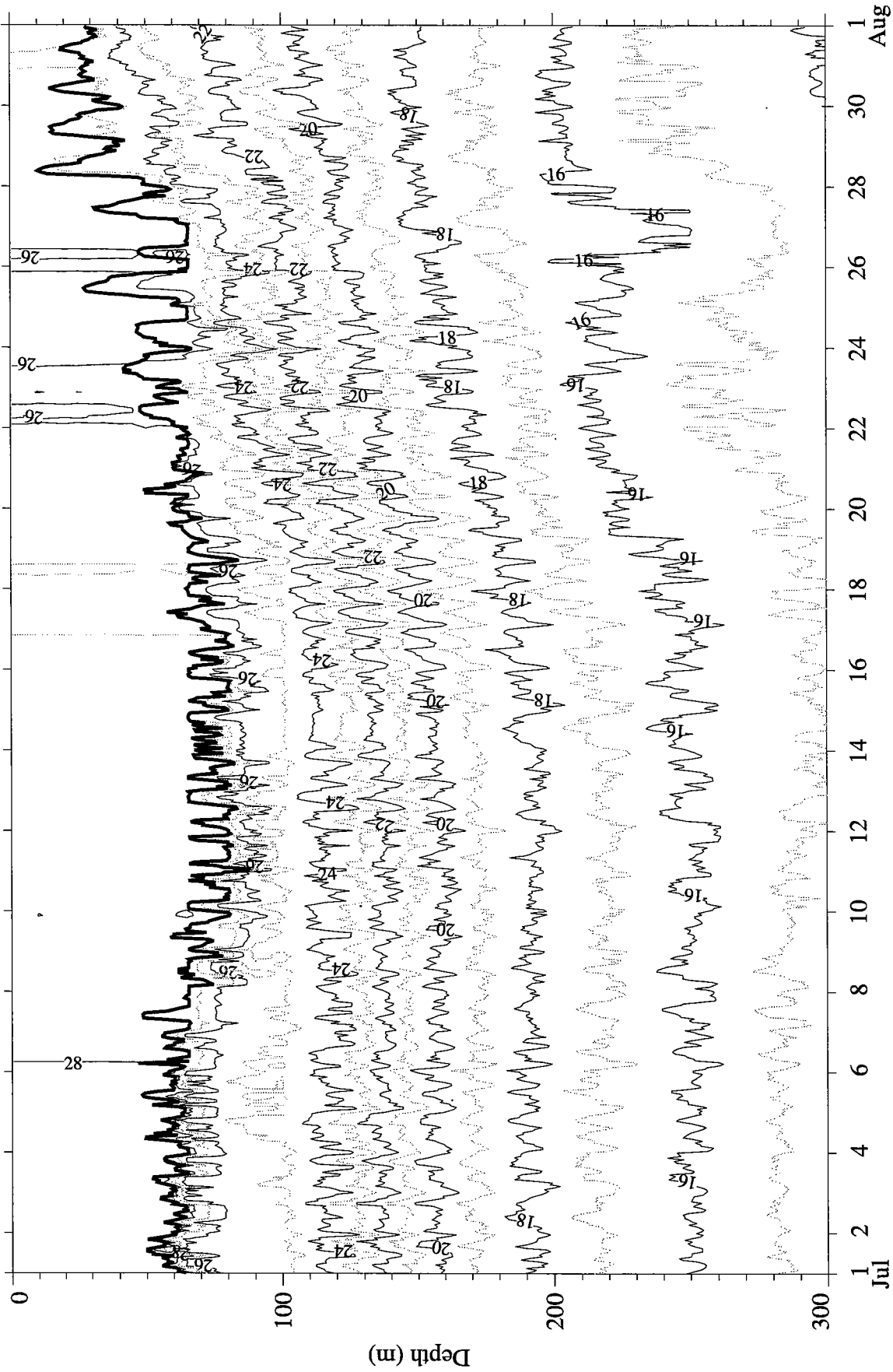


Figure 46. Contour plot of hourly averaged temperature and mixed layer depth (thick) for July, 1995. Isotherms are in units of °C.

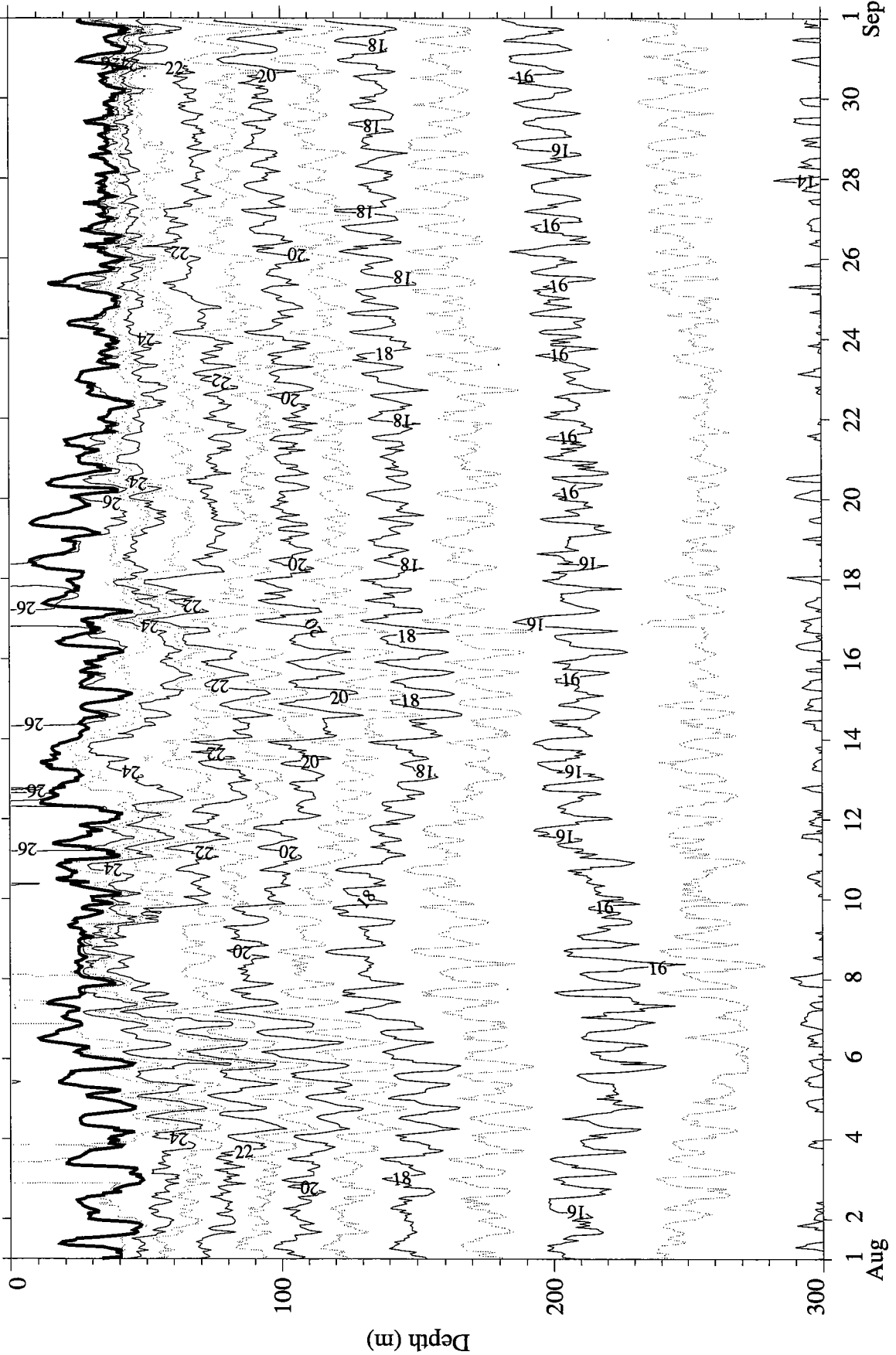


Figure 47. Contour plot of hourly averaged temperature and mixed layer depth (thick) for August, 1995. Isotherms are in units of °C.

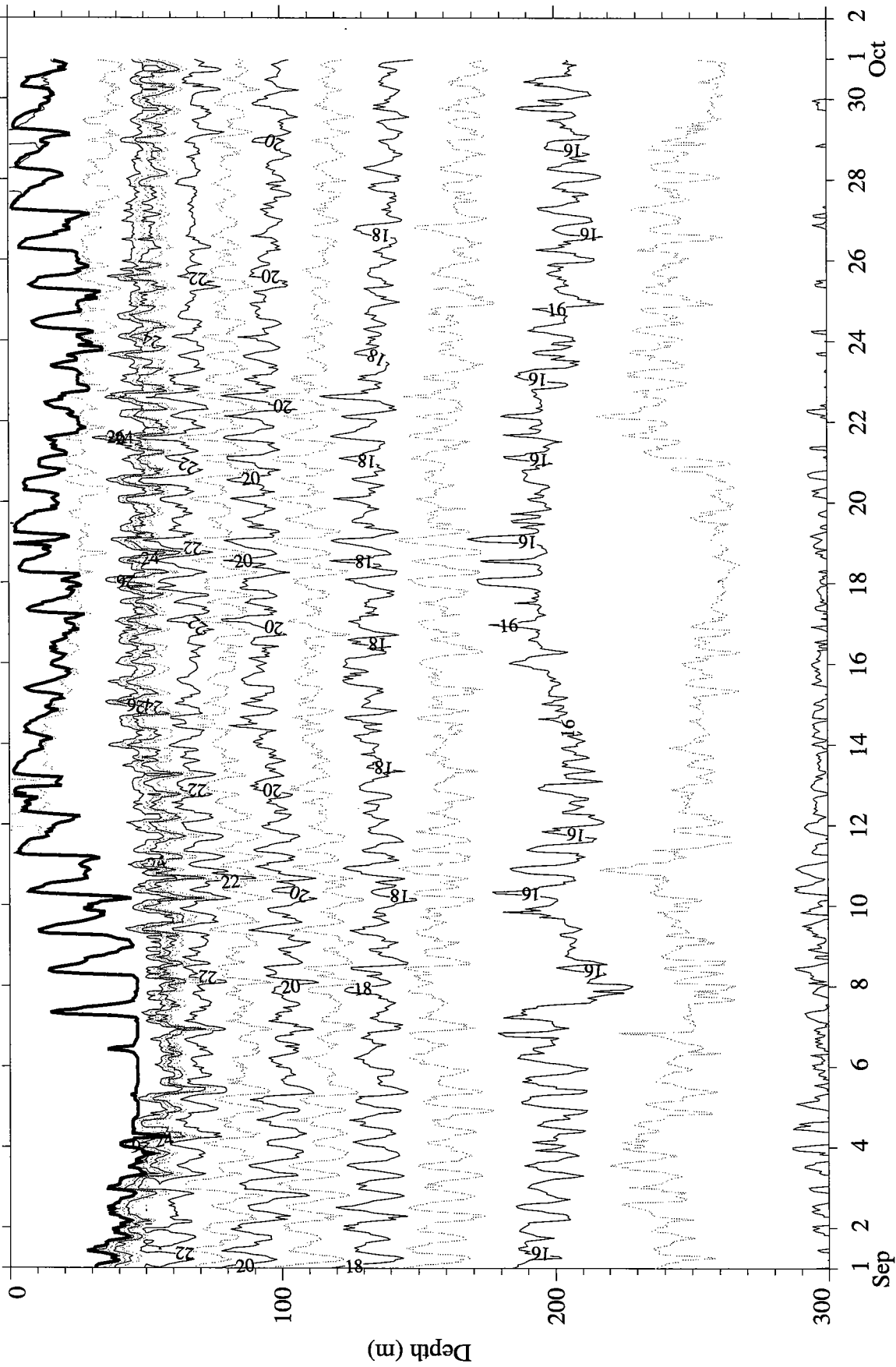


Figure 48. Contour plot of hourly averaged temperature and mixed layer depth (thick) for September, 1995. Isotherms are in units of °C.

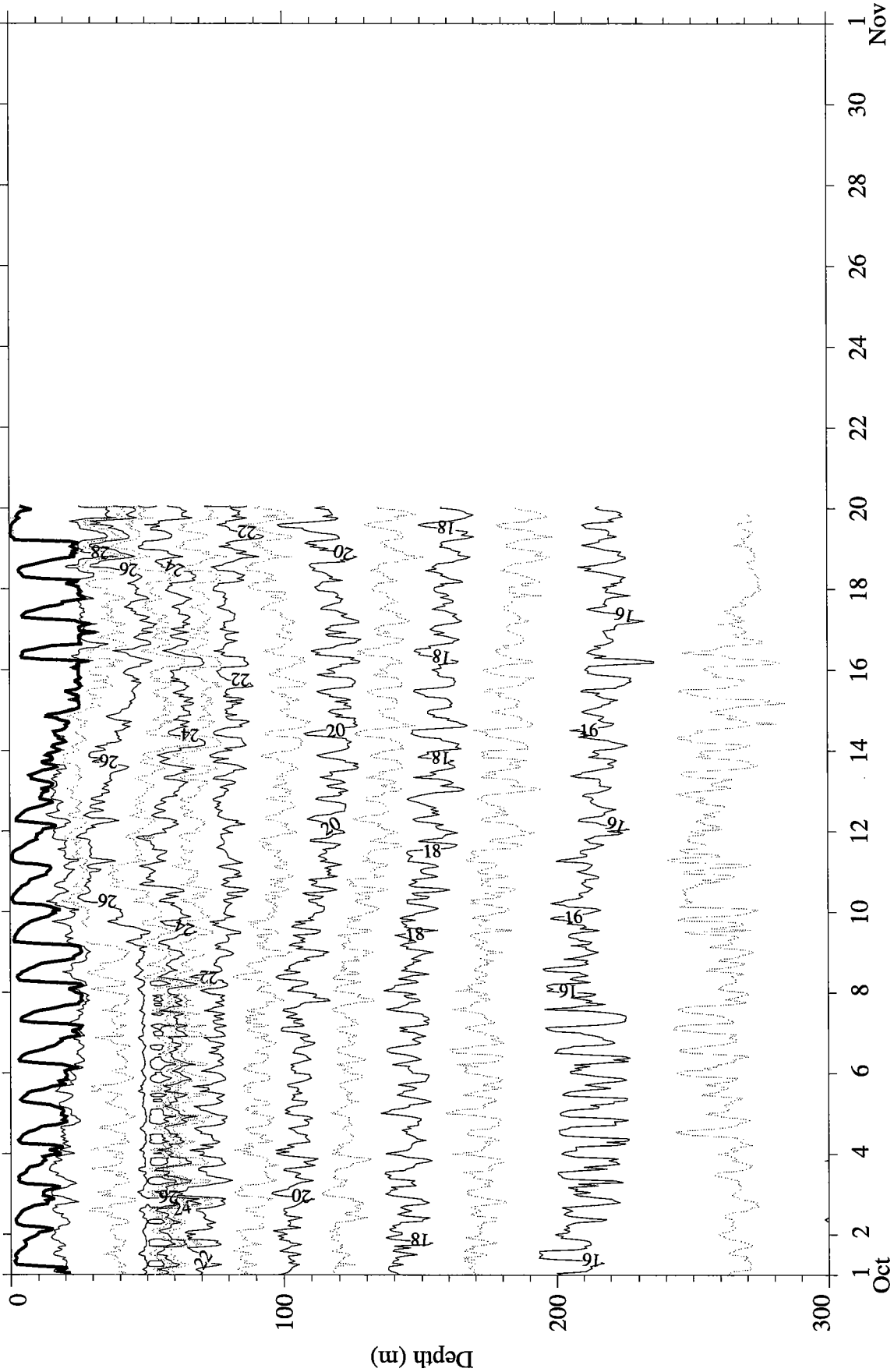


Figure 49. Contour plot of hourly averaged temperature and mixed layer depth (thick) for October, 1995. Isotherms are in units of °C.

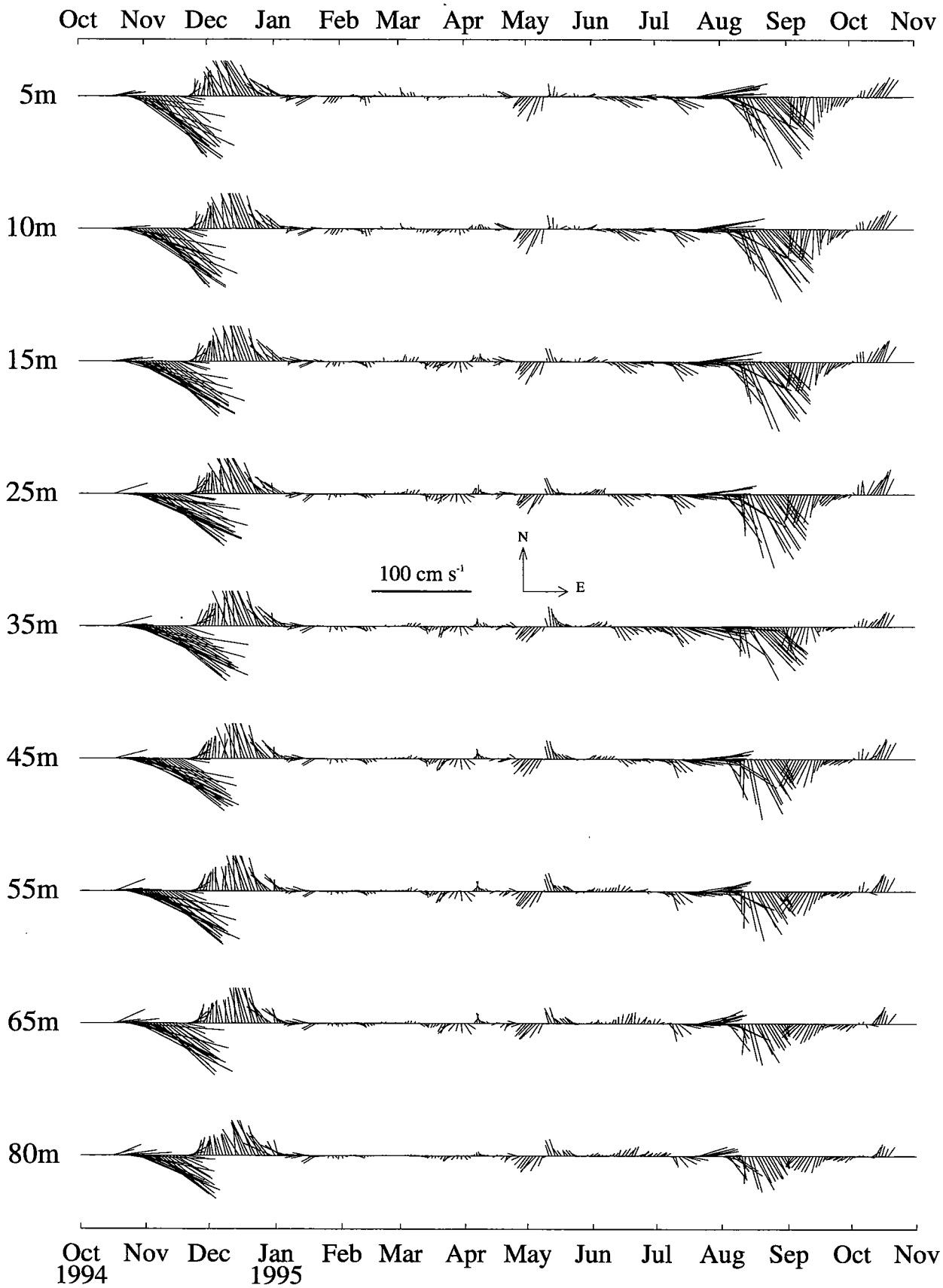


Figure 50. VMCM and MVMS 36 hour vector averaged velocity from the WHOI mooring.

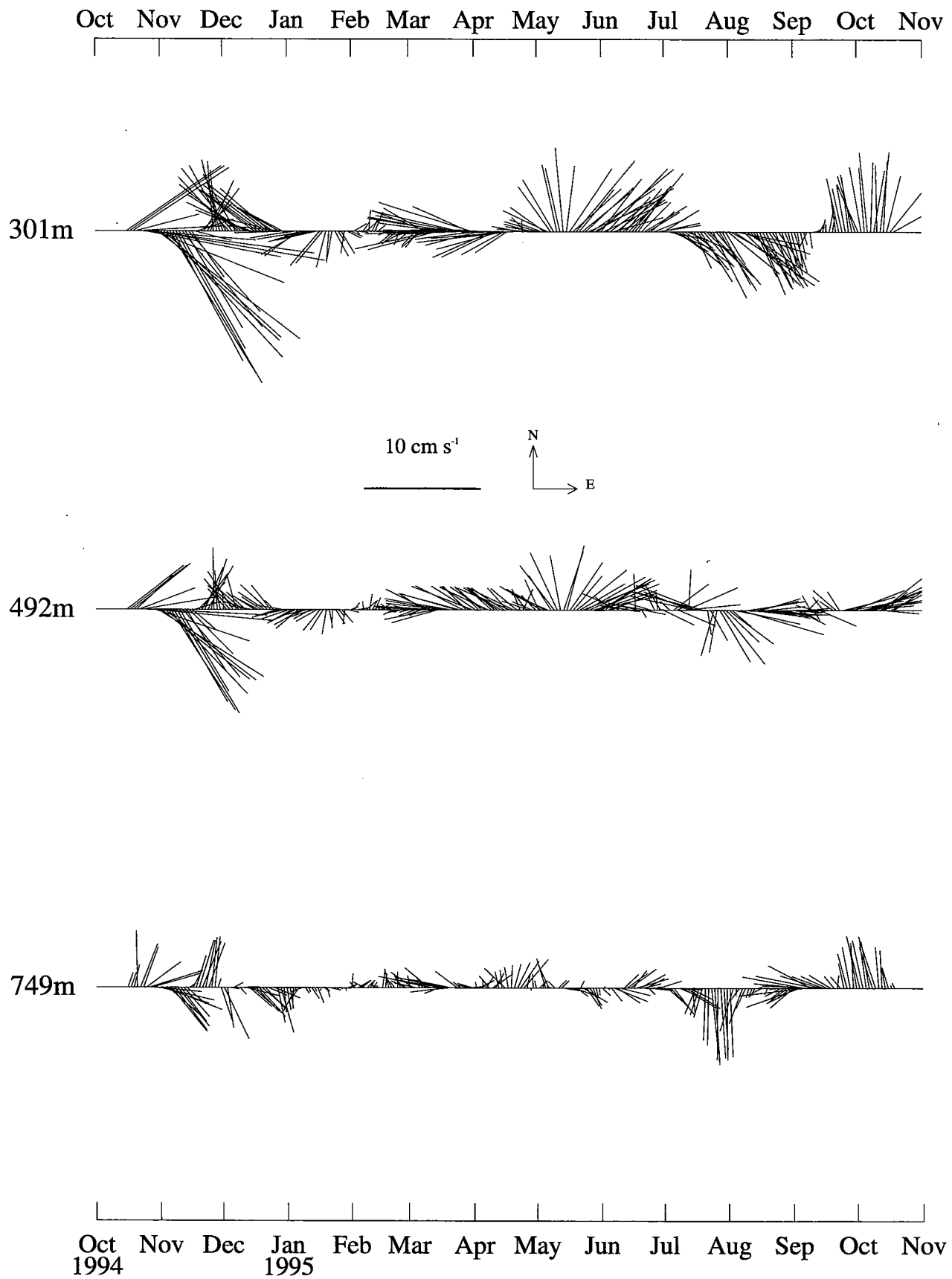


Figure 51. VMCM 36 hour vector averaged velocity from the UW Southeast mooring.

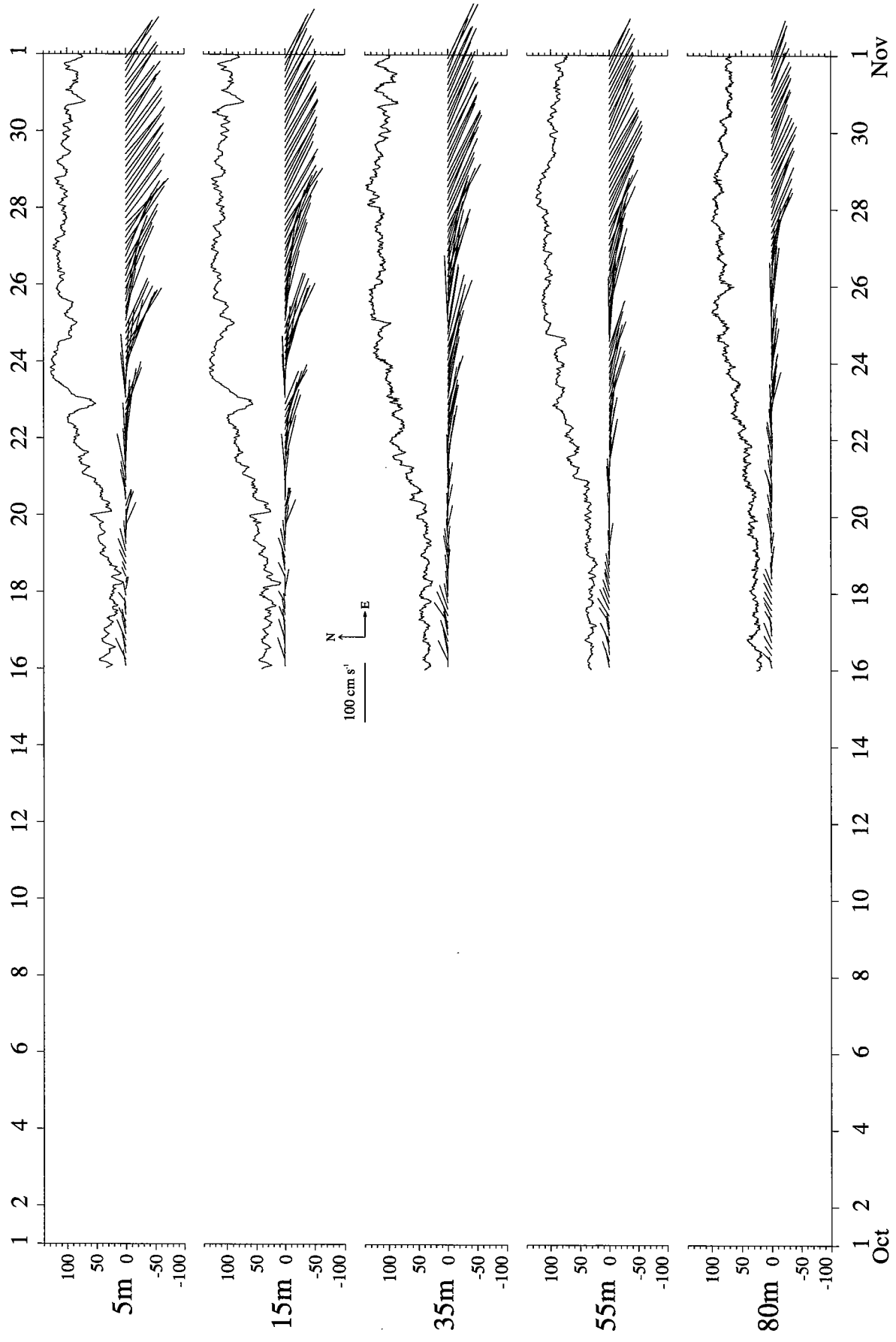


Figure 52. Four hour vector averaged velocity (sticks) and 15 minute current speed (line) in cm s⁻¹ at selected depths for October 1994.

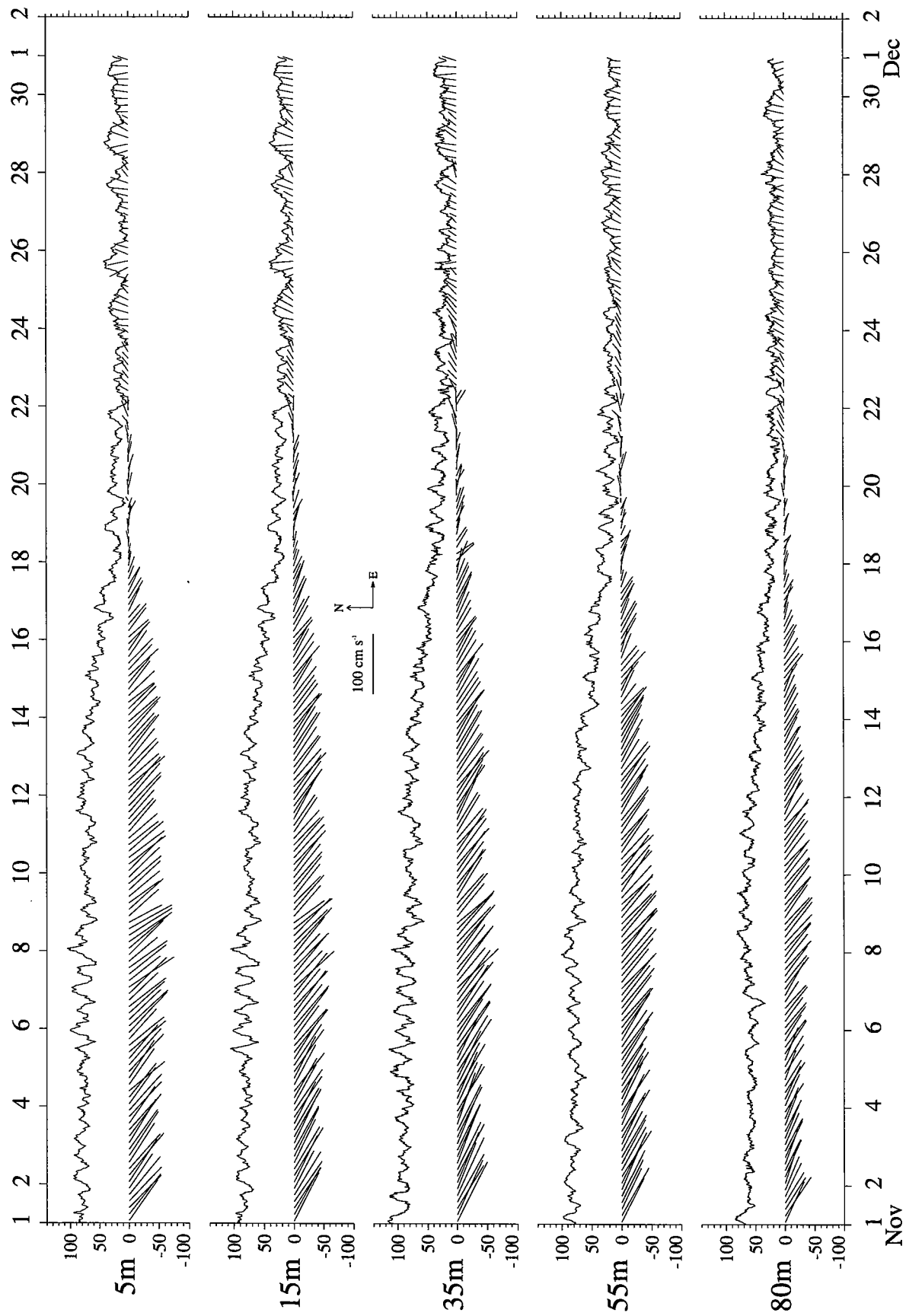


Figure 53. Four hour vector averaged velocity (sticks) and 15 minute current speed (line) in cm s^{-1} at selected depths for November 1994.

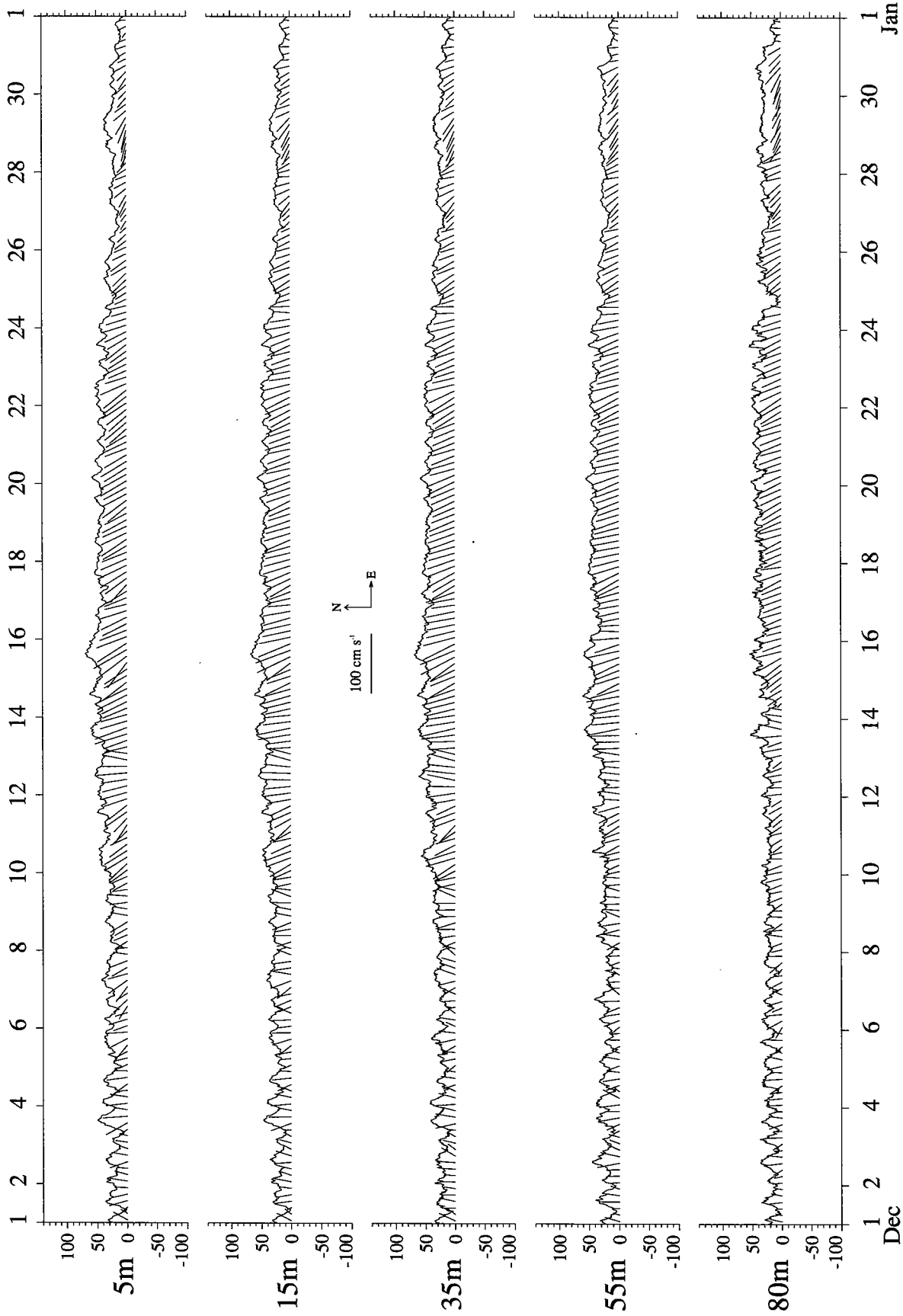


Figure 54. Four hour vector averaged velocity (sticks) and 15 minute current speed (line) in cm s^{-1} at selected depths for December 1994.

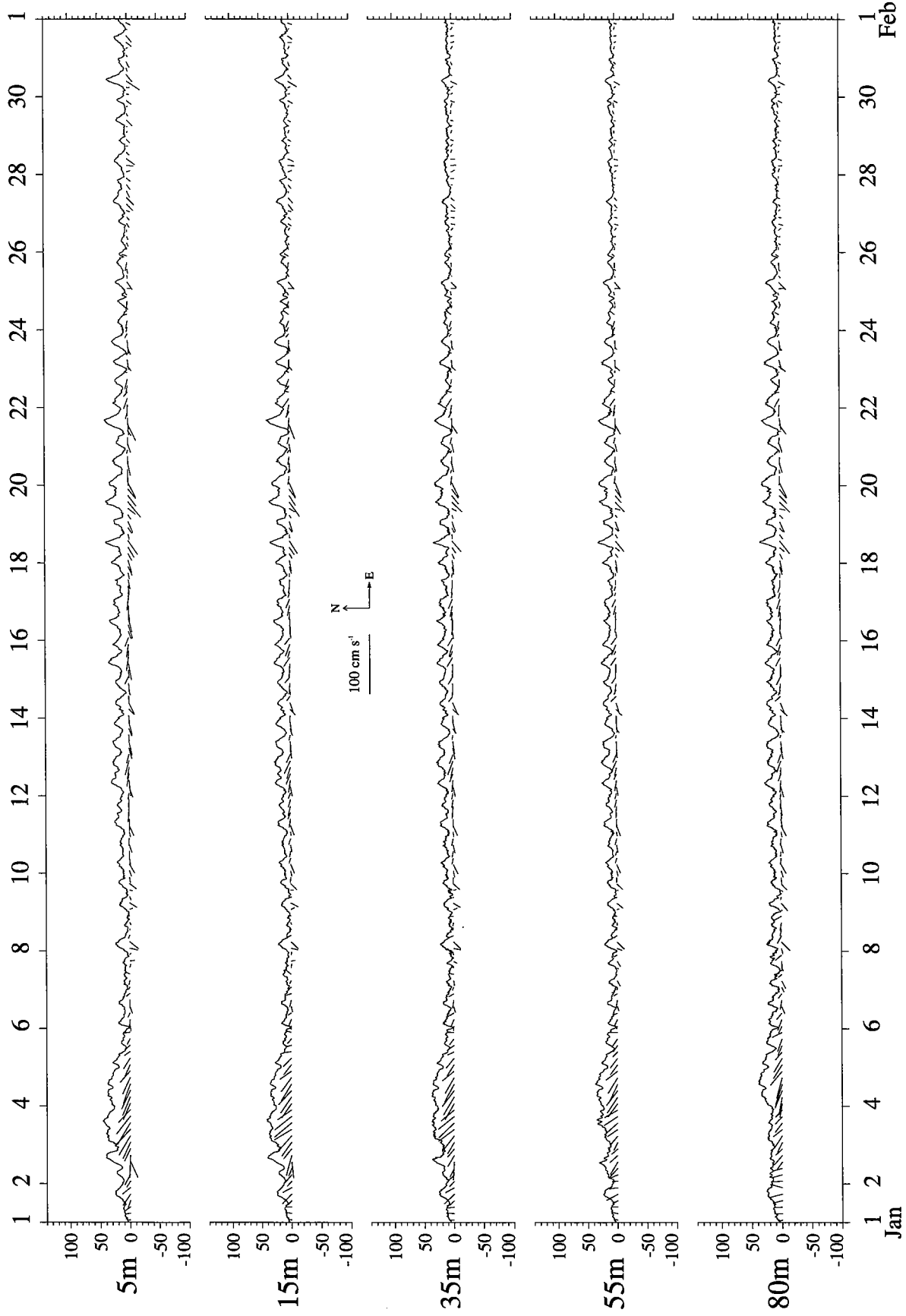


Figure 55. Four hour averaged velocity (sticks) and 15 minute current speed (line) in cm s⁻¹ at selected depths for January 1995.

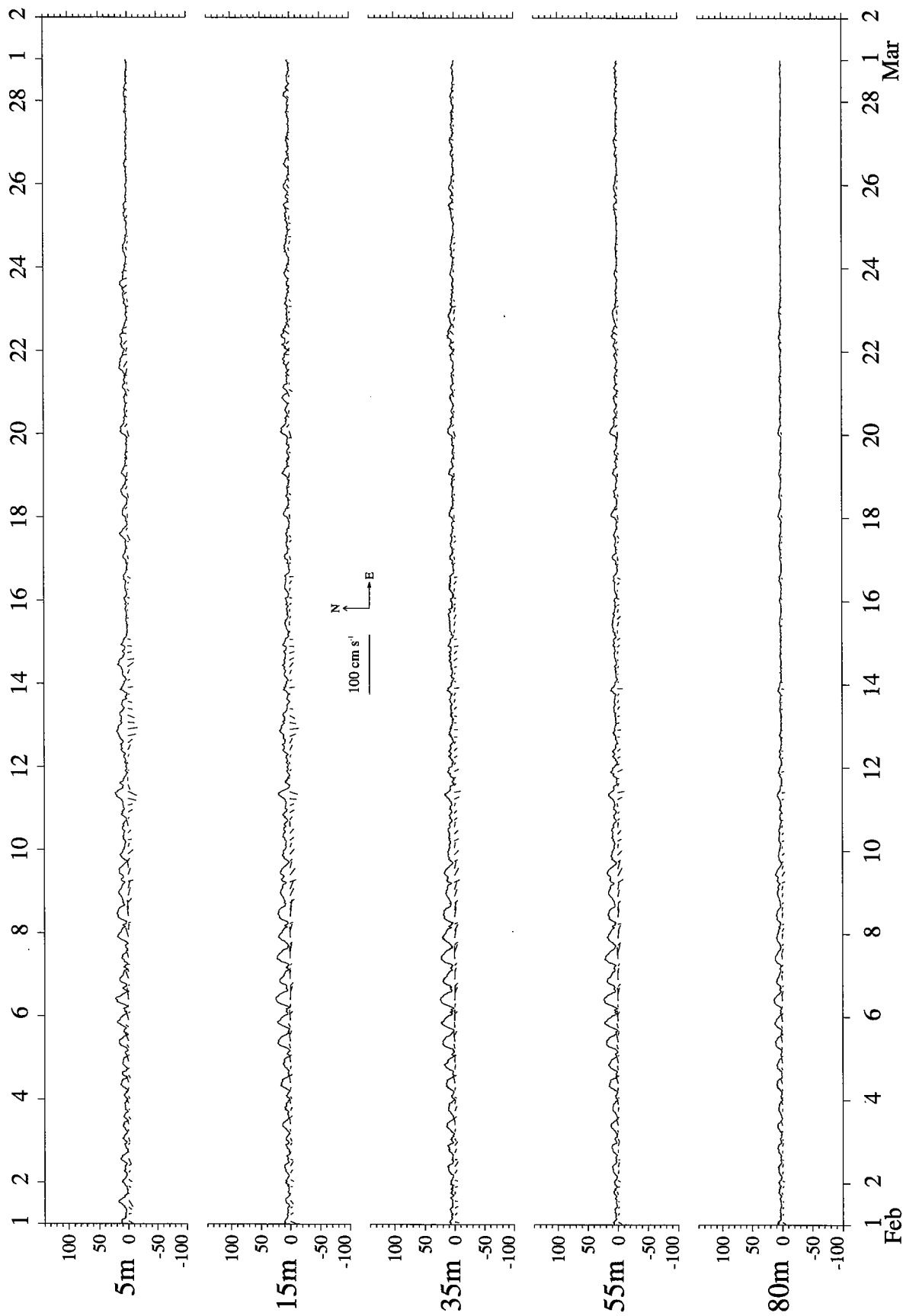


Figure 56. Four hour vector averaged velocity (sticks) and 15 minute current speed (line) in cm s⁻¹ at selected depths for February 1995.

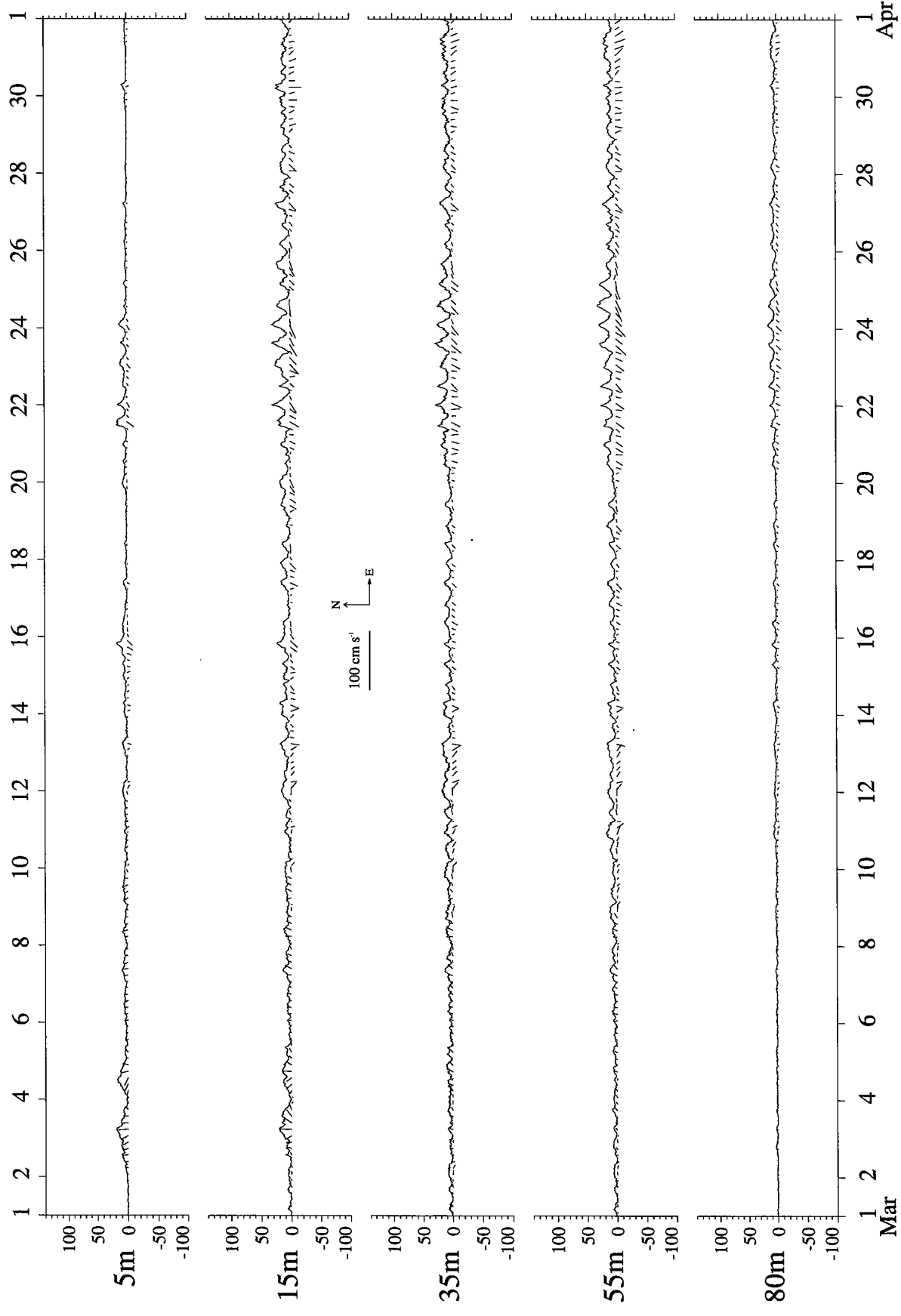


Figure 57. Four hour vector averaged velocity (sticks) and 15 minute current speed (line) in cm s^{-1} at selected depths for March 1995.

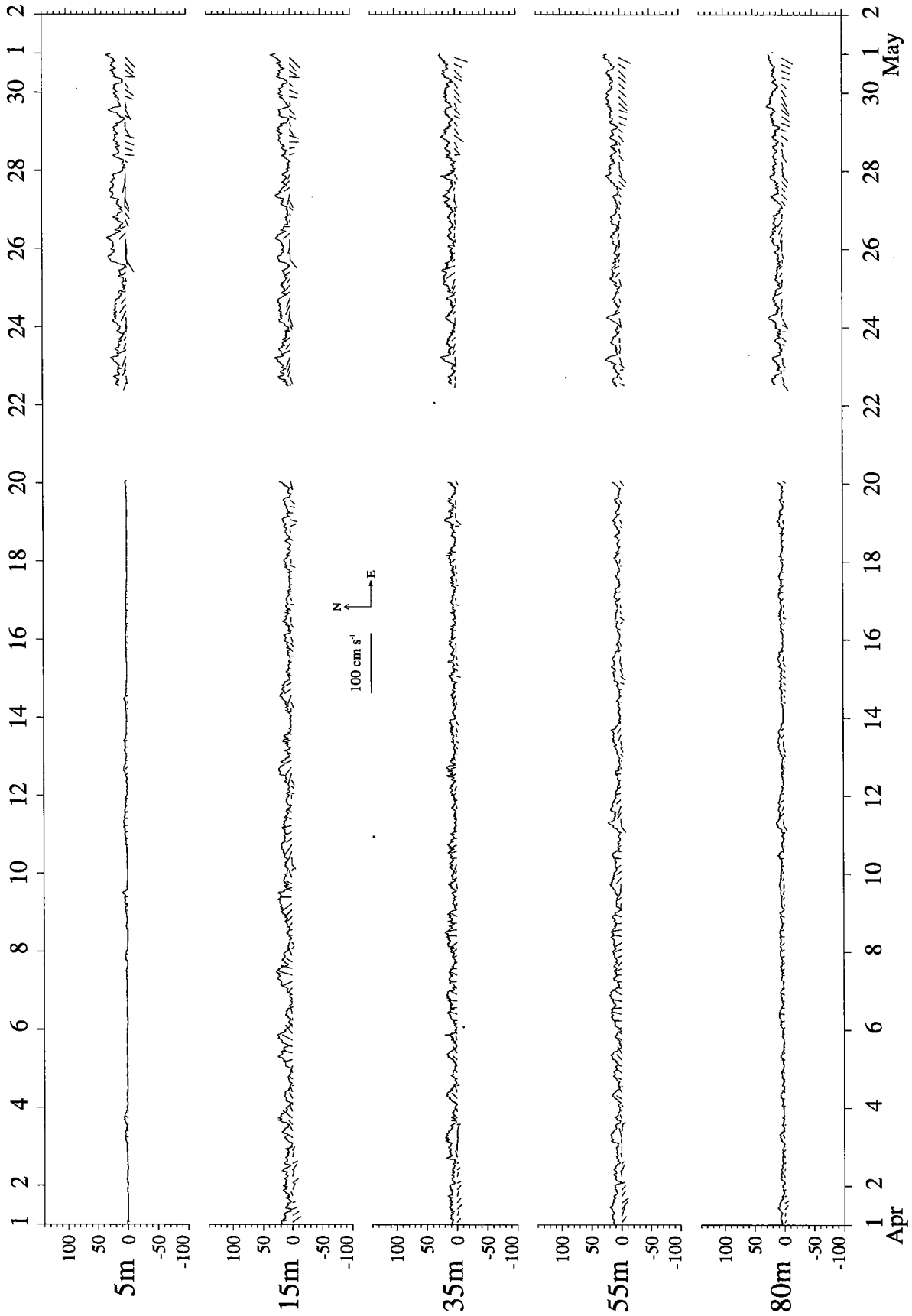


Figure 58. Four hour averaged velocity (sticks) and 15 minute current speed (line) in cm s⁻¹ at selected depths for April 1995.

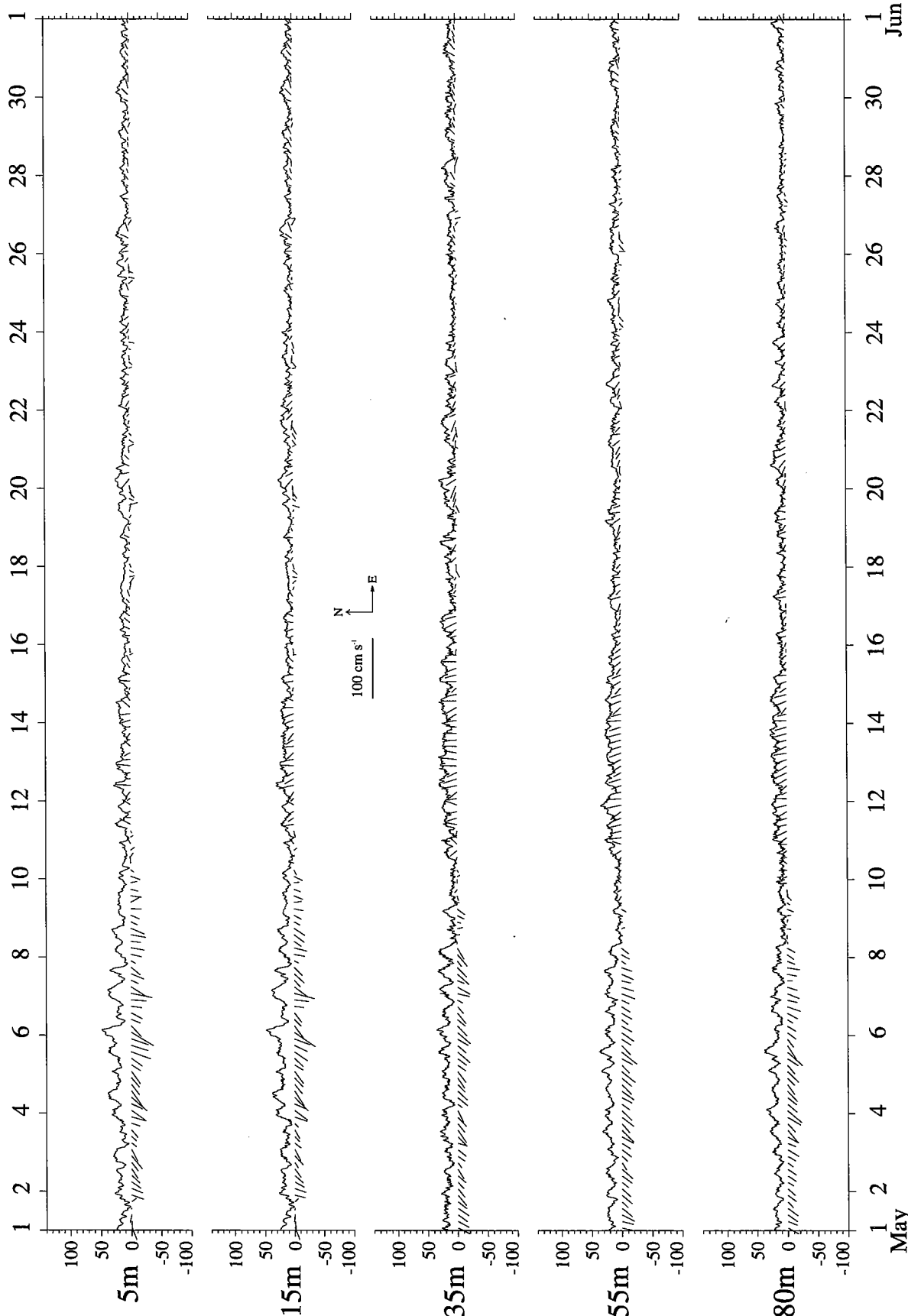


Figure 59. Four hour vector averaged velocity (sticks) and 15 minute current speed (line) in cm s⁻¹ at selected depths for May 1995.

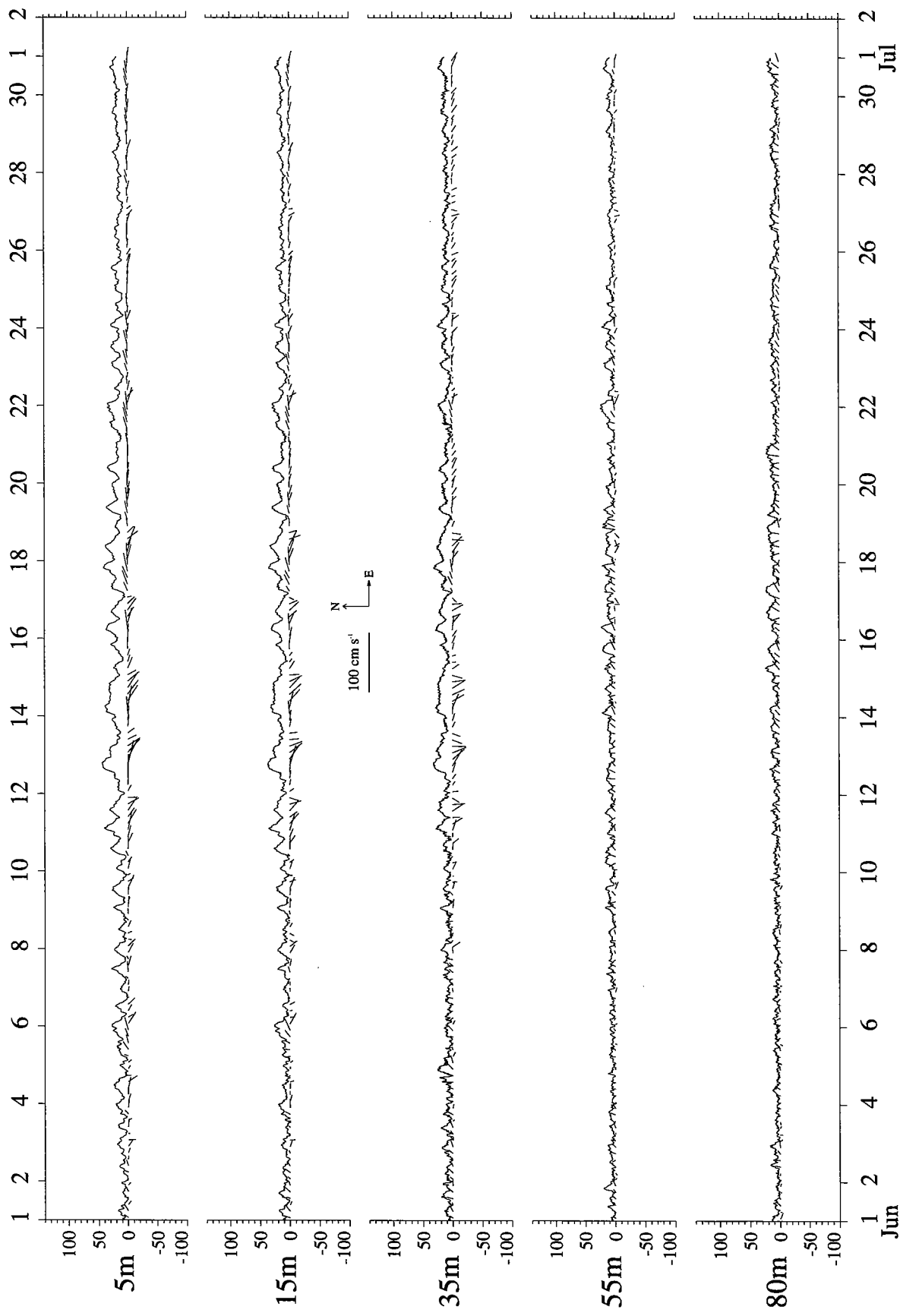


Figure 60. Four hour vector averaged velocity (sticks) and 15 minute current speed (line) in cm s⁻¹ at selected depths for June 1995.

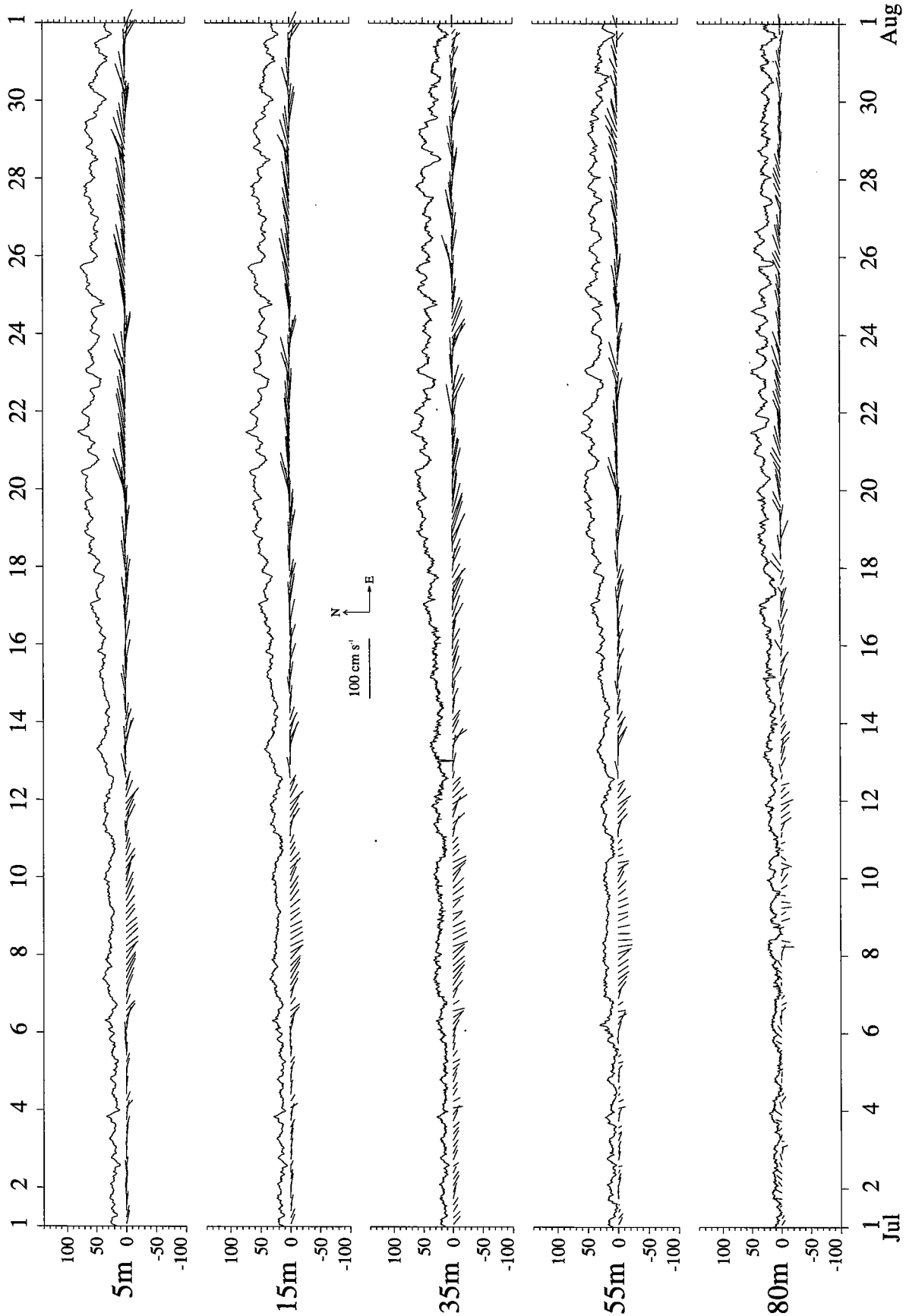


Figure 61. Four hour vector averaged velocity (sticks) and 15 minute current speed (line) in cm s⁻¹ at selected depths for July 1995.

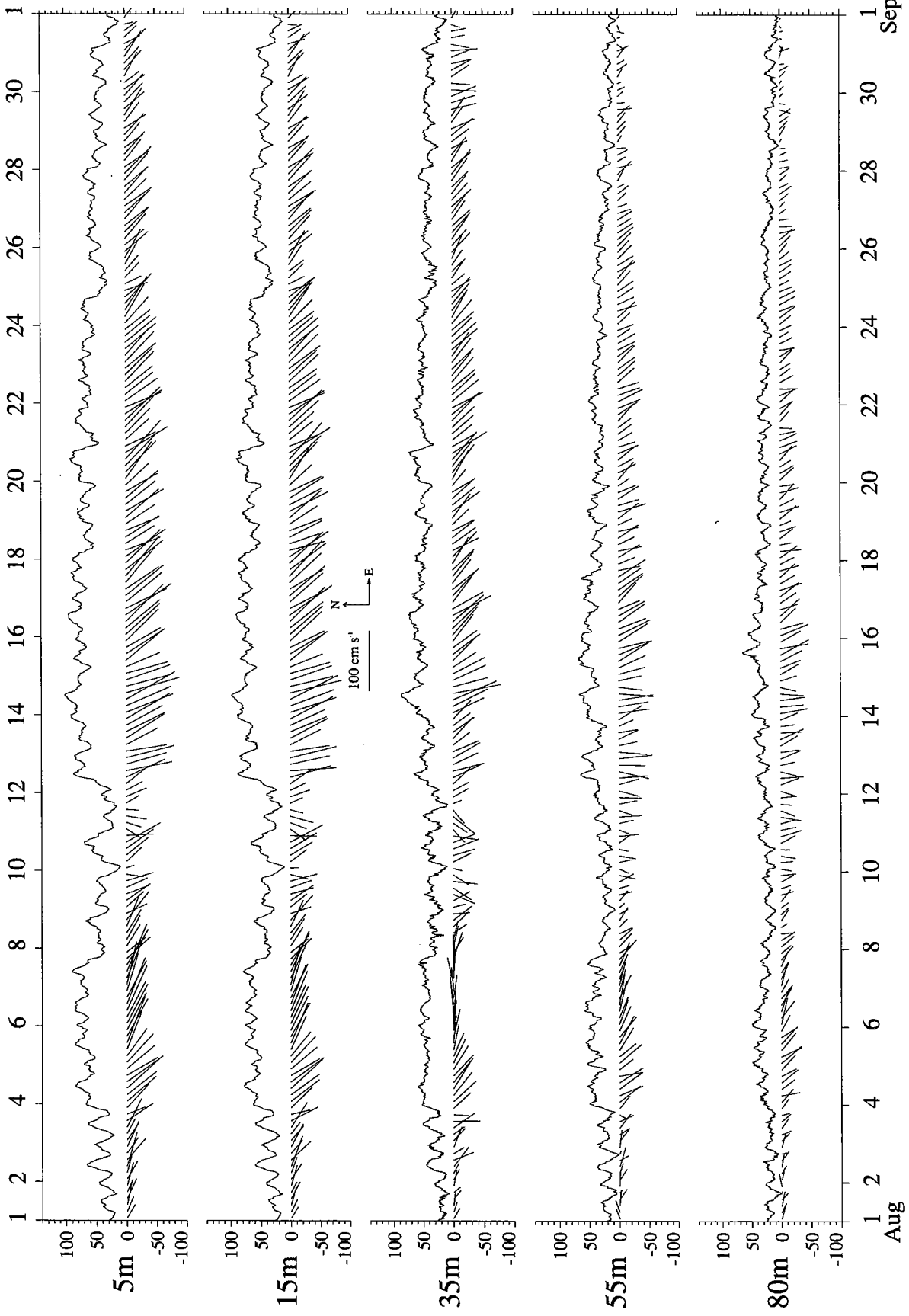


Figure 62. Four hour vector averaged velocity (sticks) and 15 minute current speed (line) in cm s⁻¹ at selected depths for August 1995.

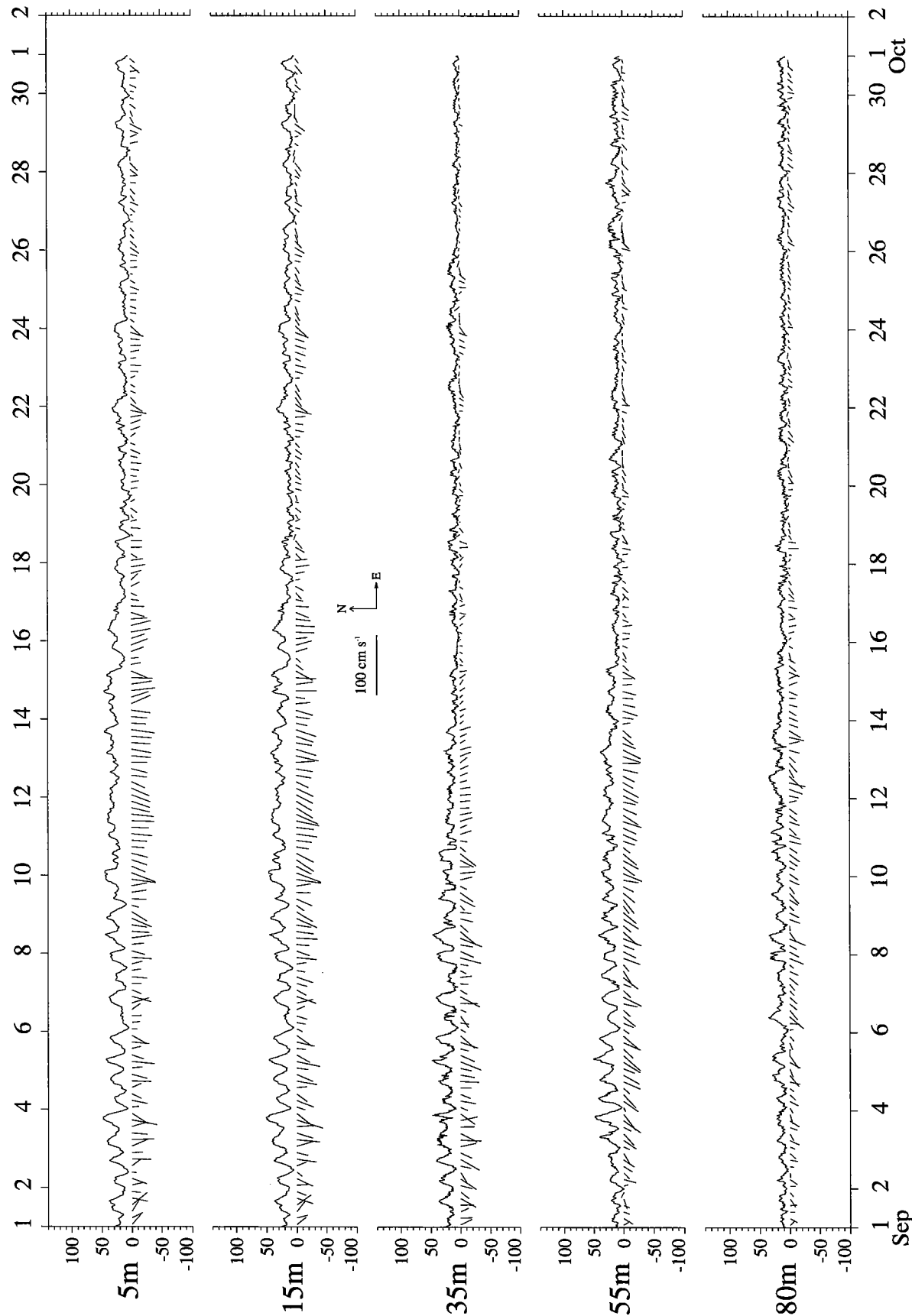


Figure 63. Four hour vector averaged velocity (sticks) and 15 minute current speed (line) in cm s⁻¹ at selected depths for September 1995.

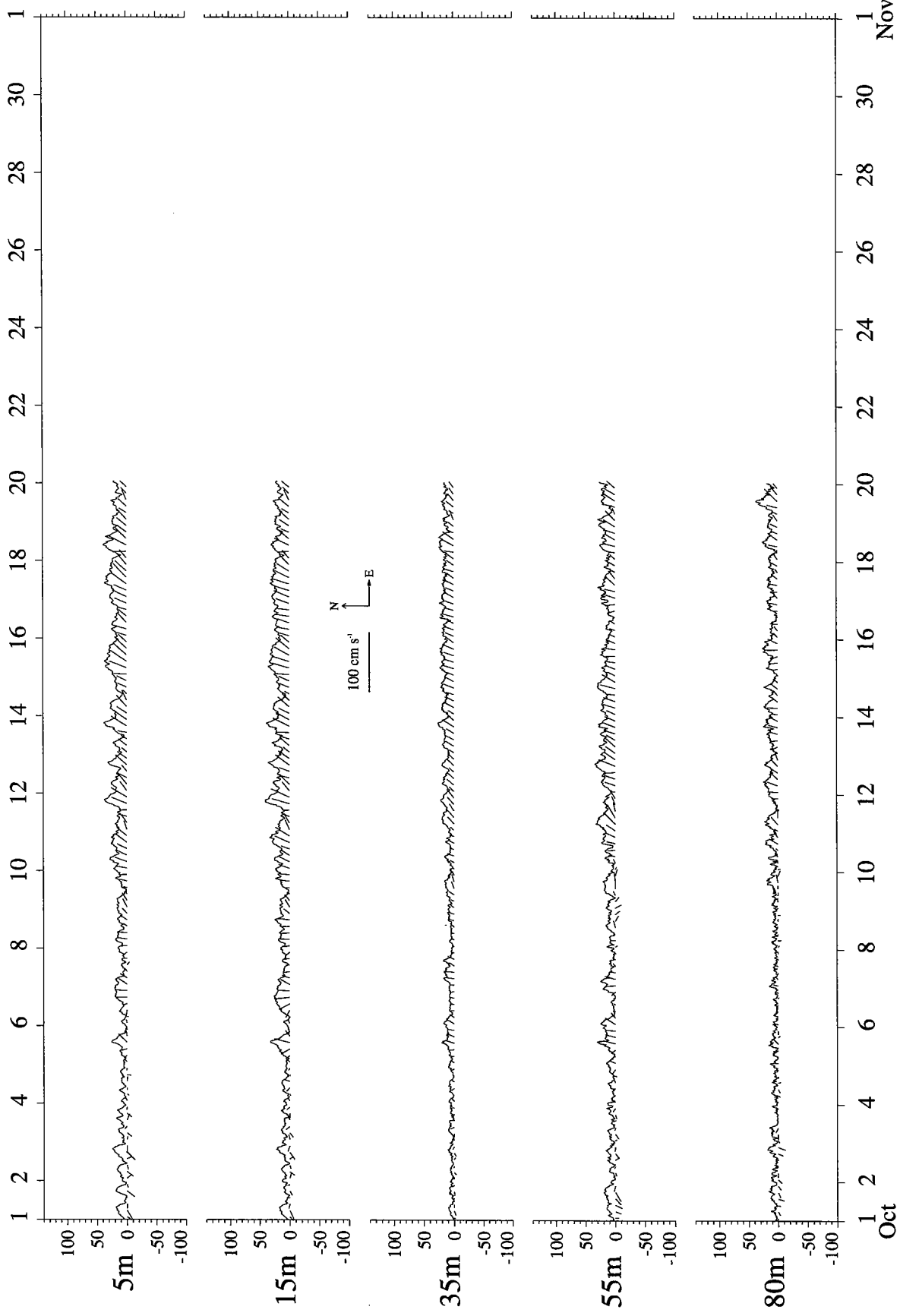


Figure 64. Four hour averaged velocity (sticks) and 15 minute current speed (line) in cm s⁻¹ at selected depths for October 1995.

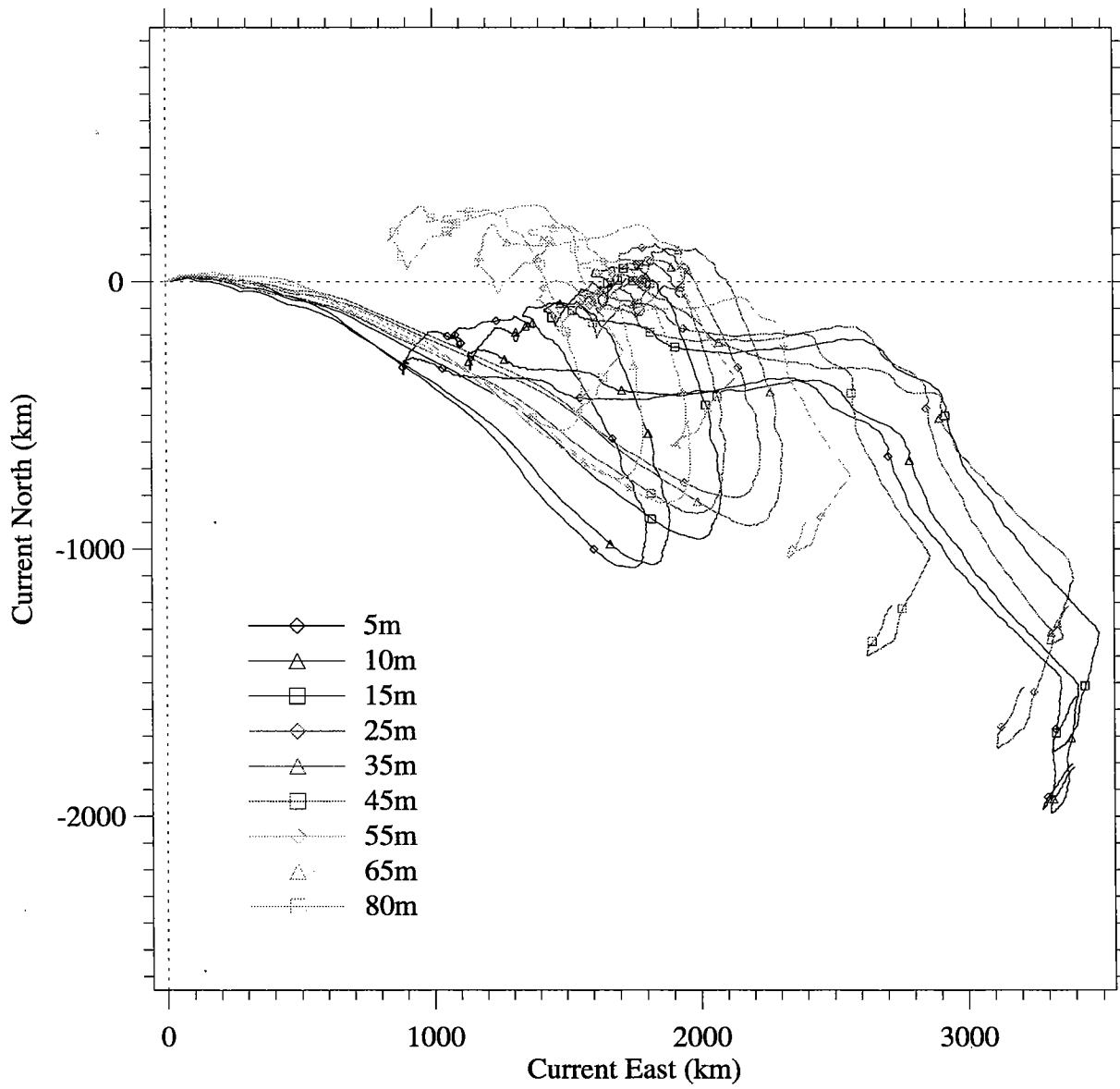


Figure 65. Progressive vectors from VMCM and MVMS current meters. Symbols are placed 30 days apart.

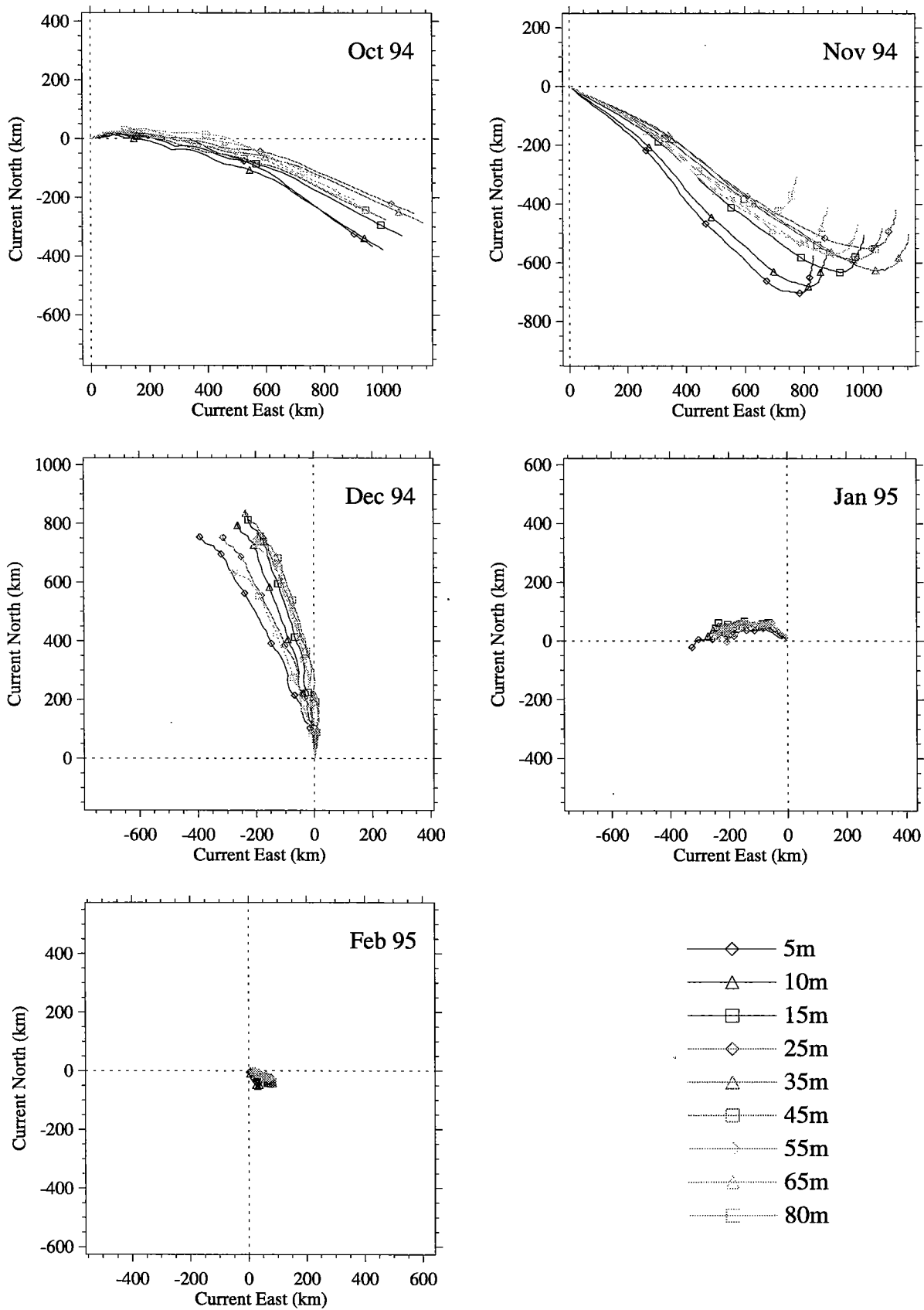


Figure 66. Progressive vectors from VMCM and MVMS current meters. Symbols are placed 5 days apart.

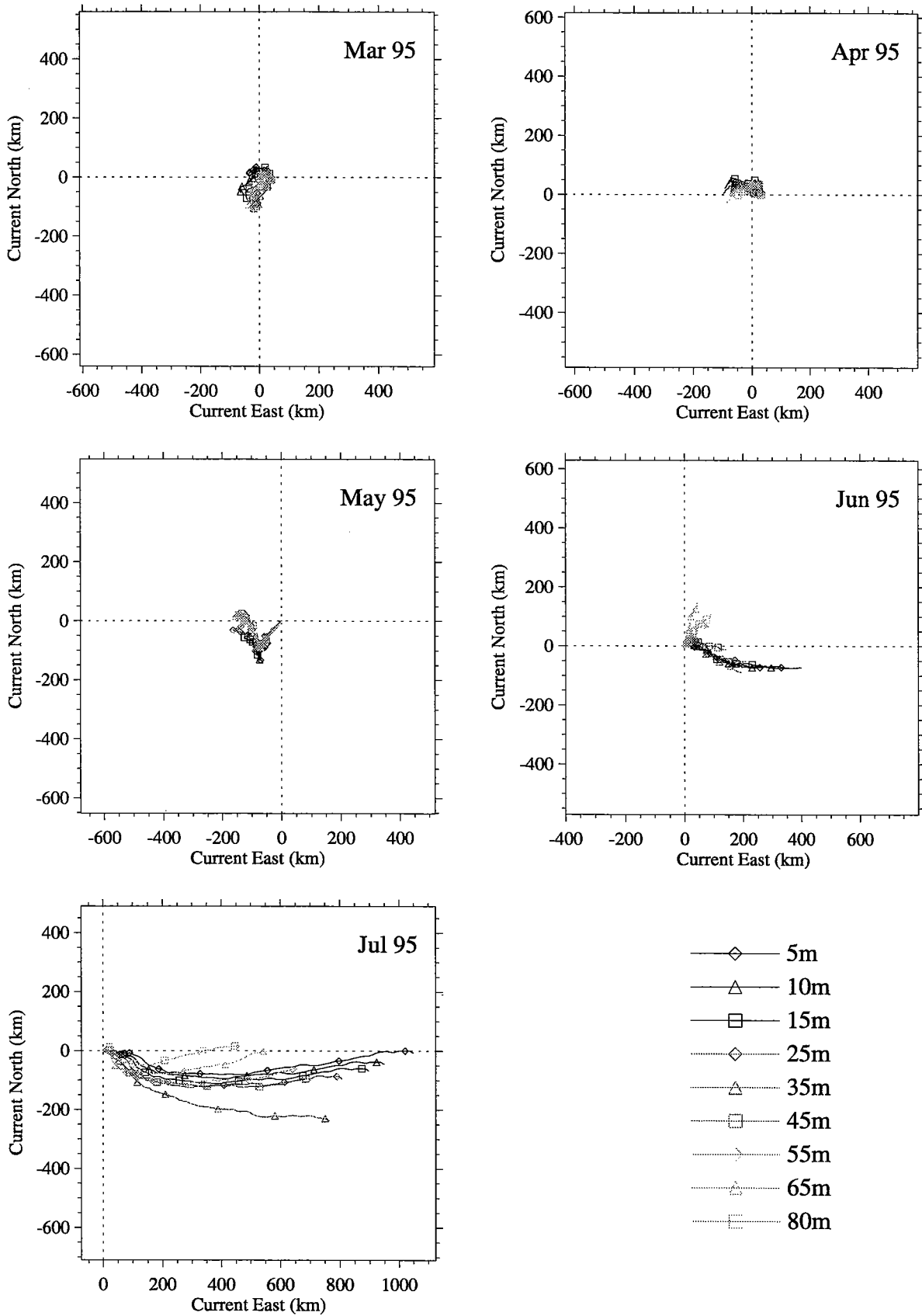
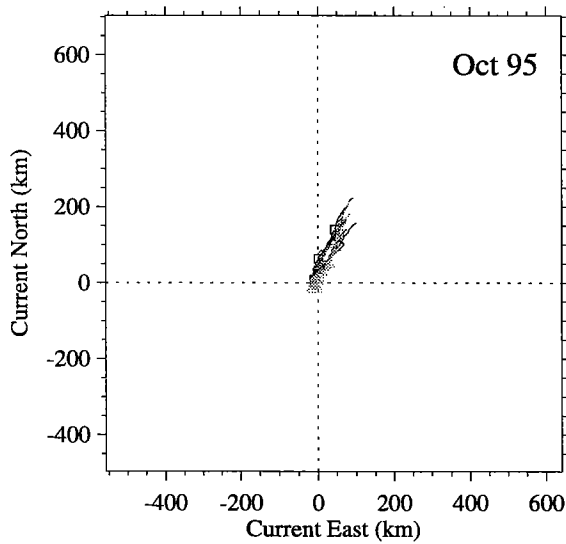
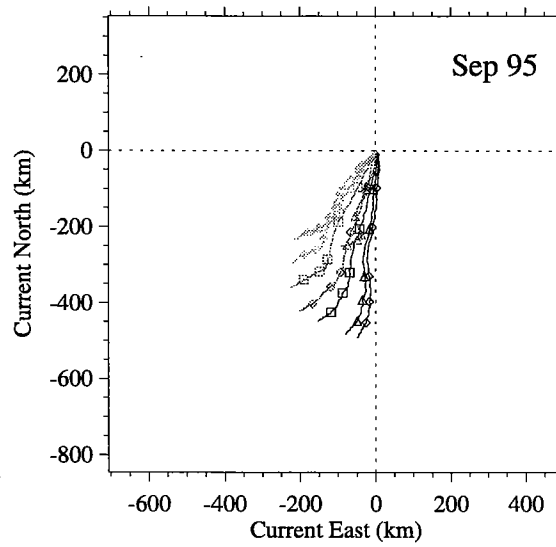
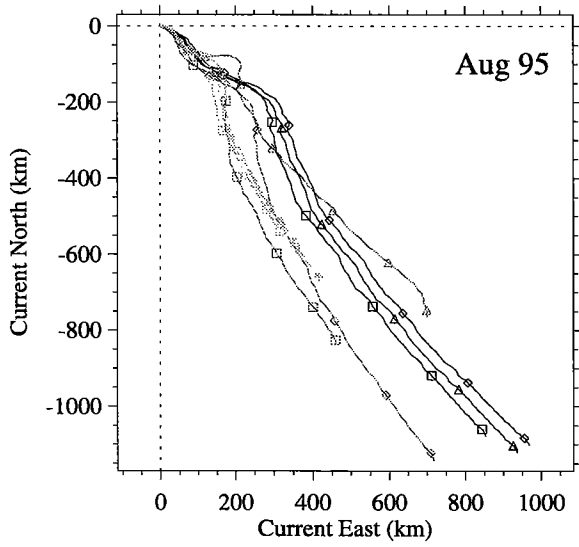


Figure 66. (continued)



- ◇— 5m
- △— 10m
- 15m
- ◇— 25m
- △— 35m
- 45m
- △— 55m
- △— 65m
- 80m

Figure 66. (continued)

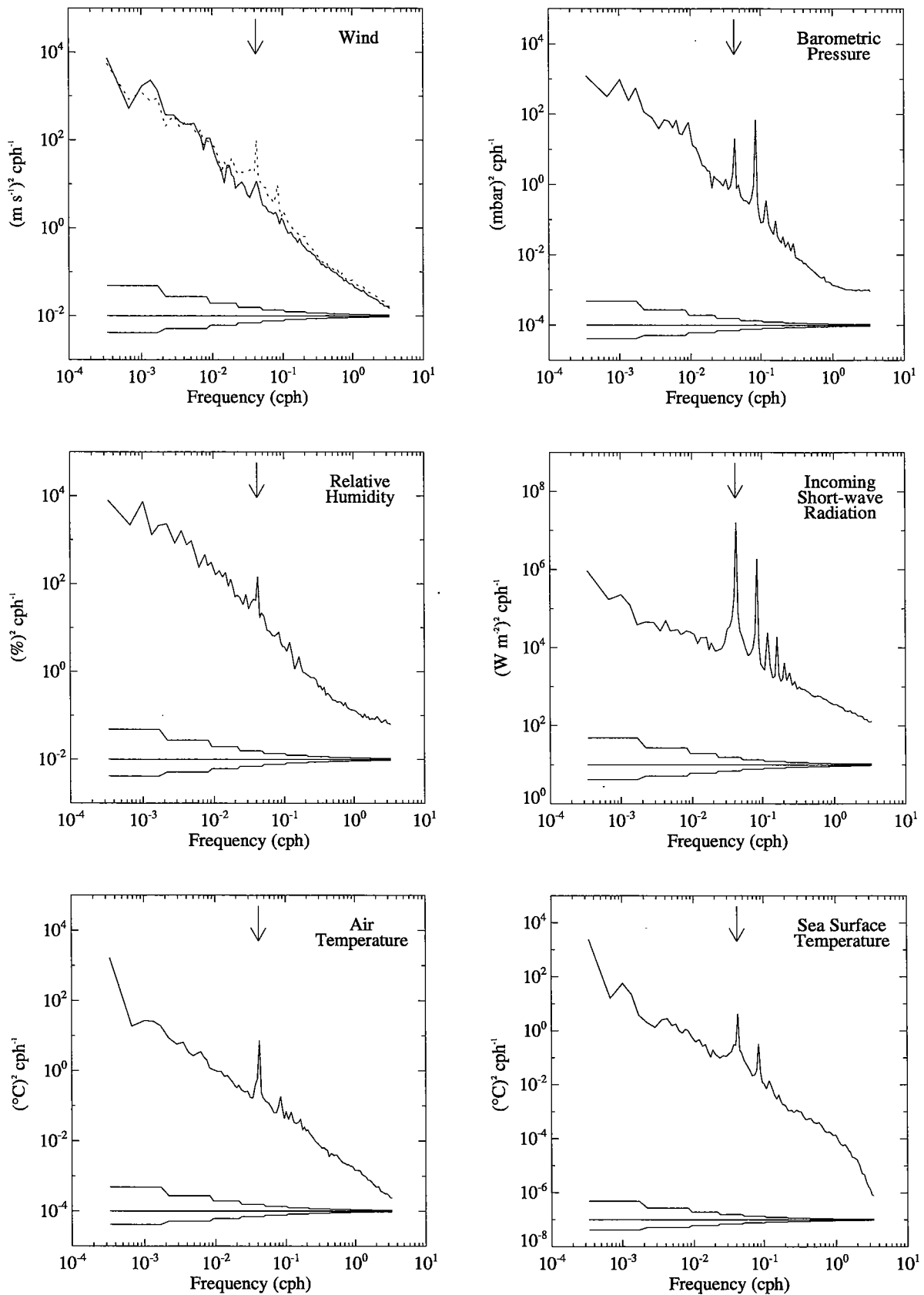


Figure 67. Autospectra of meteorological parameters. Rotary autospectra of the wind provides both clockwise (solid) and counter-clockwise (dotted) spectras. The arrow indicates the diurnal frequency (24^{-1} cph).

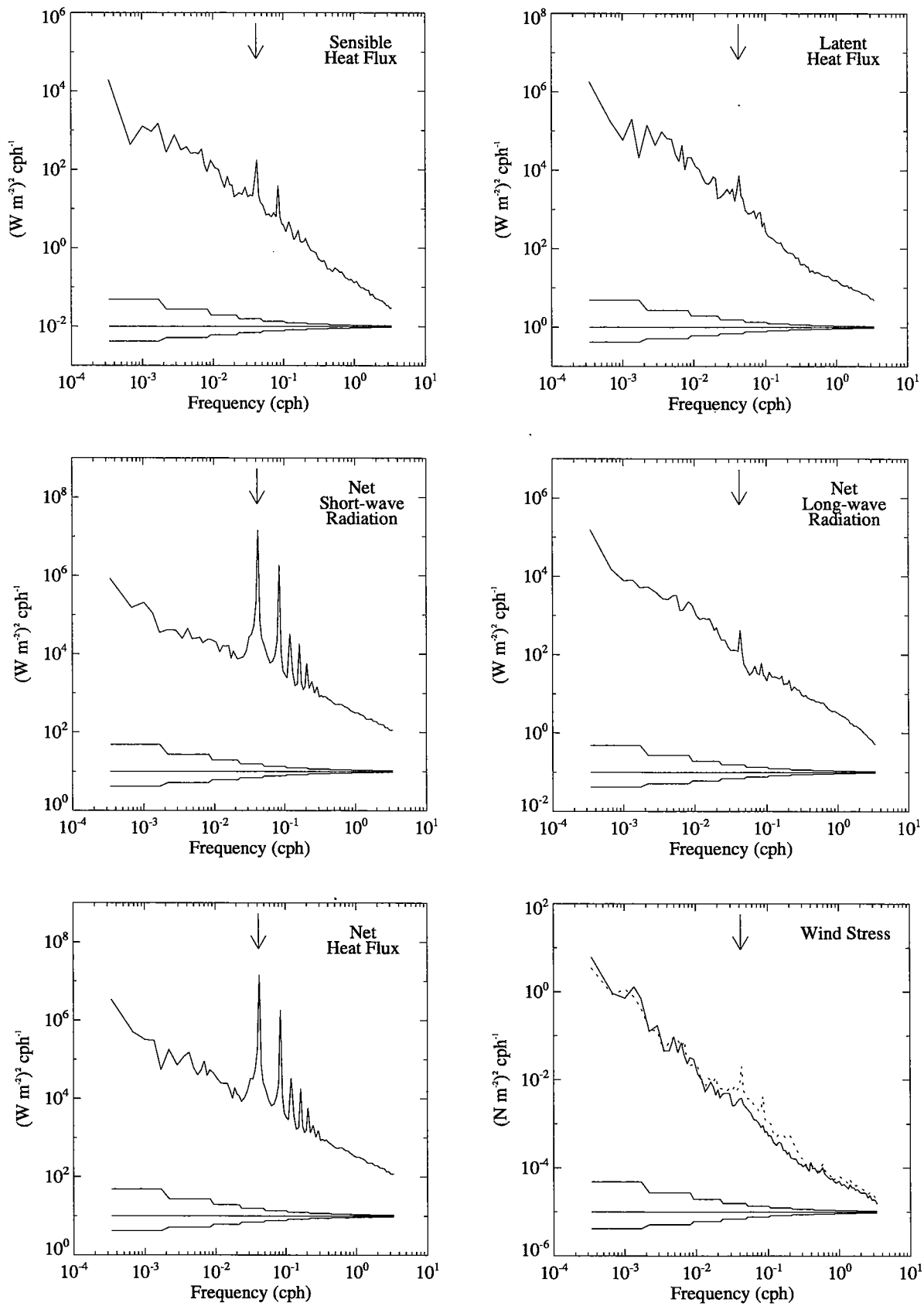


Figure 68. Autospectra of heat fluxes. Rotary autospectra of the wind stress provides both clockwise (solid) and counter-clockwise (dotted) spectras. The arrow indicates the diurnal frequency (24^{-1} cph).

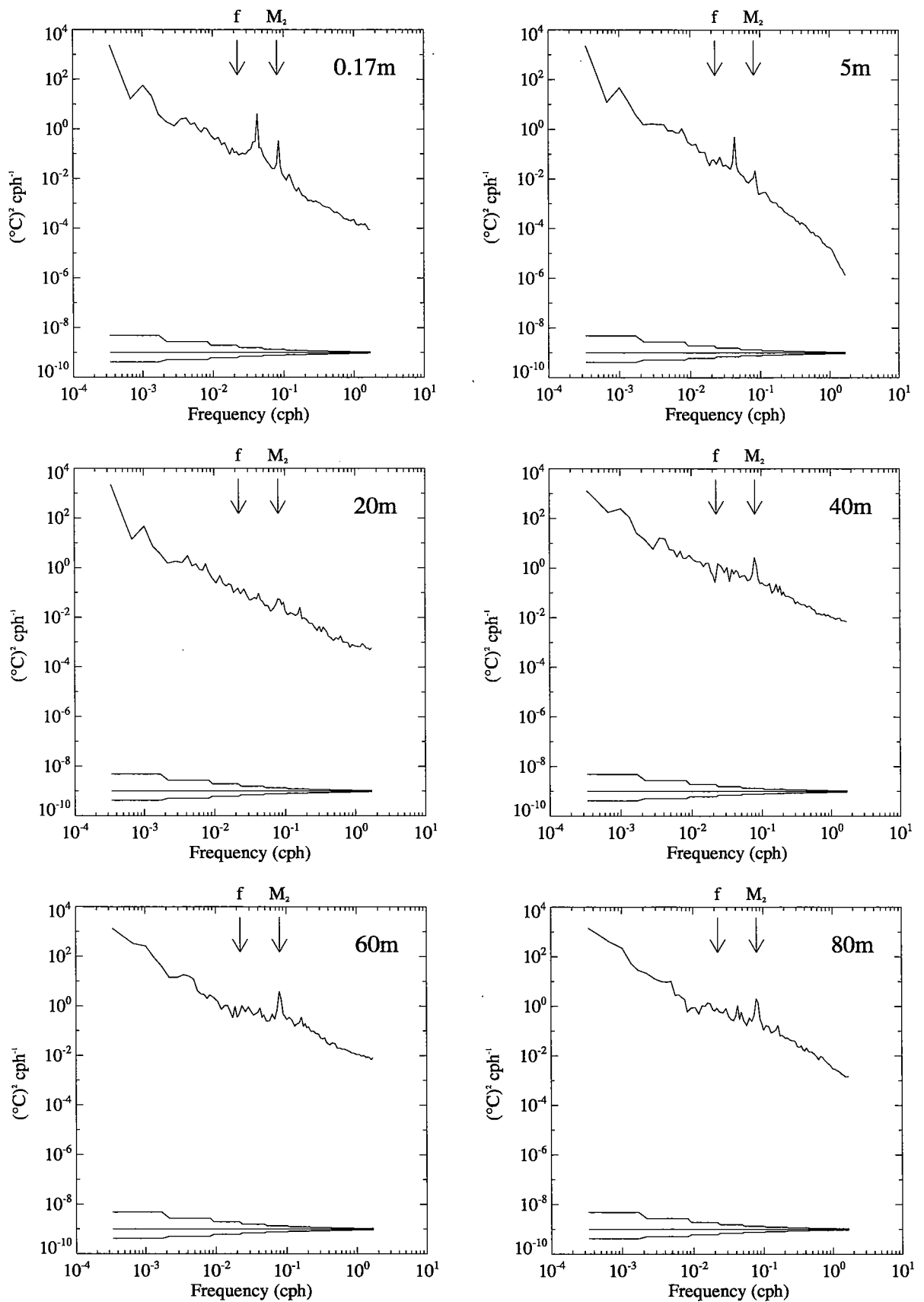


Figure 69. Autospectra of temperature at various depths. The tidal M_2 and inertial frequencies are indicated with arrows.

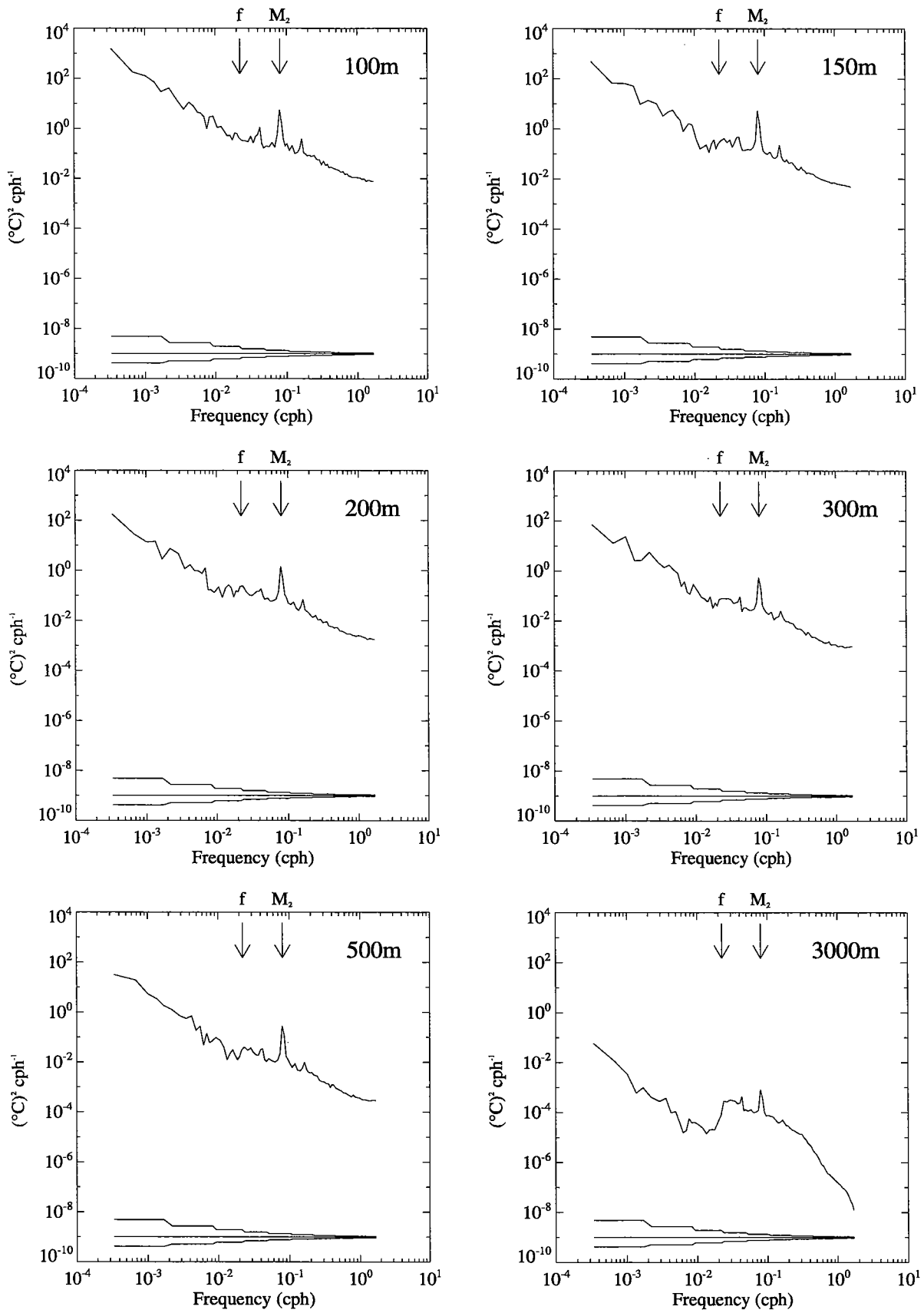


Figure 69. (continued)

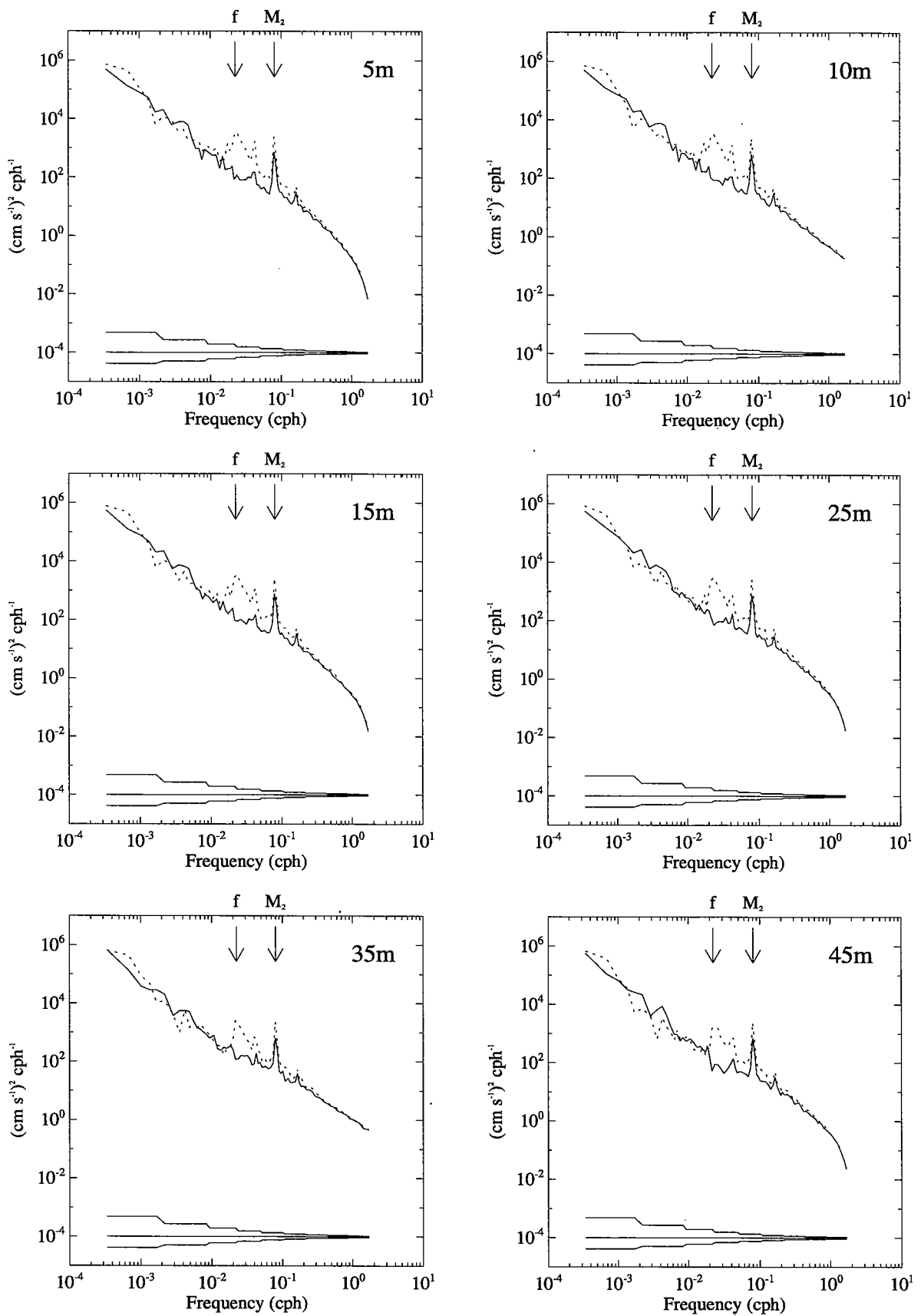


Figure 70. Rotary autospectra of velocity at various depths. The tidal M_2 and inertial frequencies are indicated with arrows. Clockwise spectra are solid and counter-clockwise spectra are dotted.

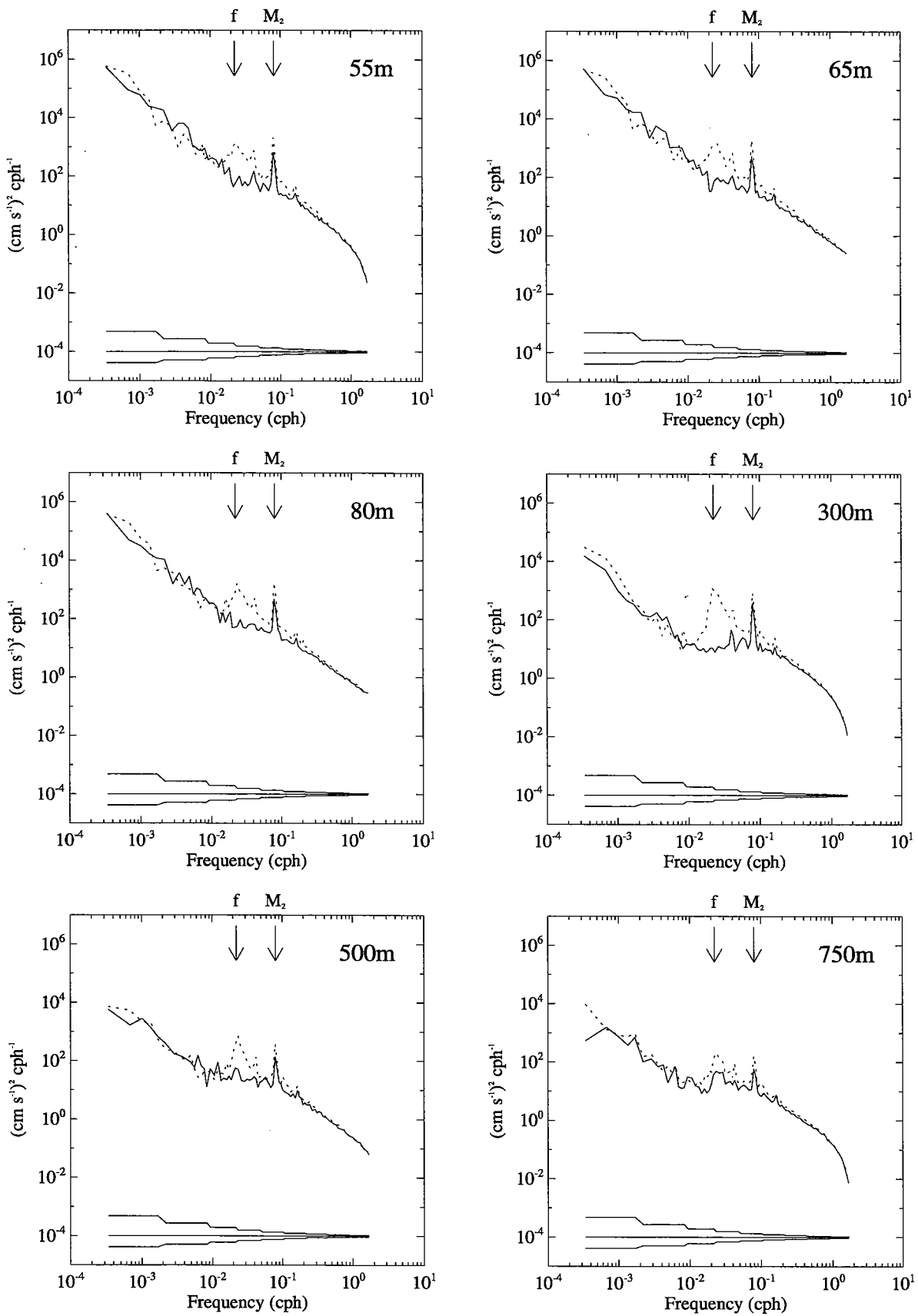


Figure 70. (continued)

Acknowledgments

The success of the Arabian Sea experiment is due to the hard work and dedication of all the members of the Upper Ocean Processes Group, including Geoff Allsup, Steve Anderson, Albert Fischer, Nancy Galbraith, Dave Hosom, Will Ostrom, Dick Payne, Rick Trask, Jonathan Ware and Bryan Way. Dave Sigurdson (UCSB) and Cheng Ho (LDEO) performed the calibrations of the MVMS data. We would like to thank the captain and crew of the R/V *Thomas Thompson* for their skillful help during deployment and recovery. This work was supported by the Office of Naval Research Grant No. N00014-94-1-0161.

Literature Cited

- Anderson, S.P. and M.F. Baumgartner, 1997. Radiative heating errors in naturally ventilated air temperature measurements made from buoys. *Journal of Atmospheric and Oceanic Technology*. in press.
- Clark, N.E., L. Eber, R.M. Laurs, J.A. Renner and J.F.T. Saur, 1974. Heat exchange between ocean and atmosphere in the eastern North Pacific for 1961–1971. NOAA Technical Report, NMFS SSRF-682. U.S. Department of Commerce, Washington, D.C.
- Denbo, D. W. and W. H. Zhu, 1993. EPS Library User's Guide. Version 2.1. Pacific Marine Laboratory, National Oceanic and Atmospheric Administration. 131pp.
- Fairall, C.W., E.F. Bradley, D.P. Rogers, J.B. Edson and G.S. Young, 1996a. Bulk parameterization of air-sea fluxes for TOGA COARE. *Journal of Geophysical Research*. **101**, 3747–3764.
- Fairall, C.W., E.F. Bradley, J.S. Godfrey, G.A. Wick, J.B. Edson, and G.S. Young, 1996b: The cool skin and the warm layer in bulk flux calculations. *Journal of Geophysical Research*. **101**, 1295–1308.
- Gill, G.C., 1983. Comparison testing of selected naturally ventilated solar radiation shields. Report submitted to NOAA Data Buoy Office, Bay St. Louis, Mississippi. In partial fulfillment of Contract #NA-82-0A-A-266. NOAA/National Data Buoy Center, Bay St. Louis, Mississippi, 39529, U.S.A.
- Ho, C., C.S. Kinkade, C. Langdon, M. Maccio and J. Marra, 1996. The forced upper ocean dynamics experiment in the Arabian Sea: Results from the multi-variable moored sensors from deployment-1 of the WHOI mooring. Lamont-Doherty Earth Observatory, Columbia University. LDEO Technical Report LDEO-96-5. 43pp.
- Ho, C., C. Langdon, M. Maccio and J. Marra, 1997. Bioluminescence and optical variability in the sea ('Marine Light-Mixed Layers'): Moored observations in the North Atlantic Ocean. LDEO Technical Report LDEO-97-1. 12pp.
- Hosom, D.S., R.A. Weller, R.E. Payne and K.E. Prada, 1995: The IMET (Improved Meteorology) ship and buoy system. *Journal of Atmospheric and Oceanic Technology*. **12**, 527–540.
- List, R.J., 1984. Smithsonian Meteorological Tables. Smithsonian Institution Press, Washington D.C. 572pp.
- Liu, W. T., K. B. Katsaros and J. A. Businger, 1979. Bulk parameterization of air-sea exchanges of heat and water vapor including the molecular constraints at the interface. *Journal of the Atmospheric Sciences*. **36**, 1722–1735.
- Ostrom, W.M., B.S. Way, R.A. Weller, J.D. Ware and R.P. Trask, 1996. Arabian Sea mixed layer dynamics experiment: Mooring recovery cruise report, R/V *Thomas Thompson* cruise number 52, 14 October – 25 October 1995. Woods Hole Oceanographic Institution. Technical Report WHOI-96-11. 72pp.

- Payne, R. E., 1972. Albedo of the sea surface. *Journal of the Atmospheric Sciences*. **29**, 959–970.
- Prada, K.E., 1992. A system for shipboard analysis of buoy data. Woods Hole Oceanographic Institution. Technical Report WHOI-92-42. 29pp.
- Rew, R., G. Davis and S. Emmerson, 1993. NetCDF users guide: An interface for data access. Version 2.3. Unidata Program Center. 186pp.
- Sigurdson, D.E., T.D. Dickey and D. Manov, 1995. Arabian Sea Mooring Data Report: Deployment #1 October 15, 1994 – April 20, 1995. University of California, Santa Barbara. Ocean Physics Laboratory Technical Report #OPL-2-95. 26pp.
- Sigurdson, D.E., T.D. Dickey and D. Manov, 1996. Arabian Sea Mooring Data Report: Deployment #2 April 22, 1995 – October 20, 1995. University of California, Santa Barbara. Ocean Physics Laboratory Technical Report #OPL-2-96. 26pp.
- Trask, R.P., B.S. Way, W.M. Ostrom, G.P. Allsup and R.A. Weller, 1995a. Arabian Sea mixed layer dynamics experiment: Mooring deployment cruise report, R/V *Thomas Thompson* cruise number 40, 11 October – 25 October 1994. Woods Hole Oceanographic Institution. Technical Report WHOI-95-01. 64pp.
- Trask, R.P., R.A. Weller and W.M. Ostrom, 1995b. Arabian Sea mixed layer dynamics experiment: Mooring deployment cruise report, R/V *Thomas Thompson* cruise number 46, 14 April – 29 April 1995. Woods Hole Oceanographic Institution. Technical Report WHOI-95-14. 92pp.
- Way, B.S., 1996: A stand-alone relative humidity and air temperature logger. Woods Hole Oceanographic Institution Upper Ocean Processes Group January 1996 Technical Note. Upper Ocean Processes Group, c/o Rick Trask, Woods Hole Oceanographic Institution, Woods Hole, Massachusetts 02543. 2 pp. Also available at <http://uop.whoi.edu>.
- Weller, R.A. and R.E. Davis, 1980. A vector measuring current meter. *Deep Sea Research*. **27A**, 1122–1136.
- Weller, R.A., D.L. Rudnick, R.E. Payne, J.P. Dean, N.J. Pennington and R.P. Trask, 1990. Measuring near-surface meteorology over the ocean from an array of surface moorings in the subtropical convergence zone. *Journal of Atmospheric and Oceanic Technology*. **7**, 85–103.

Appendix A: Ancillary Data

XBT and CTD

Expendable bathythermographs (XBT) and conductivity/temperature/depth (CTD) profiles were collected during each deployment and recovery cruise (R/V/ *Thomas Thompson* cruise 40, 46 and 52). These data, including station times, positions, water depths and plots, are described in Trask *et al.* (1995a), Trask *et al.* (1995b) and Ostrom *et al.* (1996).

Shipboard meteorological measurements

Concurrent shipboard meteorological measurements were collected after each deployment and just before recovery at an approximate distance of 0.25 miles from the buoy. These measurements provide an independent check of the buoy measurements to determine if some sensors were damaged during deployment and to provide pre-recovery calibration information should a sensor be damaged on recovery. The R/V *Thomas Thompson* carries an IMET system and during cruises 46 and 52, a second meteorological system was mounted on the ship (Trask *et al.*, 1995b; Ostrom *et al.*, 1996). Both of these systems measure air temperature, relative humidity, barometric pressure and wind speed and direction. The shipboard IMET system also records incoming short-wave radiation. All of the meteorological sensors were mounted to the jackstaff at a height of approximately 16.33 m. The ship also has a flow-through thermosalinograph capable of measuring temperature and conductivity. The intake for this flow-through system is at 4 m depth. Data from the three deployment and recovery cruises (40, 46 and 52) and four Seasoar cruises (42, 44, 48 and 51) were processed and are presented in Figures A1–A7.

The bulk flux algorithm described in Section 3 (Fairall *et al.*, 1996a) was used to estimate heat and momentum fluxes from the shipboard IMET and thermosalinograph measurements. Since no incoming long-wave radiation measurement was available, net long-wave was computed from estimated cloud cover, air and sea surface temperature and vapor pressure from Clark *et al.* (1974). Cloud cover was estimated from the observed incoming short-wave radiation and the theoretical clear-sky radiation (List, 1984) using an atmospheric transmission coefficient of 0.745. Since cloud cover can only be estimated from incoming short-wave radiation during the day, a 30 hour centered average of cloud cover was used in the net long-wave calculation as an approximation of the mean cloud cover at any one time. The estimated heat and momentum fluxes from the three deployment and recovery cruises and the four Seasoar cruises are presented in Figures A8–A14.

Drifting near-surface temperature array (DrifTAR)

A near-surface temperature array mounted to a modified three-ball radio float (DrifTAR) was used during R/V *Thomas Thompson* cruise 46 to investigate the effect of flow disturbance on the buoy-mounted near-surface temperature array (Trask *et al.*, 1995b). The DrifTAR was deployed approximately 0.25 miles from the buoy at sunrise in three 12 hour long experiments. The position of the DrifTAR relative to the buoy was tracked using range and bearing measurements of both the DrifTAR and the buoy to the ship. The near-surface temperatures for the three experiments are shown with incoming short-wave radiation and wind speed in Figures A15–A17.

Numerical Weather Prediction Models

Forecast fields generated by numerical weather prediction models from the European Centre for Medium Range Weather Forecasts (ECMWF) and the National Centers for Environmental Prediction (NCEP, formerly the National Meteorological Center [NMC]) were obtained for the duration of the Arabian Sea experiment. These fields include wind, air and sea surface temperature, a moisture variable (dew point temperature or specific humidity), barometric pressure, cloud cover, sensible and latent heat fluxes, net short- and long-wave radiation and wind stress. The NCEP model also includes predictions of precipitation rate. Both models are run four times daily at 0, 6, 12 and 18Z. To assess the accuracy of the model forecasts, each model variable was extracted at the grid point closest to the buoy (at 15.140N, 61.875E for ECMWF and 16.190N, 61.875E for NCEP) and evaluated against the corresponding in situ measurement. The ECMWF and NCEP meteorological variables were compared to 30 minute buoy averages centered on 0, 6, 12 and 18Z. Model heat and momentum fluxes were compared to 6 hour buoy averages. The moisture variable in each model was converted to relative and specific humidity for the comparisons.

Statistics of the difference between the models and the buoy observations are presented in Tables A1 and A2. These tables include the mean, standard deviation and standard error of the differences, the correlation coefficient and two sets of regression coefficients. Positive differences indicate that the model data is higher or larger than the buoy averages. The first set of regression coefficients are from a simple, linear regression yielding a slope and offset. The other regression coefficient reported in Tables A1 and A2 is the slope of a regression line forced through zero. Plots showing the ECMWF model and the buoy time series, a scatterplot and a histogram of the differences are presented in Figures A18–A30 and the same comparison plots for the NCEP model are provided in Figures A31–A43. The two sets of regression coefficients are superscripted as the simple linear regression (1) and the regression forced through zero (2) in Figures A18–A43.

Table A1. Mean, standard deviation and standard error of the difference between the ECMWF model and in situ buoy observations. Positive differences indicate that the model values are higher than those of the buoy. The correlation coefficient (r) and two sets of regression coefficients are also reported.

Variable	Unit	Mean	Std. Dev.	Std. Err.	r	Regression ^a		Slope ^b
						c ₁	c ₀	
Wind speed at 10m ^c	m s ⁻¹	0.249	1.860	0.049	0.869	0.89404	1.004	1.0065
Wind direction	°	2.2	32.9	0.9	0.957	1.0234	2.8	1.0182
Barometric pressure	mbar	0.42	0.64	0.02	0.992	0.92713	74.05	1.0004
Air temperature at 2m ^d	°C	0.070	0.796	0.021	0.895	0.98415	0.493	1.0026
Relative humidity at 2m ^d	%	-0.53	9.21	0.24	0.405	0.39051	46.99	0.98595
Specific humidity at 2m ^d	g kg ⁻¹	-0.106	1.672	0.044	0.821	0.73420	4.401	0.98637
Sea surface temperature	°C	-0.051	0.499	0.013	0.948	0.88784	3.005	0.99777
Sensible heat flux	W m ⁻²	-2.89	6.65	0.17	0.728	1.0961	-2.72	1.1994
Latent heat flux	W m ⁻²	-21.84	48.00	1.25	0.660	0.72857	-55.13	1.1028
Net short-wave radiation	W m ⁻²	-25.08	82.58	2.16	0.959	0.88289	3.42	0.88874
Net long-wave radiation	W m ⁻²	-2.06	19.53	0.51	0.697	0.68749	-20.39	0.98070
Net heat flux	W m ⁻²	-51.87	90.40	2.36	0.952	0.88739	-45.06	0.85747
Wind stress	N m ⁻²	0.00485	0.04734	0.00124	0.898	0.86395	0.01856	0.95106

^a Model = c₁ · Buoy + c₀

^b Model = Slope · Buoy

^c The 10m buoy wind speed was estimated from the boundary layer profile computed in the bulk flux algorithm.

^d The 2m buoy air temperature, relative humidity and specific humidity were estimated from the boundary layer profile computed in the bulk flux algorithm.

Table A2. Mean, standard deviation and standard error of the difference between the NCEP model and in situ buoy observations. Positive differences indicate that the model values are higher than those of the buoy. The correlation coefficient (r) and two sets of regression coefficients are also reported.

Variable	Unit	Mean	Std. Dev.	Std. Err.	r	Regression ^a		Slope ^b
						c ₁	c ₀	
Wind speed at 10m ^c	m s ⁻¹	-0.256	1.632	0.043	0.892	0.75426	1.494	0.9216
Wind direction	°	-1.9	31.4	0.8	0.964	1.0584	-0.6	1.0595
Barometric pressure	mbar	-0.31	1.30	0.03	0.976	1.13218	-133.88	0.9997
Air temperature at 2m ^d	°C	-0.414	0.830	0.022	0.914	1.12313	-3.698	0.9850
Relative humidity at 2m ^d	%	4.11	7.04	0.18	0.591	0.43179	48.42	1.04528
Specific humidity at 2m ^d	g kg ⁻¹	0.477	1.200	0.031	0.914	0.91162	1.976	1.02484
Sea surface temperature	°C	-0.124	0.461	0.012	0.956	0.92654	1.878	0.99524
Sensible heat flux	W m ⁻²	-4.74	9.47	0.25	0.761	1.5883	-3.76	1.7304
Latent heat flux	W m ⁻²	-32.30	46.54	1.22	0.736	0.91552	-42.66	1.2051
Net short-wave radiation	W m ⁻²	-21.82	83.72	2.19	0.959	0.86417	11.24	0.88340
Net long-wave radiation	W m ⁻²	-6.88	25.59	0.67	0.511	0.53322	-34.26	1.02583
Net heat flux	W m ⁻²	-65.71	93.45	2.44	0.949	0.87106	-57.91	0.83256
Wind stress	N m ⁻²	-0.00959	0.04454	0.00116	0.909	0.78639	0.01197	0.84254

^a Model = c₁ · Buoy + c₀

^b Model = Slope · Buoy

^c The 10m buoy wind speed was estimated from the boundary layer profile computed in the bulk flux algorithm.

^d The 2m buoy air temperature, relative humidity and specific humidity were estimated from the boundary layer profile computed in the bulk flux algorithm.

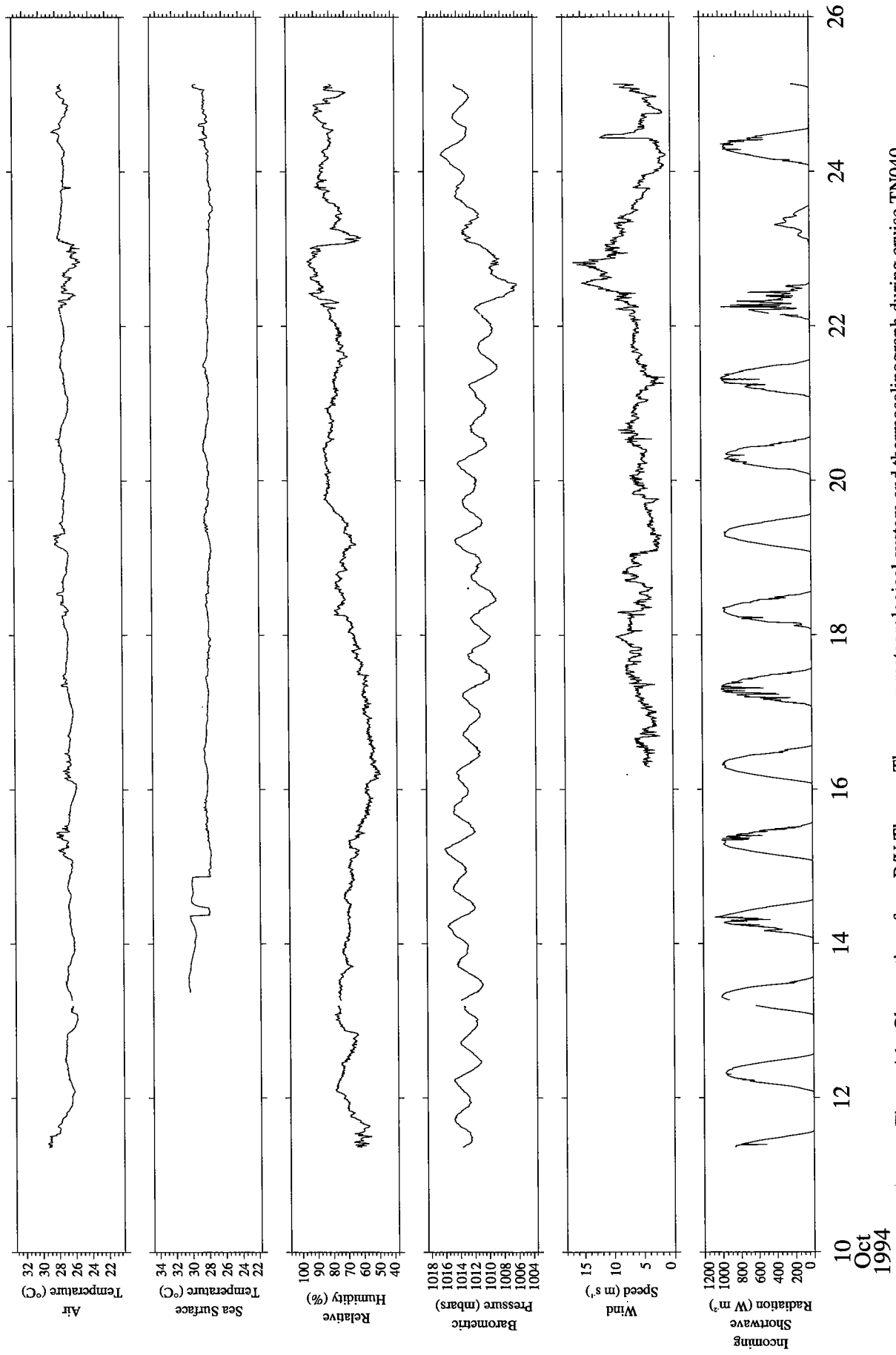


Figure A1. Observations from R/V Thomas Thompson meteorological system and thermalinograph during cruise TN040.

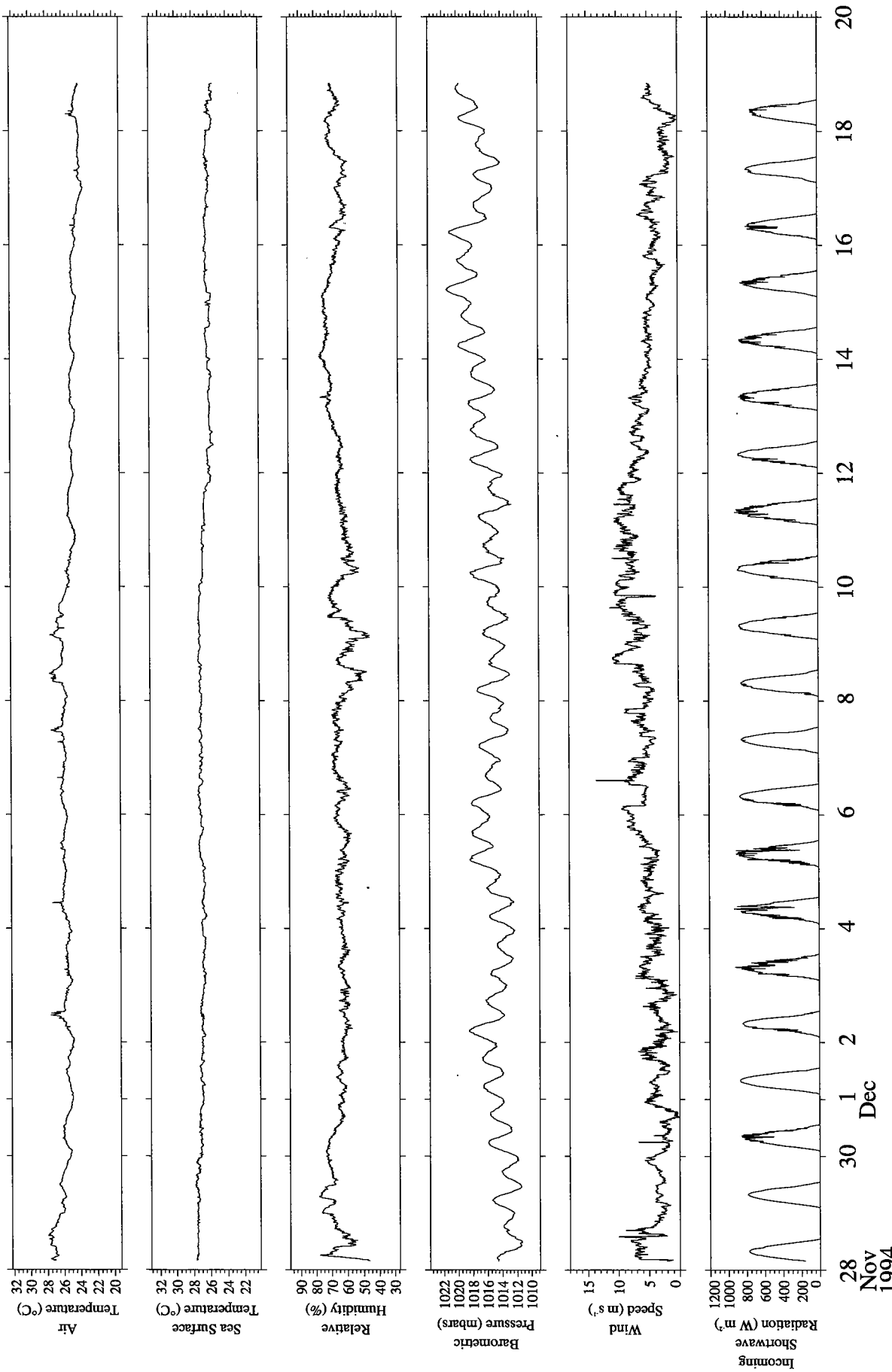


Figure A2. Observations from R/V Thomas Thompson meteorological system and thermosalinograph during cruise TN042.

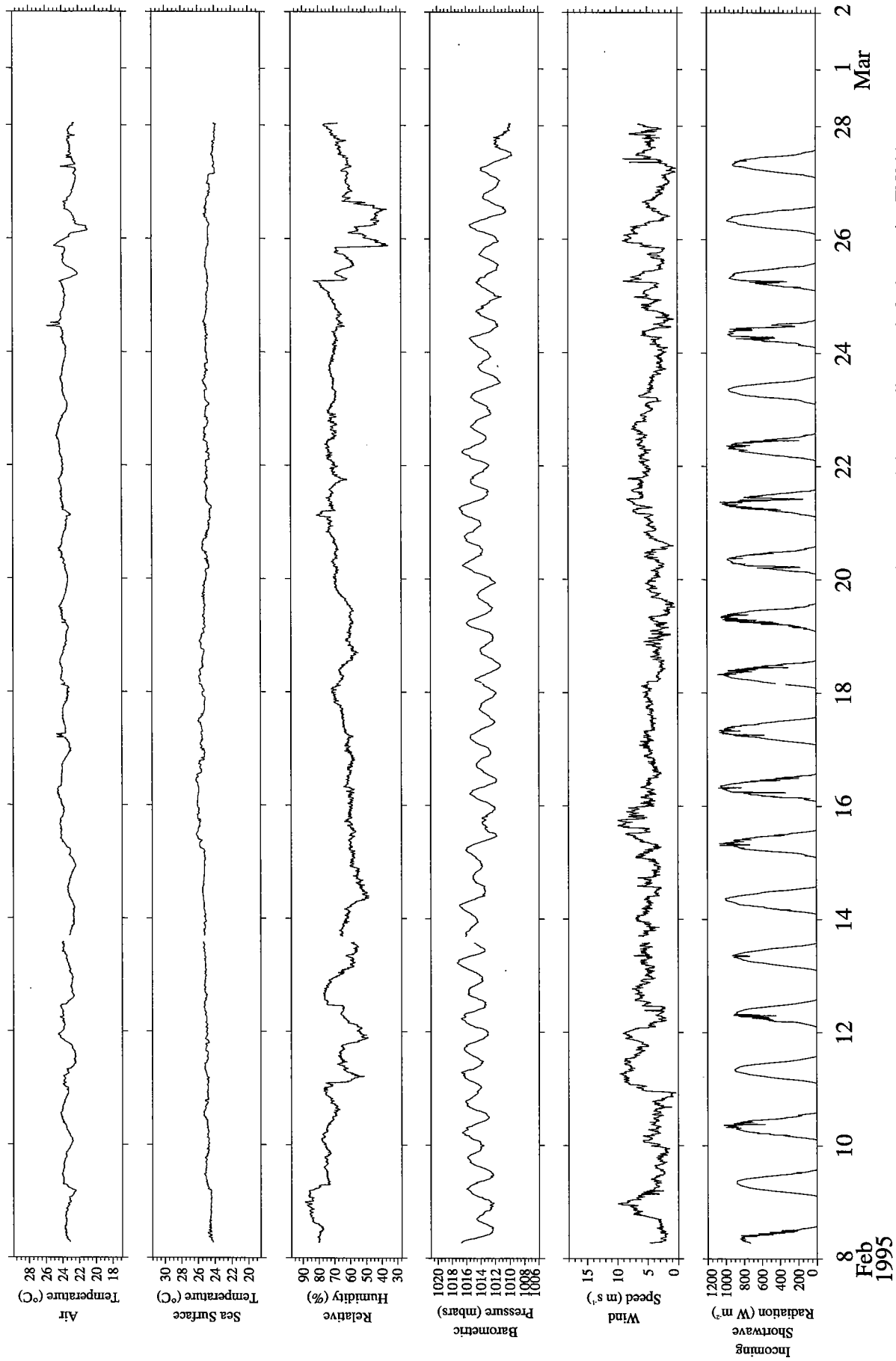


Figure A3. Observations from R/V Thomas Thompson meteorological system and thermosalinograph during cruise TN044.

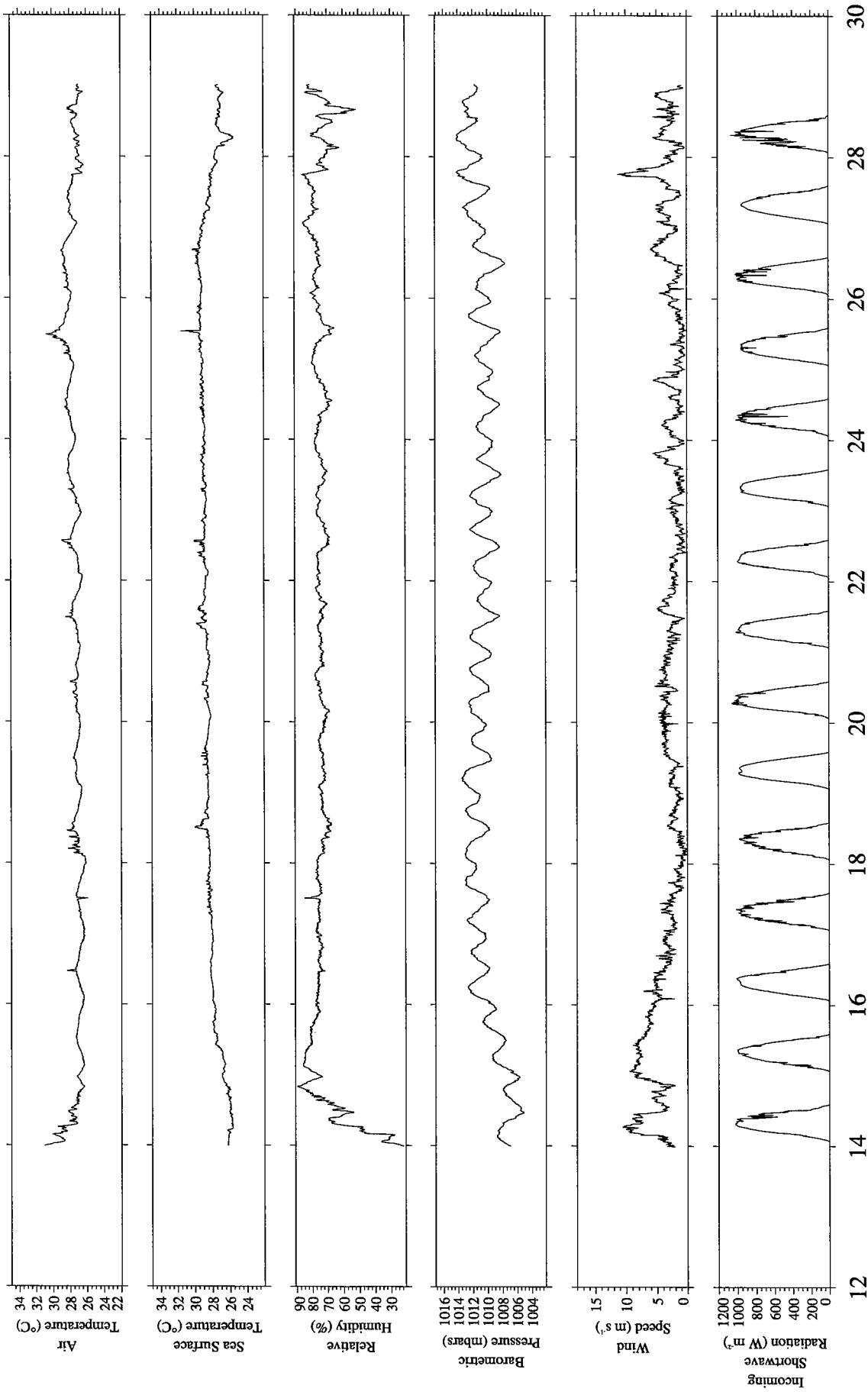


Figure A4. Observations from R/V Thomas Thompson meteorological system and thermosalinograph during cruise TN046.

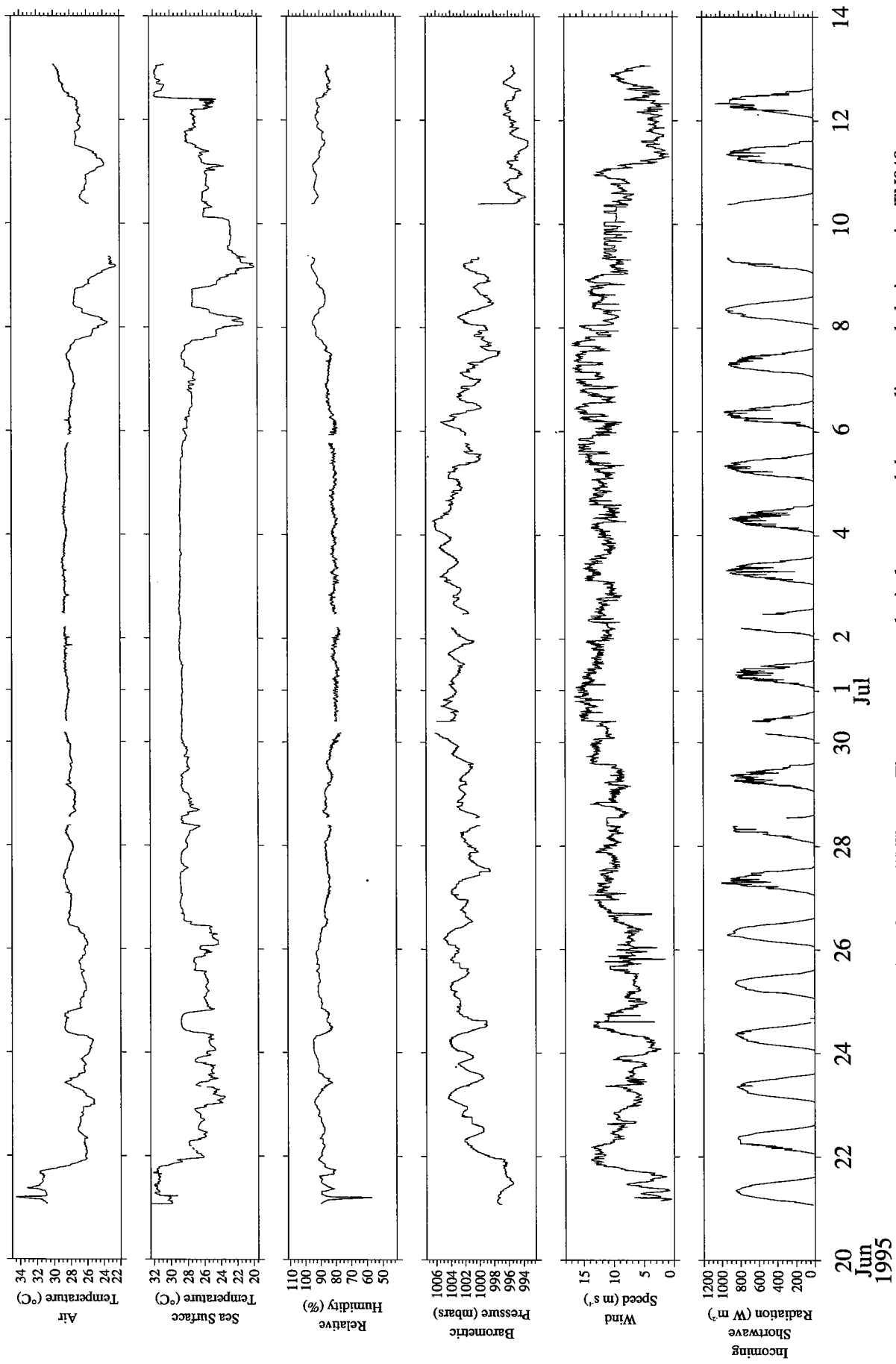


Figure A5. Observations from R/V Thomas Thompson meteorological system and thermalinograph during cruise TN048.

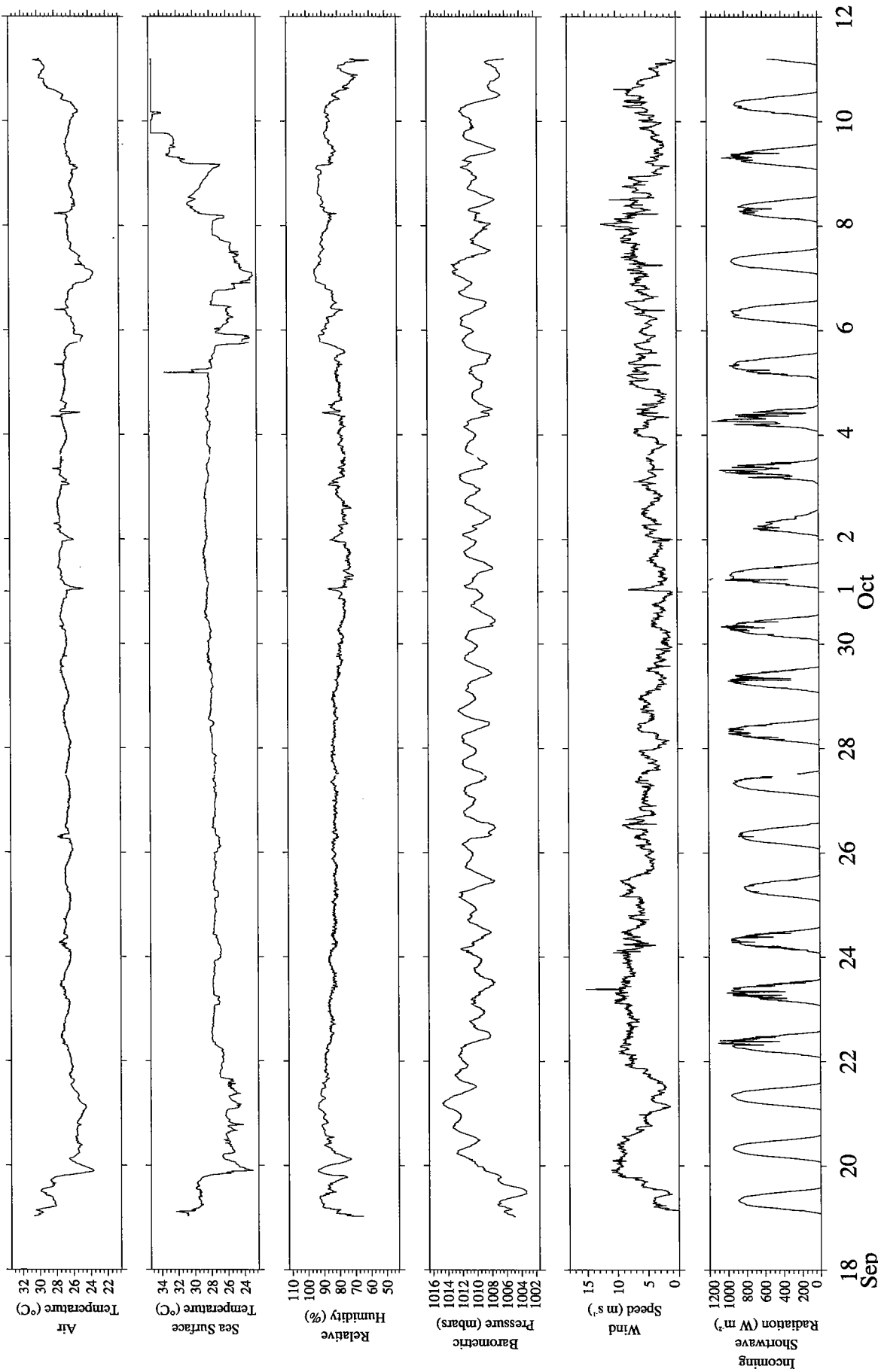


Figure A6. Observations from R/V Thomas Thompson meteorological system and thermosalinograph during cruise TN051.

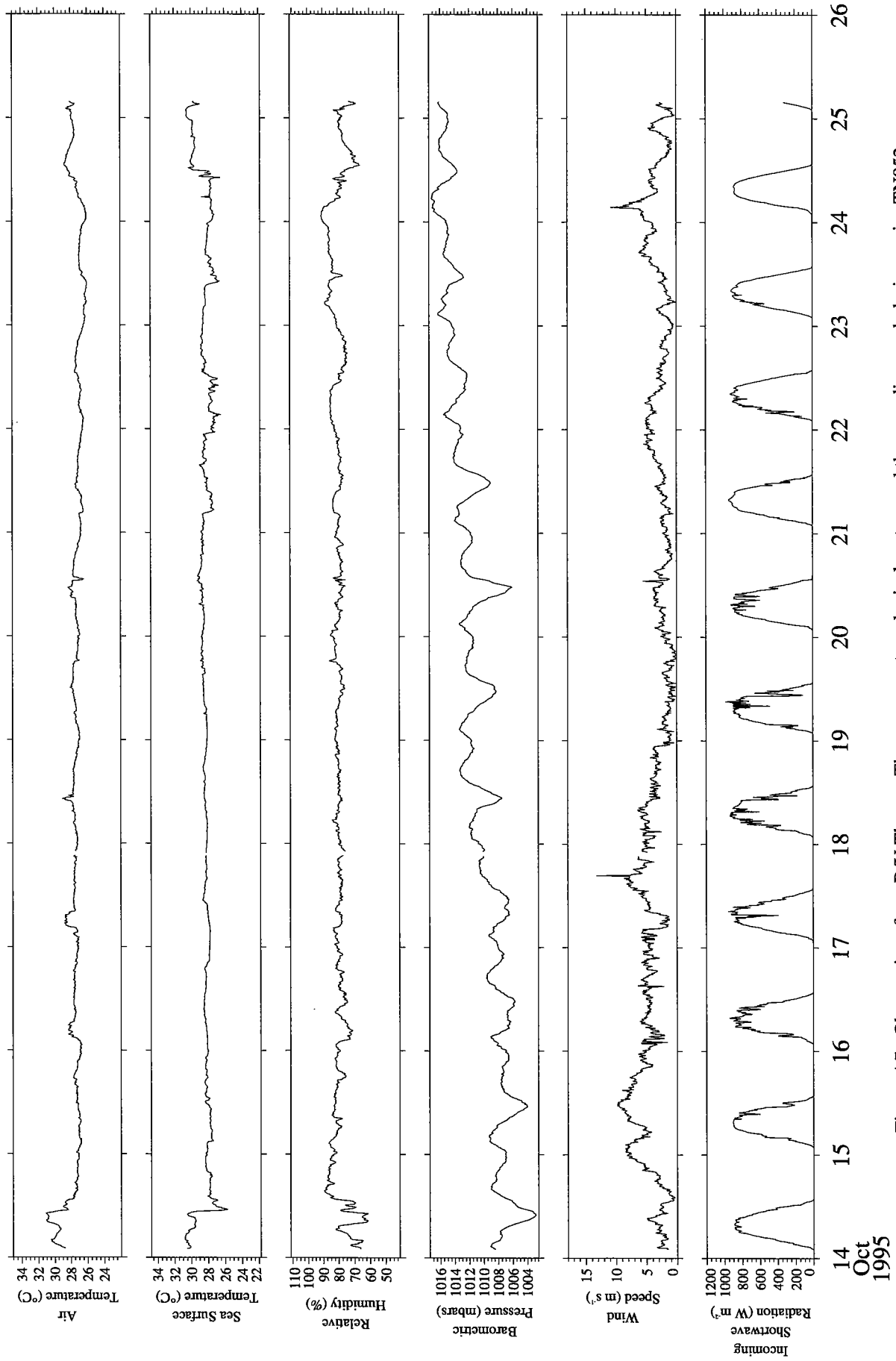


Figure A7. Observations from R/V Thomas Thompson meteorological system and thermosalinograph during cruise TN052.

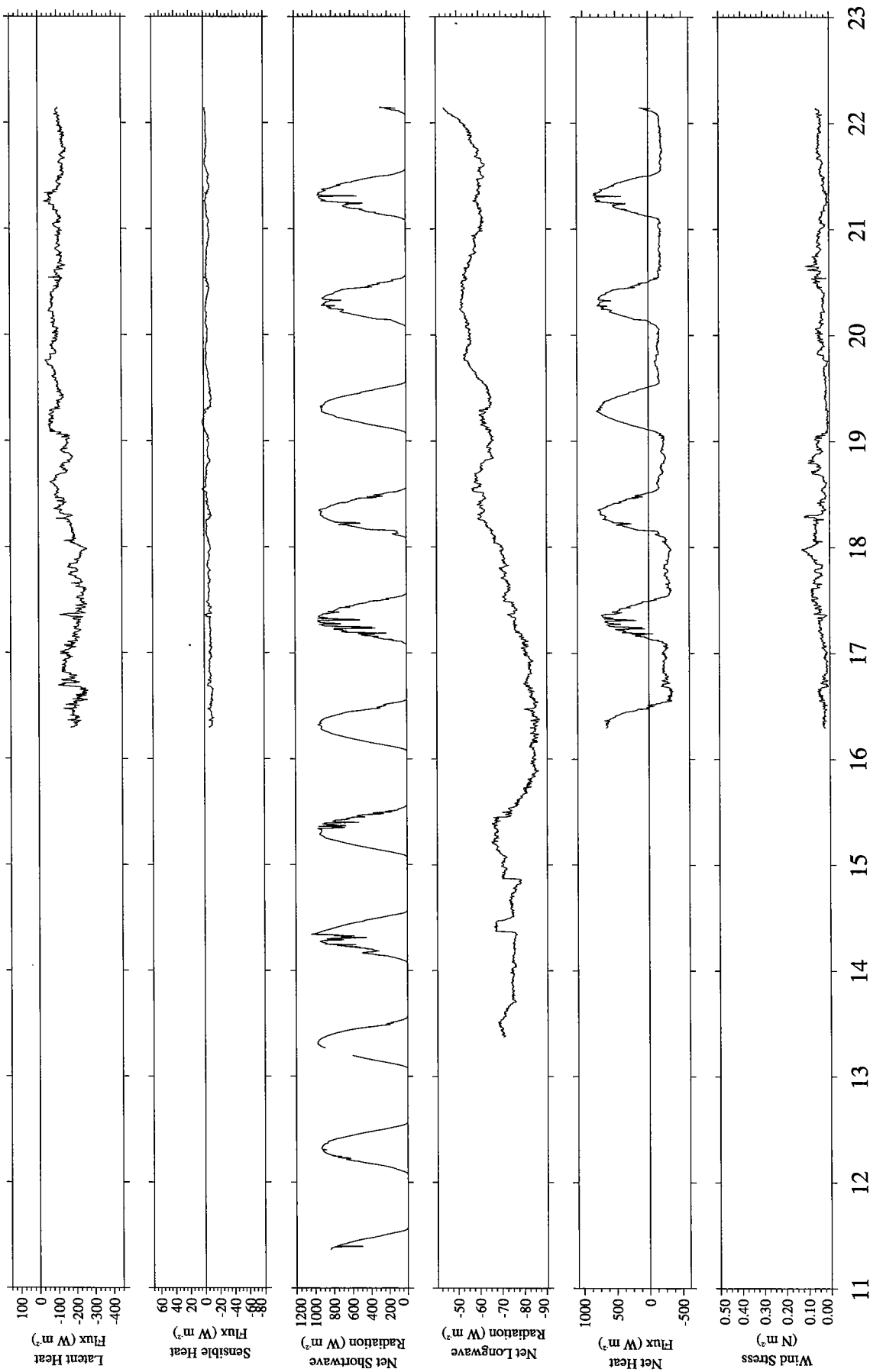


Figure A8. Estimated heat and momentum fluxes from R/V Thomas Thompson during cruise TN040.

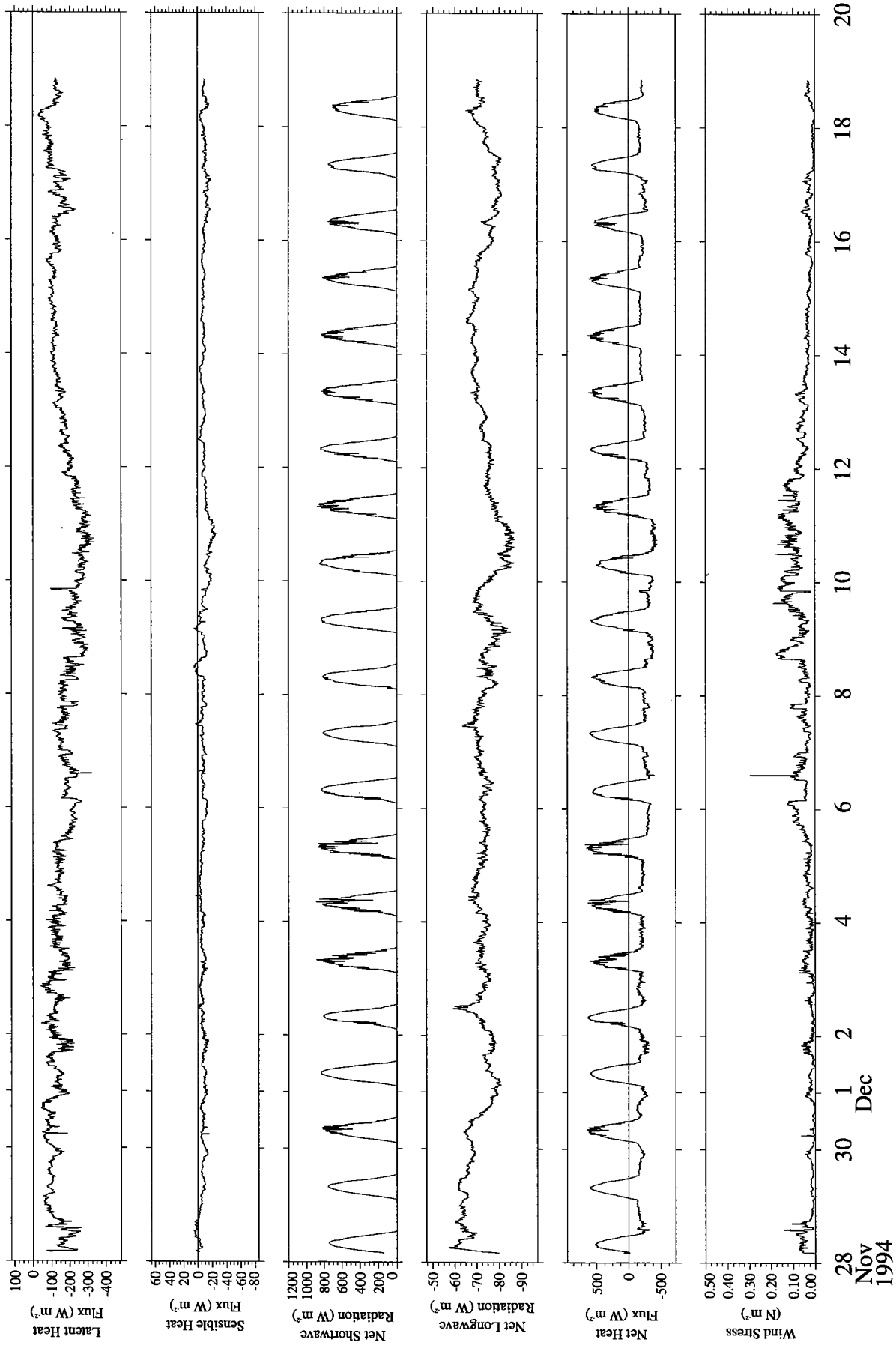


Figure A9. Estimated heat and momentum fluxes from R/V Thomas Thompson during cruise TN042.

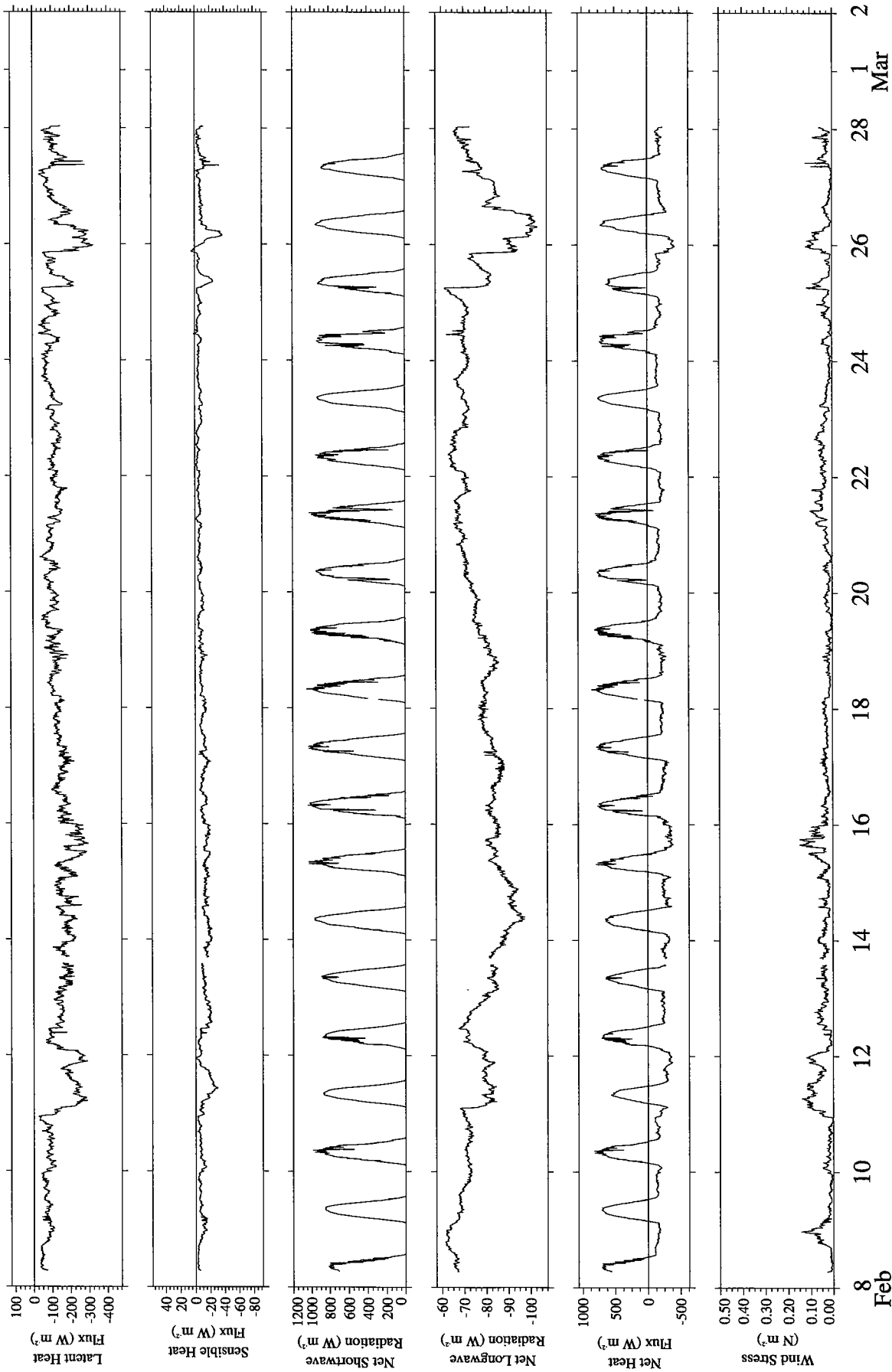


Figure A10. Estimated heat and momentum fluxes from R/V Thomas Thompson during cruise TN044.

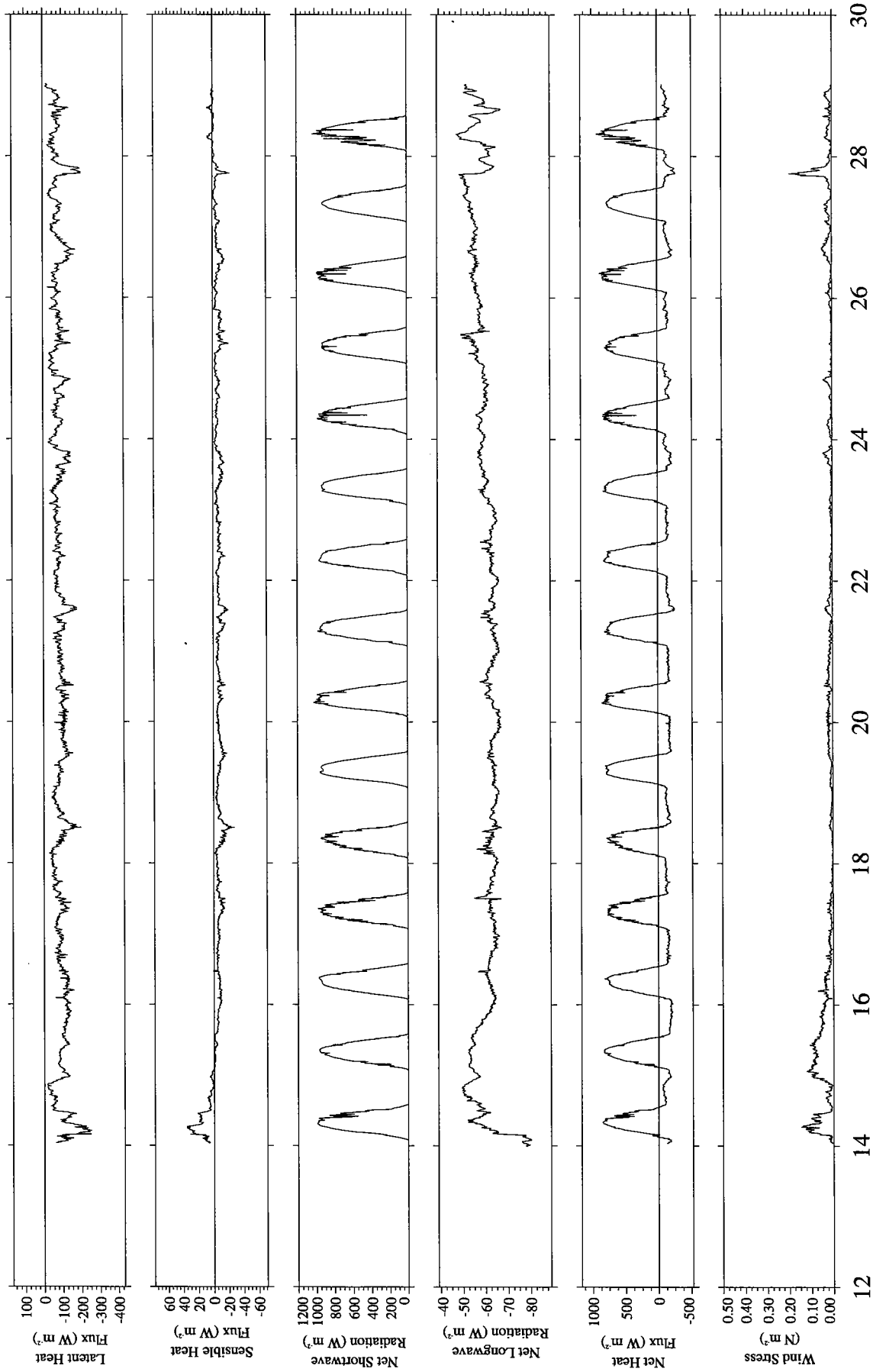


Figure A11. Estimated heat and momentum fluxes from R/V Thomas Thompson during cruise TN046.

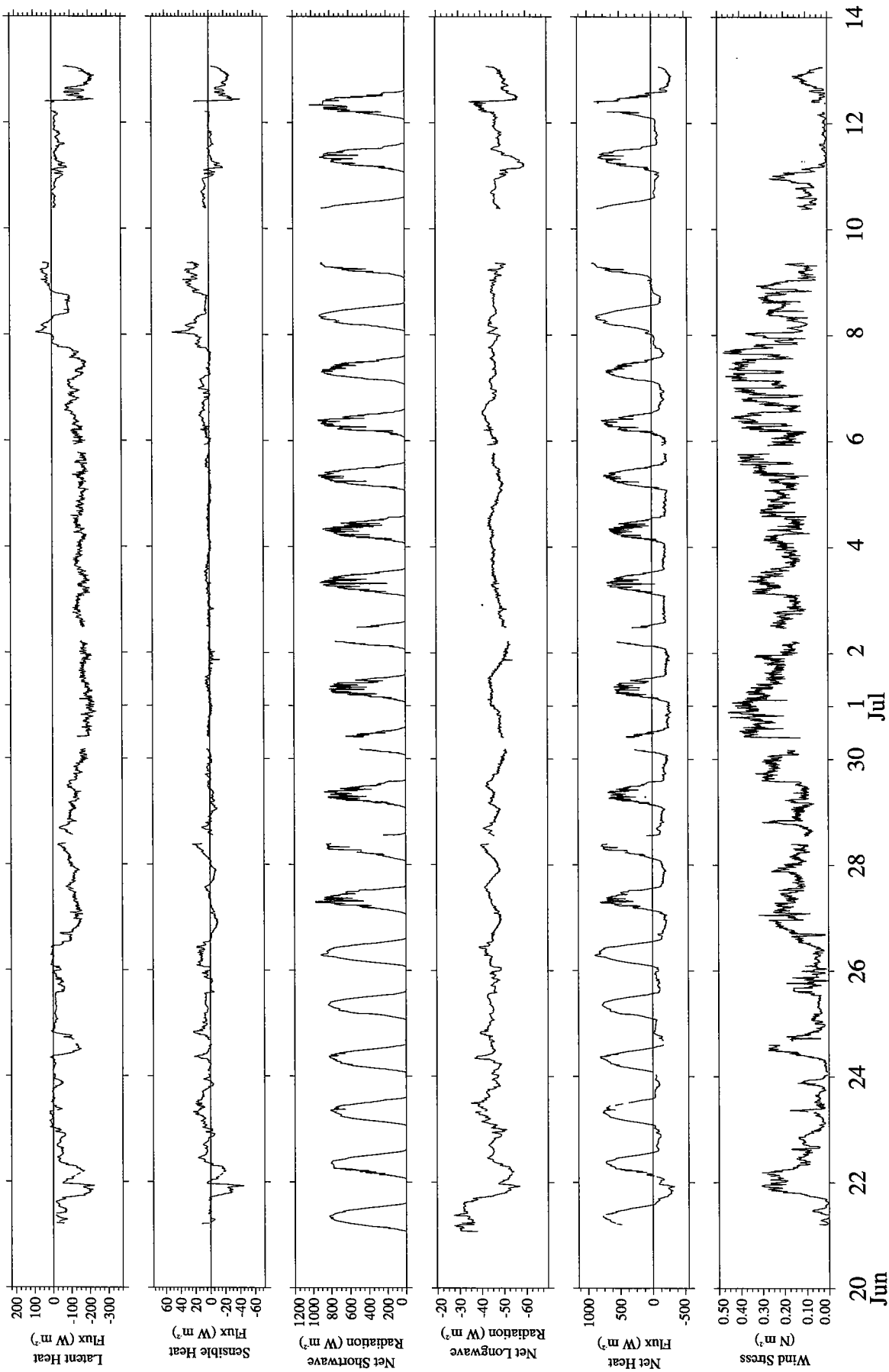


Figure A12. Estimated heat and momentum fluxes from R/V Thomas Thompson during cruise TN048.

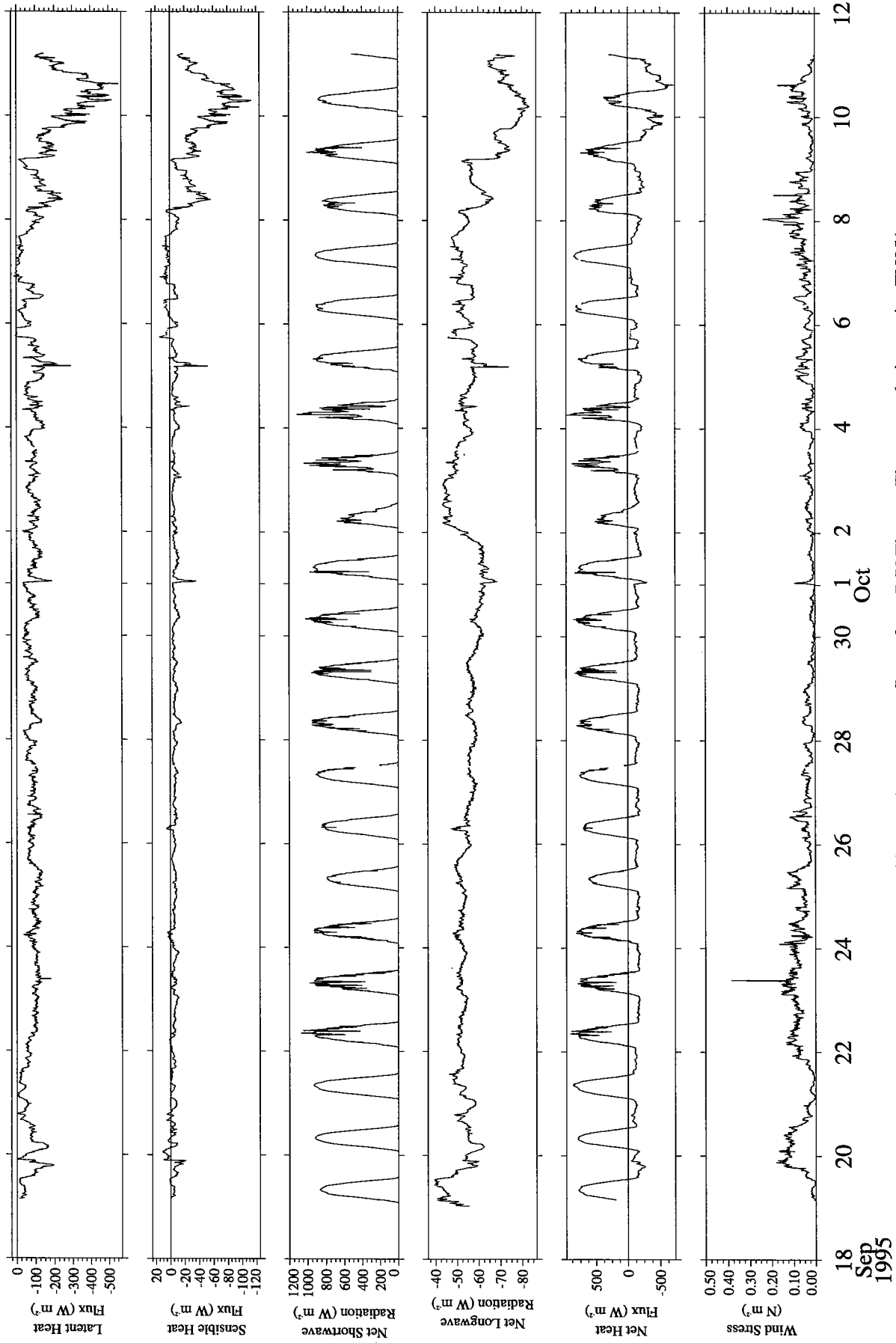


Figure A13. Estimated heat and momentum fluxes from R/V Thomas Thompson during cruise TN051.

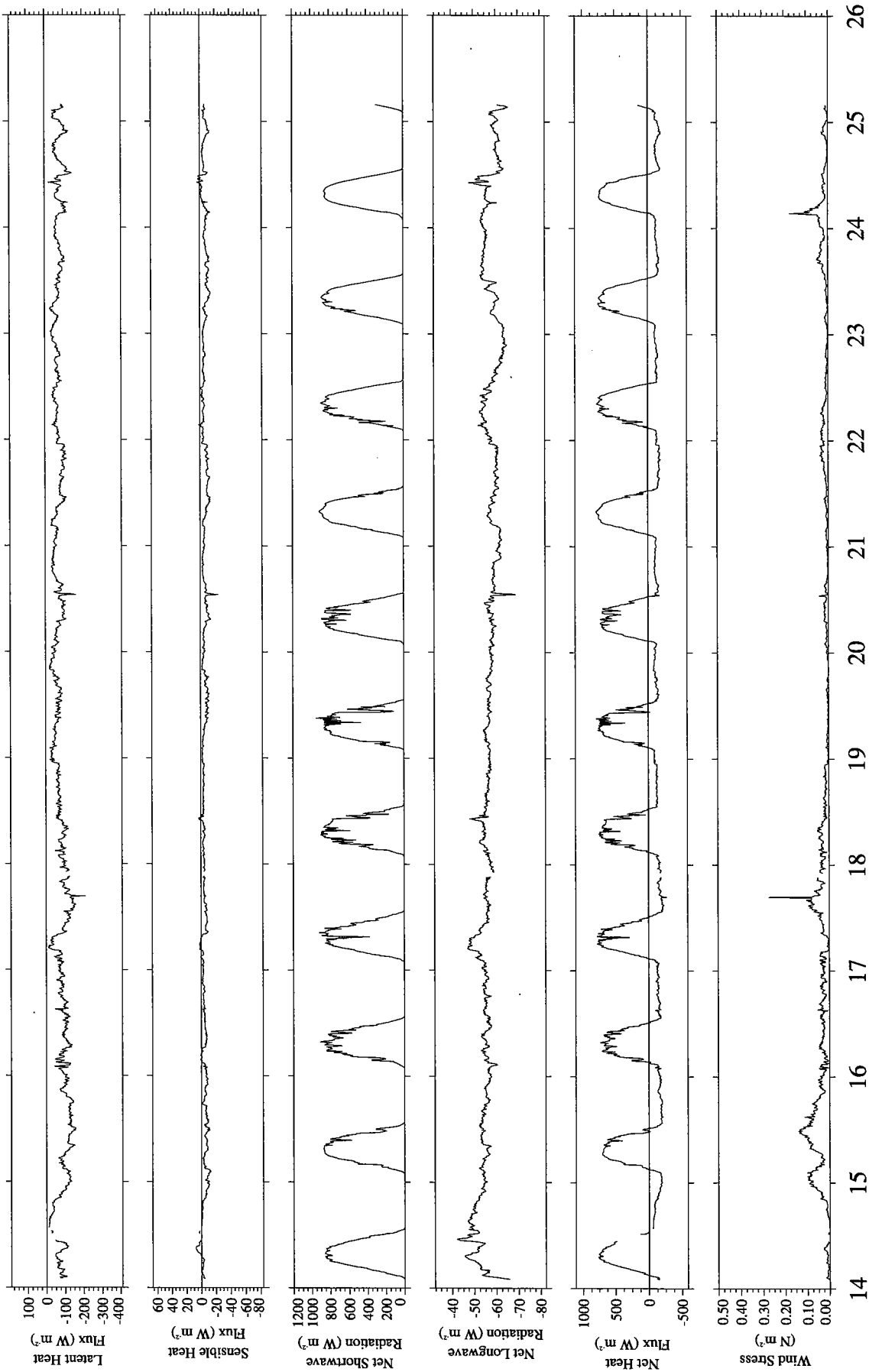


Figure A14. Estimated heat and momentum fluxes from R/V Thomas Thompson during cruise TN052.

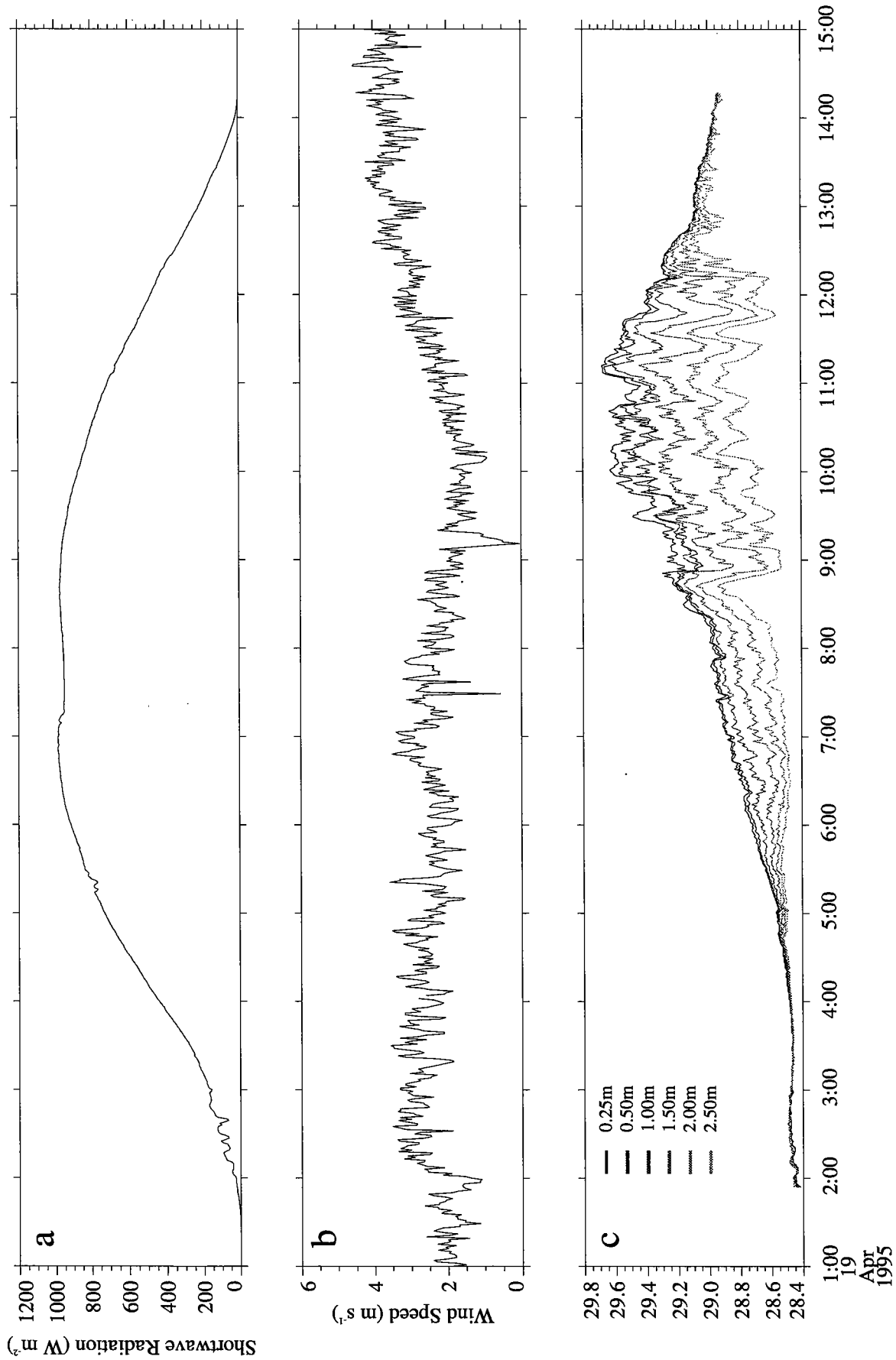


Figure A15. (a) Incoming short-wave radiation, (b) wind speed and (c) near-surface temperature during DriftAR experiment 1. Short-wave radiation and wind speed were measured aboard the R/V Thomas Thompson. Near surface temperatures were measured by the DriftAR.

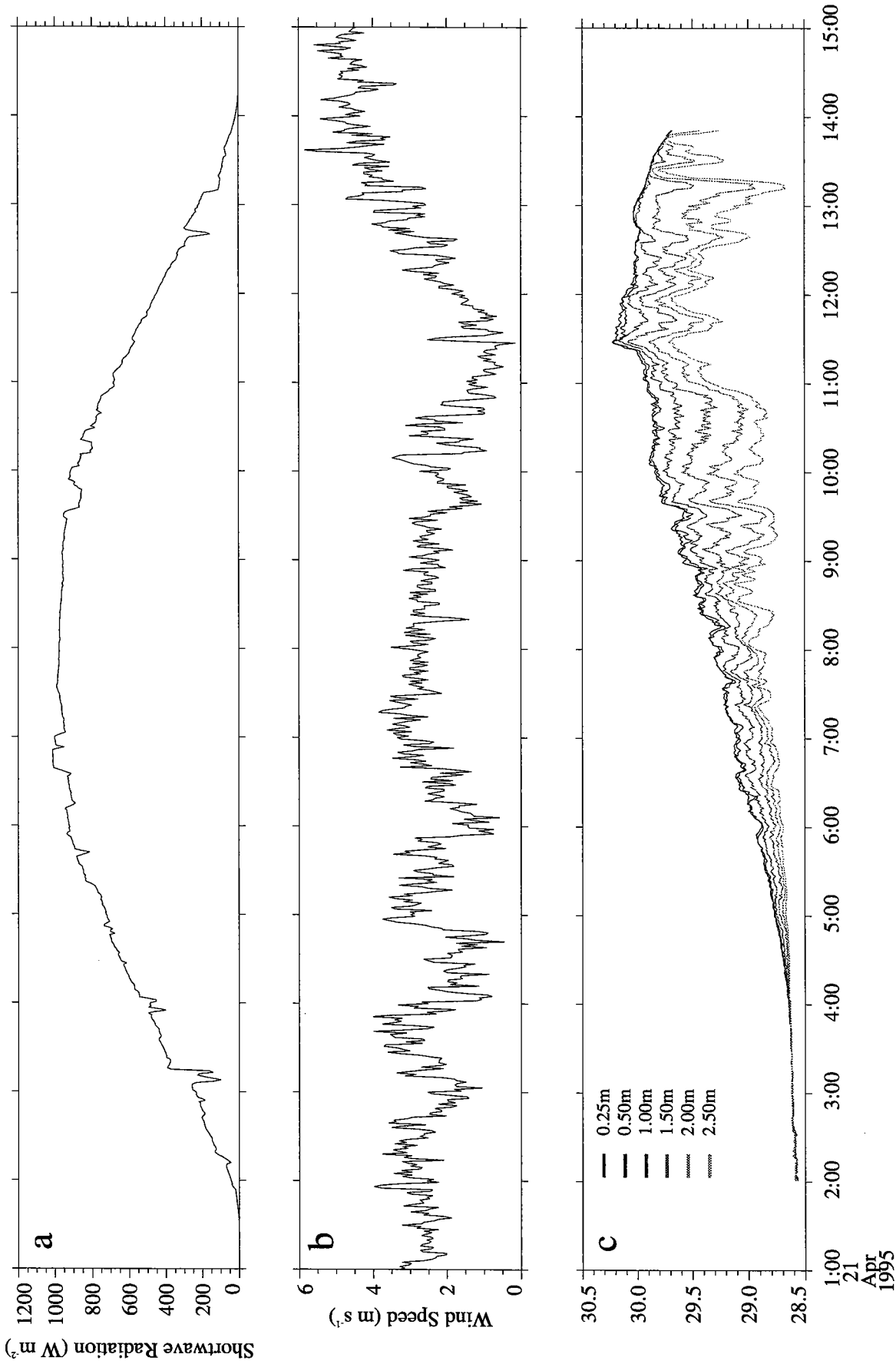


Figure A16. (a) Incoming short-wave radiation, (b) wind speed and (c) near-surface temperature during DriftAR experiment 2. Short-wave radiation and wind speed were measured aboard the R/V Thomas Thompson. Near surface temperatures were measured by the DriftAR.

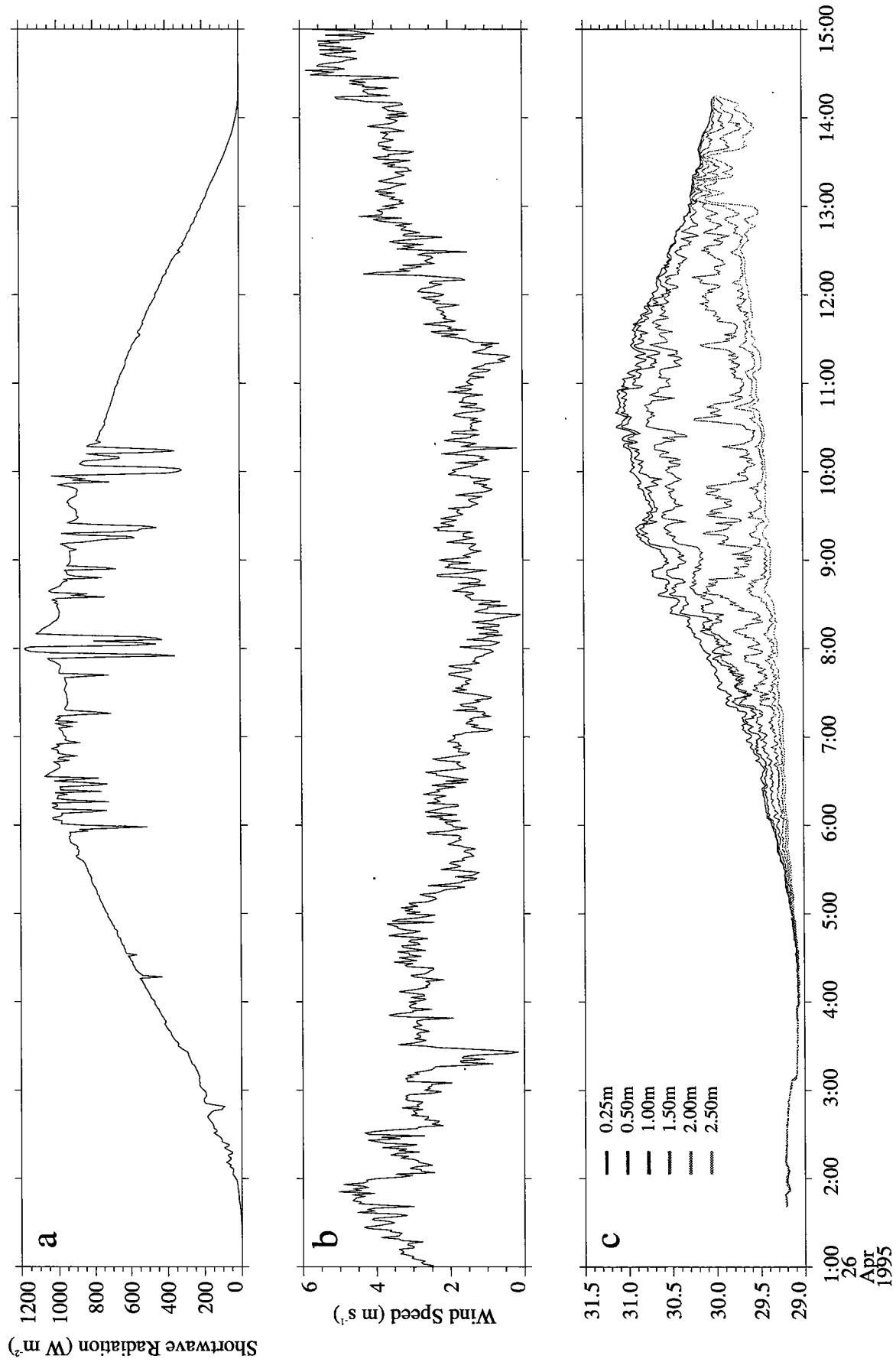
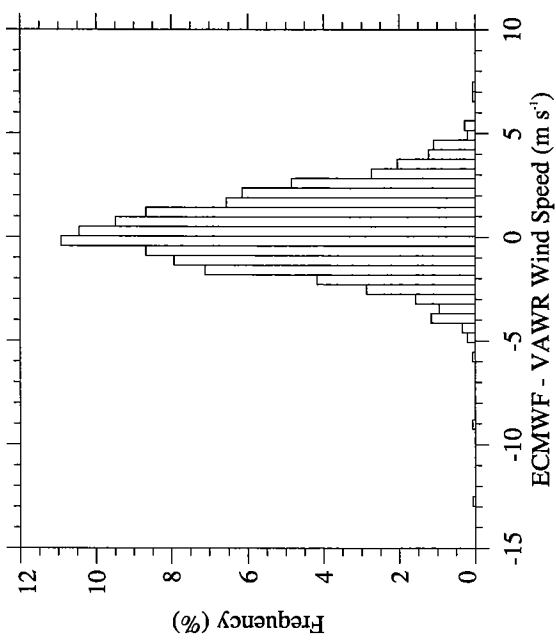
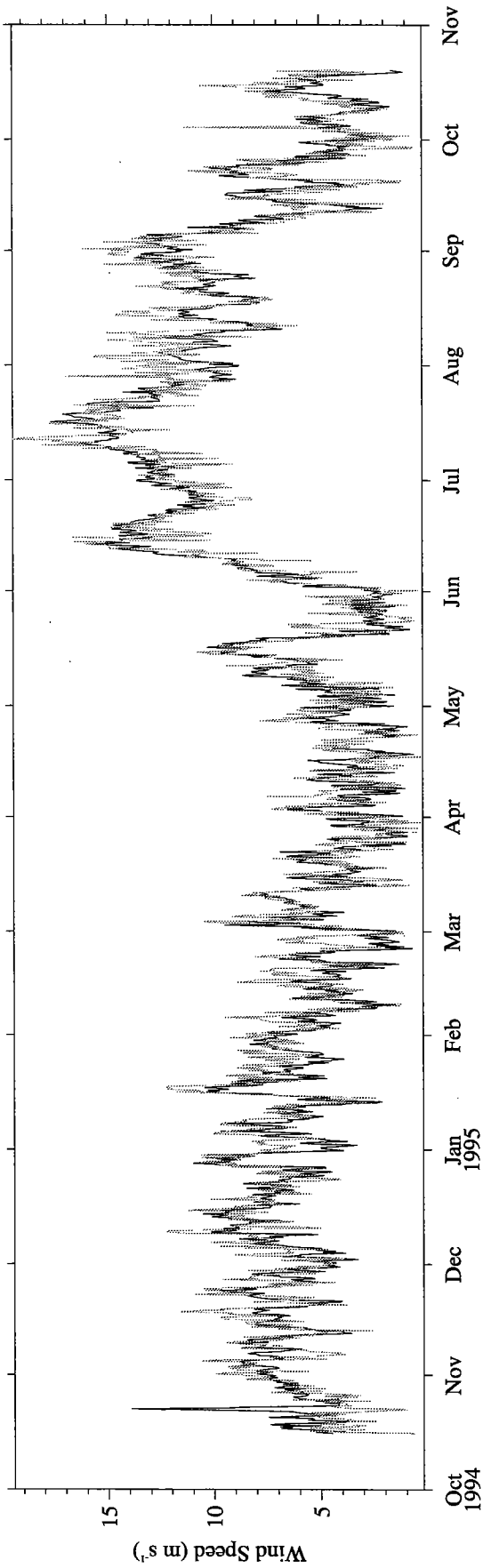


Figure A17. (a) Incoming short-wave radiation, (b) wind speed and (c) near-surface temperature during DriftAR experiment 3. Short-wave radiation and wind speed were measured aboard the R/V Thomas Thompson. Near surface temperatures were measured by the DriftAR.



Statistics	
N:	1464
Median(ECMWF - VAWR):	0.219727
Mean(ECMWF - VAWR):	0.248845
Stdev(ECMWF - VAWR):	1.85990
Stderr(ECMWF - VAWR):	0.0486094
Correlation:	0.869460
ECMWF = 0.894041 VAWR + 1.00368	
ECMWF² = 1.00649 VAWR	

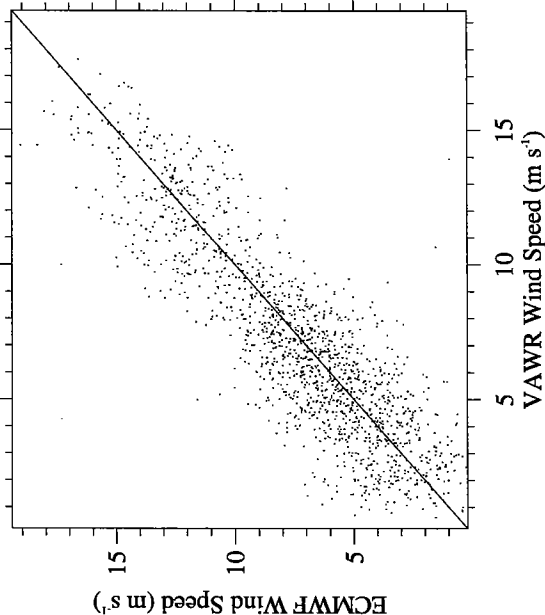


Figure A18. ECMWF (gray) vs. VAWR (black) wind speed.

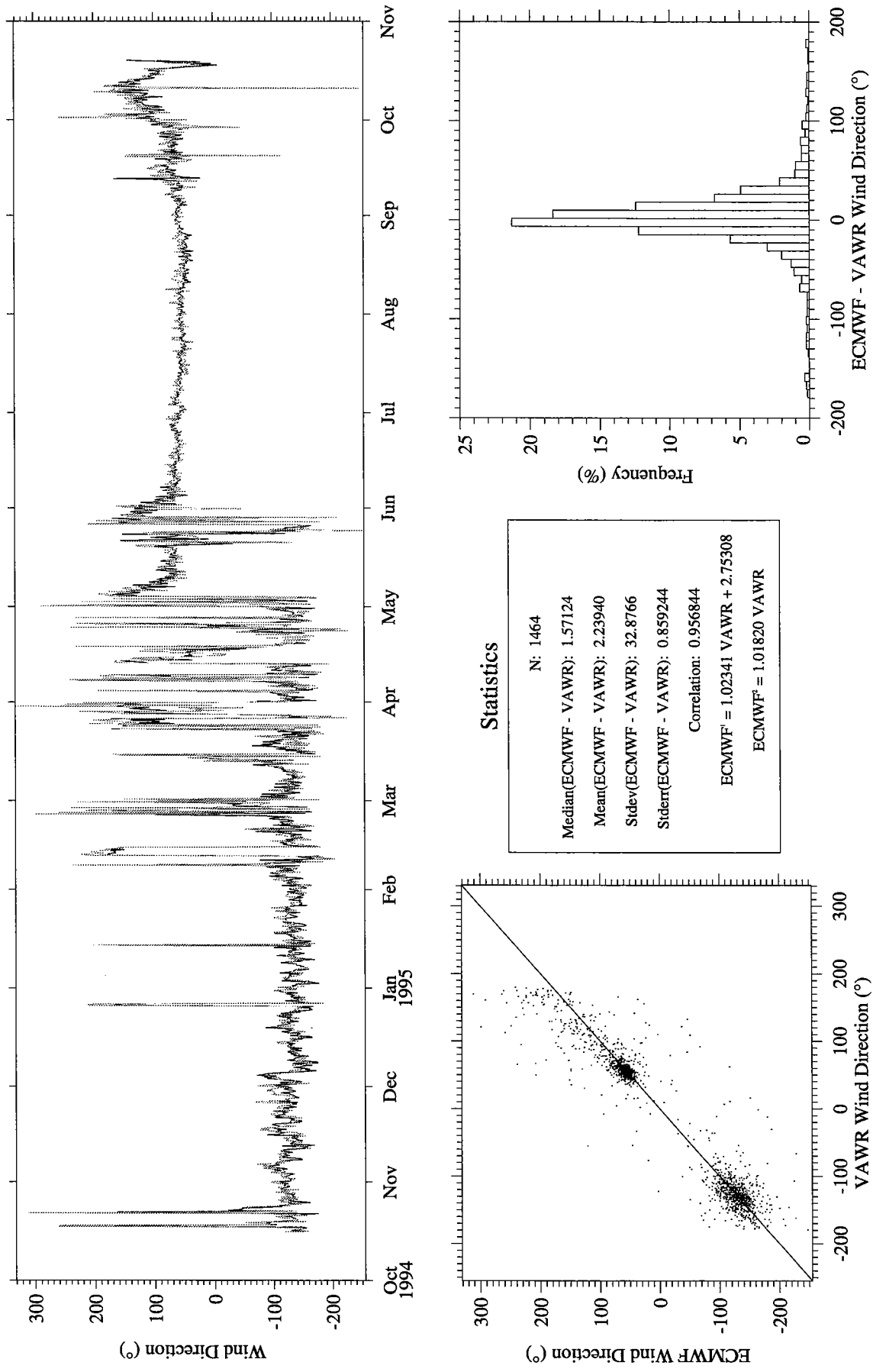


Figure A19. ECMWF (gray) vs. VAWR (black) wind direction.

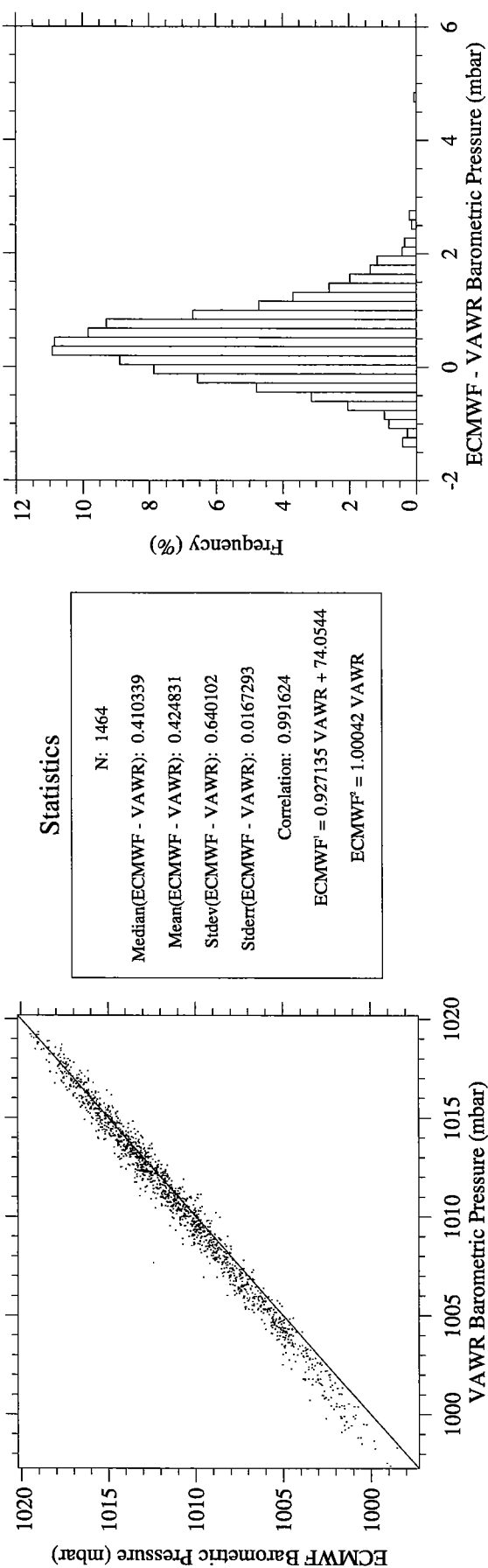
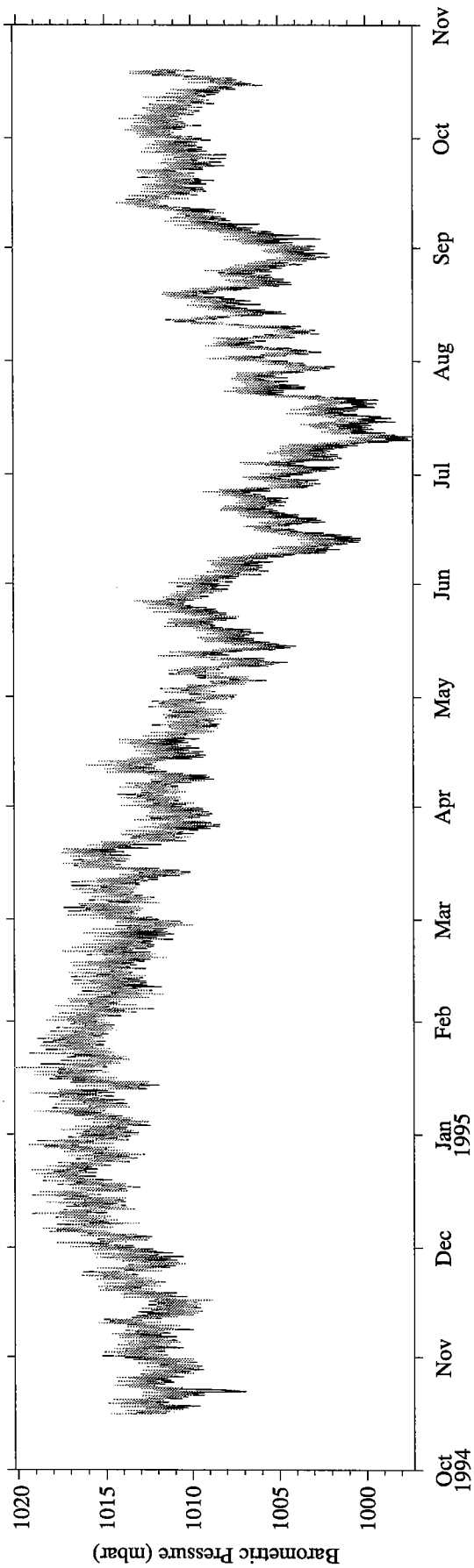


Figure A20. ECMWF (gray) vs. VAWR (black) barometric pressure.

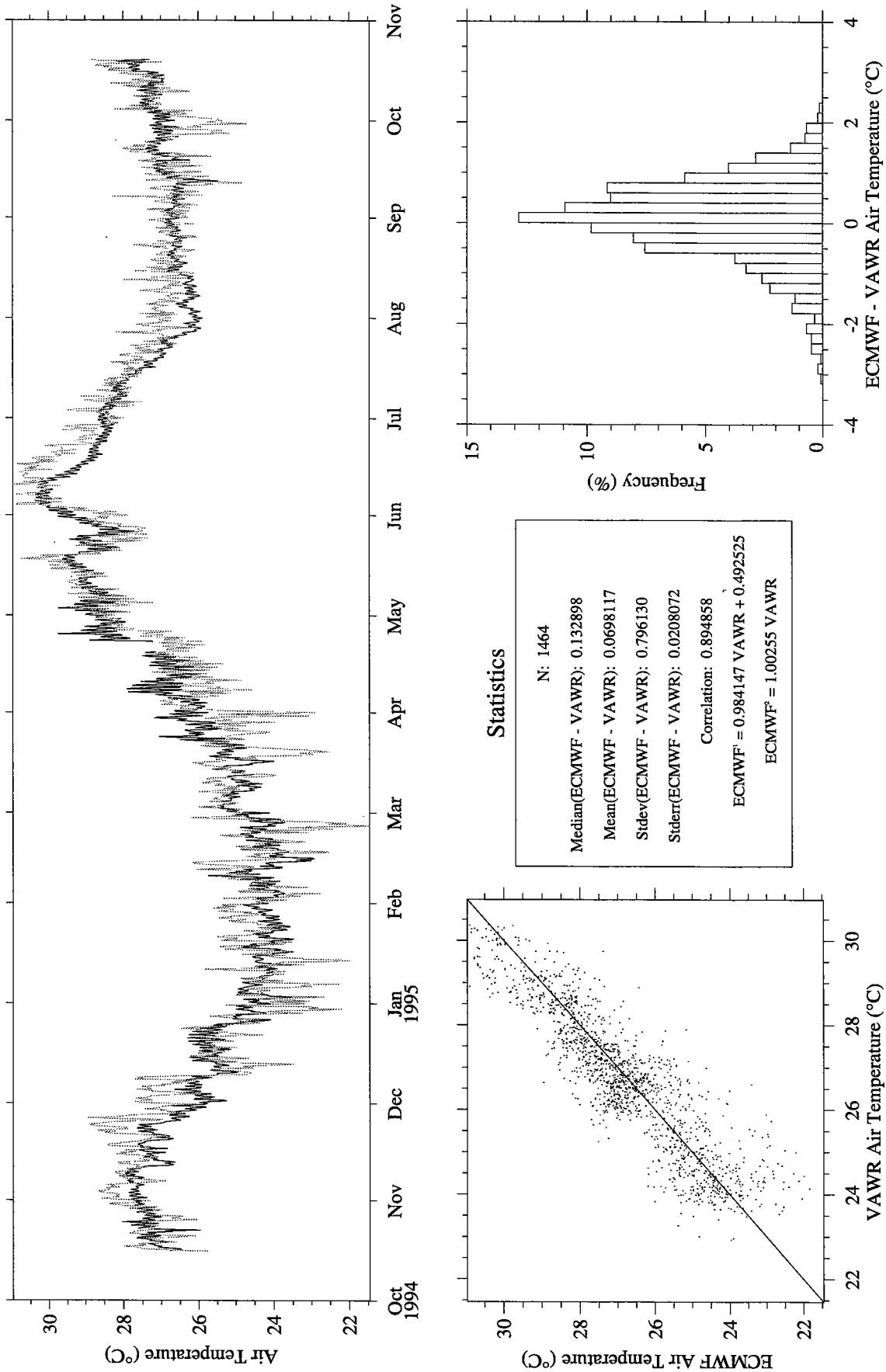
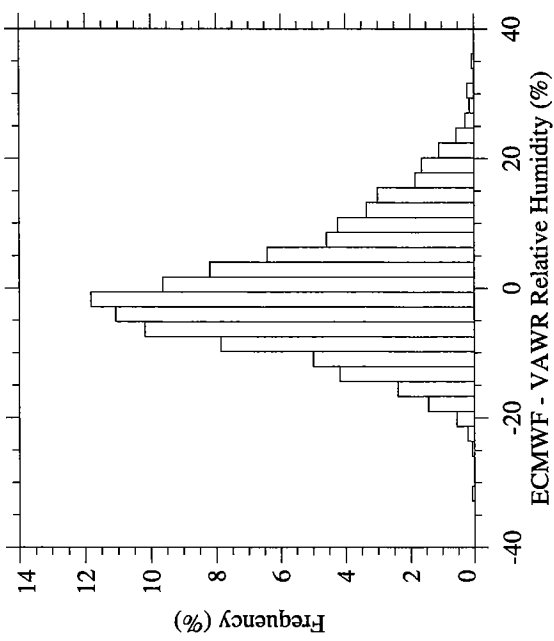
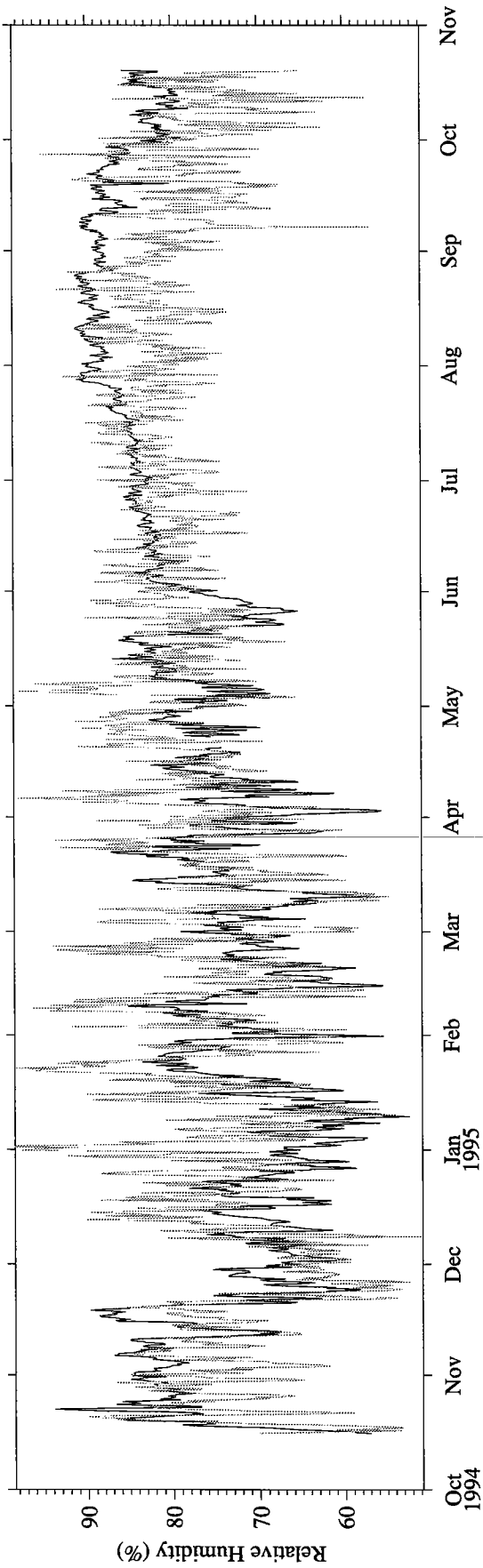


Figure A21. ECMWF (gray) vs. VAWR (black) air temperature.



Statistics

N:	1464
Median(ECMWF - VAWR):	-1.38358
Mean(ECMWF - VAWR):	-0.531728
Stdev(ECMWF - VAWR):	9.20802
Stderr(ECMWF - VAWR):	0.240655
Correlation:	0.405236
ECMWF =	0.390513 VAWR + 46.9947
ECMWF =	0.985952 VAWR

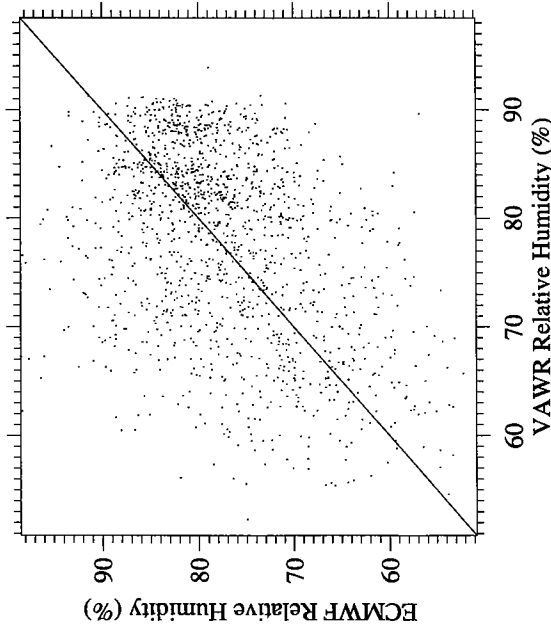


Figure A22. ECMWF (gray) vs. VAWR (black) relative humidity.

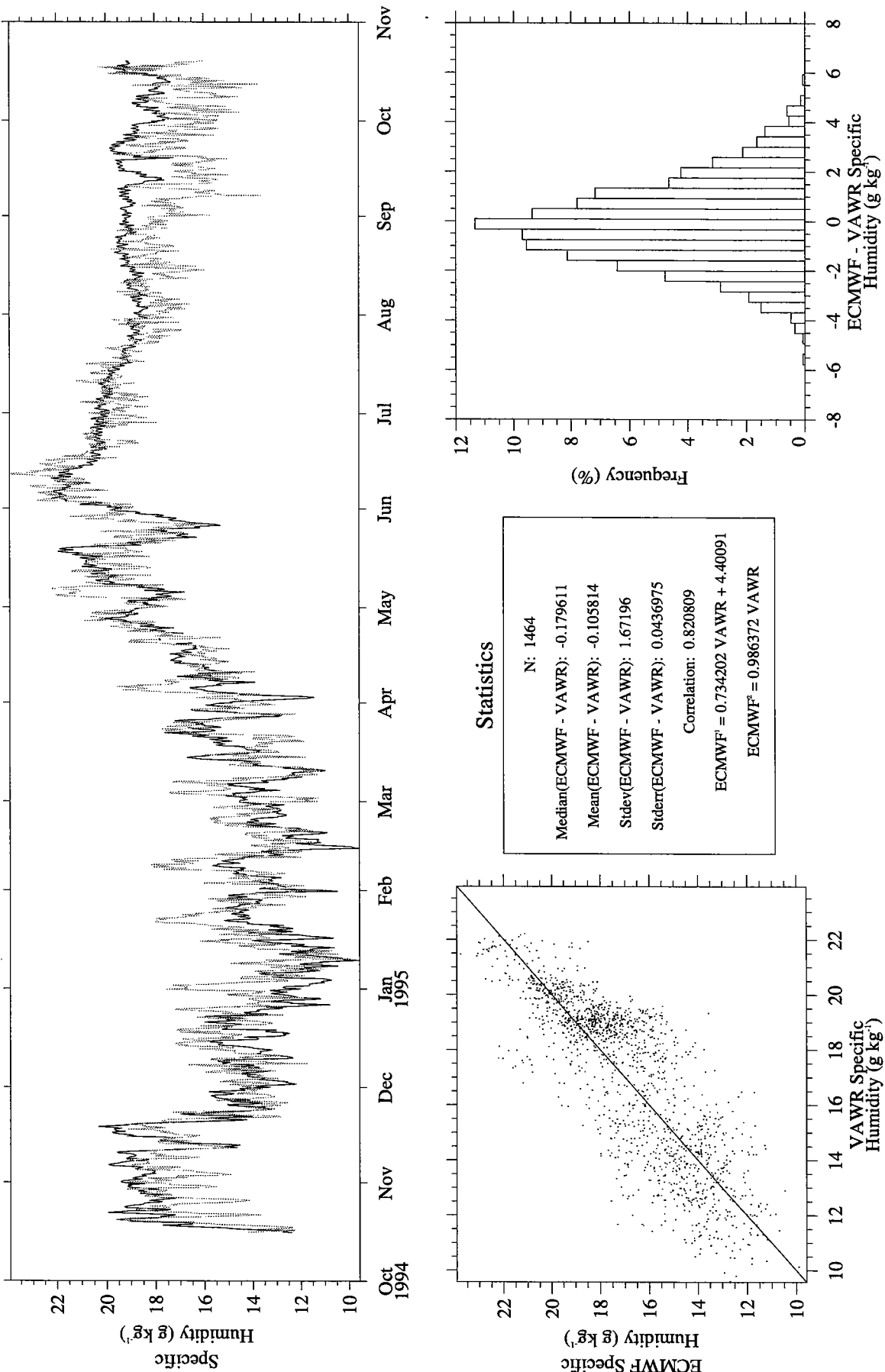
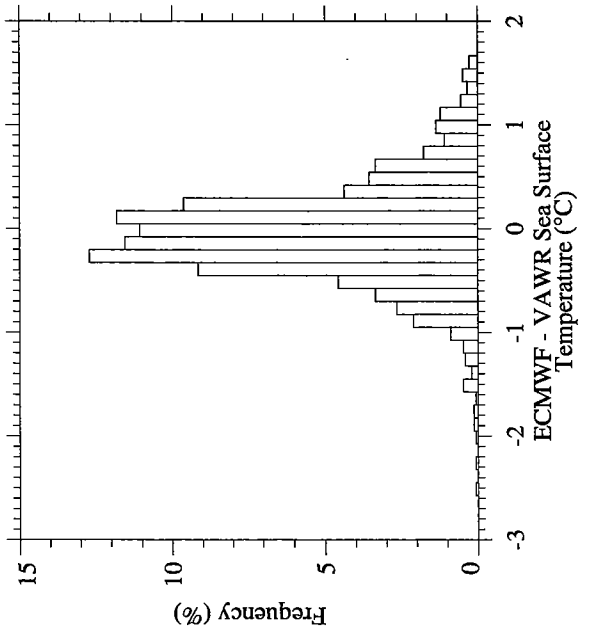
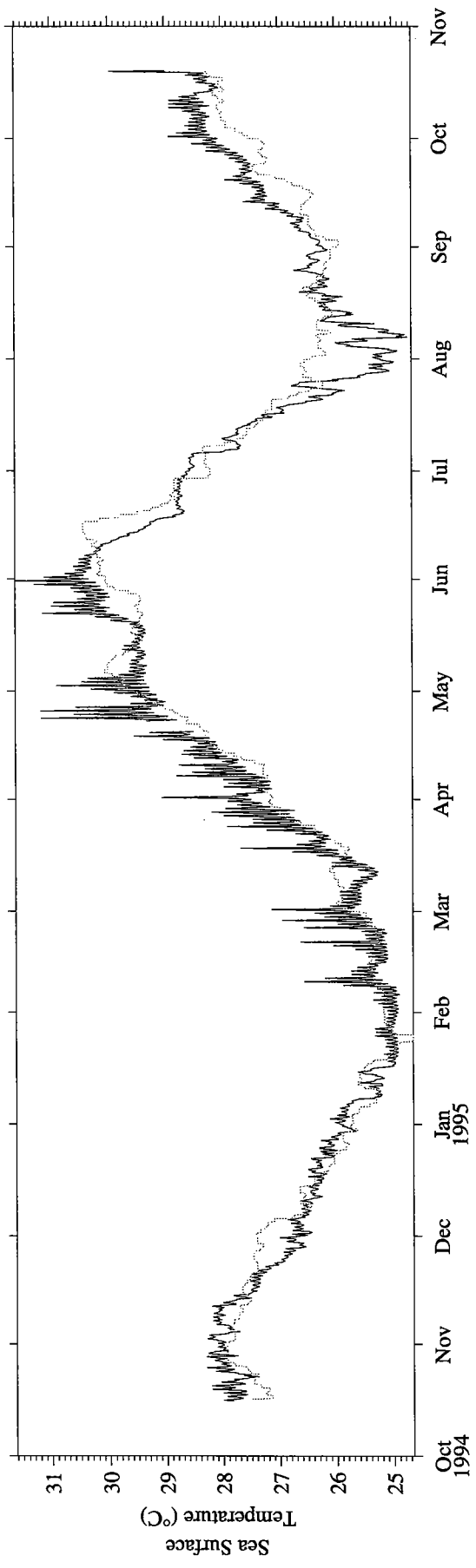


Figure A23. ECMWF (gray) vs. VAWR (black) specific humidity.



Statistics

N: 1464

Median(ECMWF - VAWR): -0.0688019

Mean(ECMWF - VAWR): -0.0510007

Stdev(ECMWF - VAWR): 0.498772

Stderr(ECMWF - VAWR): 0.0130356

Correlation: 0.947900

ECMWF = 0.887837 VAWR + 3.00474

ECMWF² = 0.997767 VAWR

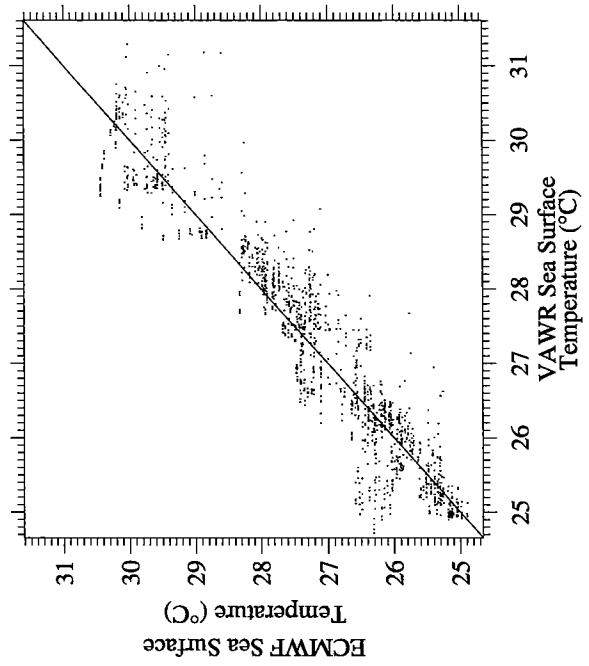


Figure A24. ECMWF (gray) vs. VAWR (black) sea surface temperature.

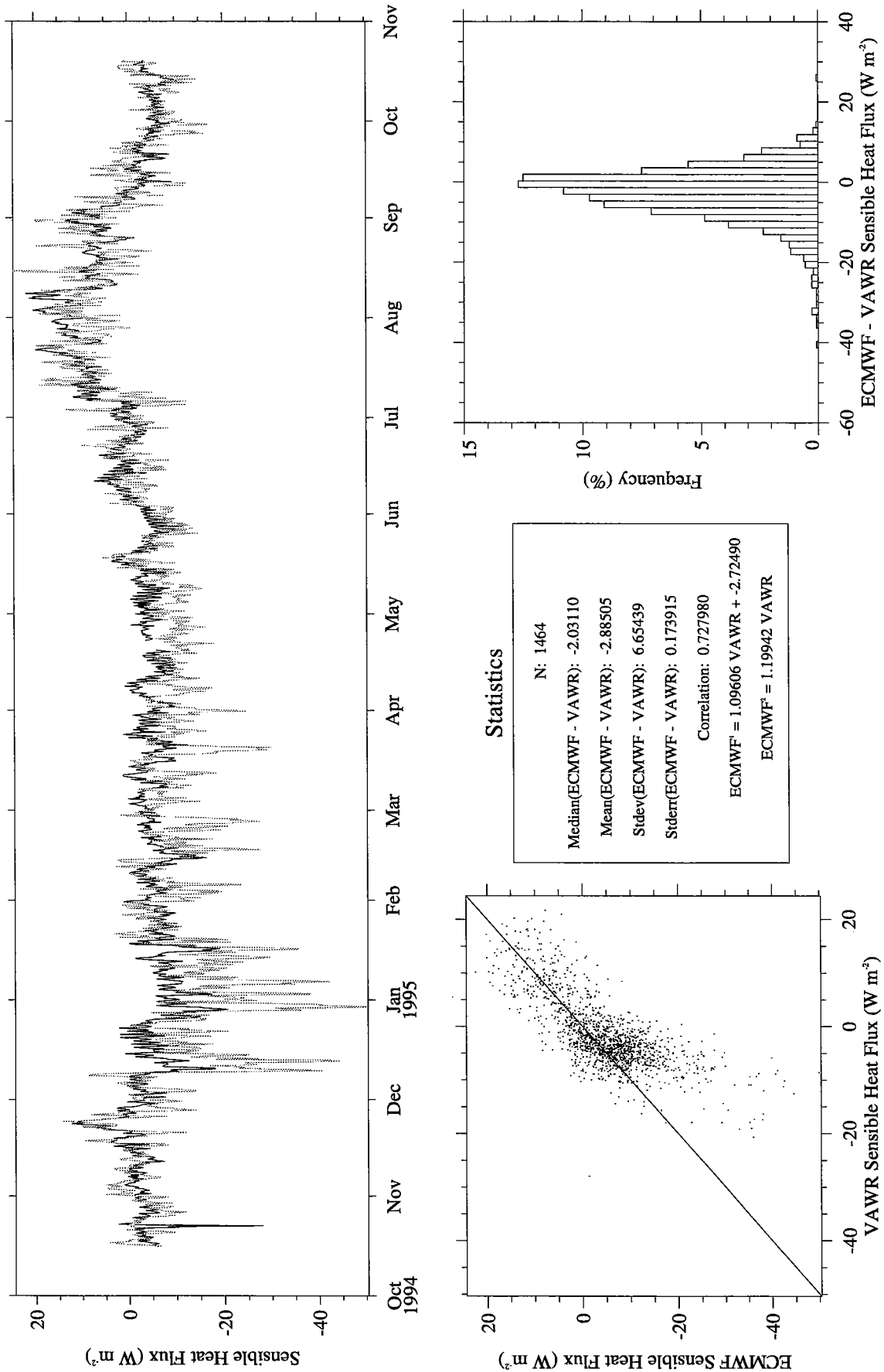


Figure A25. ECMWF (gray) vs. VAWR (black) sensible heat flux.

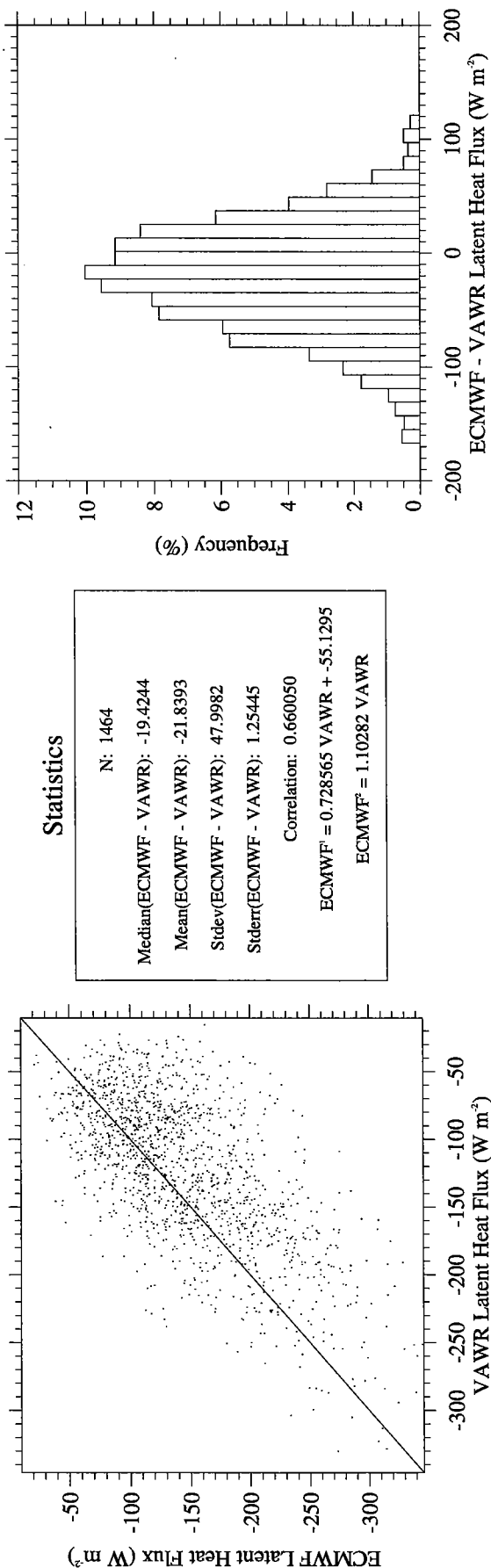
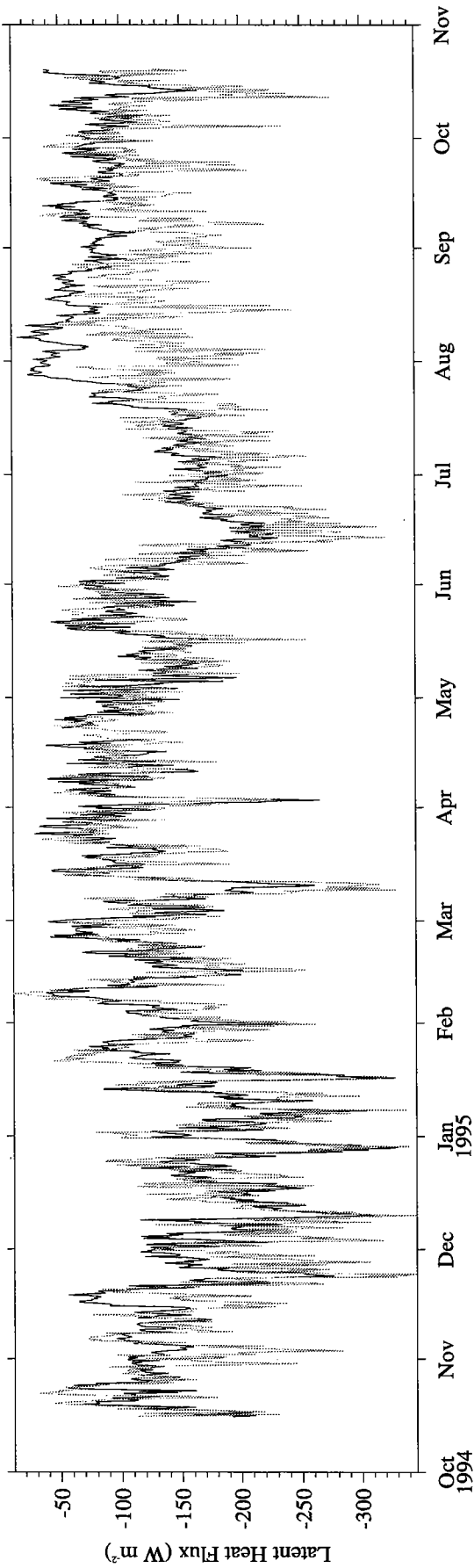


Figure A26. ECMWF (gray) vs. VAWR (black) latent heat flux.

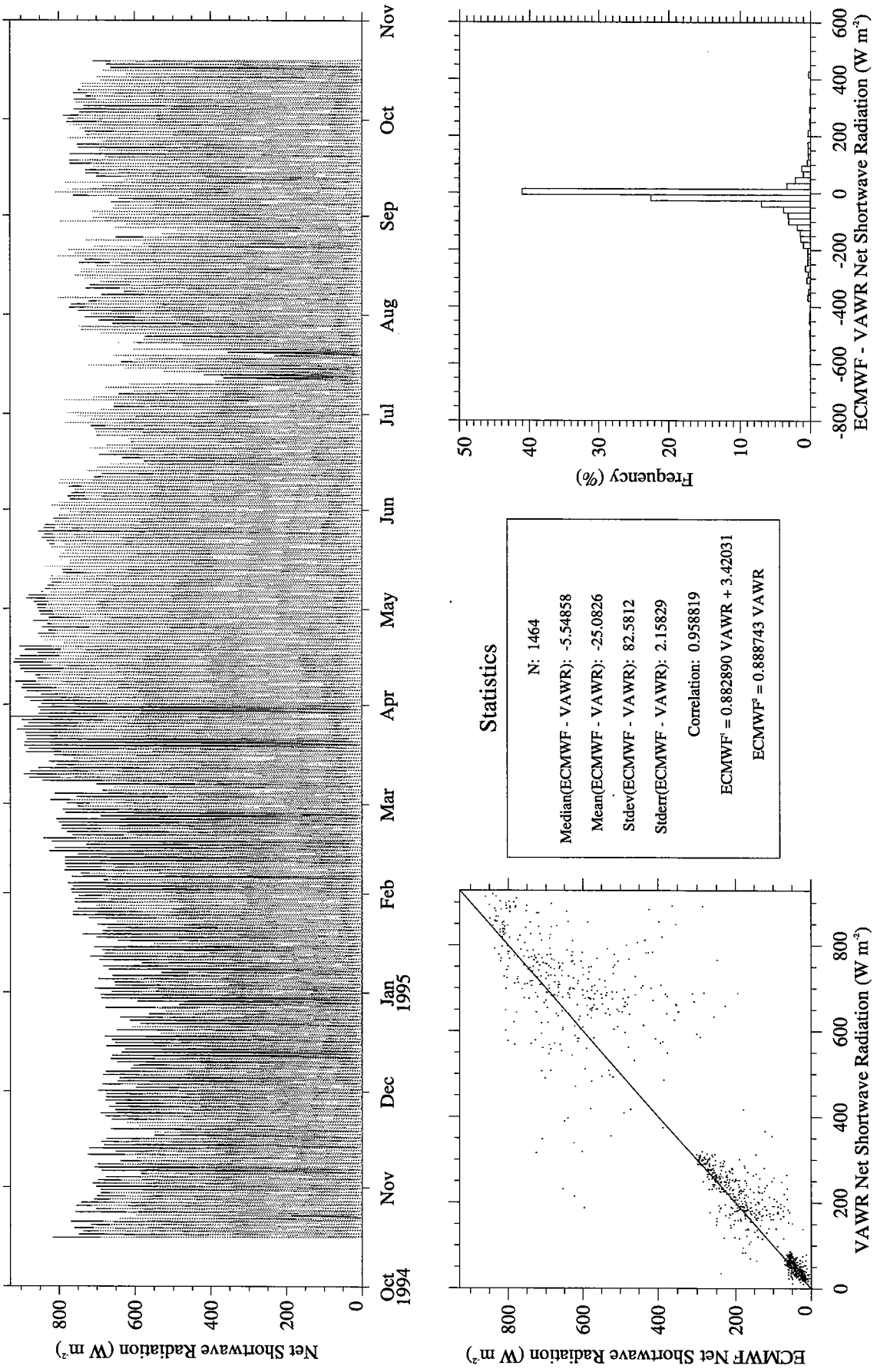
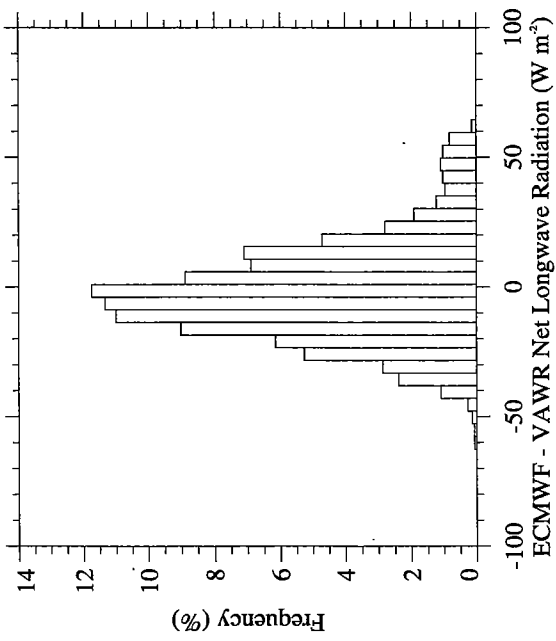
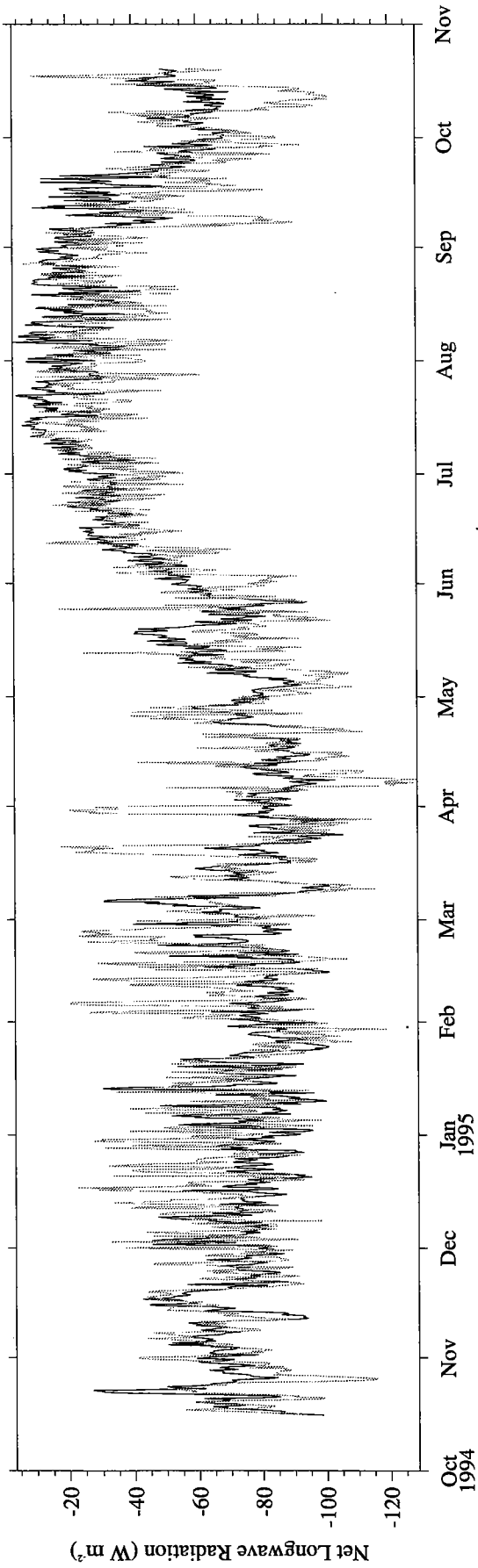


Figure A27. ECMWF (gray) vs. VAWR (black) net shortwave radiation.



Statistics

N: 1464

Median(ECMWF - VAWR): -3.80608

Mean(ECMWF - VAWR): -2.06123

Stdev(ECMWF - VAWR): 19.5317

Stderr(ECMWF - VAWR): 0.510470

Correlation: 0.697368

ECMWF = 0.687485 VAWR + -20.3909

ECMWF² = 0.980702 VAWR

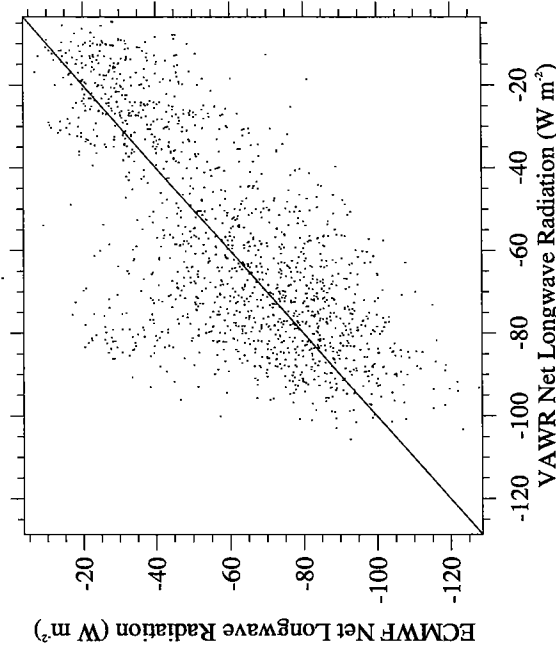


Figure A28. ECMWF (gray) vs. VAWR (black) net longwave radiation.

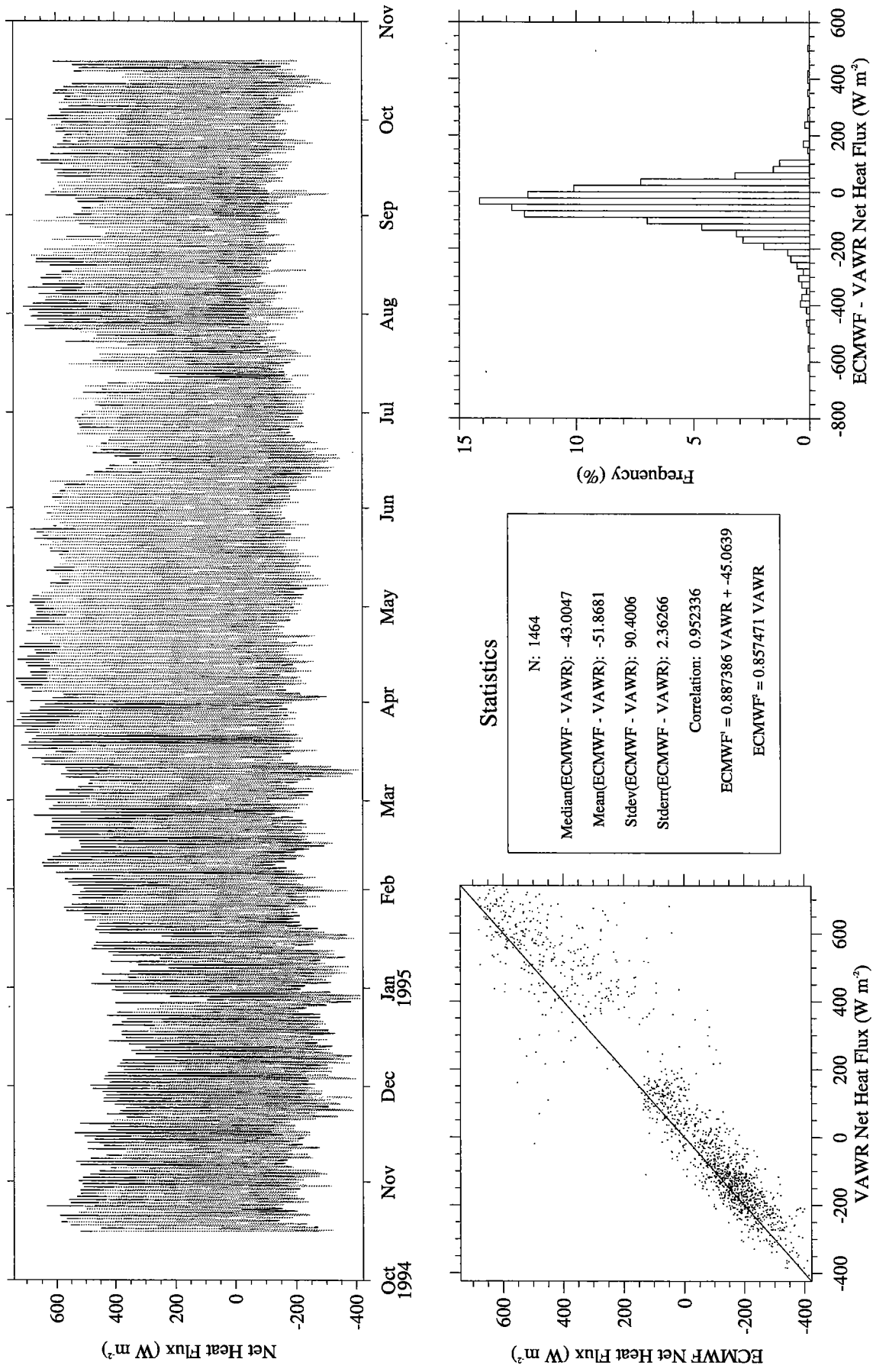


Figure A29. ECMWF (gray) vs. VAWR (black) net heat flux.

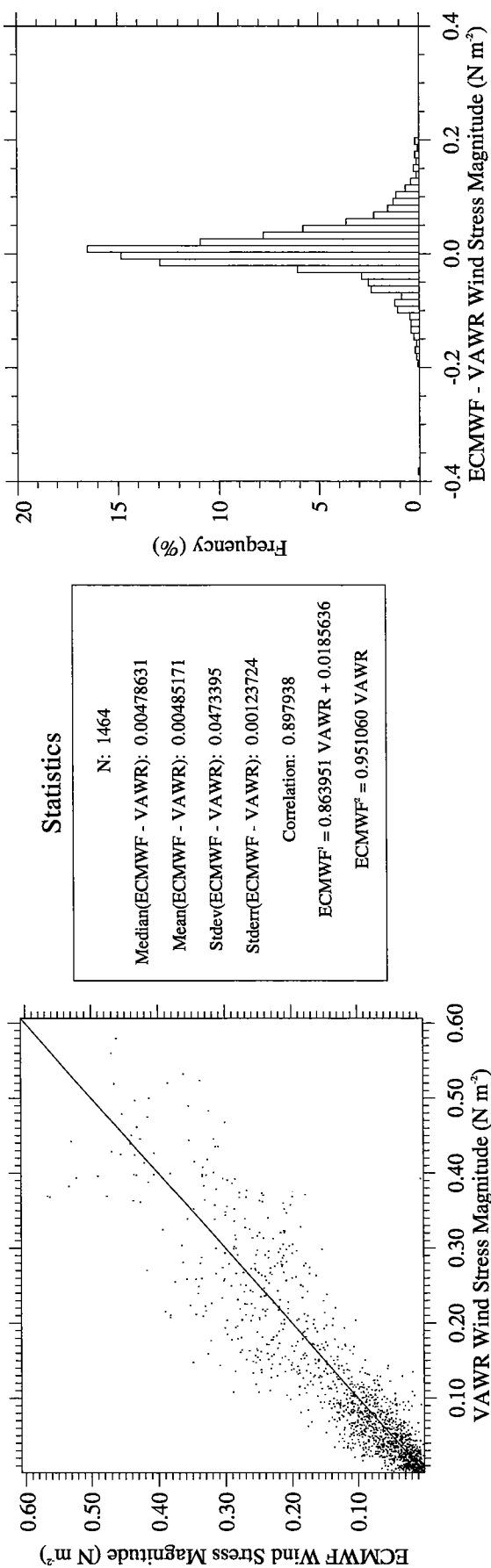
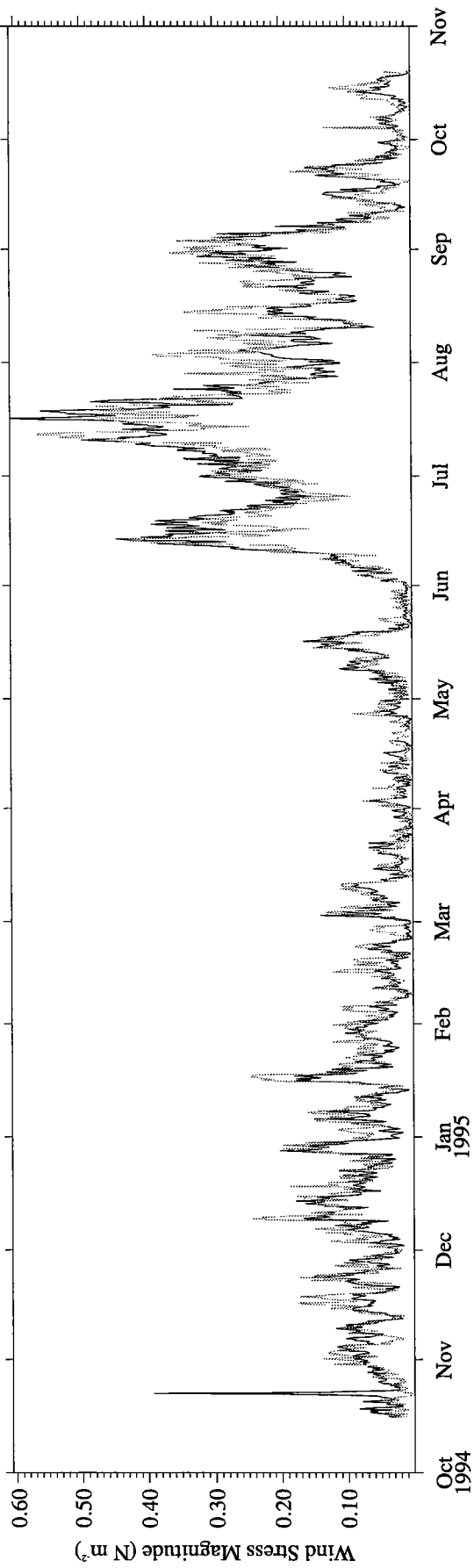


Figure A30. ECMWF (gray) vs. VAWR (black) wind stress magnitude.

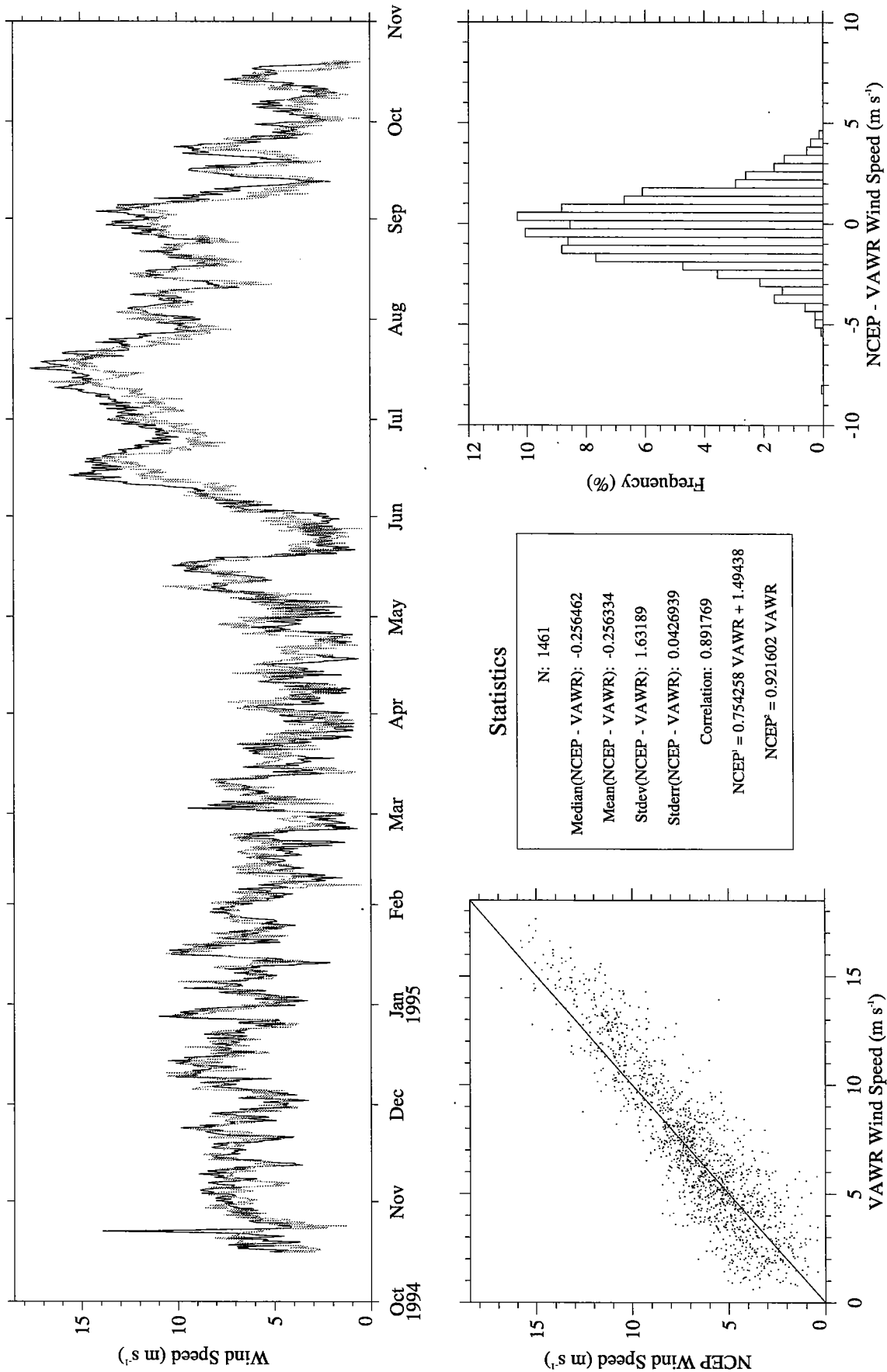
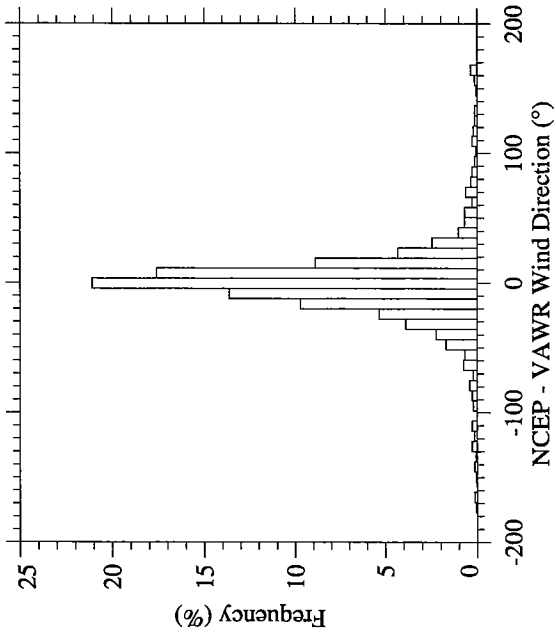
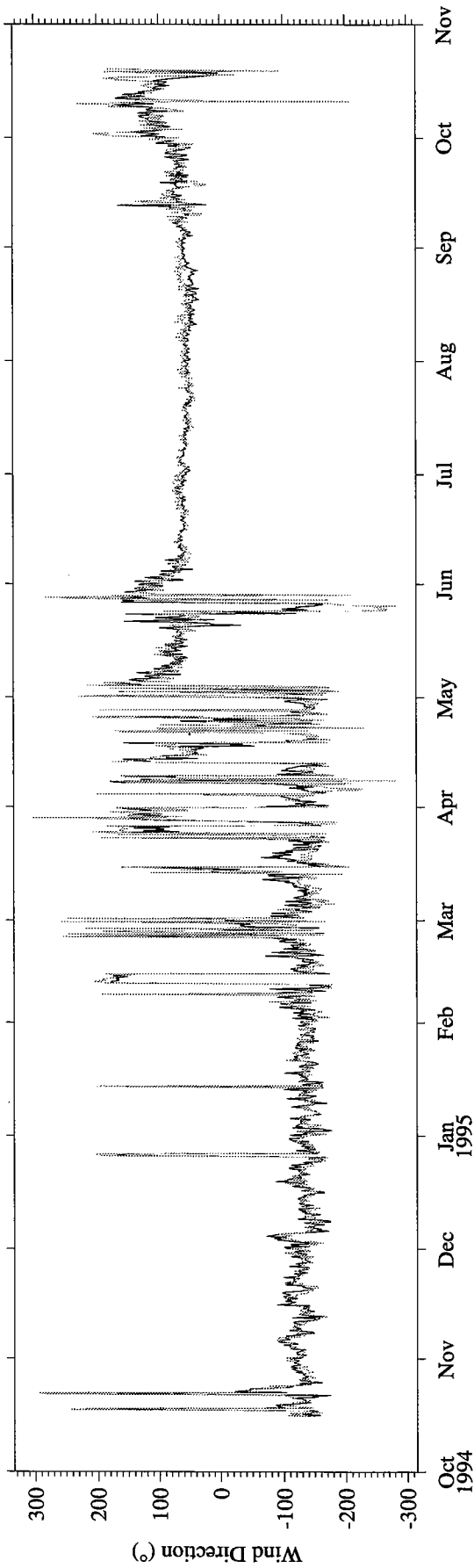


Figure A31. NCEP (gray) vs. VAWR (black) wind speed.



Statistics

N: 1461
 Median(NCEP - VAWR): -0.994446
 Mean(NCEP - VAWR): -1.87003
 Stdev(NCEP - VAWR): 31.3880
 Stderr(NCEP - VAWR): 0.821180
 Correlation: 0.964054
 NCEP = 1.05841 VAWR + -0.599188
 NCEP² = 1.05953 VAWR

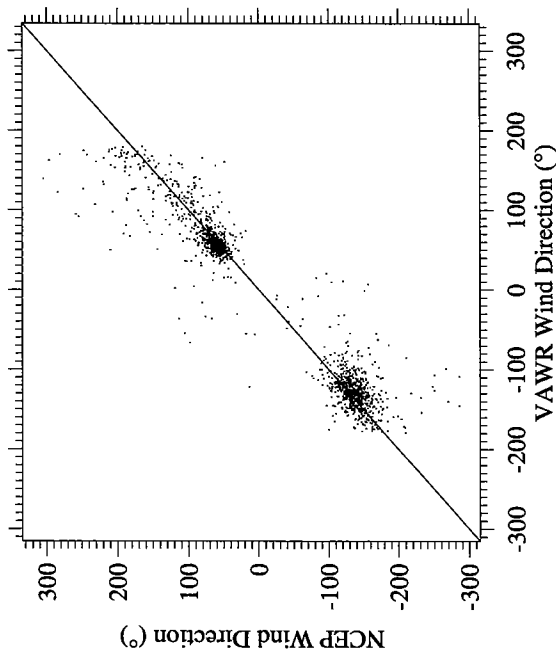


Figure A32. NCEP (gray) vs. VAWR (black) wind direction.

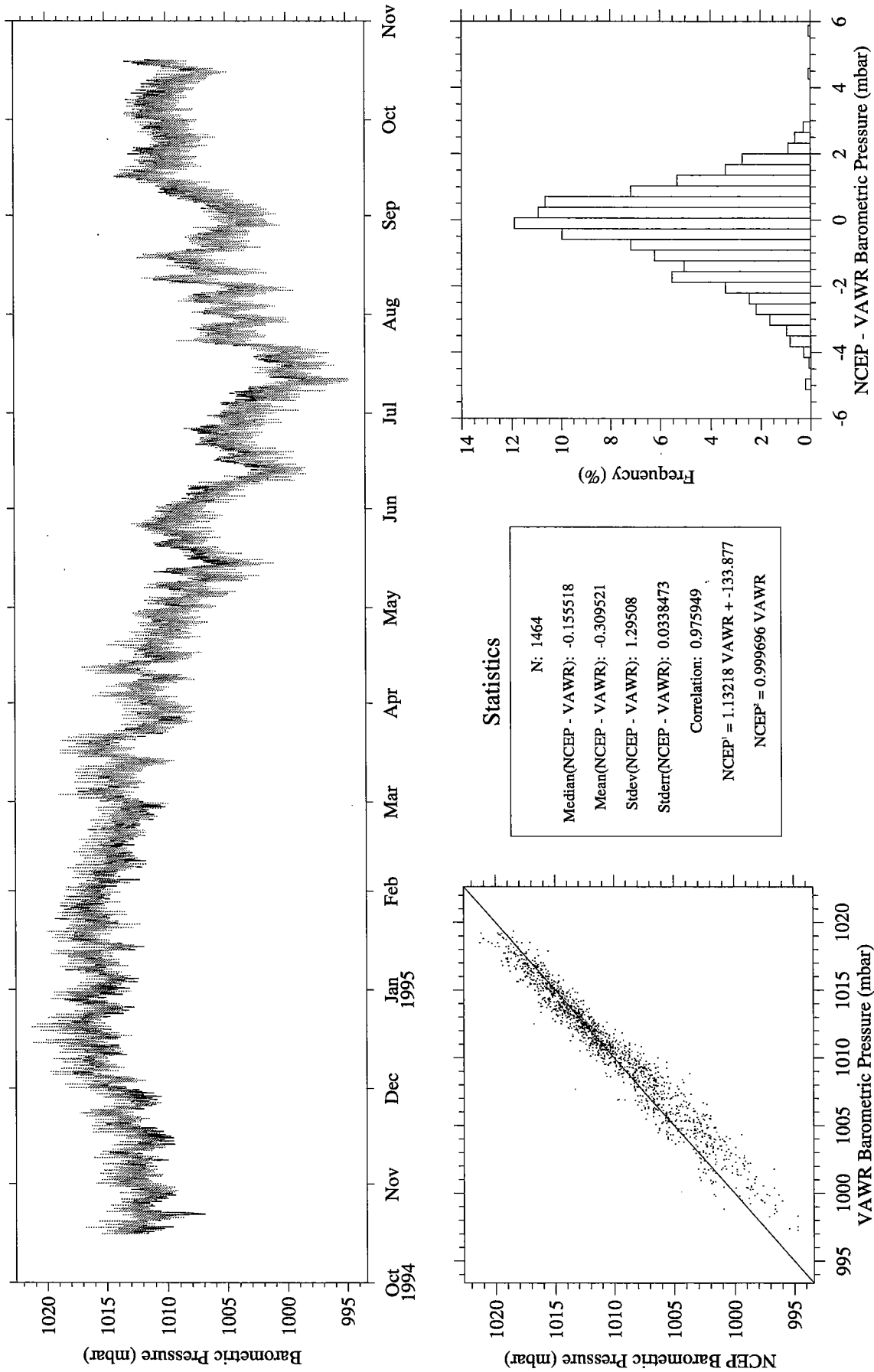


Figure A33. NCEP (gray) vs. VAWR (black) barometric pressure.

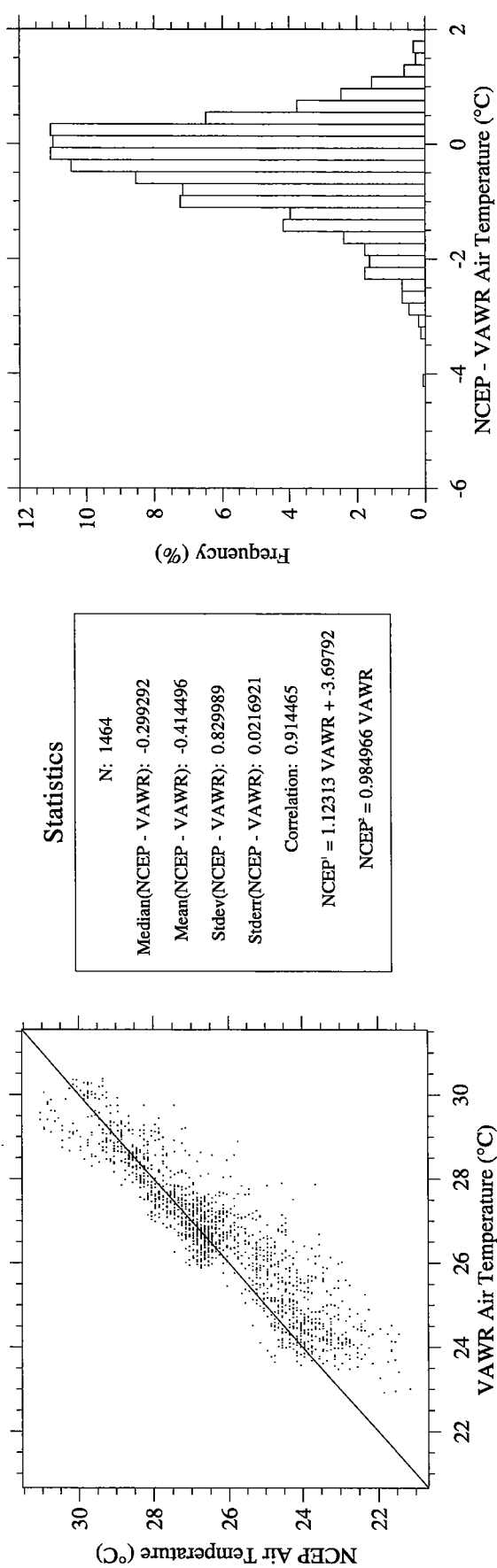
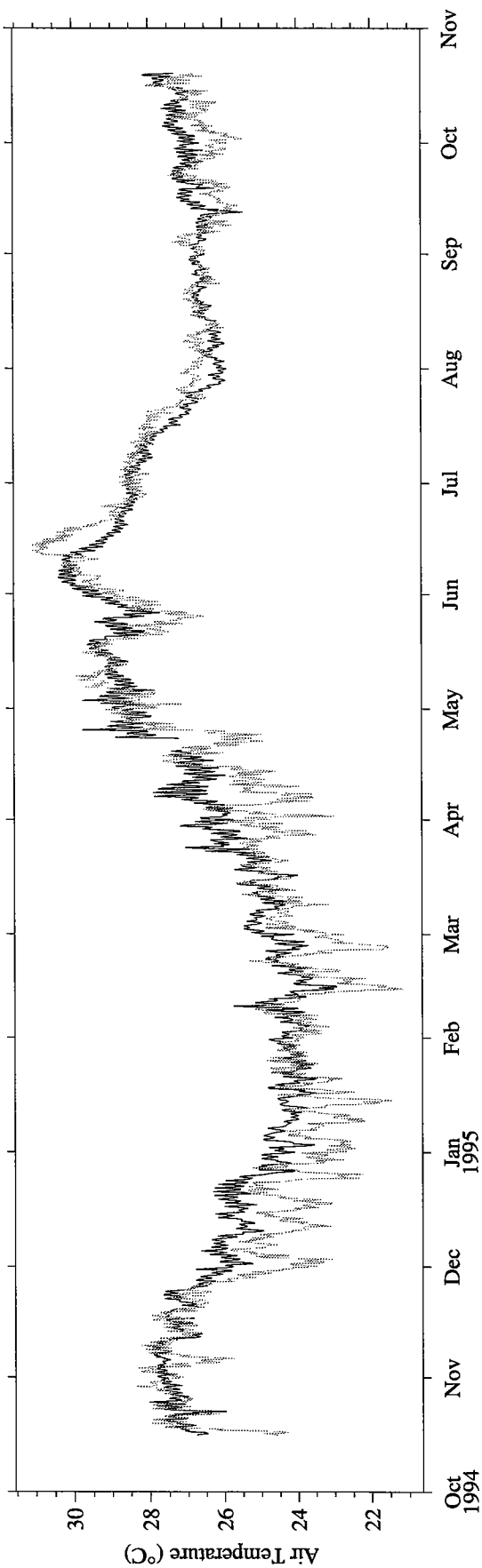


Figure A34. NCEP (gray) vs. VAWR (black) air temperature.

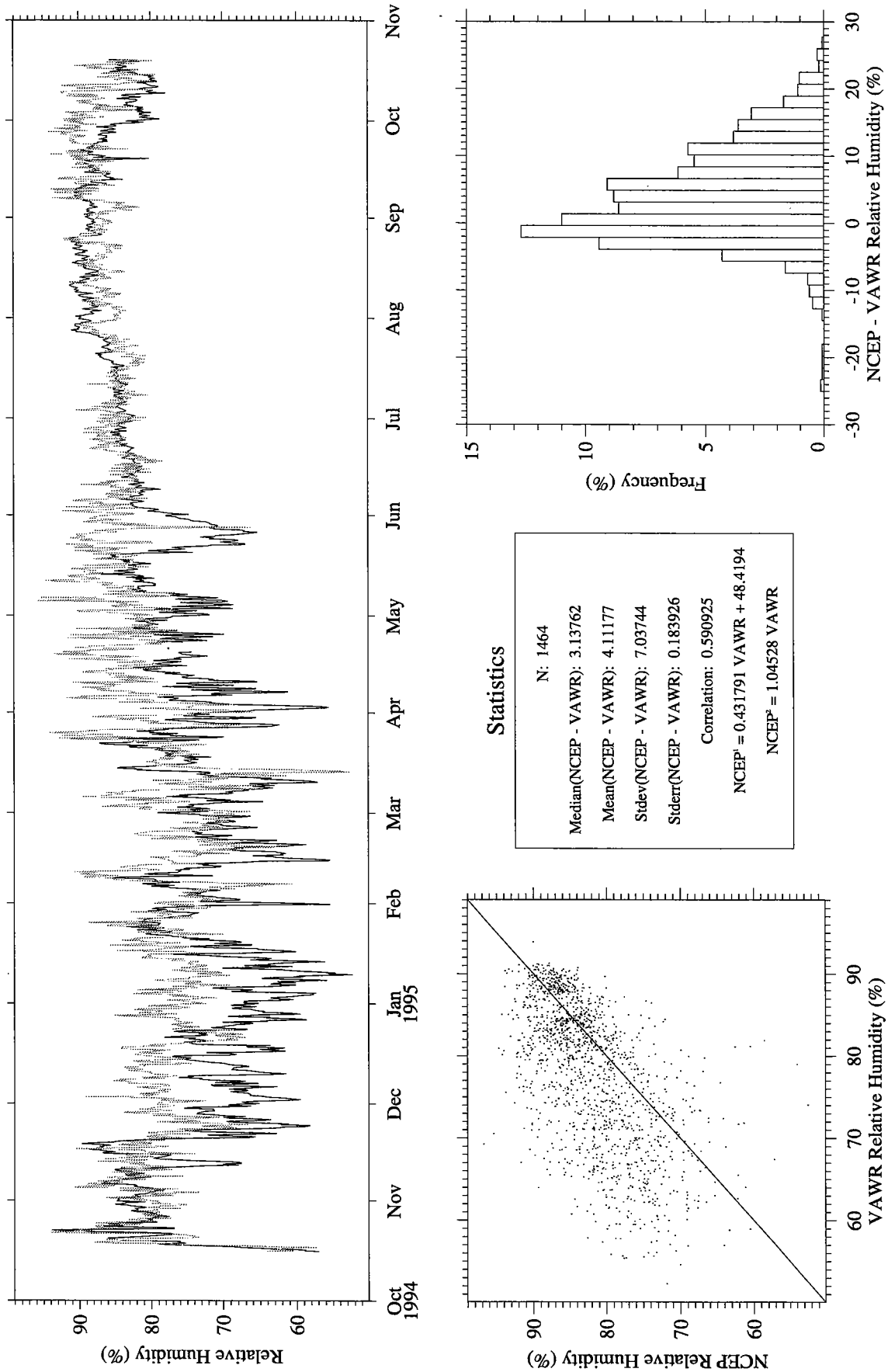
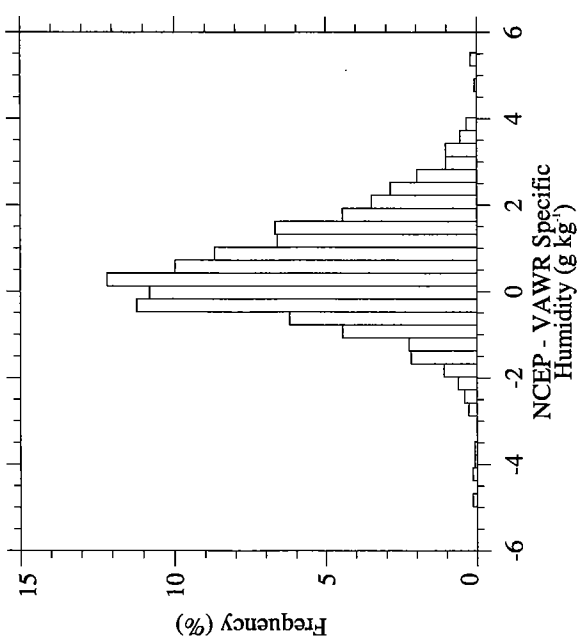
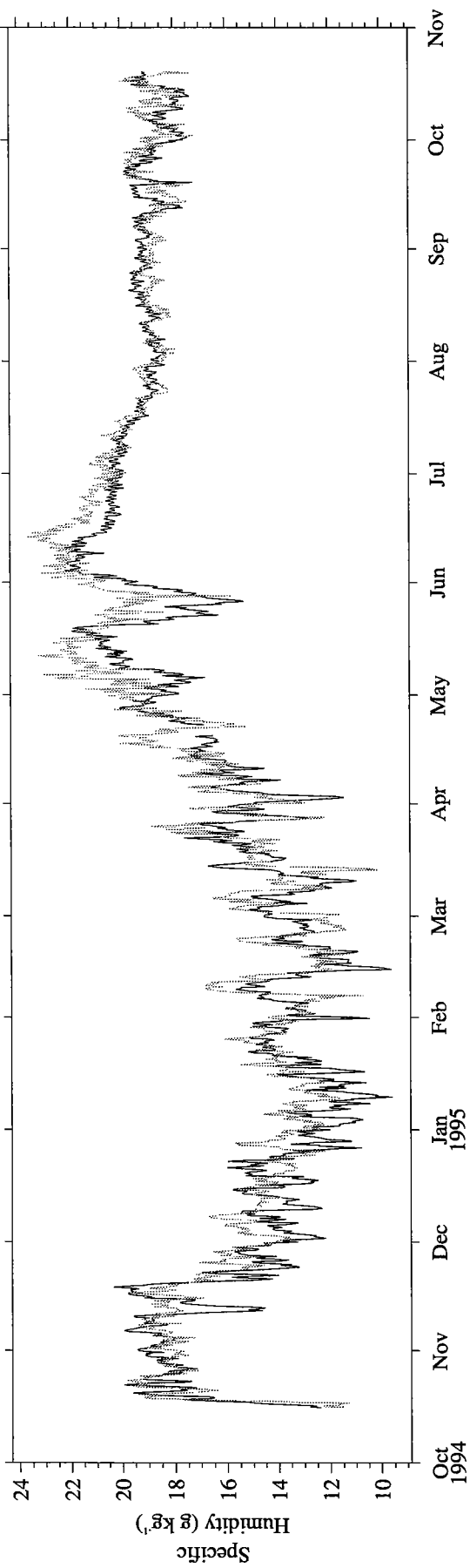


Figure A35. NCEP (gray) vs. VAWR (black) relative humidity.



Statistics

N: 1464
 Median(NCEP - VAWR): 0.383183
 Mean(NCEP - VAWR): 0.477359
 Stdev(NCEP - VAWR): 1.20047
 Stderr(NCEP - VAWR): 0.0313749
 Correlation: 0.914257
 $NCEP = 0.911618 VAWR + 1.97592$
 $NCEP = 1.02484 VAWR$

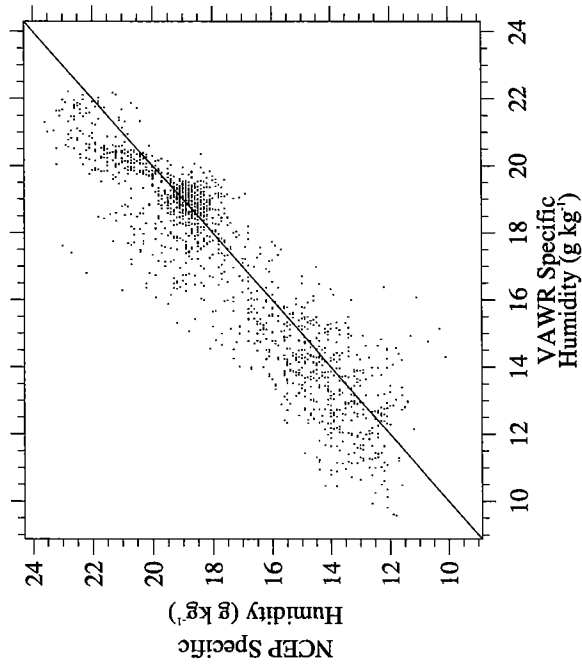


Figure A36. NCEP (gray) vs. VAWR (black) specific humidity.

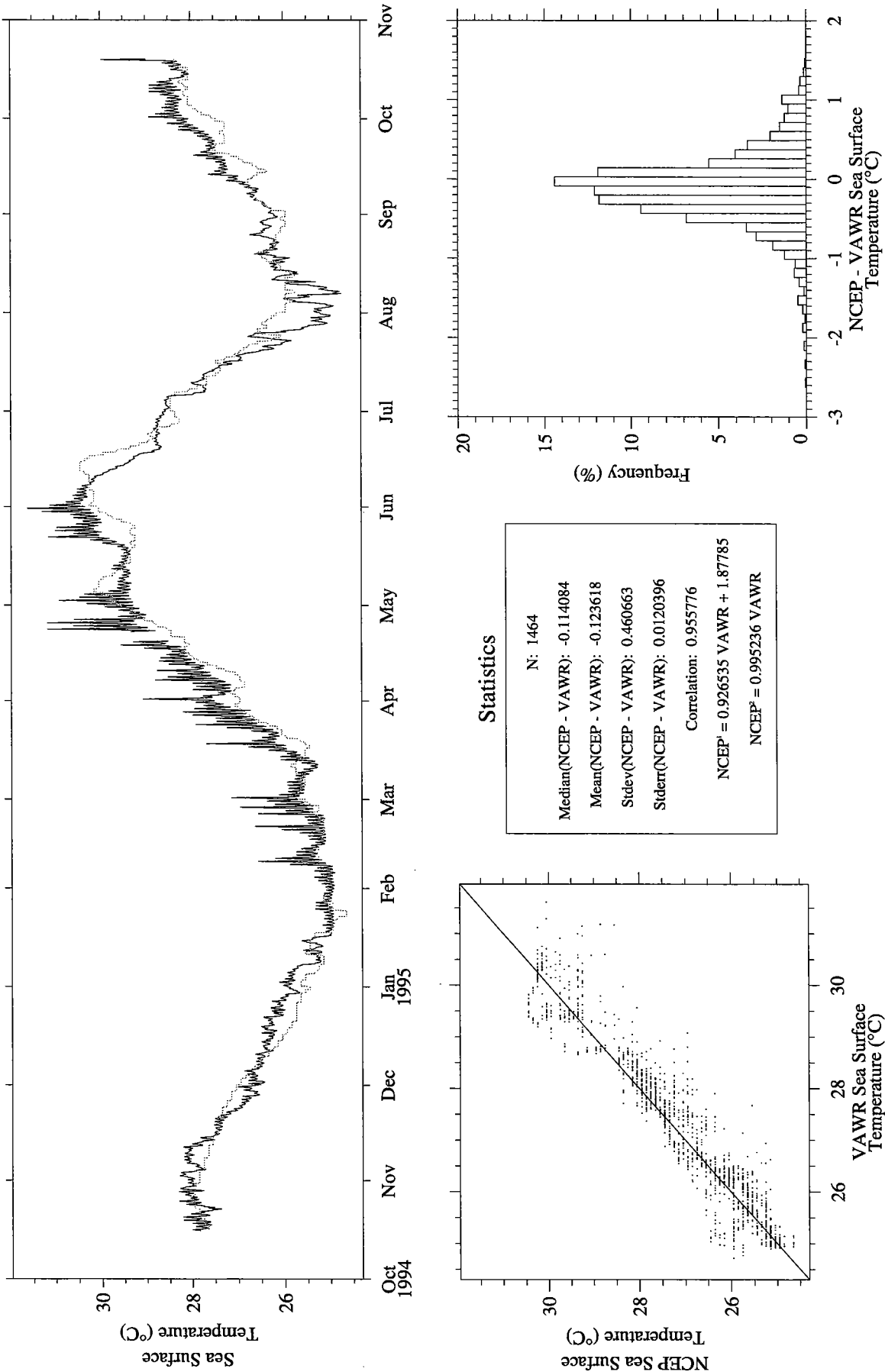
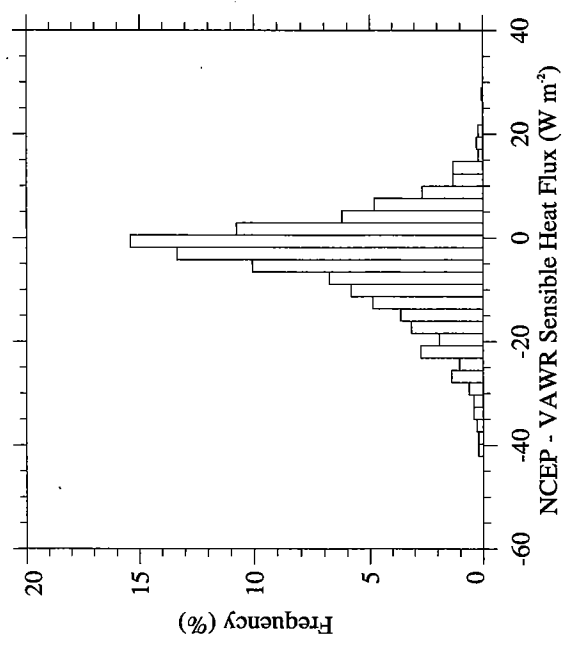
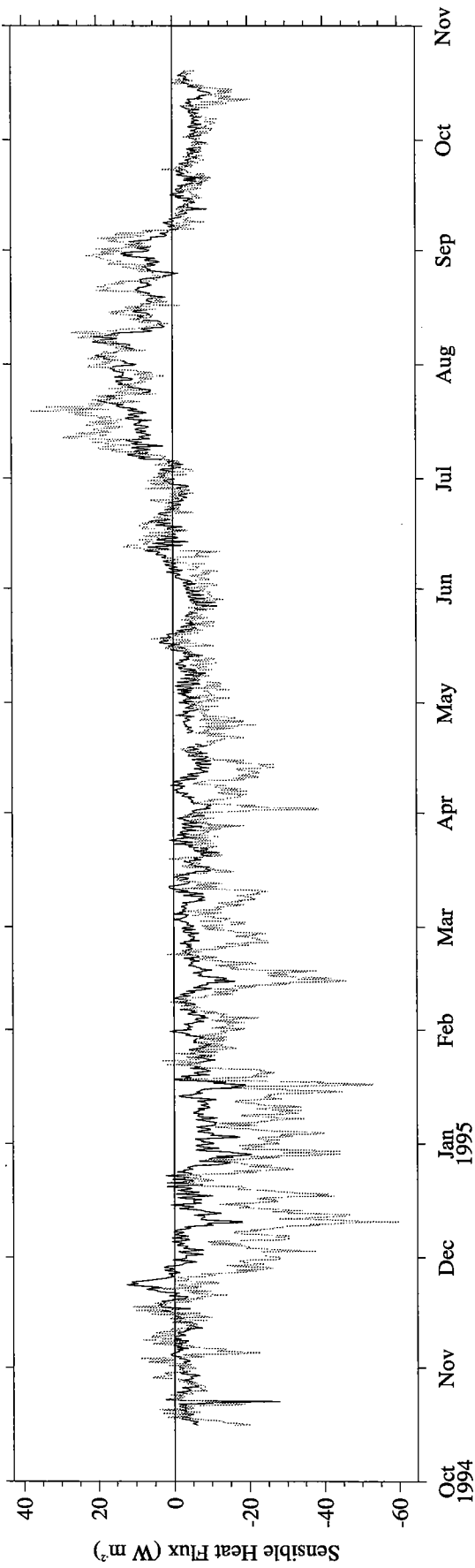


Figure A37. NCEP (gray) vs. VAWR (black) sea surface temperature.



Statistics

N: 1461
 Median(NCEP - VAWR): -3.17167
 Mean(NCEP - VAWR): -4.74130
 Stdev(NCEP - VAWR): 9.47155
 Stderr(NCEP - VAWR): 0.247797
 Correlation: 0.761400
 NCEP = 1.58832 VAWR + -3.76482
 NCEP = 1.73042 VAWR

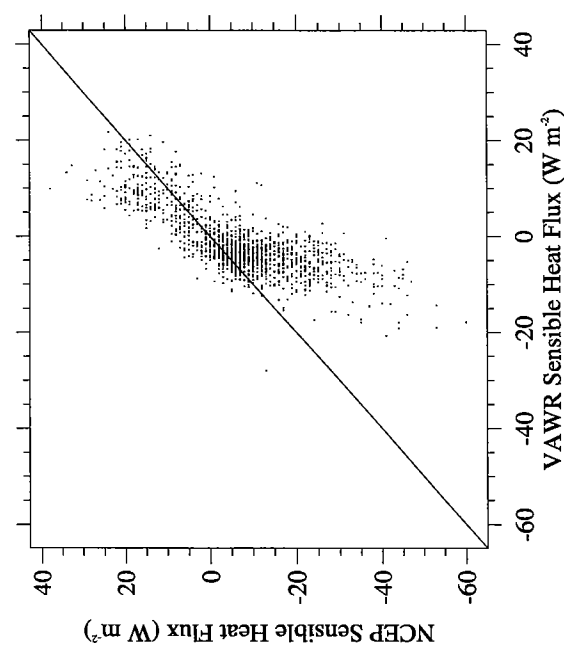


Figure A38. NCEP (gray) vs. VAWR (black) sensible heat flux.

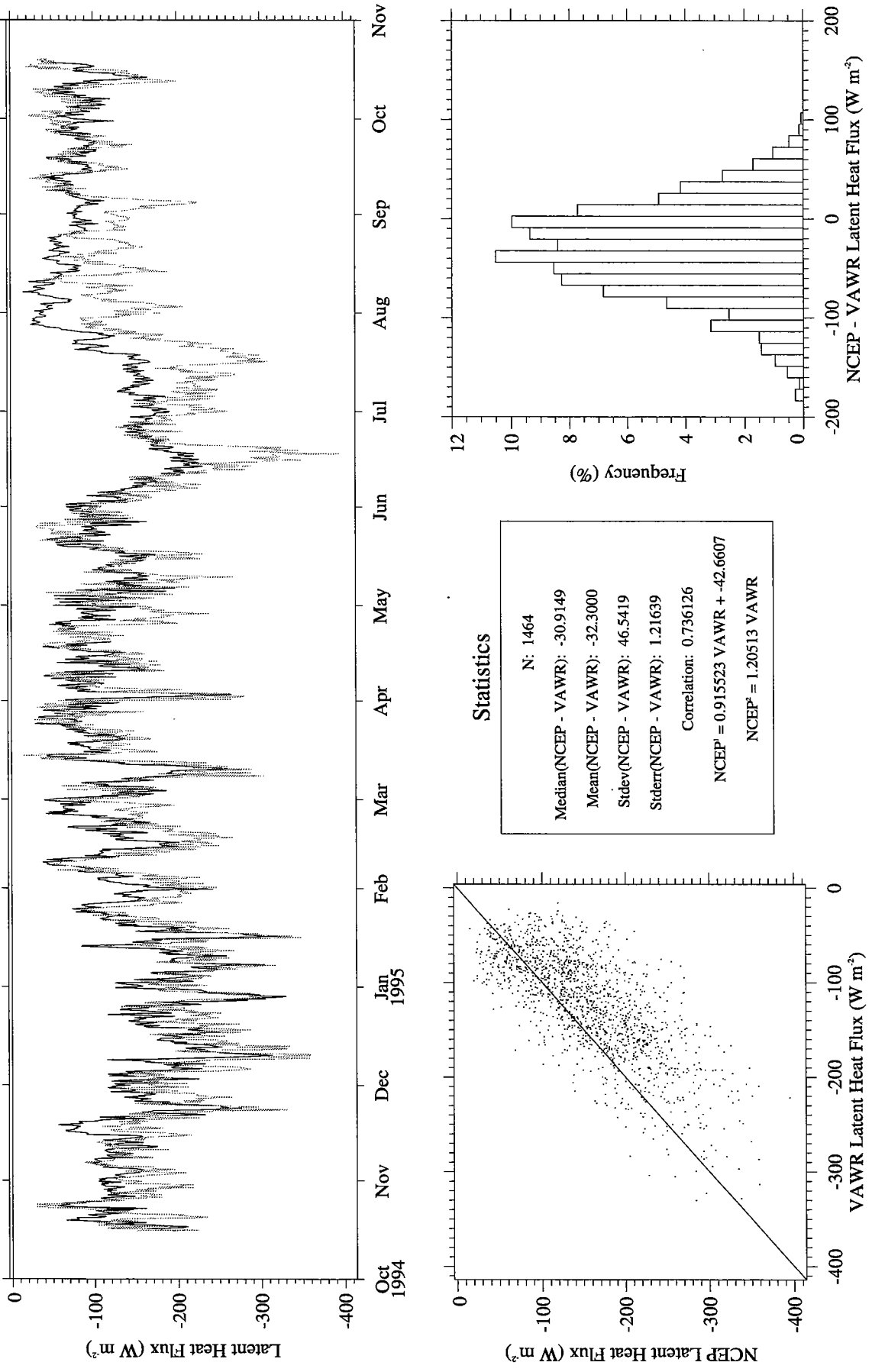


Figure A39. NCEP (gray) vs. VAWR (black) latent heat flux.

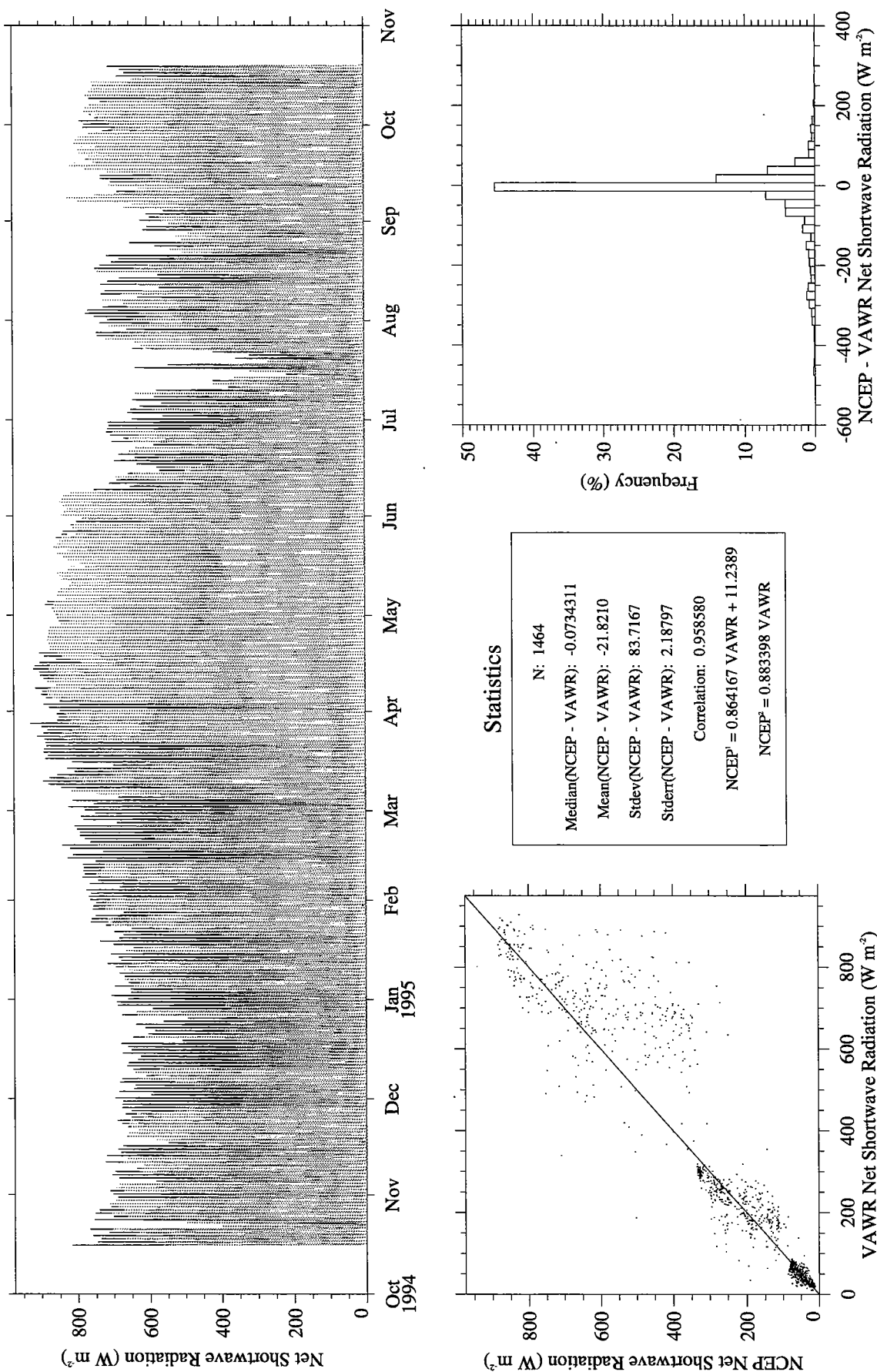


Figure A40. NCEP (gray) vs. VAWR (black) net shortwave radiation.

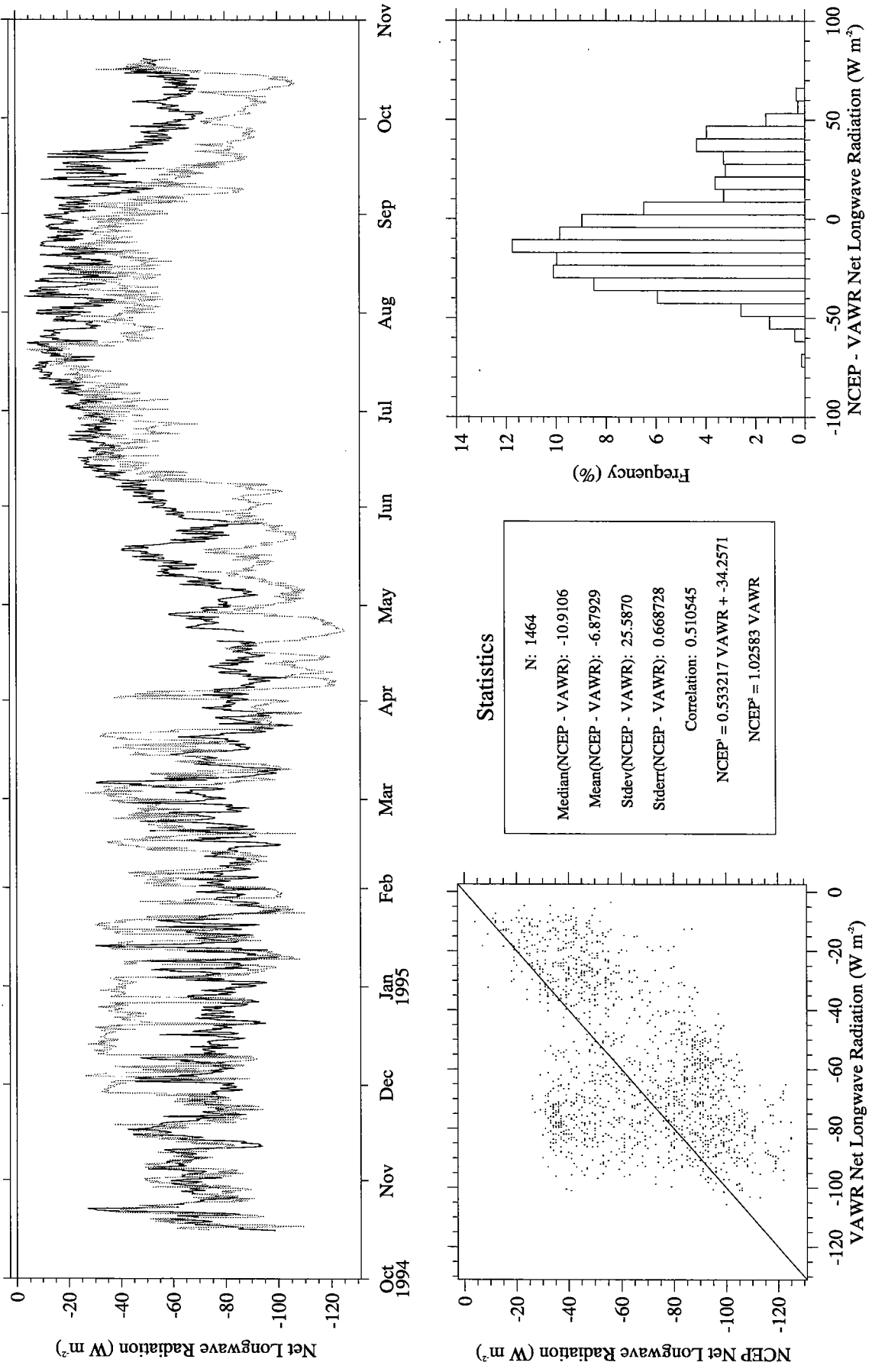
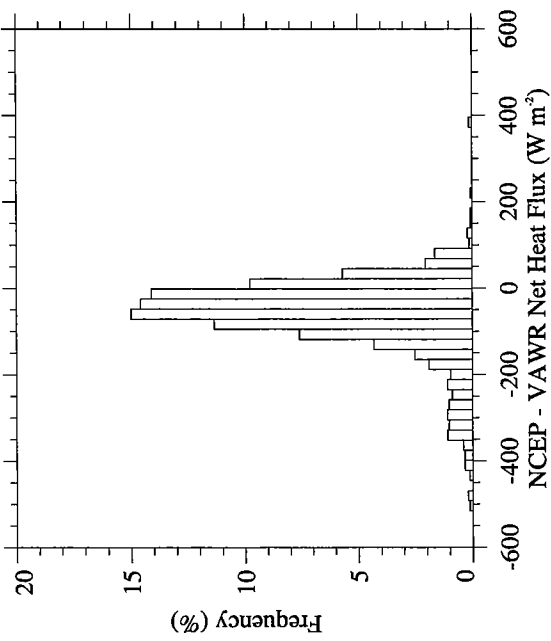
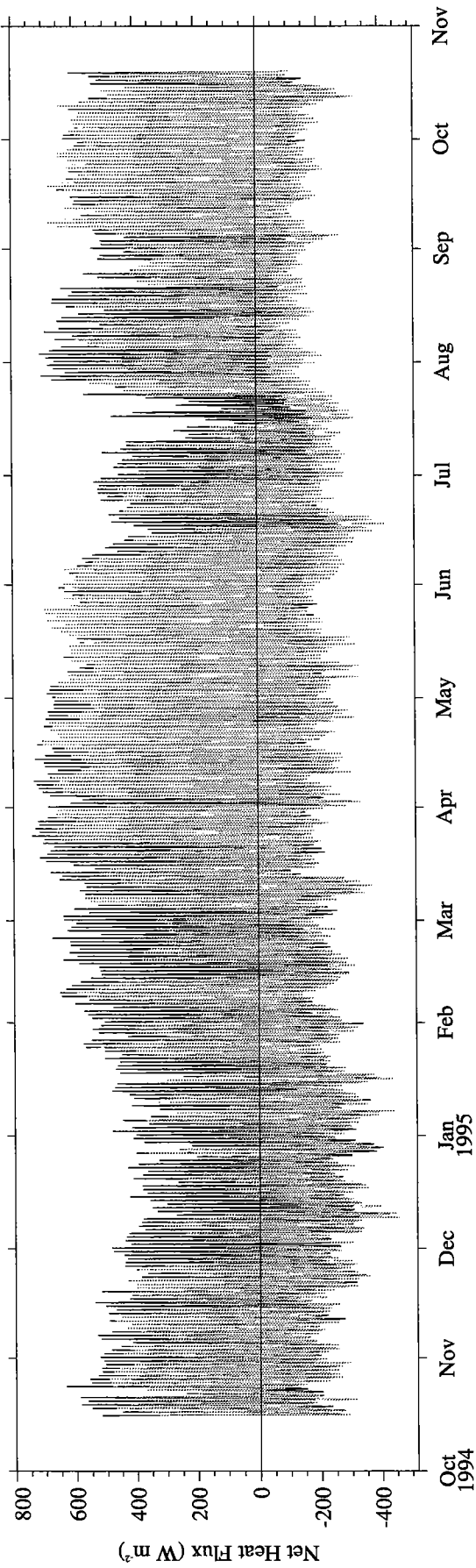


Figure A41. NCEP (gray) vs. VAWR (black) net longwave radiation.



Statistics

N: 1461
 Median(NCEP - VAWR): -50.1566
 Mean(NCEP - VAWR): -65.7119
 Stdev(NCEP - VAWR): 93.4485
 Stderr(NCEP - VAWR): 2.44482
 Correlation: 0.949272
 NCEP = 0.871057 VAWR + -57.9091
 NCEP = 0.832561 VAWR

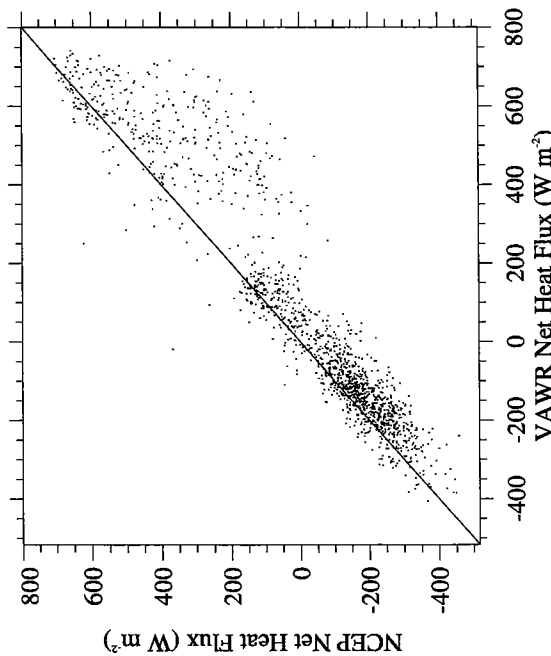


Figure A42. NCEP (gray) vs. VAWR (black) net heat flux.

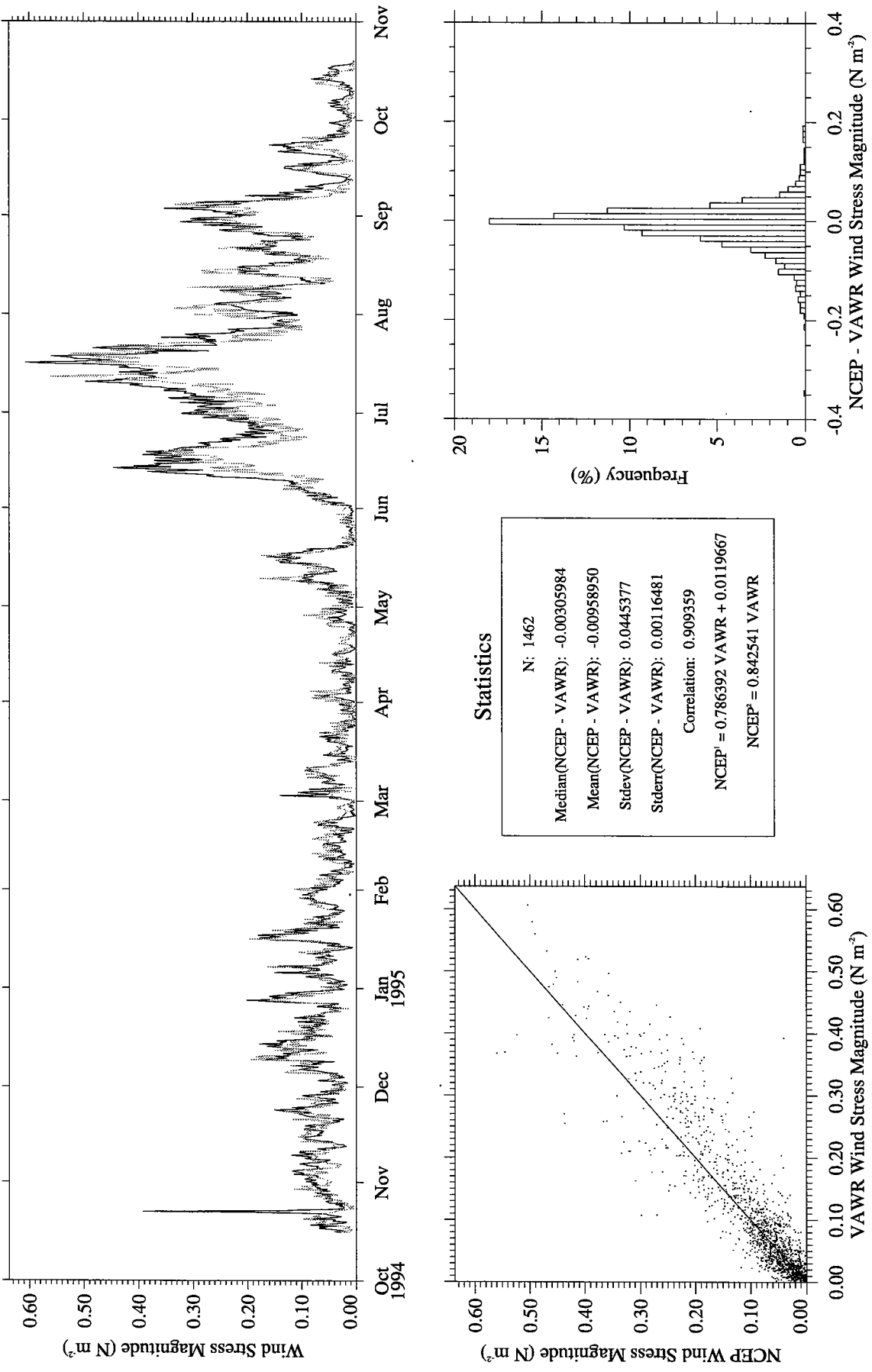


Figure A43. NCEP (gray) vs. VAWR (black) wind stress magnitude.

Appendix B: Instrument Serial Numbers

Table B1. Serial numbers of meteorological instrumentation on the WHOI buoy.

Parameter	Arab 1	Arab 2
<u>VAWR</u>	V721WR	V720WR
Air temperature	Thermistor 5804	Thermistor 5854
Relative humidity	V-034-001	V-029
Barometric pressure	46398	44147
Wind speed	V721WR	V720WR
Wind direction	V721WR	V720WR
Short-wave radiation	25418	21972
Long-wave radiation	28463	28459
Sea temperature	Thermistor 5005	Thermistor 5568
<u>IMET</u>	Logger 226	Logger 228
Air temperature	TMP 101	TMP 105
Relative humidity	HRH 111	HRH 108
Barometric pressure	BPR 107	BPR 106
Wind speed	WND 104	WND 111
Wind direction	WND 104	WND 111
Short-wave radiation	SWR 109	SWR 104
Long-wave radiation	LWR 101	LWR 103
Sea temperature	SST 106	SST 006
Aspirated air temperature	TMP 108	TMP 106
Precipitation	PRC 101	PRC 108
Stand-alone		
Relative humidity with air temp.	002	005 / 27439

Table B2. Serial numbers of WHOI instrumentation deployed on UW moorings.

Depth (m)	Sensor	Arab 1	Arab 2
<u>UW South</u>			
20	Brancker	T-3265	T-3835
250	Brancker	T-2537	T-2533
300	VMCM	VM-016	VM-016
500	VMCM	VM-018	VM-018
750	VMCM	VM-021	VM-021
1500	VMCM	VM-025	VM-025
3025	VMCM	VM-038	VM-038
<u>UW North</u>			
20	Brancker	T-3279	T-3279
250	Brancker	T-2541	T-2541

Table B3. Serial numbers of subsurface instrumentation on the WHOI buoy.

Depth (m)	Sensor	Arab 1	Arab 2
0.17	Brancker	T-3836	T-3291
0.43	Brancker	T-3662	T-3299
0.92	Brancker	T-4483	T-3280
1.37	Brancker	T-5432	None deployed
1.41	Brancker	T-3667	T-3263
1.42	Seacat	1179	928
1.91	Brancker	T-3839	T-3274
2.42	Brancker	T-3762	T-3271
3.5	MTR	3240	3250
4.5	Brancker	T-3763	T-3341
5	VMCM	VM-011	VM-050
10	MVMS	302703-LD	203805-LD
15	VMCM	VM-037	VM-030
20	Brancker	T-3259	T-4488
25	VMCM	VM-039	VM-034
30	Brancker	T-3305	T-3283
35	MVMS	500501-UCSB	200203-UCSB
40	Brancker	T-3703	T-3309
45	VMCM	VM-033	VM-003
50	Brancker	T-4489	T-4492
55	VMCM	VM-015	VM-014
60	Brancker	T-4487	T-3296
65	MVMS	401405-LD	500301-LD
72.5	Brancker	T-4481	T-3699
80	MVMS	500601-UCSB	200201-UCSB
90	Brancker	T-3301	T-2535
100	Seacat	357	927
125	Brancker	T-4491	T-2536
150	Seacat	994	144
175	Brancker	T-3761	T-3308
200	Seacat	992	929
225	Brancker	T-4493	T-3702
250	Seacat	993	142
300	Brancker	T-2534	T-4495

Appendix C: VMCM Record Format

1. RECORD COUNTER (TIME)

The first 16 bits (4 characters) of data comprise the record number. The counter is incremented once each data record. The first record number is one and is used to initialize the instrument. The data and length of the first record may be invalid and should be ignored. Record two contains data for the first record interval. After 65535 records, the record counter will reset to zero and begin its normal counting.

2. NORTH VECTOR

Each vector is scaled from a 24 bit accumulator and stored in a 16 bit floating point representation. This vector is the algebraic sum of the NORTH component of current flow from each sample.

3. EAST VECTOR

Each vector is scaled from a 24 bit accumulator and stored in a 16 bit floating point representation. This vector is the algebraic sum of the EAST component of current flow from each sample.

4. ROTOR 2 (X CURRENT FLOW) (UPPER)

The rotor counts are an algebraic sum of the counts for a record interval. Rotor counts are scaled from a 24 bit accumulator and stored as a 16 bit floating number.

5. ROTOR 1 (Y CURRENT FLOW) (LOWER)

The rotor counts are an algebraic sum of the counts for a record interval. Rotor counts are scaled from a 24 bit accumulator and stored as a 16 bit floating number.

6. COMPASS

The compass field is an 8 bit, 2's complement number (-128 to 128 decimal). The stored value is measured at the beginning of the last sample of the record interval.

7. TEMPERATURE

One temperature sample is taken just before the end of the last record interval.

Record interval = 2 seconds to 2 hours

Sample interval = 0.25 seconds to 2 seconds in quarter second steps

PREAMBLE	TIME	NORTH	EAST	R2	R1	COMPASS	TEMP	PARITY
(2)	(4)	(4)	(4)	(4)	(4)	(2)	(4)	(1)

(X) = Number of characters

REPORT DOCUMENTATION PAGE	1. REPORT NO. WHOI-97-08	2.	3. Recipient's Accession No.
4. Title and Subtitle Arabian Sea Mixed Layer Dynamics Experiment Data Report		5. Report Date July 1997	
7. Author(s) Mark F. Baumgartner, Nancy J. Brink, William M. Ostrom, Richard P. Trask, Robert A. Weller, Tommy D. Dickey and John Marra		8. Performing Organization Rept. No. WHOI-97-08	
9. Performing Organization Name and Address Woods Hole Oceanographic Institution Woods Hole, Massachusetts 02543		10. Project/Task/Work Unit No. 11. Contract(C) or Grant(G) No. (C) N00014-94-1-0161 (G)	
12. Sponsoring Organization Name and Address Office of Naval Research		13. Type of Report & Period Covered Technical Report	
15. Supplementary Notes This report should be cited as: Woods Hole Oceanog. Inst. Tech. Rept., WHOI-97-08.			
16. Abstract (Limit: 200 words) The Arabian Sea is characterized by strong, large-scale atmospheric forcing during the summer (southwest) and winter (northeast) monsoons. To investigate air-sea interactions related to this unique surface forcing, a moored array was deployed from 15 October 1994 to 19 October 1995 just south of a region that experiences the climatological maximum winds during the summer monsoon. The array consisted of two Scripps Institution of Oceanography surface toroid buoys, two University of Washington subsurface moorings and a surface 3 m discus buoy deployed by the Woods Hole Oceanographic Institution (WHOI). The WHOI buoy carried redundant meteorological packages to measure wind speed and direction, air temperature, relative humidity, barometric pressure, incoming short- and long-wave radiation and precipitation. Oceanographic instrumentation was deployed on the WHOI buoy's bridle and mooring line to collect time series of temperature, salinity and velocity at various depths. Four multi-variable moored systems (MVMS) were also deployed along the mooring line by the Lamont-Doherty Earth Observatory and the University of California at Santa Barbara to record both bio-optical and physical parameters. This report describes the instrumentation deployed on the WHOI buoy and the processing and editing of the returned data. The data are then summarized in graphical and tabular formats.			
17. Document Analysis a. Descriptors air-sea interaction moored data Arabian Sea b. Identifiers/Open-Ended Terms c. COSATI Field/Group			
18. Availability Statement Approved for public release; distribution unlimited.		19. Security Class (This Report) UNCLASSIFIED	21. No. of Pages 169
		20. Security Class (This Page)	22. Price

DOCUMENT LIBRARY

Distribution List for Technical Report Exchange – February 1996

University of California, San Diego
SIO Library 0175C
9500 Gilman Drive
La Jolla, CA 92093-0175

Hancock Library of Biology & Oceanography
Alan Hancock Laboratory
University of Southern California
University Park
Los Angeles, CA 90089-0371

Gifts & Exchanges
Library
Bedford Institute of Oceanography
P.O. Box 1006
Dartmouth, NS, B2Y 4A2, CANADA

Commander
International Ice Patrol
1082 Shennecossett Road
Groton, CT 06340-6095

NOAA/EDIS Miami Library Center
4301 Rickenbacker Causeway
Miami, FL 33149

Research Library
U.S. Army Corps of Engineers
Waterways Experiment Station
3909 Halls Ferry Road
Vicksburg, MS 39180-6199

Institute of Geophysics
University of Hawaii
Library Room 252
2525 Correa Road
Honolulu, HI 96822

Marine Resources Information Center
Building E38-320
MIT
Cambridge, MA 02139

Library
Lamont-Doherty Geological Observatory
Columbia University
Palisades, NY 10964

Library
Serials Department
Oregon State University
Corvallis, OR 97331

Pell Marine Science Library
University of Rhode Island
Narragansett Bay Campus
Narragansett, RI 02882

Working Collection
Texas A&M University
Dept. of Oceanography
College Station, TX 77843

Fisheries-Oceanography Library
151 Oceanography Teaching Bldg.
University of Washington
Seattle, WA 98195

Library
R.S.M.A.S.
University of Miami
4600 Rickenbacker Causeway
Miami, FL 33149

Maury Oceanographic Library
Naval Oceanographic Office
Building 1003 South
1002 Balch Blvd.
Stennis Space Center, MS, 39522-5001

Library
Institute of Ocean Sciences
P.O. Box 6000
Sidney, B.C. V8L 4B2
CANADA

National Oceanographic Library
Southampton Oceanography Centre
European Way
Southampton SO14 3ZH
UK

The Librarian
CSIRO Marine Laboratories
G.P.O. Box 1538
Hobart, Tasmania
AUSTRALIA 7001

Library
Proudman Oceanographic Laboratory
Bidston Observatory
Birkenhead
Merseyside L43 7 RA
UNITED KINGDOM

IFREMER
Centre de Brest
Service Documentation - Publications
BP 70 29280 PLOUZANE
FRANCE